NEONOR
Neotectonics in Norway

NGU Report 2000.001

Neotectonics in Norway

Annual Technical Report 1999

NGU
Norges geologiske undersøkelse
Geological Survey of Norway
N-7491 Trondheim, Norway
Tel.: 47 73 90 40 11

REPORT

Report no.: 2000.001	ISSN 0800-3416	Grading: Åpen

Title:

Neotectonics in Norway, Annual Technical Report 1999

Editors:	Client:
John Dehls and Odleiv Olesen	BP-Amoco, Norsk Hydro, Phillips Petroleum, Statkraft, NFR, NGU, NORSAR, NPD and SK
Contributors:	**Contributing institutes:**
E. Anda, L. Blikra, L. Bockmann, A. Braathen, H. Bungum, J. Dehls, W. Fjeldskaar, I. Fjeldskaar, L. Grimstveit, E. Hicks, F. Krüger, C. Lindholm, O. Longva, O. Olesen, L. Olsen, G. Richter, F. Riis, D. Roberts, J. Schweitzer, T. Skogseth, K. Sletten, M. Thoresen	NGU, NORSAR, NPD, RF, County Council of Møre and Romsdal, Norwegian Mapping Authority, University of Potsdam, NTNU, UiB
Deposit name and grid-reference:	Number of pages: 187 Price (NOK): Kr. 730,- Map enclosures: 0

Fieldwork carried out:	Date of report:	Project no.:	Person responsible:
1999	17/02-2000	2757.00	Odleiv Olesen

Summary:

The NEONOR project represents a national effort by several national research and mapping institutions to study neotectonic phenomena through a multidisciplinary approach. Information on present land uplift, seismicity, rock stress and postglacial faults is compiled in a 1: 3 million map of Norway and adjacent areas.

Four new possible neotectonic locations were visited. None are considered to be of neotectonic origin. Two areas in the northern North Sea were selected for bathymetry surveys. The survey south of Kvetebjørn supports the interpretation that faults offset the sea floor and Quaternary sediments to the west of Bergen. Two of the N-S trending faults continue through most of the survey area. The survey east of Troll shows no evidence of neotectonic faulting. Considerable work went into evaluating the connection between large-scale slope failures and neotectonics. Large concentrations of these failures are found in several areas in Norway. Some of these concentrations are linked with the increased seismicity that followed the deglaciation of Norway. Others are younger, and more work needs to be done to evaluate the importance of neotectonics in initiating these failures. A new excavation was made at the Båsmoen fault, and the results from previous excavations re-evaluated. New radiocarbon dating indecates that the last significant fault activity occurred during the middle Holocene, between about 8700 and 3850 ^{14}C-yr BP. A new GPS campaign was carried out on the Rana network. Due to poor quality of previous campaigns, no assesment of deformation can be made at this time. However, the ground has been laid for future work. Differential GPS levelling of paleoshorelined in Østerdalen did not support the claim by Holmsen that there was neotectonic movement in the area. The seismic network in Rana continued to operate. The seismic network in Bremanger had many technical problems, but recorded a number of events. A microseismic study of Finnmark was carried out in cooperation with the University of Potsdam. The study was succesful in identifying numerous events, but the results are still being processed. Modelling of current postglacial uplift patterns has identified areas with positive or negative deviations between theoretical and observed rates. Areas with significant positive deviations are located in the mountainous areas onshore southeastern Norway and the northern part of western Norway. There is an area with a significant negative deviation along the northern part of the Baltic Sea. Both of these regions correspond to areas of above average seismicity.

Keywords: Geofysikk	Geologi	Seismologi
Neotektonikk	Geologisk risiko	Forkastning
Skred	Landhevning	Fagrapport

CONTENTS

LIST OF FIGURES

1 INTRODUCTION

By John Dehls and Odleiv Olesen, NGU

The initiative for a national neotectonic research project was taken in 1995 by NORSAR and the Geological Survey of Norway (NGU). The Norwegian Petroleum Directorate (OD) and NGU did at the same time make plans for compiling a neotectonic map of Norway at the scale 1:3 million. These two initiatives were merged into the 'Neotectonics in Norway' - NEONOR Project in 1996. The Norwegian Mapping Authority (SK) has joined the project and is contributing with expertise on geodesy. The Norwegian Research Council (NFR) has financed three years of a four-year Doctoral fellowship (Dr. Scient for Erik Hicks at NORSAR/UiO and a two-year Post Doctoral fellowship for John Dehls at NGU, until 1 June, 1999). Mark Shahly (Amoco), Chris Dart (Norsk Hydro), Robert Hunsdale (Phillips Petroleum) and Ivar Hågensen (Finnmark Energiverk) are representatives of the four industrial partners in the steering committee. Mark Shahly replaced Philip J. Goldsmith as chairman after August 1998. NGU, NORSAR, OD and SK are represented by Odleiv Olesen, Hilmar Bungum, Fridtjof Riis and Lars Bockmann, respectively. Stein Fanavoll (SINTEF Petroleum Research), Willy Fjeldskaar (Rogaland Research), Ægir Jóhannsson (SINTEF Civil and Environmental Engineering) and Terje Skogseth (NTNU, Dept. of Surveying and Mapping) are carrying out substantial parts of the research project on a contract basis. Conrad Lindholm and Hilmar Bungum (NORSAR) were instrumental in the planning phase of the project proposal.

The project started in June 1997 and the activities for the first two years were reported in previous NEONOR Annual Technical Reports (NGU Reports 98.016 and 99.007). The present report documents the status for the activities that have been carried out by NGU, NORSAR, NPD, SK, NTNU, Sintef and RF during 1999 (task numbers refer to the project proposal):

1. Classification and quality assessment of reported neotectonic phenomena.
2. Collation and interpretation of marine seismic data (both 2D and 3D) from Sintef Petroleum Research (former IKU), Norwegian Petroleum Directorate and the petroleum industry, aimed at mapping recent offshore faulting.
3. Production of a 1:3 million scale map on neotectonic phenomena in Norway.
4. Geological and geophysical investigations.

5-7.Acquisition and interpretation of local and regional high-resolution geodetic data, also by means of GPS networks.

8. Drilling through faults; *In situ* stress measurements.
9. Trenching of postglacial faults.
10. Acquisition of local seismological data by means of new seismic stations (micro-networks).
11. Joint interpretation of acquired neotectonic data and geodynamic modelling aimed to understand the recent and present day crustal dynamics.

The NEONOR activities in 1999 have largely been focused on follow-up work, reporting and integrated interpretation of the compiled neotectonic data sets. Four locations of reported neotectonic activity were investigated in the field. New bathymetry data was collected in two areas offshore western Norway to investigate possible neotectonic faults. A new excavation was made at the Båsmoen fault, and the results from previous excavations re-evaluated. Investigations of large-scale slope failures and avalanches, while only partly financially sup-

ported by NEONOR, are reported here due to their possible relationship to seismic events. The GPS network in the Mo i Rana area was remeasured, and the previous vectors recalculated. Reportedly offset shorelines in Østerdalen were also investigated using GPS levelling. An opportunity for a microseismic study of Finnmark came with an initiative from the University of Potsdam, Germany. The results of this cooperative study are presented here. Finally, the results of modelling the relationship between post-glacial uplift, seismicity and neotectonic activity is presented.

2 CLASSIFICATION AND QUALITY ASSESSMENT OF REPORTED NEOTECTONIC PHENOMENA (TASK 1)

2.1 NEOTECTONIC PHENOMENA IN SOUTHERN NORWAY (PART 2)

By Odleiv Olesen, John Dehls and Alvar Braathen, NGU

2.1.1 Introduction

Dehls and Braathen (1998) reported on the results from studies and evaluations of neotectonic indications in southern Norway. During their study some locations were not visited in the field because of poor weather conditions and for other reasons. Four new possible neotectonic locations are reported herein. The first two, the Rudihø and Gnedden locations, were visited immediately after an excursion in 1998 on the Caledonian geology of the Sel-Vågå area. The two other locations, Ytre Byrknes and Grytehorgi, were visited during the summer of 1999. The results are included in the present account.

2.1.2 Rudihø, Heidal, Sel, Oppland

(Map sheet 1718 IV Otta, UTM 514,000 – 6850,000, Zone 32)

In this area, Werenskiold (1931) reported up to 1 metre wide, open fractures. He said that one side seemed to be down-faulted; the turf was hanging down into the fracture; the local population had reported rumbling from the mountain.

We visited the location in June 1998. Two 100-200 metres long and one metre wide SE-NW trending fractures were observed. The southwestern sides seem to be down-faulted up to 1 metre and the fractures are 1-2 metres wide and up to 6 metres deep. The clefts are arc-shaped with the concave side facing a 500 m high, almost vertical mountain side (Fig. 2.1.1). Rock avalanches are situated below the steep mountain. The average strike of the fractures is 113°. The horizontal distance from the fractures to the steep mountainside is between 10 and 40 metres. The bedrock in the area consists of psammite with a foliation striking 070°/02°. Conclusion - the fractures are interpreted to be gravity-induced.

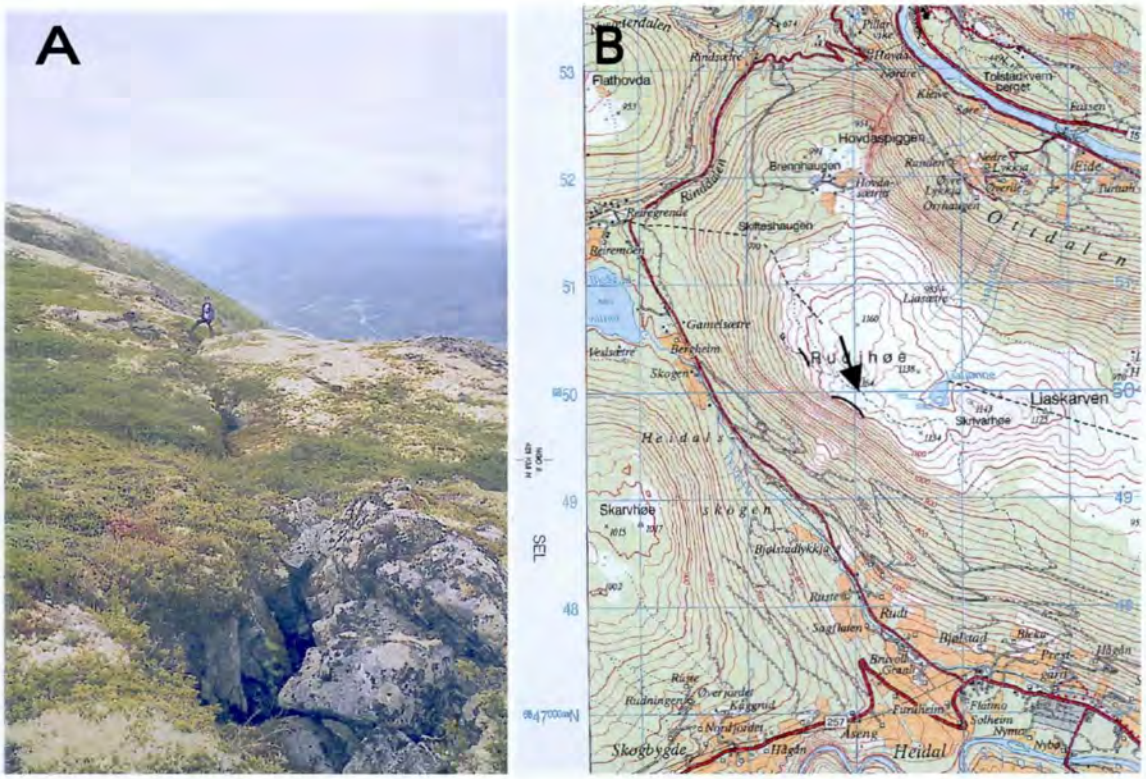

Fig. 2.1.1 A) Photograph towards the southwest of one of the gravitational faults on Rudihø. The valley Heidal can be seen in the background. B) Location of open fractures on 1:50.000 map sheet 1718 IV Otta. The arrow indicates the location and direction of view of the photo.

2.1.3 Gnedden, Holsætrin, Sel, Oppland

(Map sheet 1718 II Vinstra, UTM 532,500 – 6842,550, Zone 32)

Werenskiold (1931) also mapped some NNE-SSW striking and approximately 1-metre high fault scarps south of the barren mountain Gnedden. He suggested that the scarps were formed by faulting after the deglaciation.

In this area, an up to 7 metres high and 1 km long escarpment trends ENE-WSW and can be followed across a small mountain crest (Figs. 2.1.2 and 2.1.3). There is a large variation in scarp height along the western part of the scarp, but it is more constant to the east (3-5 m). The escarpments seem to be sculptured by the inland ice. The local bedrock consisting of phyllite within the Kvitvola Nappe (Englund 1986) has a foliation of 295°/40°.

Conclusion - the escarpment is most likely formed by erosion by the inland ice along a pre-existing steeply dipping fracture in the bedrock.

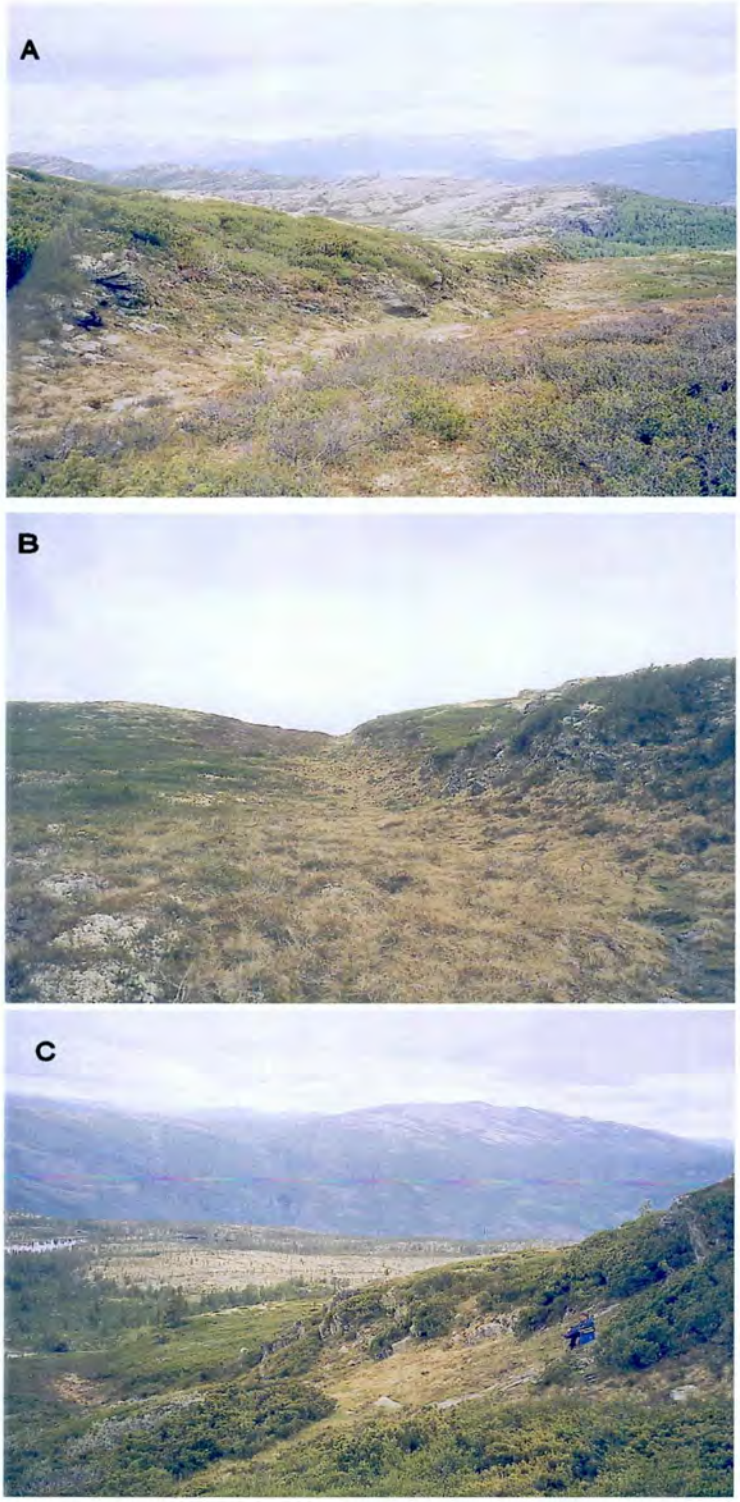

Fig. 2.1.2 Photographs of the reported postglacial fault to the south of Gnedden (Werenskiold 1931). A) Towards the northeast along the eastern part of the scarp. B) Central part of scarp looking to the west. C) View to the west of the western part of scarp. There are large variations in scarp height along the western part of the scarp (1-7 m), while it is more constant to the east (3-5 m). The escarpments seem to be sculptured by the inland ice.

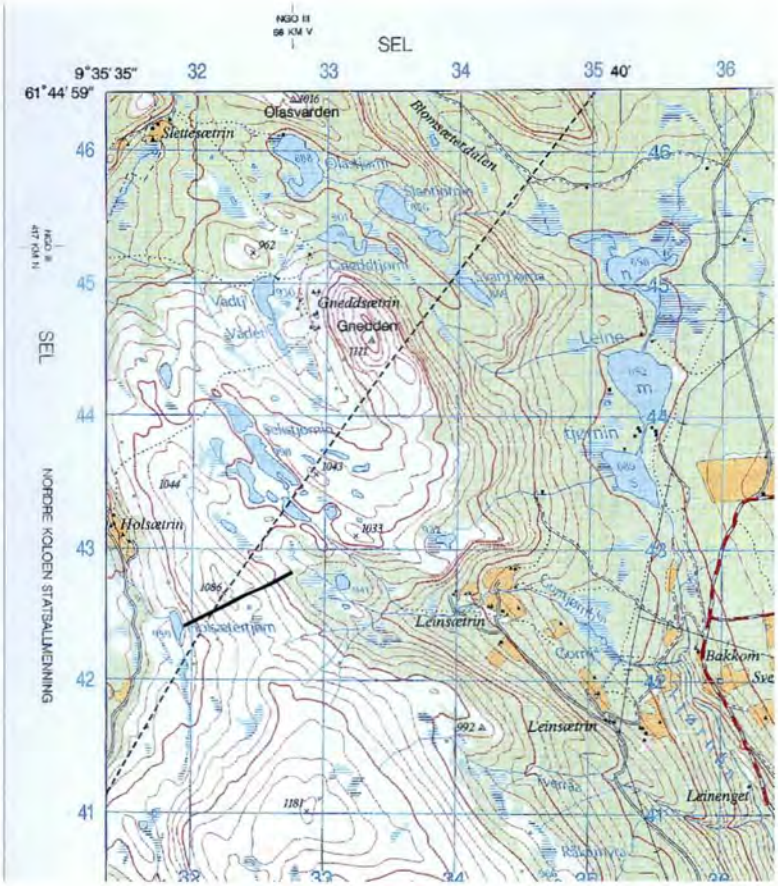

Fig. 2.1.3 Location of the scarp interpreted as a postglacial fault by Werenskiold (1931) on 1:50.000 map sheet 1718 II Vinstra. The black line to the south of Gnedden indicates the location of the scarp.

2.1.4 Ytre Byrknes Archipelago, Gulen, Sogn og Fjordane

(Map sheet 1116 IV Mongstad, UTM 268,200 – 6757,600, Zone 32)

Michelsen *et al.* (1986) mapped NNE-SSW trending open fractures that were 0.5-3 m wide (Fig. 2.1.4a). They occurred *ca.* 50-100 m apart on Ytre Byrknes Archipelago. Some normal faults had vertical displacements in the order of 0.5-2 m. One of the faults was said to displace a glacial splay channel.

We visited the location in June 1999. The sedimentary rocks are situated within the Devonian Fensfjord Basin, which is the southernmost rock unit of this age on mainland Norway. The two main orientations of the fractures in the Devonian conglomerate are 090°/85° and 005°/90°. The scarps have been sculptured by the moving inland ice and vary considerably in height (0-3 m) along the strike (Fig. 2.1.4b, c). The walls are smooth and rounded by ice and melt-water. The scarp, which was said to displace the splay channel, is actually a part of the channel (Fig. 2.1.5). We conclude that the scarps are due to glacial and melt-water erosion and are not caused by any tectonic process.

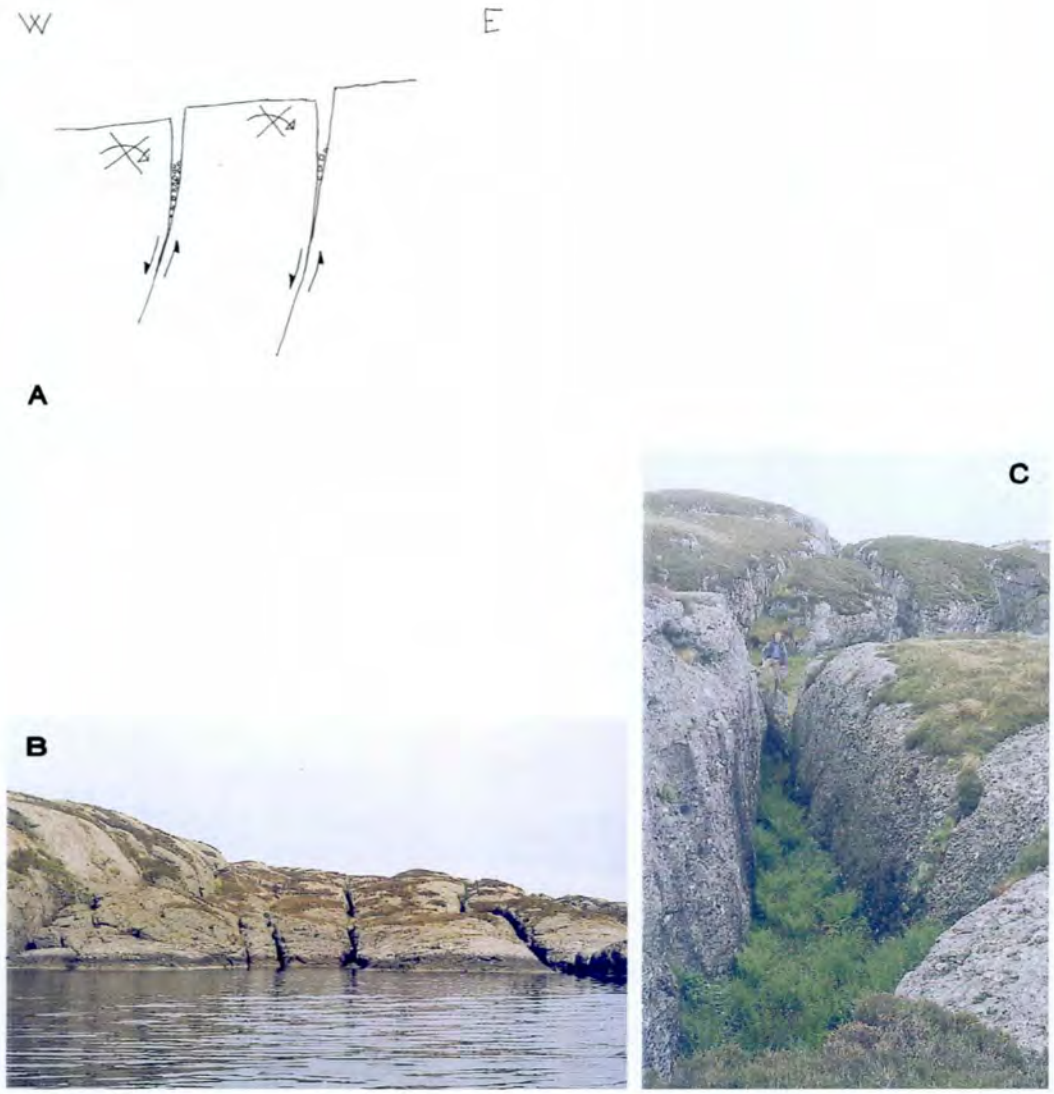

Fig. 2.1.4 A) Sketch by Michelsen et al. (1986) illustrating the formation of the suggested postglacial normal faults on the Byrknes Archipelogo. B) Photograph of the southern part of Kjellingøyna looking to the north. Several vertical open fractures can be seen. C) One of the N-S trending open clefts on Vassøyna. The scarp height varies considerable along strike and the scarps seem to be sculptured by the moving inland ice. The clefts are up to 3 m wide, with a maximum depth of 5 m.

Fig. 2.1.5 Michelsen et al. (1986) reported that a postglacial fault is cutting a glacial splay channel on the northeastern shore of Vassøyna (as seen on these photographs). However, we find it more viable that the melt water has eroded along the ice-sculptured, pre-existing fracture. In conclusion, we have not found any evidence for postglacial faulting in the area. The photos are looking to the east. The strike and dip of the fracture are 090°/85°.

2.1.5 Grytehorgi, Ullensvang, Hordaland

(Map sheet 1415 IV Eidfjord, UTM 406,600 – 6699,500, Zone 32)

Reusch (1901) described a NNE-SSW striking and steeply dipping fault on Grytehorgi, with the down-faulted block to the west (Fig. 2.1.6 and 2.1.8a). Ice-striation seemed to be offset by 1 metre (normal fault). Other N-S sharp escarpments in the Vøringsfossen area were also suggested to be effects of postglacial faulting. The bedrock geology of map sheet Eidfjord has later been mapped by Jorde (1978). Løset (1981) questioned the postglacial age of the Grytehorgi fault since it is filled with till and erratic blocks. Neotectonic movements along the N-S striking faults may, however, be possible.

We visited the location in August 1999. The height of the scarp is generally between 0 and 3 metres, but varies along the scarp (within approximately 30-40 metres length). The foliation of the phyllite (Cambro-Silurian Hardangervidda Group) is flat lying (194°/5°). The lowermost part of the scarp is towards the west. The fracture zone is most likely eroded (Fig. 2.1.7a). The apparent fault scarp varies between 1 and 3 metres and the scarp seems to be rounded by the ice (Fig. 2.1.7). We conclude that the scarp is caused by plucking by the westward-moving inland ice along a pre-existing, steeply dipping fracture zone (200° strike). The central part of the fracture zone is partly eroded along the scarp to form a local trench (Fig. 2.1.7a).

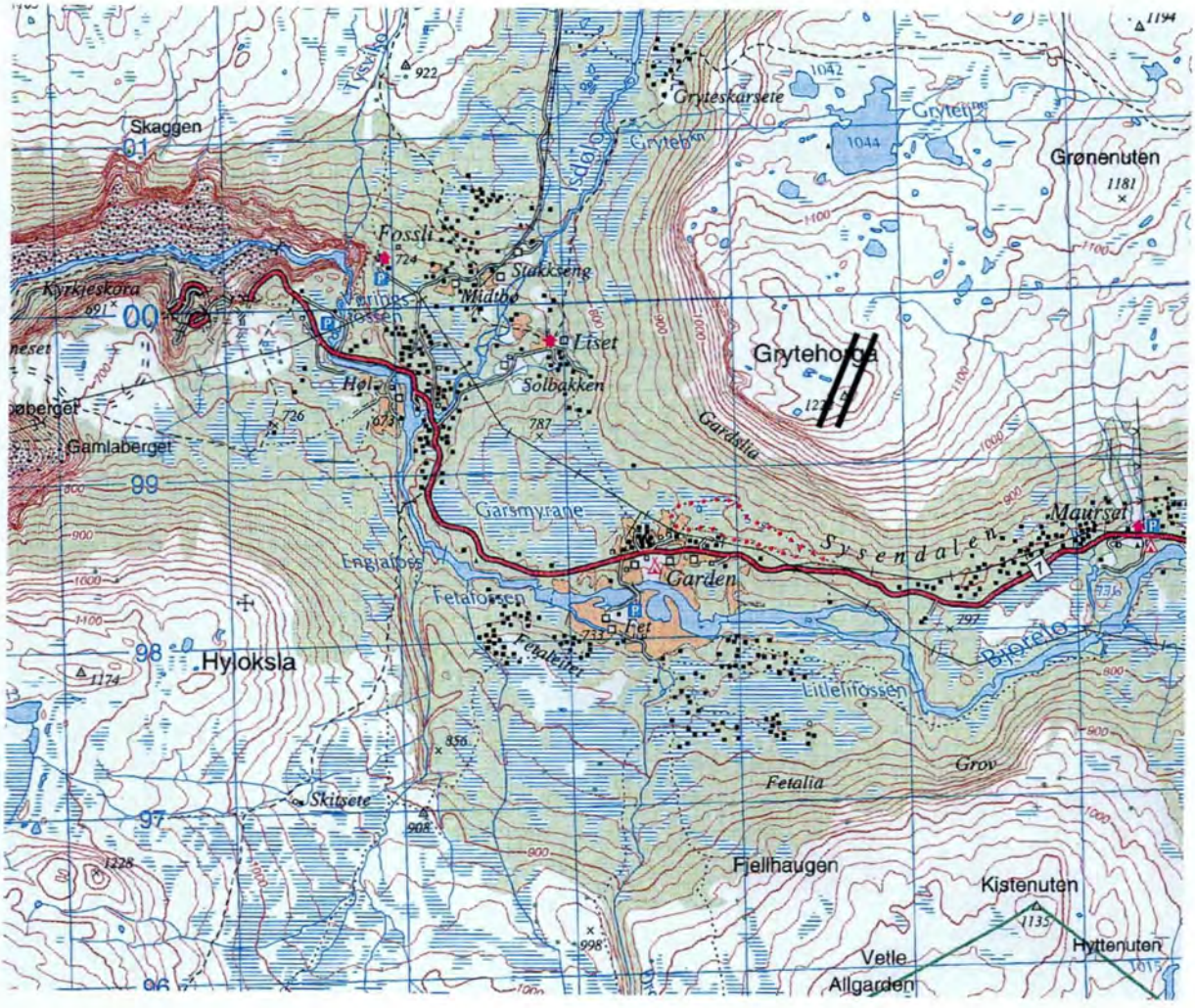

Fig. 2.1.6 Reusch (1901) interpreted two scarps on Grytehorgi to the east of Vøringsfossen to represent postglacial faults. The black lines show the location on 1:50.000 topographic map sheet 1415 IV Eidfjord.

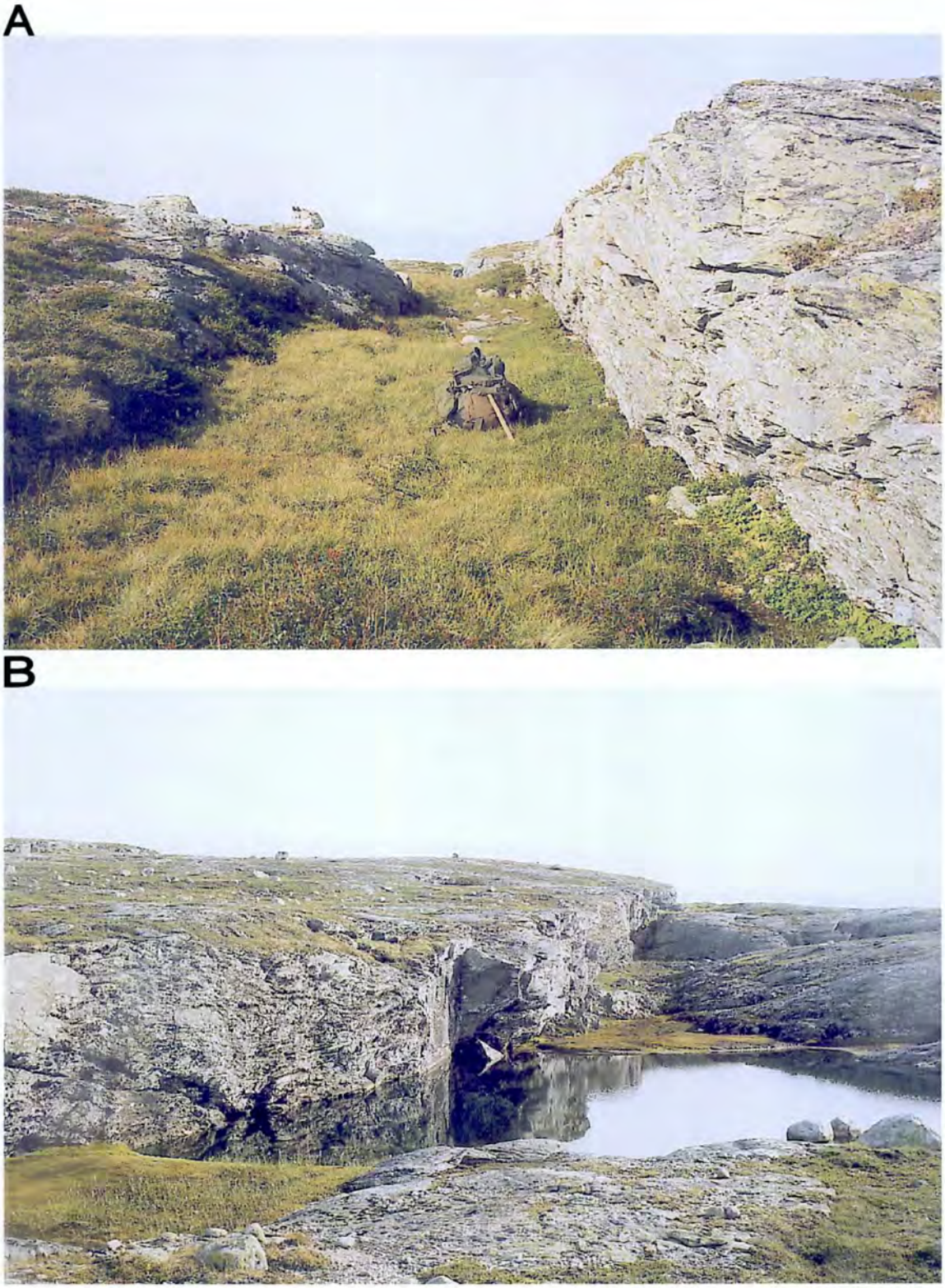

Fig. 2.1.7 Photographs of the westernmost scarp on Grytehorgi. A) View towards the north along the southernmost part. The central part of the fracture zone is most likely eroded. B) The Reusch (1901) locality (Fig. 2.1.8a) with a view towards the south along the northernmost section. The apparent fault scarp varies between 1 and 3 metres and the scarp seems to be sculptured by the ice.

A

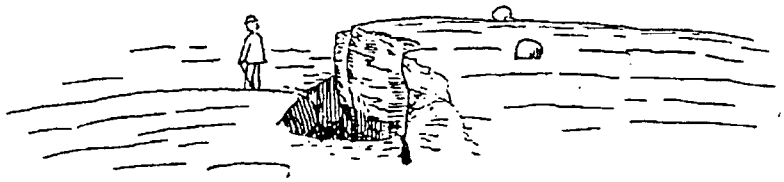

Spalte, langs hvilken der synes at gaa en postglacial forskydning. Grytefjeldets ryg.

B

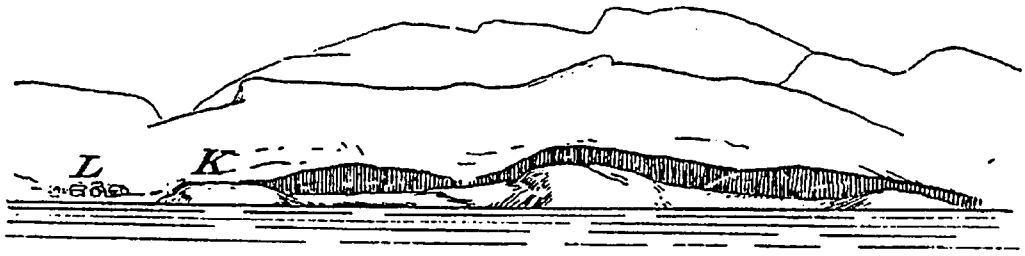

Fjeldvægge (skraferede) langs Lygrefjord.
L. Gaarden Lygre. *K.* Kløft parallelt med strandbredden.

Fig. 2.1.8 A) The interpretation of a postglacial fault on Grytehorgi by Reusch (1991). B) Postglacial fault interpretation from Lygre Hardangerfjord (Reusch 1888). We have attributed both of these scarps to a plucking effect by the Weichselian inland ice. The latter locality is described by Dehls and Braathen (1998).

2.1.6 Conclusions

We conclude that there is no evidence for postglacial faulting on any of the four studied localities. We have graded the Gnedden and Grytehorgi reports as a 'D - Probably not neotectonics' and the Rudihø and Byrknes localities with an 'E - Very unlikely to be neotectonics'. The most likely cause of the proposed neotectonic deformation on Rudihø is gravity-induced sliding, while the other three are classified as erosional phenomena. The Grytehorgi and Gnedden localities bear some resemblance to the localities Austerdalsisen and Handnesøya (Olesen and Dehls 1998) since the scarps are best developed on the crest of the mountain where the erosion from the moving inland ice was most pronounced. We have also found that a flat lying foliation (subparallel to the rock surface) is typical for three of the locations (Austerdalsisen, Handnesøya and Grytehorgi). Plucking and removal of blocks can be easily accommodated along these two surfaces: the flat lying foliation and the steeply dipping fractures zones. This process is shown in Fig. 2.1.9. A photograph (Fig. 2.1.19 in Olesen and Dehls 1998) illustrates this mechanism in the Austerdalsisen area where a boulder is left behind some 1-2 m from the scarp. The resulting escarpment may appear as a postglacial fault scarp at a first glance.

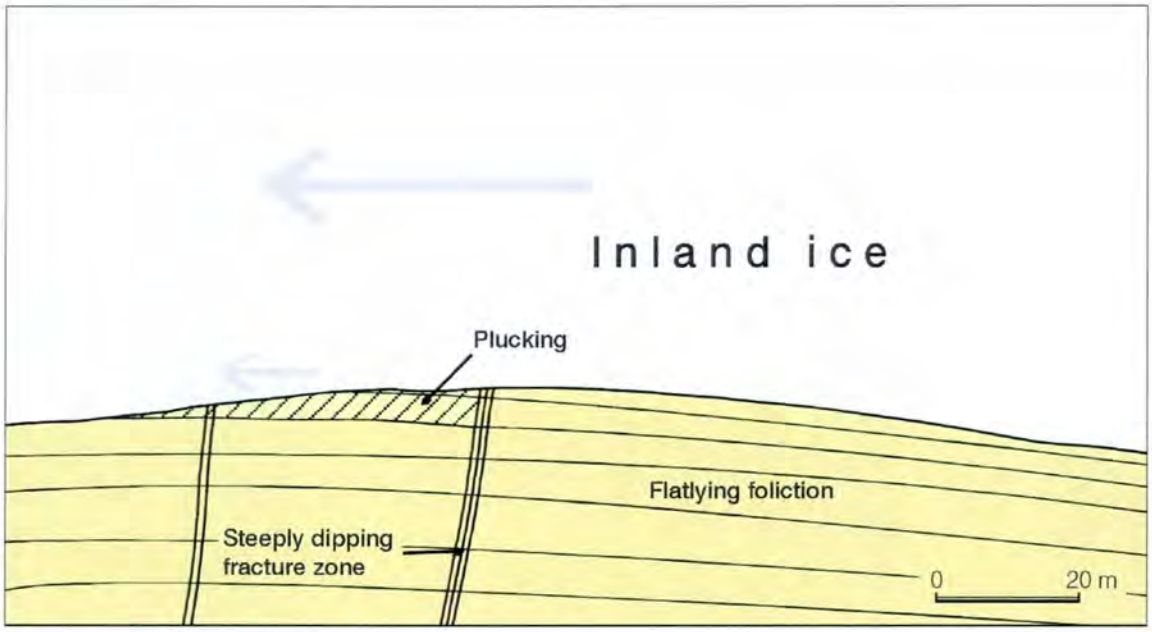

Fig. 2.1.9 Sketch illustrating the formation of erosional scarps at Austerdalsisen, Handnesøya, Gnedden and Grytehorgi. The inland ice has been plucking blocks from the bedrock along steeply dipping fracture zones. The blocks have loosened along the subhorizontal foliation. These scarps have earlier been misinterpreted as postglacial faults.

We also visited the Geitura locality in Ulvik, Hardanger on the field trip to Gryehorgi. There, Simonsen (1963) reported a rock avalanche in a gently dipping slope. He concluded that an earthquake must have triggered the avalanche. We agree in this conclusion, since the angle of the slope is only 20°. Blikra *et al.* describe this locality in the present report. Appendix A and B in the NEONOR Final Report (Olesen *et al.* 2000) summarise the classification of the neotectonic claims in Norway.

2.1.7 References

Dehls, J. and Braathen, A. 1998: Neotectonic phenomena in southern Norway. *In:* Dehls, J. and Olesen, O. 1998 (eds.) *Neotectonics in Norway, Annual Technical Report 1997,* NGU Report 98.016, 31-39.

Englund, J.O. 1986: Berggrunnskart Vinstra 1718 II – M. 1:50.000. Nor. geol. unders.

Jorde, K. 1978: Berggrunnskart Eidfjord 1415 IV – M. 1:50.000. Preliminær utgave. Nor. geol. unders.

Løset, F. 1981: Neotectonic movements in Norway. Literature review of neotectonic movements in Norway, and results from field investigations on Hardangervidda. Norwegian Geotechnical Institute (NGI) Internal Report 40009-7.

Michelsen, J. K., Lund, T., and Hansen, H. J. 1986: *The geology of the Devonian Fensfjord Basin.* University of Bergen, Unpublished Manuscript, 41 pp.

Olesen, O., Dehls, J., Bungum, H., Riis, F., Hicks, E., Lindholm, C., Blikra, L.H., Fjeldskaar, W., Olsen, O., Longva, O., Faleide, J.I., Bockmann, L., Rise, L., Roberts, D., Braathen, A. and Brekke, H. 2000: NEONOR Final Report. NGU Report 2000.002.

Olesen, O. and Dehls, J. 1998: Neotectonic phenomena in northern Norway. *In:* Dehls, J. and Olesen, O. 1998 (eds.) *Neotectonics in Norway, Annual Technical Report 1997,* NGU Report 98.016, 3-30.

Reusch, H. 1888: Bømmeløen og Karmøen med omgivelser. Nor. geol. unders., Oslo, 423 pp.

Reusch, H. 1901: Nogle bidrag til forstaaelsen af hvorledes Norges dale og fjelde er blevne til. *Nor. geol. unders. Bulletin, 32*, 125-217.

Simonsen, A. 1963: Kvartærgeologiske undersøkelser i Indre Hardanger, Ulvik hd. Hordaland. Unpubl. M.Sc. Thesis, University of Bergen. 67 pp.

Werenskiold, W. 1931: Ett sprekkesystem i Gudbrandsdalen. *Norsk Geologisk Tidsskrift 12*, 575-576.

3 OFFSHORE FAULTING (TASK 2)

3.1 Multi-beam echo-sounding (swath) surveys in the North Sea

By Odleiv Olesen, John Dehls (NGU) and Fridtjof Riis (NPD)

3.1.1 Introduction

Two areas in the northern North Sea were selected for multi-beam echo-sounding surveying (Fig. 3.1.1). The northernmost area is located to the east of the Troll area and is 2.5 km x 5 km. Riis (1998) interpreted a potential postglacial fault from high-resolution 2D seismic data in the area. The other area to the south of the Kvitebjørn petroleum-field, at the foot of the western slope of the Norwegian Trench, was surveyed to study the postglacial faulting associated with gas leakage as proposed by Hovland (1983) (Fig. 3.1.2). The surveyed area is 2.5 km by 6 km.

The Norwegian Hydrographic Survey (part of the Norwegian Mapping Authority) was contracted to carry out the surveys. The data were collected during good weather conditions during June 1999 using a multi-beam echo-sounder (Simrad EM-1002) from the vessel M/S Sjømålaren. The data were processed by the Norwegian Hydrographic Survey. The bathymetric data were of high quality, and the digital model was based on a 2 m x 2 m grid produced by a minimum curvature gridding method. ER-Mapper software was used to produce artificial shaded relief image maps (Figs. 3.1.3, .4 and .5).

3.1.2 Kvitebjørn South survey

The data set supports the interpretation by Hovland (1983) that faults offset the sea floor and Quaternary sediments to the west of Bergen. Two of the N-S trending faults continue through most of the survey area and are longer than 3.5 km. The offsets of the faults are 1-2 metres. The faults are similar to the N-S trending postglacial faults to the north of the Storegga landslide scar (Evans *et al.* 1996). The considerable length of the faults indicates a significant depth extent. On the other hand, the faults do not coincide with deeper Mesozoic faults. Similar faults have also been interpreted within the NEONOR project from 3D seismic data in the northern North Sea (Riis *et at.* 2000). The faulting may be connected to venting of gas or fluids in these areas. The faults seem to be related to the formation of the numerous pockmarks in the area. The elongated depressions associated with the pockmarks are probably caused by a combination of shallow gas seepage, the geometry of subsurface bedding and the action of bottom currents (Hovland 1983).

An azimuth map of the sea floor generated from 3D seismic data in the Kvitebjørn area, slightly to the north of the bathymetry survey, indicates a similar set of structures (Fig. 2.11 in Riis *et al.* 2000). In this area, there are spots of high gas saturation at shallow depth. The shape and orientation of the faults suggest that they were neither formed by gravity sliding, or by glacial deformation. This supports Hovland's explanation that they are connected to gas release.

3.1.3 Troll East survey

The bathymetry indicates that pockmarks with an average diameter of 40 m and an average depth of 5 m are more or less randomly distributed in the surveyed area east of Troll (Fig. 3.1.5). There is no obvious correlation to the deep-seated faults, which trend in a NNW-SSE

direction in the area. Similar relations have been interpreted from the 3D seismic surveys in the main Troll area (NEONOR final report; Riis *et al.* 2000). It appears to be a coincidence that a pockmark was situated straight above the deep fault in the seismic line studied in the 1998 report. The structure, which was interpreted as a recent fault, can now be better explained as a seismic "pullup" which is not related to the Mesozoic fault.

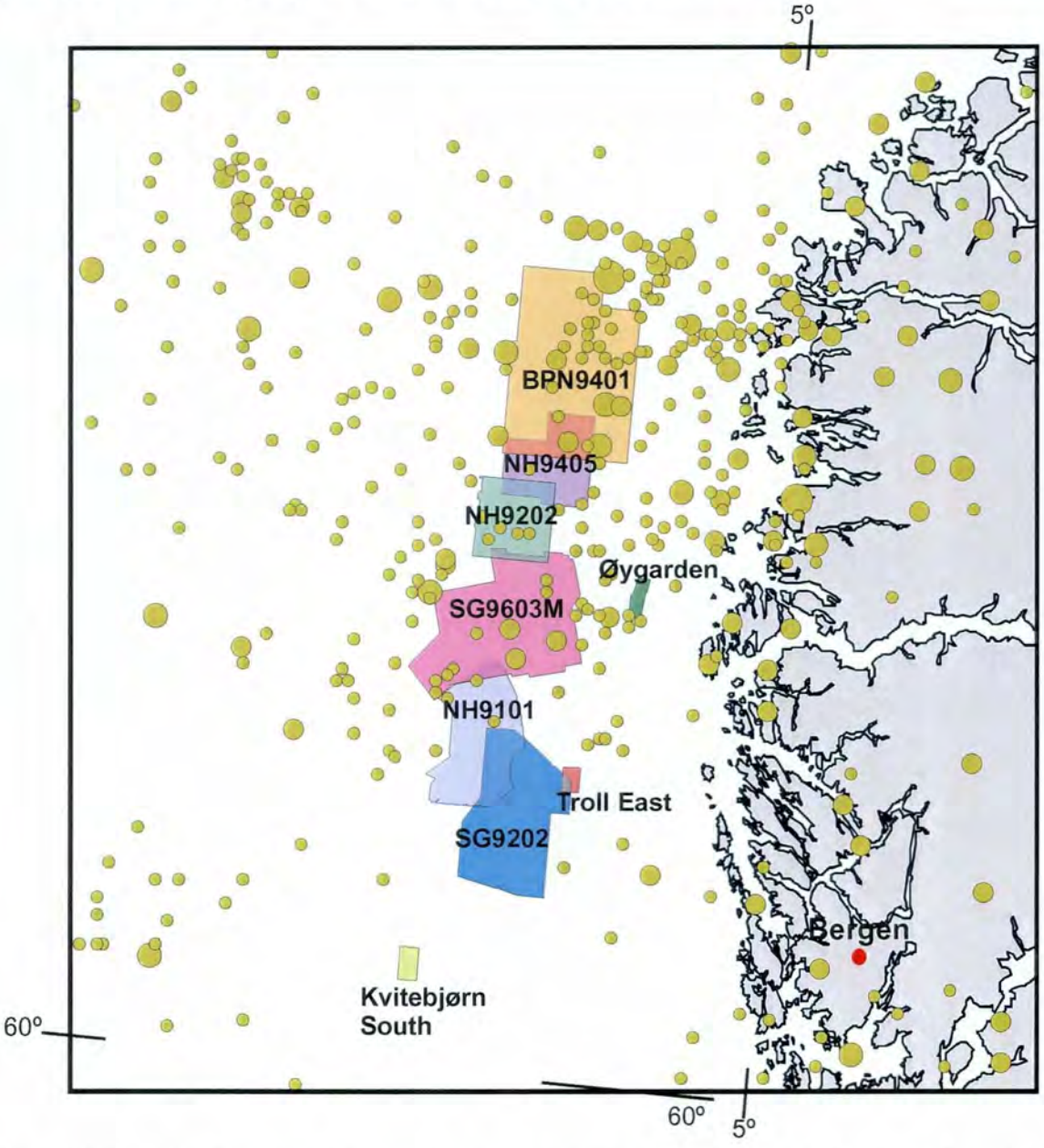

Fig. 3.1.1 Map showing location of the two survey areas to the east of Troll and south of Kvitebjørn. The interpreted 3D surveys are also shown.

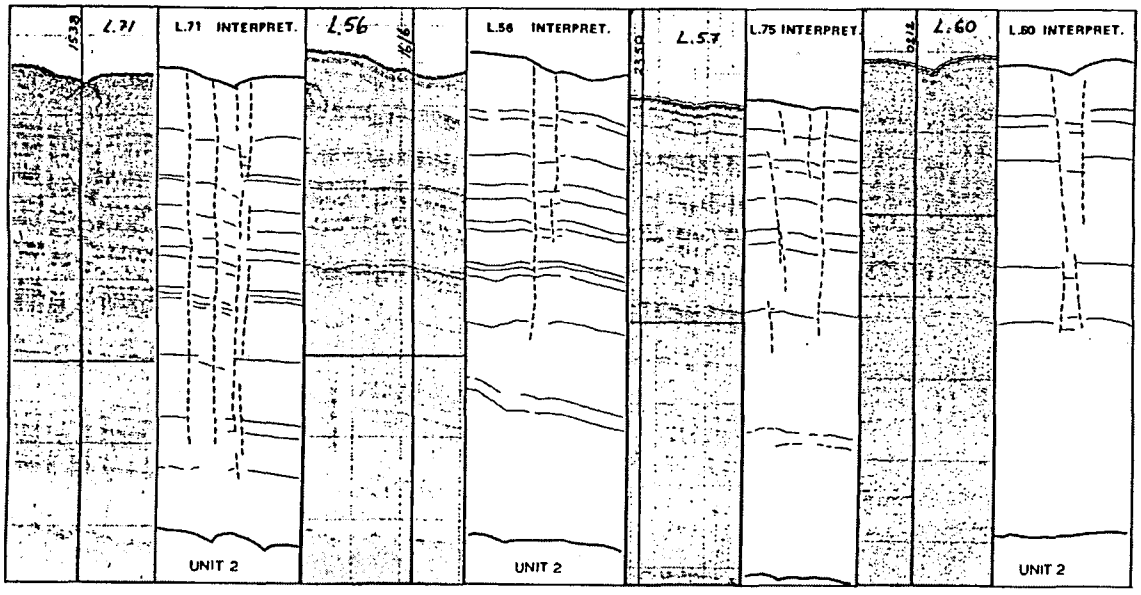

Fig. 3.1.2 Postglacial faulting of a soft, silty clay at the foot of the western slope of the Norwegian Channel to the south of Kvitebjørn (Hovland 1983). A total of nine parallel boomer profiles have been acquired along a 2 km wide corridor as part of the Statpipe route survey. The net slip of the vertical fault is in the order 1-2 m (Hovland 1983). The fault is trending N-S (parallel to the slope of the Norwegian Trench) and is evident on nearly all boomer profiles run in the corridor.

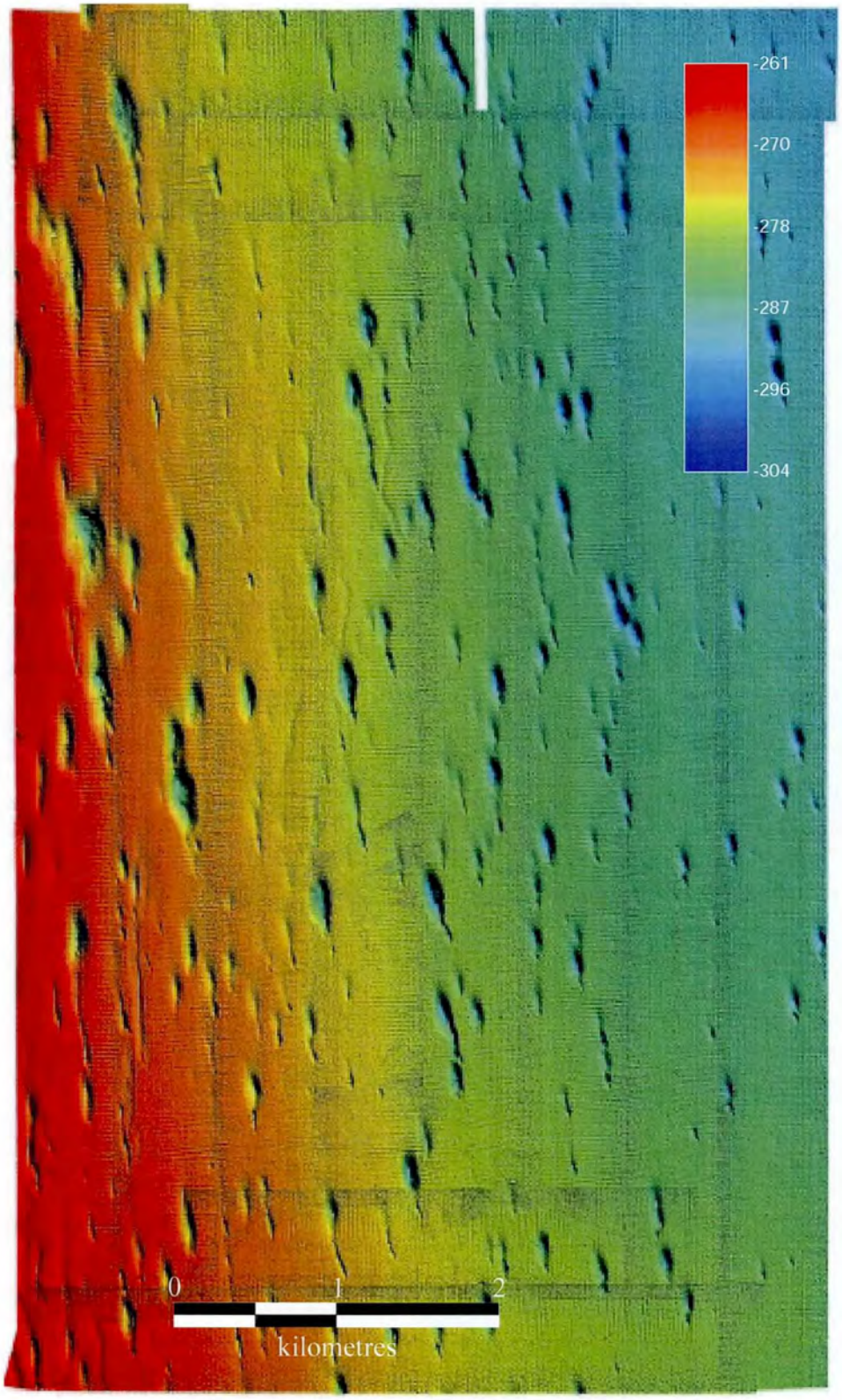

Fig. 3.1.3 Sea floor relief image map from the south of Kvitebjørn area.

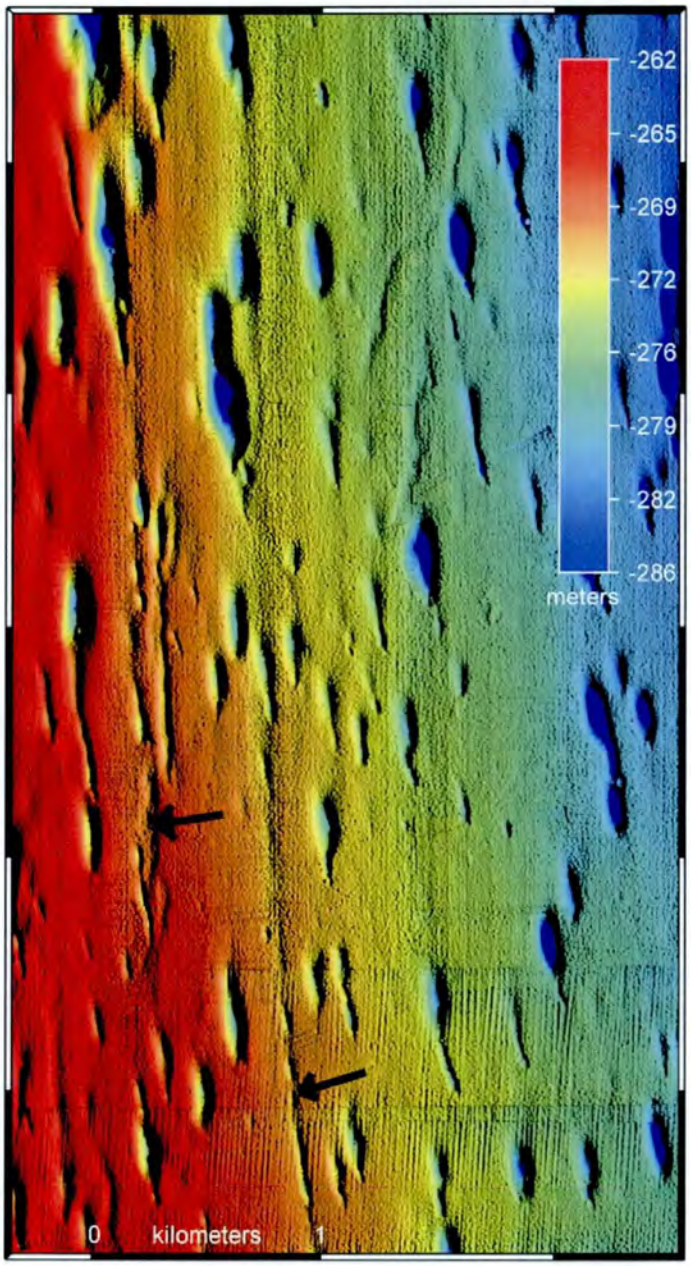

Fig. 3.1.4 Close up of the southwestern part of the bathymetric map from south of Kvitebjørn area. The arrows indicate the postglacial faulting associated with the pock-mark formation.

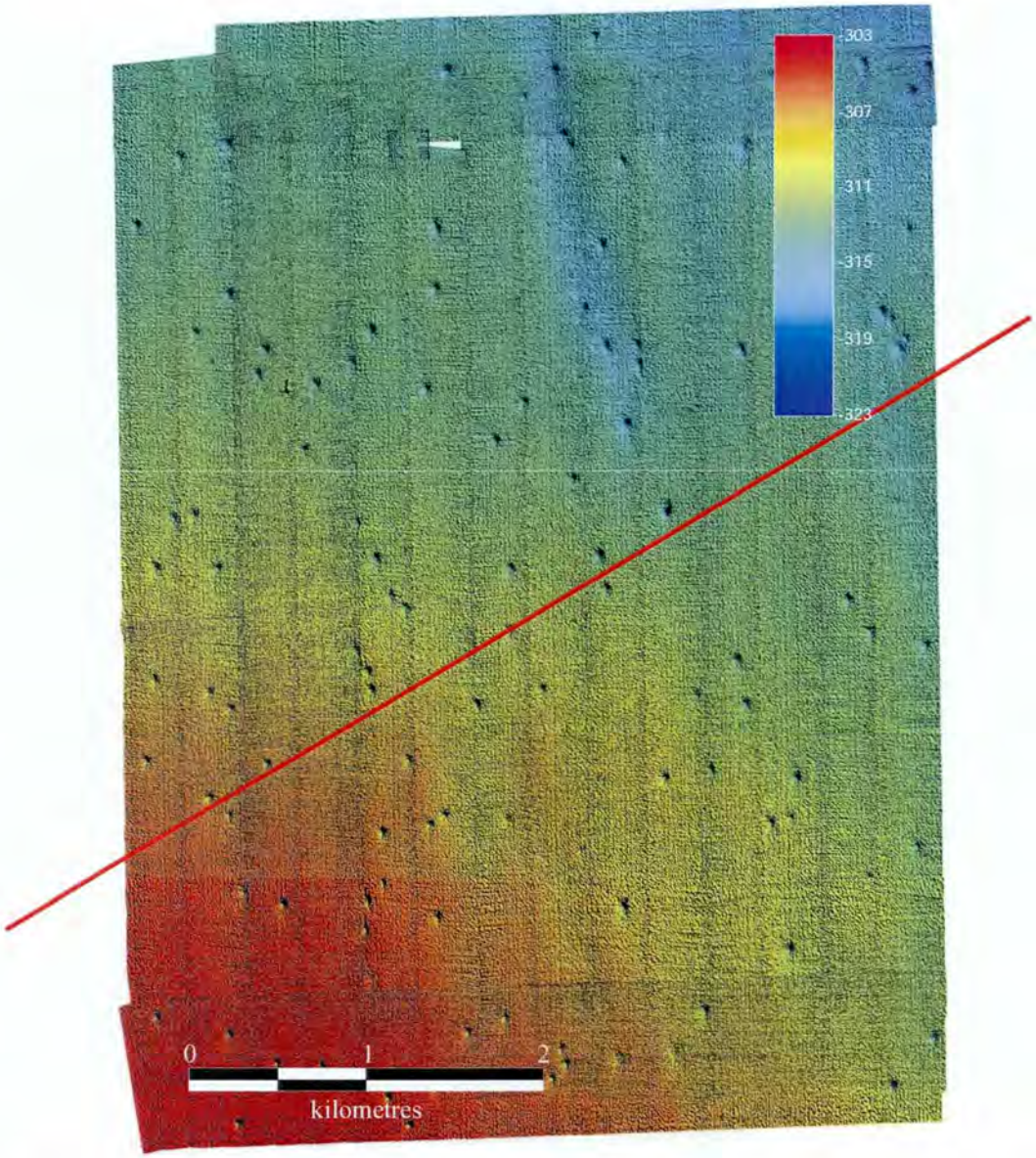

Fig. 3.1.5 Sea floor relief image map from the east of Troll area. Part of Seismic line KYST-115 is shown.

3.1.4 References

Evans, D., King, E.L., Kenyon, N.H., Brett, C. and Wallis, D. 1996: Evidence for long-term instability in the Storegga Slide region of western Norway. *Marine Geology* 130, 281-292.

Hovland, M. 1983: Elongated depressions associated with pockmarks in the western slope of the Norwegian Trench. *Marine Geology 50*, M11-M20.

Riis, F. 1998: Seismic investigations in the North Sea. *In:* J. F. Dehls and O. Olesen (Eds.), *Neotectonics in Norway, Annual Technical Report 1997.* NGU Report 98.016, 59-70.

Riis, F., Faleide, J.I. and Olesen, O. 2000: Offshore neotectonics. *In*: Olesen, O. (Ed.) . NGU Report 2000.002, 54-79.

4 GEOLOGY AND GEOPHYSICS (TASKS 4 AND 9)

4.1 LARGE-SCALE SLOPE FAILURES IN MØRE AND ROMSDAL – PALAEOSEISMIC EVIDENCE?

By Einar Anda (The County Council of Møre and Romsdal), Lars Harald Blikra (NGU) and Oddvar Longva (NGU)

4.1.1 Introduction

A project aimed at evaluating the risk of large rock avalanches has been going on in Møre and Romsdal county since 1996. Potential triggering by large earthquakes needs to be addressed, and the newly reported "Seismic Zonation of Norway", claims that one should be aware of future earthquakes of relatively large magnitudes, compared to the historic events (NORSAR and NGI 1998). The largest future earthquakes in Norway are expected in a region around Stadt, including the western part of Møre and Romsdal.

The present section shortly presents and discusses four localities that might be considered to be an effect of palaeoseismic activity. Furthermore, the distribution map of large rock avalanches in the region shows a zonation which might be controlled by seismic activity (Blikra and Anda 1997; Blikra 1998, Blikra *et al.* 1999).

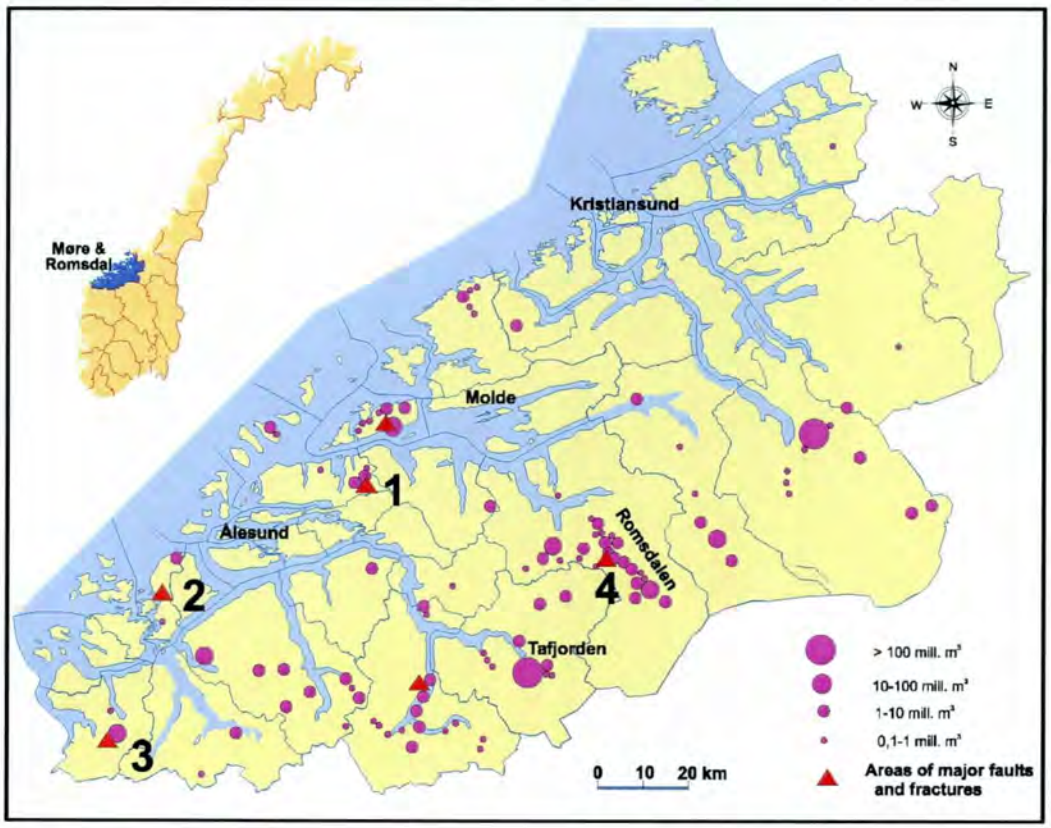

Fig. 4.1.1 Location map of rock avalanches in the Møre and Romsdal county (blue filled circles are individual rock avalanches with estimated volumes). Red triangles show areas with major rock deformations, numbers refers to localities described in the text. Modified from Blikra et al. (1999).

4.1.2 Gravitational faults and fractures in bedrock

Within the NEONOR project, claims of neotectonic activity have been classified into five grades:

(A) Almost certainly neotectonics,

(B) Probably neotectonics,

(C) Possibly neotectonics,

(D) Probably not neotectonics

(E) Very unlikely to be neotectonics.

Otrefjellet in Haram (grade B)

The site is located midway between the cities Molde and Ålesund (Fig. 4.1.1). A two kilometre long, N-S trending mountain ridge, 100-300 m high above the surrounding terrain, is heavily fractured. Locally there are crushed or collapsed bedrock within a 500 m wide zone (Fig. 4.1.2). Vertical or subvertical fractures occur in two directions, parallel (E-W) and subperpendicular (SSW-NNE) to the foliation of the gneiss. Large rock avalanches have been triggered at both sides of the northern and steepest part of the mountain ridge. Earthquakes might have triggered many of the large rock avalanches in Møre and Romsdal, but we can not normally exclude the possibility that they are formed by gravitation alone. The slopes of the southern part of the mountain Otrefjellet are too gentle to create slope failures based only on gravitational forces. Earthquake triggering is also a plausible explanation for the collapsed bedrock zone. An alternative explanation would be frost shattering, with production of extensive boulder fields by *in situ* bedrock weathering, within nunatak phases during ice ages. But the mountain surface is situated 200-300 m below a distinct regional "weathering zone" interpreted to be formed by such processes (Larsen *et al.* 1988) and this fact more or less excludes the hypothesis.

We do not know the age of the proposed palaeoseismic event, except that the failures are generated after the deglaciation, some 12 000 ^{14}C years BP (Larsen *et al.* 1988). Possible neotectonic lineaments (grade C) occur outside the central part of the area, towards both the east and the west. A possible large earthquake that created these deformations may also have triggered a rock slide on a mountain slope of Otrøya, 14 km toward NE (Robinson *et al.* 1997), and also three nearby rock avalanches on the same island (Blikra and Anda 1997), see also Fig. 4.1.1.

Fig. 4.1.2 Heavily fractured and crushed or collapsed bedrock on Otrefjellet in Haram (see locality 1 in Fig. 4.1.1). View towards the south.

Ringstadhornet-Haddalsura in Ulstein (grade C)

This site is located 25 km SW of Ålesund, on the island Hareidlandet. A 300-500 m high and 2 km long mountain ridge, trending SW-NE, is heavily deformed in a reach of 500-1000 m. The deformed bedrock surface on top of the mountain ridge (300-600 m a.s.l.) is only studied from vertical aerial photos. Lineaments have two main trends; SW-NE (along the foliation) and perpendicular to this (SE-NW). A rock avalanche has developed from the western part (Haddalsura), from a level of 300 m a.s.l and down into the sea. The rock avalanche is dated to Younger Dryas or older due to the occurrence of a distinct zone of frost-weathered debris (Blikra and Longva 1995). It is not unlikely that a single, major earthquake has both generated the deformation structures on top of the mountain and triggered the rock avalanche that evolved on the relatively gentle slope (about 30°).

Storhornet in Vanylven (grade C)

This site is located in the south-western part of Møre og Romsdal, 15 km east of Stadtlandet. A N-S orientated, 600-700 m high mountainside is heavily fractured along a length of 2 km and in a 500 m wide zone on the mountain plateau above the valley. One or more large rock avalanches have been triggered from this mountainside, extending down into the valley Sørdalen, covering the entire valley floor in a distance of 2 km. The mountain is only studied from vertical, aerial photos, but the deformation structures are very distinct. They occur both within exposed and till-covered parts of the bedrock surface. The glacial till show several sink-in features. Fractures and other lineaments are trending along the foliation (SSW-NNE), and they occur as tensional features. A major earthquake might be the cause of these features, but we can not exclude gravitational forces as the single process.

Børa in Romsdalen (grade C)

The site is located in the central part of Romsdalen, 45 km SE of Molde. An extraordinary rock deformation occurs within a three kilometre long zone of the 1000-1200 m high valley side of Romsdalen, at the mountains of Børa and Mannen. Fractures and lineaments occur

within a 200-300 wide zone, into the plateau, mainly within a till-covered bedrock surface, with typically sink-in features. Open fractures in directions E-W, NW-SE and N-S (Berg *et al.*, in press). These are mainly tensional and probably toppling features. This mountainside has generated several rock avalanches during the last 5000 years. We find a palaeoseismic event likely as an explanation, but we can not exclude gravitational forces as the only mechanism.

Fig. 4.1.3 A deep crevasse on the mountain plateau Børa in Romsdalen (locality 4 on Fig. 4.1.1). See person for scale.

4.1.3 Concentrations of rock avalanches

The distribution map shows at least two regions with distinct concentrations of large rock-avalanche events, in the Romsdalen and Tafjorden area (Fig. 4.1.1). We have no clear evidence of any palaeoseismic triggering mechanism, but we cannot exclude that large earthquakes might be the cause. The Romsdalen area might be correlated with remnants of a 500 m high regional escarpment of the land surface (Anda 1995). Five kilometres south of Åndalsnes, at the northern part of Trolltindan, the highest summits rises from 1200-1300 to 1700-1800 m a.s.l. from the northern to the southern side of this lineament. The escarpment is interpreted as a possible fault zone connected to the Cenozoic uplift of Norway (Anda 1995). The escarpment starts gradually 10-20 km west of Romsdalen and can be followed 50 km further to the east, to Sunndalsøra. The old, main water divide between western and eastern Norway (Ahlmann 1919), was situated close to this escarpment. Crustal deformations during the uplift may have created fractures into the raised block on the southern side of the escarpment. This can explain the large-scale backward erosion of the valleys Romsdalen and Eikesdalen, with a gradual change of the water divide toward the south (Anda 1995).

4.1.4 Debris flow events in Voldafjorden

A well-dated core from Voldafjorden shows three distinct turbidite layers within the Holocene unit (Grøsfjeld *et al.* 1999). The two uppermost turbidites are dated to approximately 7000 BP and 2000 BP, with the 7000 BP layer correlating in age to tsunami-sediments from the Storegga slide which has been described from lower-lying lakes in the region (Bondevik *et al.* 1997). No evidence has been found, however, for more than one huge tsunami in these lakes.

A detailed seismic survey of the fjord in 1999 revealed at least two seismic horizons that are related to regional slump-events with collapses of sediments along the fjord margin all around

the basin (Fig. 4.1.4). The failures developed debris flows, which seems to have transformed into turbidites and cover the entire sea floor in the deepest part of the fjord. A correlation between the turbidites in the core with the debris flow deposits seen from the seismic data seems quite clear, but so far there is a misfit in stratigraphic positions. This may be explained by compaction of the core during sampling.

The 7000 BP turbidite in Voldafjorden was tentatively interpreted to have been formed by a tsunami (Flatebø 1998). However, since the geologic setting, as interpreted from the seismic data, seems to have been the same for both the two upper turbidites and only one tsunami layer is found in lakes, an alternative explanation would be that the regional failure-events were caused by strong earthquakes. If this is the case, similar horizons should be found in other fjords and a challenge would be to relate such horizons to rock avalanches found in the successions of fjord sediments.

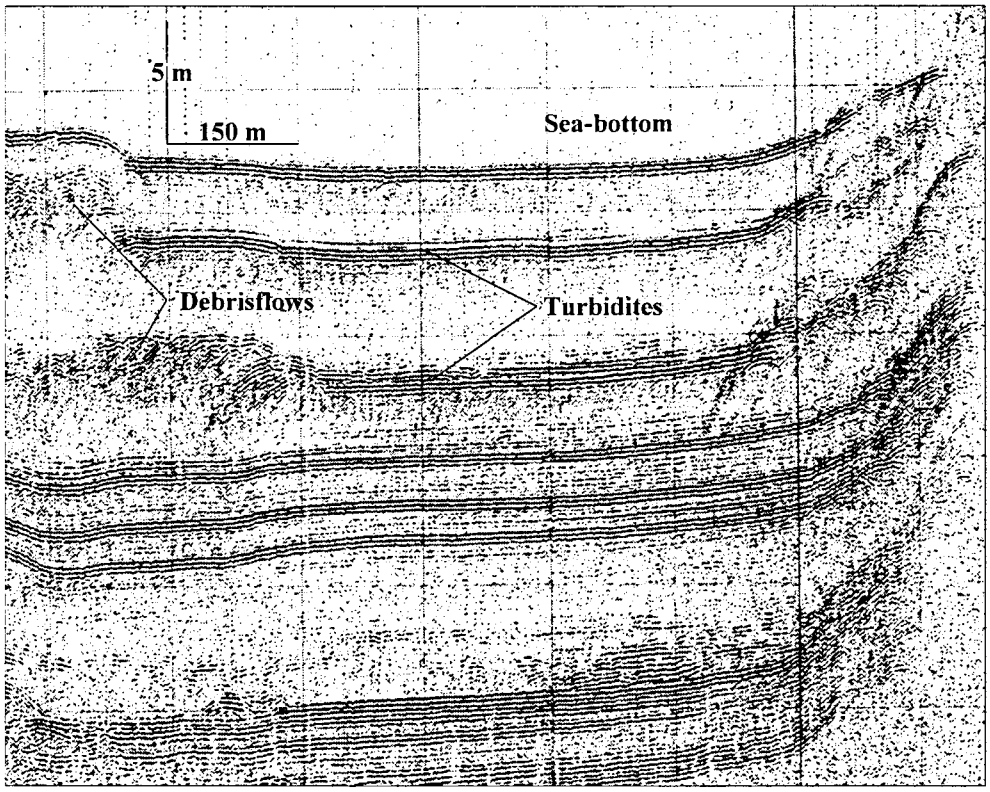

Fig. 4.1.4 High resolution seismic cross profile in the outer part of Voldafjorden.

4.1.5 Conclusions and further work

So far the locality on Otrefjellet in Haram is considered to be classified as grade B (probably neotectonics), while the other localities presented are classified as grade C (possibly neotectonics). The concentrations of rock-avalanche events is so far also classified as grade C (possibly neotectonics), but a better age control is needed on individual events.

Further studies need to be carried on in order to evaluate possible palaeoseismic causes of some of the slope failures in the region. Some of the localities need to be studied in more detail, and more focus should also be paid on studies in the fjords. The potential of dating rock-avalanche events and other sediment failures in fjords are much higher than on land. The regional view of instability features with data of their spatial occurrence and dating of individual

events is essential for palaeoseismic analysis (Jibson 1994). The effect of future large earthquakes should be modelled.

4.1.6 References

Ahlmann, H. W. 1919: Geomorphological studies in Norway. *Geografiska Annaler*, Stockholm I, 193-252.

Anda, E. 1995: Romsdalen og Romsdalsfjorden. Hovedtrekkene i landskapet. In Sanden, J. (Ed.) Romsdalen, natur og kultur. Romsdalsmuseet, årbok 1995, 14-34.

Berg, S. S., Braathen, A., Blikra, L. H. and Anda, E. in press: Structural analyses of a source area for large rock avalanches, Børa in Romsdalen, Møre og Romsdal. Abstract Nordic geological winter meeting.

Blikra, L.H. 1998: Rock avalanches, gravitational faulting and its potential palaeoseismic cause. In Dehls, J. and Olesen, O. (Eds.) Neotectonics in Norway, Annual Technical Report 1998. *NGU Report* 99.007, 88-92.

Blikra, L. H. and Anda, E. 1997: Large rock avalanches in Møre og Romsdal, western Norway (Extended abstract). *Nor. geol. unders, Bull.* 433, 44-45.

Blikra, L. and Longva, O. 1995: Frost-shattered debris facies of Younger Dryas age in the coastal sedimentary successions in western Norway. Palaeogeography, Palaeoclimatology, *Palaeoecology* 118, 89-110.

Bondevik, S., Svendsen, J. I., Johnson, G., Mangerud, J. and Kaland, P. E. 1997: The Storegga tsunami along the Norwegian coast, its age and runup. *Boreas* 26, 29 – 53.

Flatebø, T. 1998: Miljøvariasjoner i Voldafjorden de siste 11 ka BP belyst ved bentiske foraminiferer og stabile isotoper. Cand . scient. Thesis, University of Bergen. 102 pp.

Grøsfjeld, K., Larsen, E., Sejrup, H. P., de Vernal, A., Flatebø, T., Vestbø, M., Haflidason, H. and Aarseth, I. 1999: Dinoflagellate cysts reflecting surface-water conditions in Voldafjorden, western Norway during the last 11300 years. *Boreas* 28, 403-415.

Jibson, R.W. 1994: Using landslides for Paleoseismic analysis. In McCalpin (ed.) Paleoseismology. International geophysics series 62, 397-438. Academic press.

Larsen, E., Klakegg, O. and Longva, O. 1988: Brattvåg and Ona. Quaternary geological maps 1220 II and 1220 IV - scale 1:50,000 with description. *Nor. geol. unders, Skrifter* 85, 1-41.

NORSAR and NGI 1998: Development of Seismic Zonation for Norway: Final Report. Report for Norwegian Council for Building Standardization (NBR), 162 pp.

Robinson, P., Tveten, E. and Blikra, L. H. 1997: A Post-glacial bedrock failure at Oppstadhornet, Oterøya, Møre og Romsdal: a potential major rock avalanche (Extended abstract). *Nor. geol. unders, Bull.* 433, 46-47.

4.2 GRAVITATIONAL-SLOPE FEATURES FROM ODDA IN HARDANGER TO AURLAND IN SOGN, WESTERN NORWAY.

By Lars Harald Blikra, John Dehls and Odleiv Olesen (NGU)

4.2.1 Introduction

Several gravitational-slope failures have been observed earlier in the Hardangerfjorden area, e.g. a gravitational fracture zone at Geitura east of Granvin (Simonsen 1994) and features possible related to neotectonic activity in Hardangerfjorden (Hoel 1992, Helle *et al.* 2000). A reconnaissance study based on air-photo interpretations has been done along a 20 km wide zone from Odda in Hardanger to Aurland in Sogn. This shows a series of gravitational-slope features lining up between Odda and Aurland (Fig. 4.2.1)

Many gravitational faults and fractures developed in bedrock are found on the western side of Sørfjorden, but occur also northeast of Granvin, northeast of Ulvik and in Flåmsdalen-Aurland area. Large rock avalanches are often formed in connection with these fracture zones (see Fig. 4.2.1). The failure zone in Flåmsdalen-Aurland are characterised by a series of faults and crevasses on the plateau on the eastern side of valley, cut by distinct slide scars with rock-avalanche deposits below (Fig. 4.2.2).

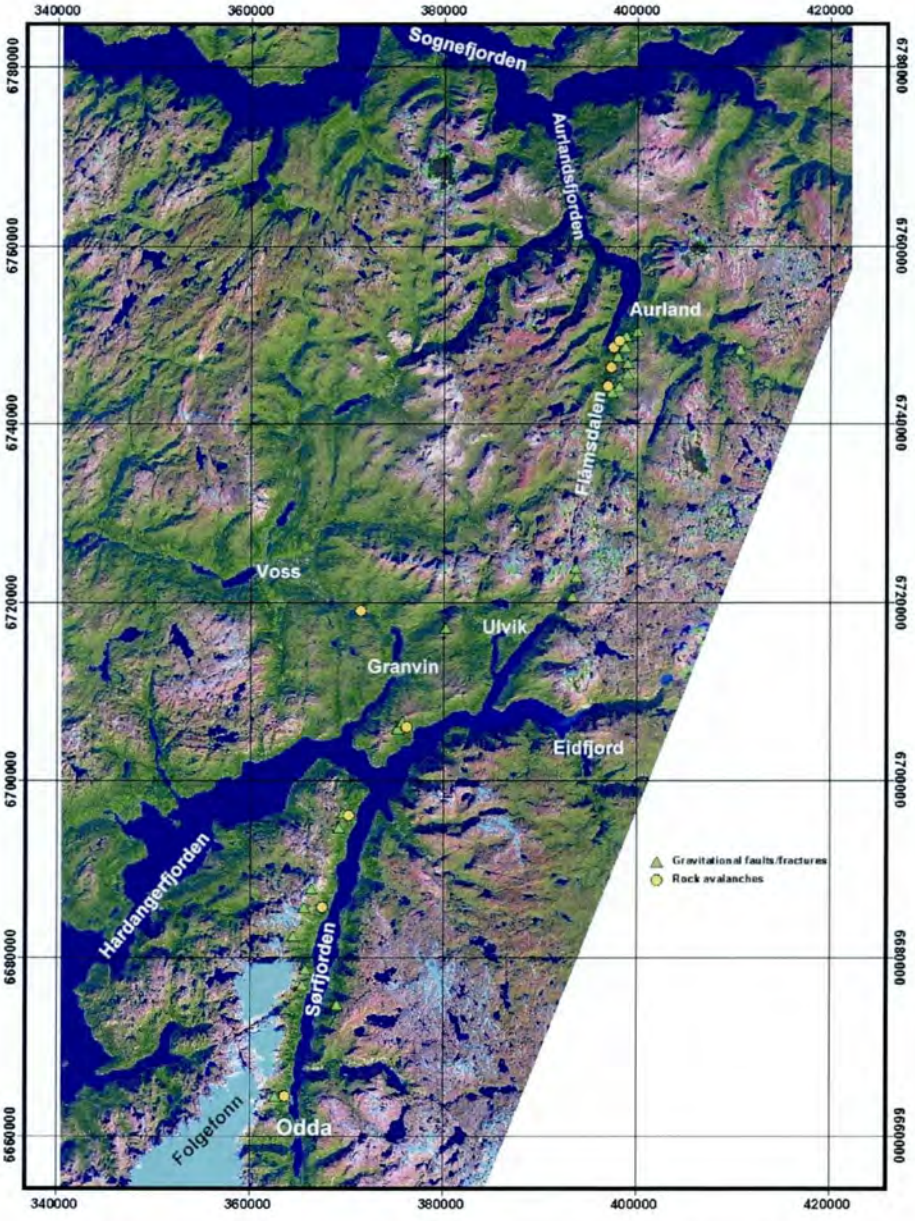

Fig. 4.2.1 A satellite image showing locations of gravitational-slope features in an area from Odda in Hardanger to Aurland in Sogn. The aerophoto interpretation was done in a 20 km wide area from Odda to Aurland. The line spacing is 20 km.

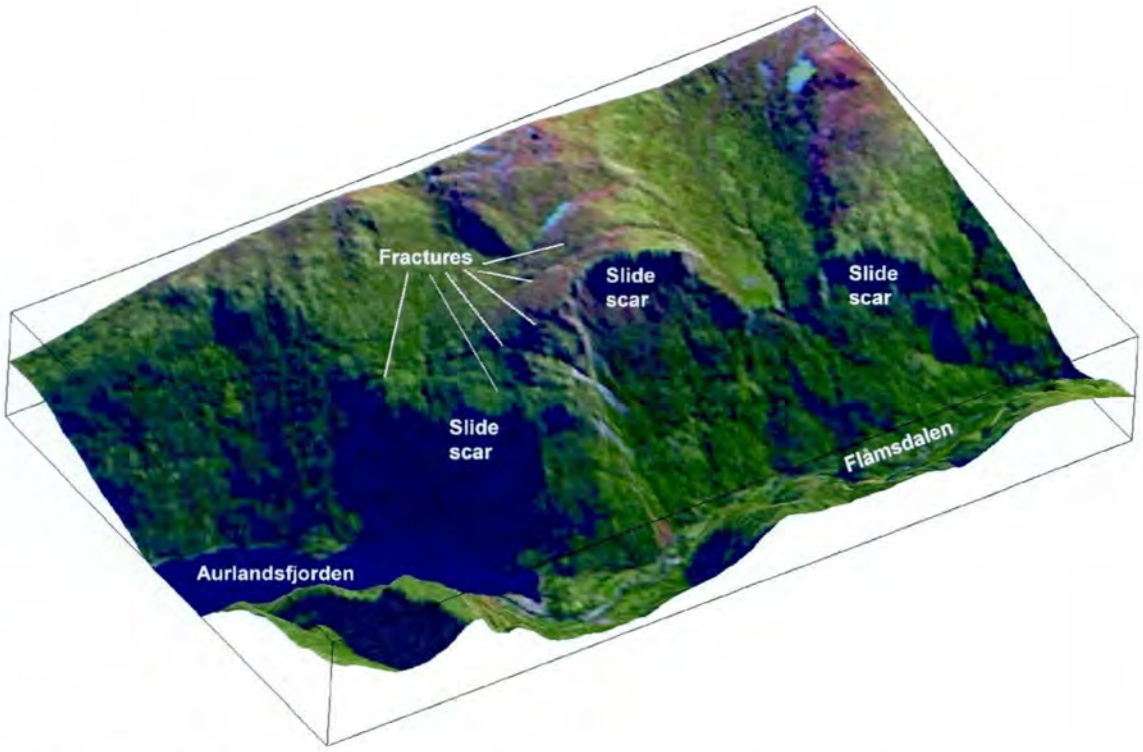

Fig. 4.2.2 A 3D model of satellite and topographic data showing the gravitational-slope features in Flåmsdalen, south of Aurland. View towards southeast.

The gravitational faults and fractures on Geitura, northeast of Granvin (see location on Fig. 4.2.1), are characterised by distinct faults and crevasses in the uppermost part, but are more fractured in lower part (Fig. 4.2.3). Some of the faults and fractures are situated on relatively gentle slopes. The local bedrock consists of mica schist of the Upper Bergsdals Nappe. The orientation of the foliation is 142°/18°. A 400 m wide and 300 m long rock avalanche occurs towards the valley (i.e. in a NW direction). Some of the boulders in the avalanche have dimensions of several metres. The terrain is gently dipping with a slope of approximately 20°. There is a sharp boundary between collapsed and undisturbed bedrock. An up to 20-m high scarp occurs at the slide scar. The fractures and faults on the plateau are curved in a NE-SW direction behind the scarp. Due to the fairly gentle terrain slope, Simonsen (1963) concluded that the fractures and related rock avalanche were most likely triggered by earthquakes.

It is likely that many of the gravitational-slope features observed in the area from Odda in Hardanger to Aurland in Sogn were triggered by large earthquakes. More detailed field studies including dating of individual events are needed in order of trying to verify this hypothesis.

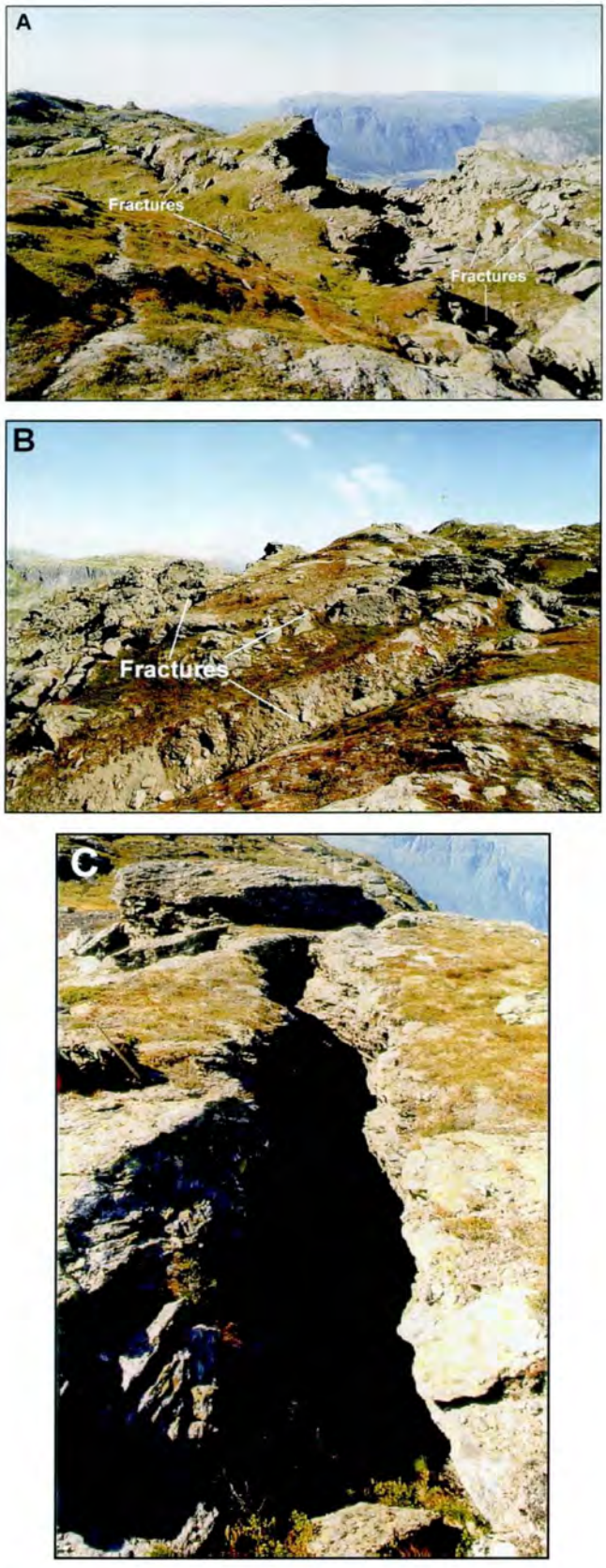

Fig. 4.2.3 Gravitational faults and fractures on Geitura, northeast of Granvin.

4.2.2 References

Helle, S.K., Rye, R. and Stabell, B. 2000: Shoreline displacement and fault activity in the Hardangerfjord, western Norway, after the deglaciation. Abstract 24th Nordic Geological Winter-Meeting, 6-9 January, Geonytt 1-2000, p. 82.

Hoel, C. 1992: Sesimisk stratigrafi av sedimentene i Hardangerfjorden og sidefjorder. Unpubl. M.Sc. thesis, University in Bergen, 121 pp.

Simonsen, A. 1963: Kvartærgeologiske undersøkelser i Indre Hardanger, Ulvik hd. Hordaland. Unpubl. M.Sc. Thesis, University of Bergen. 67 pp.

4.3 GRAVITATIONAL-SLOPE FAILURES IN TROMS: INDICATIONS OF PALAEOSEISMIC ACTIVITY?

By Lars Harald Blikra and Oddvar Longva, NGU

4.3.1 Introduction

Geological studies on land and in the fjords of Troms county have encountered a large number of gravitational-induced failures, in bedrock, glacial tills and in the fjord sediments. The studies are part of a project evaluating the risk for different types of avalanches, and in locating regional differences in hazard level.

Regional geological mapping performed by NGU in Troms demonstrates concentrations of large-scale failure events in specific zones (Sveian *et al.* in prep). Some of these deposits have been studied earlier by Corner (1972) and Tolgensbakk and Sollid (1988). A high number of rock avalanches and bedrock fractures are registered in northern Troms, in an area from Balsfjord to Kåfjord (Fig. 4.3.1). A series of gravitational faults and crevasses are found along mountain plateaux in the same area. Large-scale collapse features of fine-grained fjord sediments along the fjord margin in Balsfjorden and Ullsfjorden (Longva *et al.* 1999) have also been identified. Some scattered rock avalanches are mapped in the southern part of the county, from Astafjorden to Sørreisa and on Grytøya.

We speculate that the triggering mechanisms for the observed failures are tectonic movements and/or high-magnitude seismic shocks. The present section describes some of the observed failures and discusses briefly the possible palaeoseismic cause. The grading of areas follows the scheme used within the NEONOR project, with five categories:

(E) Almost certainly neotectonics,

(F) Probably neotectonics,

(G) Possibly neotectonics,

(H) Probably not neotectonics

(E) Very unlikely to be neotectonics.

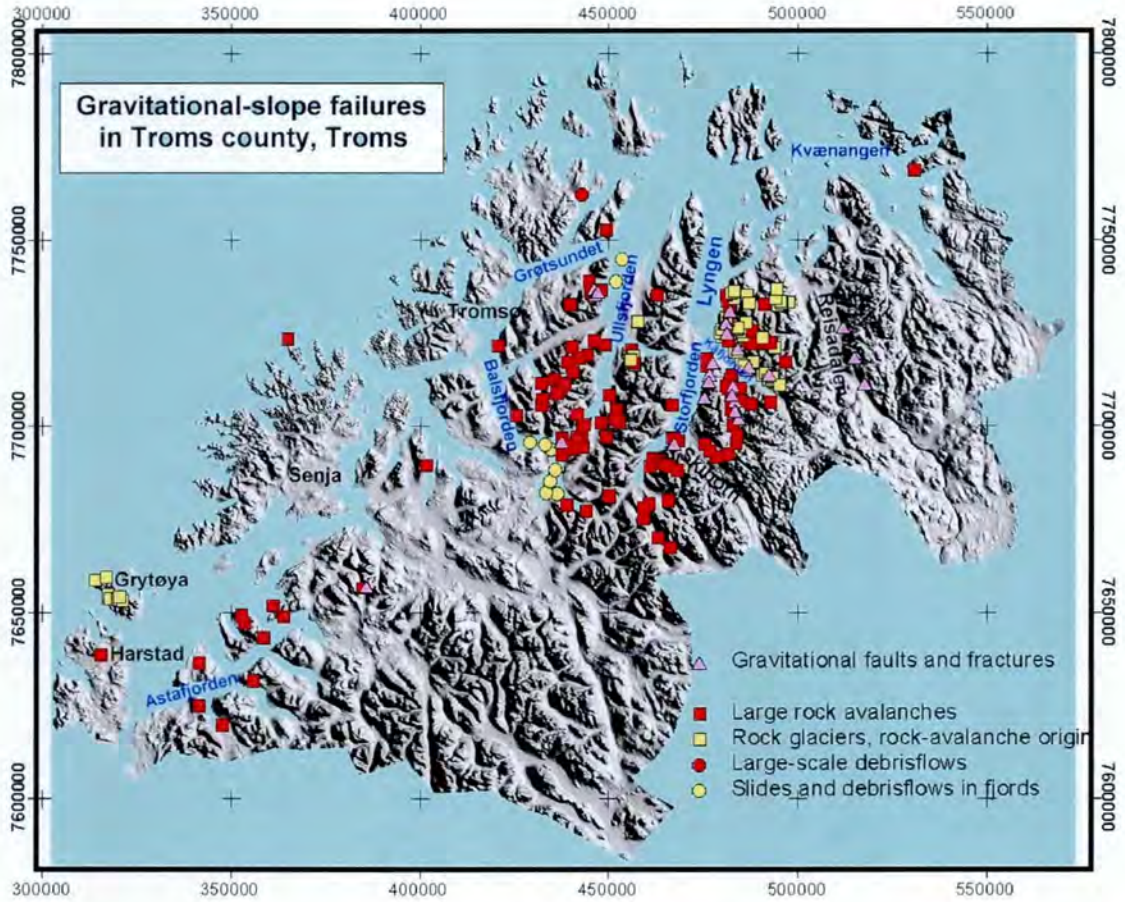

Fig. 4.3.1 Gravitational slope failures in Troms county. The northeastern part (Kvænangen area) has not yet been mapped. The grid spacing is 50 km.

4.3.2 Concentrations of rock-avalanche events

The distribution map of gravitational-slope failures in Troms demonstrate distinct grouping of rock-avalanche events to specific zones (Fig. 4.3.1). We will here briefly describe these zones.

Possible rock glaciers initiated by rock avalanches in Kåfjord area (grade B)

Numerous large bouldery deposits have been mapped in a 25-km wide zone in the Kåfjord area (Fig. 4.3.1). Many of them have been interpreted to be rock glaciers of non-glacial origin (Tolgensbakk and Sollid 1988). These deposits have now been restudied from aerial photos and a few visits in the field. These lead us to conclude that nearly all of them are related to major bedrock failures and large rock avalanches. They may have been further modified by rock glacier movement. We have classified those deposits to be rock glaciers of rock-avalanche origin (see Fig. 4.3.1), although some might still be primary rock-avalanche deposits. To find a climate which is cold enough to get active rock glaciers we must go back to the Younger Dryas period, 11 000 – 10 000 radiocarbon years before present. The original rock-avalanche deposits thus seem to have been formed during or before the Younger Dryas period. The fjords in Kåfjorden and areas south of Kåfjord were covered by glaciers during the Younger Dryas, and thus we should not expect to find this type of deposits there.

Possible rock glaciers on Grytøya (grade C)

Deposits similar to those described above have been mapped on Grytøya (Bergstrøm *et al.* in press; Fig. 4.3.1). The primary origin is definitively large bedrock failures, although some of them might have been modified by rock glacier movement. It is worth noting that these types of deposits have not been found on the alpine western part of Senja.

Rock avalanches in the Balsfjord-Kåfjord area (grade B)

More than 90 individual large rock-avalanche deposits have been registered in an area from Balsfjorden to Kåfjord, covering a distance of *ca.* 80 km (Fig. 5.3.1). Some of them have been possible to date and all dates indicate that the events occurred shortly after the deglaciation (Fig. 4.3.2), 10 000 – 9500 radiocarbon years before present (Blikra 1999). The geographic concentrations of events and their grouping in age indicate that seismic triggering of the avalanches is probable.

Fig. 4.3.2 Sandy infill and growth of balanoides between blocks from a rock avalanche in Balsfjord. The balanoides have been dated to ca. 9500 radiocarbon years BP. The lens cap is 5 cm.

Rock avalanches in Astafjorden-Sørreisa area (grade C)

A less distinct grouping of rock-avalanche events occur in the southwestern part of the county (Fig. 4.3.1). The largest event comprises a total volume of more than 100 mill. m^3 and is thus one of the largest rock avalanches in Norway and Europe (Fig. 4.3.3). The runout distance is *ca.* 4 km.

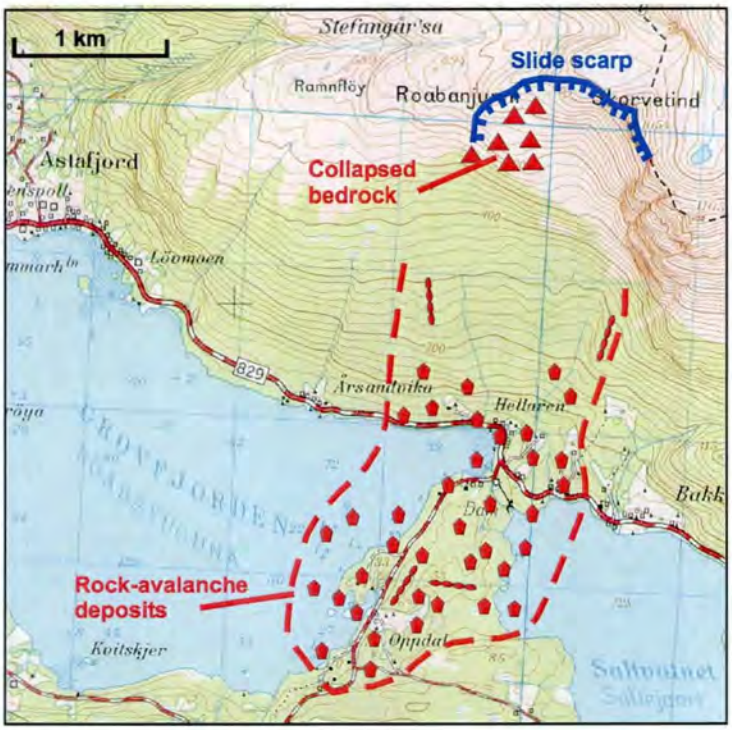

Fig. 4.3.3 A rock avalanche in Grovfjorden on the southern side of Astafjorden (see Fig. 4.3.1) showing the slide scar and the deposits.

Several rock avalanches reached the fjord margin in this area, and a section through one of them was studied (Fig. 4.3.4). Mollusc shells, which occupied the openwork-textured topmost part of the deposit, were dated to *ca.* 9900 radiocarbon years BP, suggesting that the failures occurred shortly after the deglaciation. This deposit lies inside the Younger Dryas ice-marginal zone and the maximum age is thus *ca.* 10,300 radiocarbon years BP.

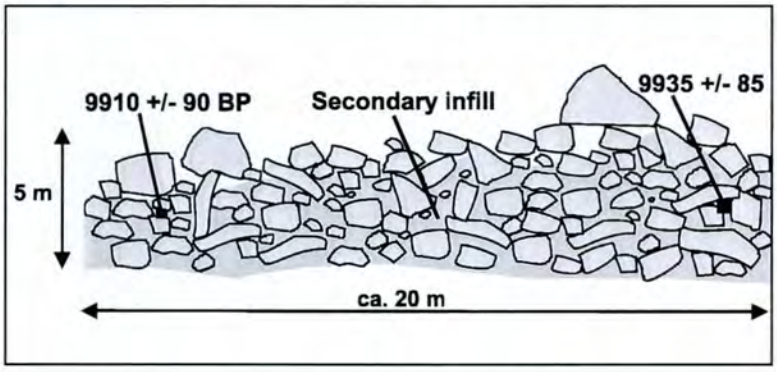

Fig. 4.3.4 Exposure of rock-avalanche deposit at Grøtura on the northern side of Astafjorden (see Fig. 4.3.1). The section shows that the primary topmost part of the rock avalanche had an openwork texture, which later have been filled with finer-grained sand and silt. Mollusc shells are common in these secondary deposits, and radiocarbon dates show that the avalanche is older than 9900 radiocarbon years BP.

4.3.3 Gravitational faults and fractures in bedrock

There are many areas characterised by gravitational failures in bedrock in the northern part of Troms (Fig. 4.3.1). They often occur in connection with large rock avalanches. Some of the

mountain plateaux between fjords are highly fractured and flanked by gravitational faults and rock avalanches, for example in an area between Grøtsundet and Ullsfjorden, northeast of Tromsø (Fig. 4.3.5). The crevasses on the plateau itself show no vertical movement; they seem only to have been stretched. The fractures are filled with coarse-grained sediments due to extensive creep transport of material, indicating that they were formed early in postglacial time. The gravitational faults on the western margin are formed in thick glacial tills, and they often show a rotational pattern (Fig. 4.3.5).

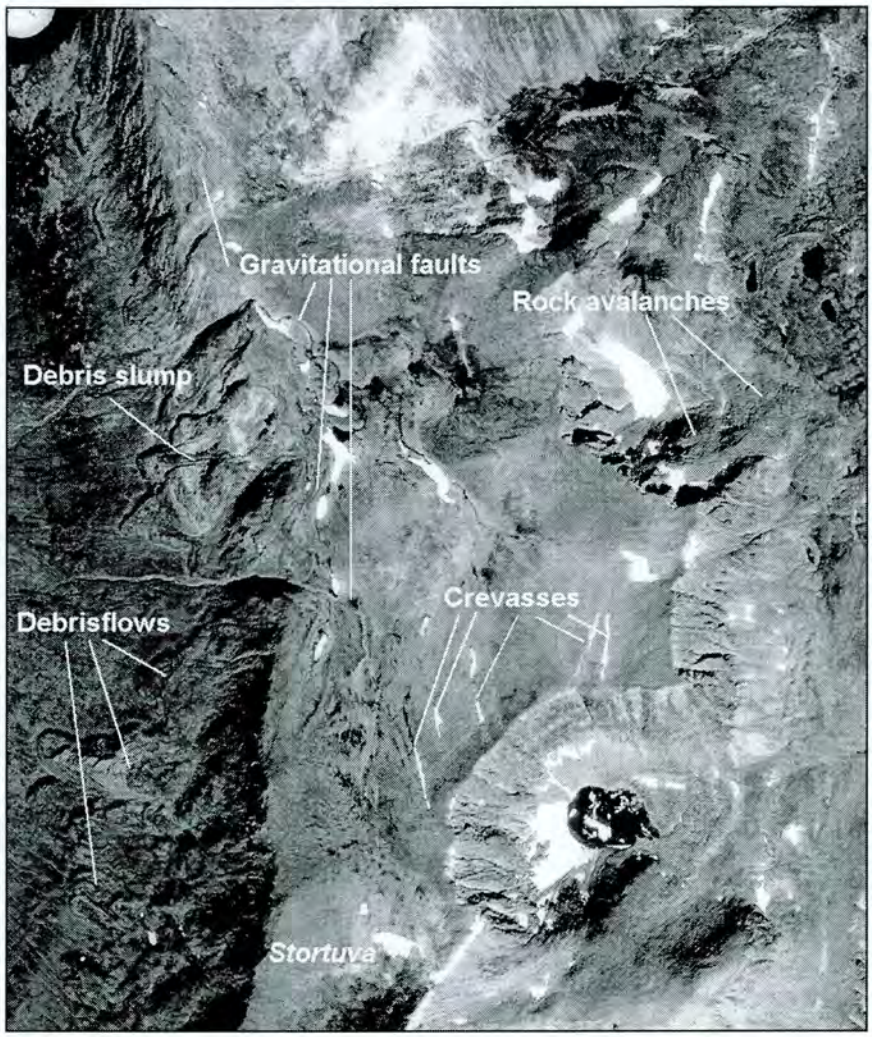

Fig. 4.3.5 Gravitational-slope failures on a mountain plateau northeast of Tromsø. Note also prominent crevasses in the middle part. The aerial photo covers an area of ca. 3.5 km x 4 km.

Fig. 4.3.6 Rotational slide in bedrock from Falsnestind, south of Skibotn. The slide is ca. 100 m long.

A series of gravitational faults occurs on the eastern side of Lyngen and Storfjorden (Fig. 4.3.1), with the southernmost failure south of Skibotn.

Detailed mapping on Nordnesfjellet, north of Skibotn, shows a series of large gravitational fault blocks (Fig. 4.3.7). Several fractures occur internally in the blocks, and even graben structures have been observed (Fig. 4.3.8). Detailed studies in this area have demonstrated detachment zones following the low-angle foliation, with dips in the range of 10-15°. Normally a gradient of *ca.* 30° is needed for failures in bedrock to occur.

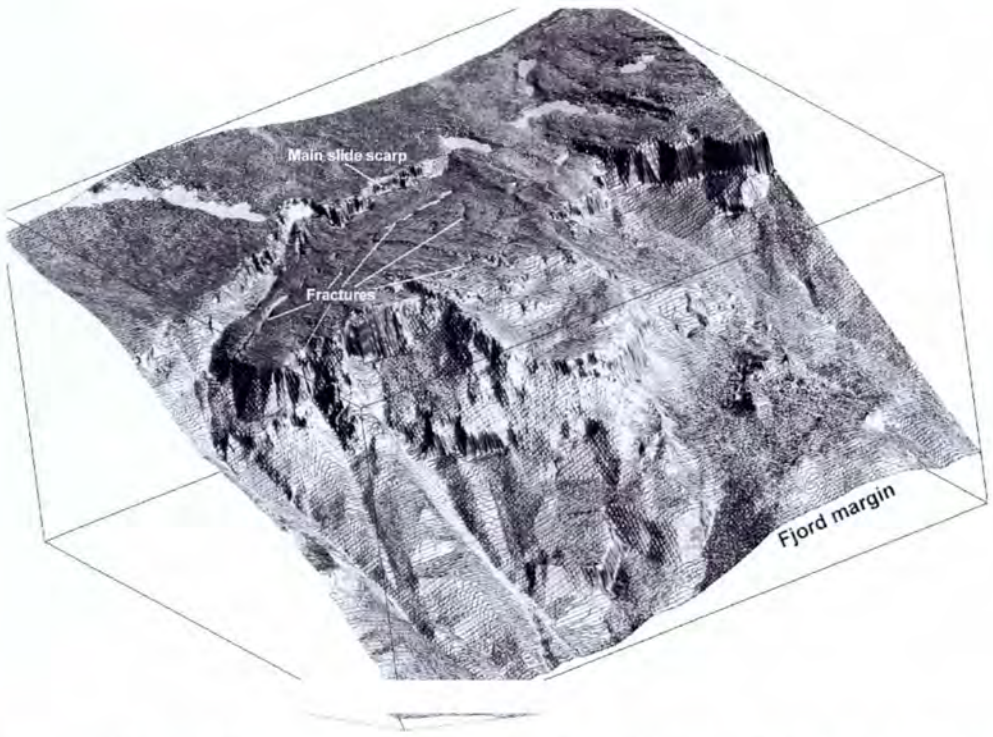

Fig. 4.3.7 3D model of one of the gravitational-slide blocks on Nordnesfjellet showing a well-defined main slide scar and several other fractures within the block. The area is about 1 km long.

Fig. 4.3.8 Innermost part of the fault block shown in Fig. 4.3.7. The length of the fault scarp shown here is ca. 200 m. The vertical drop of the fault is ca. 25 m.

4.3.4 Large-scale debris flows (grade B)

Large-scale failures of the glacial till with the development of extensive debris slumps and debris flows have occurred on the western side of the plateau shown in Figure 4.3.5 (Fig. 4.3.9). They are very different from debris flows occurring today. Present debris flow events are triggered by extreme rainfall events, and involve only the weathered upper 0.5 to 1 m of the glacial till. Their deposits are often characterised by bouldery lobes and blocky lateral levees. The deposits in this area are totally different as they lack lateral levees, are finer-grained, and they seem to have been formed by more cohesive debris flows. The large gravitational faults in the source area also document their initiation from deeper-seated sliding surfaces.

Fig. 4.3.9 Large viscous debrisflow deposits in Olderviklangdalen in Troms. See also Fig. 4.3.5.

4.3.5 Slides and debris flows in fjords (Balsfjorden and Ullsfjorden).

In Balsfjorden, a seismic unit with chaotic signature is found between layered glaciomarine sediments and marine sediments of Holocene age (Longva *et al.* 1999). The sub-surface of the unit is locally sharp, but in other places it is a gradual transition from glaciomarine sediments

via a deformed zone into a zone with massive seismic signature. The unit may contain blocks of undeformed glaciomarine sediments floating in the chaotic matrix (Fig. 4.3.10).

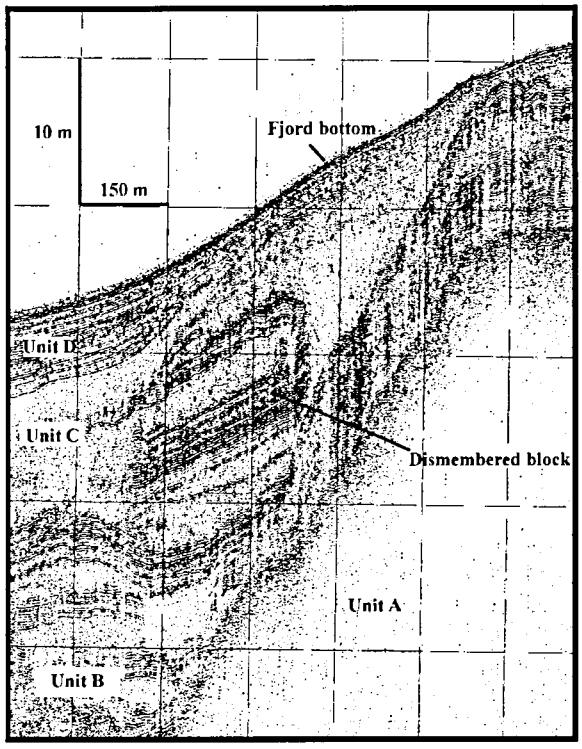

Fig. 4.3.10 Seismic profile from Balsfjord. Unit A;bedrock, Unit B: glaciomarine sediments – here partly deformed, Unit C: deformed and chaotic glaciomarine sediments, Unit D: Holocene, marine sediments. Note the block of undeformed glaciomarine sediments floating in unit C.

Along the margins of the fjord many "old" slide depressions are found (Fig. 4.3.11). These depressions are partly covered by Holocene sediments. They are interpreted to have been formed shortly after the deglaciation of the area. Unit C (Fig. 4.3.10) can be traced backwards to these depressions and it seems obvious that the unit is formed by a collapse of the fine-grained glaciomarine sediments along the fjord margins.

A high number of failures also occur along the margins of Sørfjorden and Ullsfjorden. Seismic studies demonstrate that both rock avalanches and submarine debris flows were triggered shortly after the deglaciation (before 9600 BP).

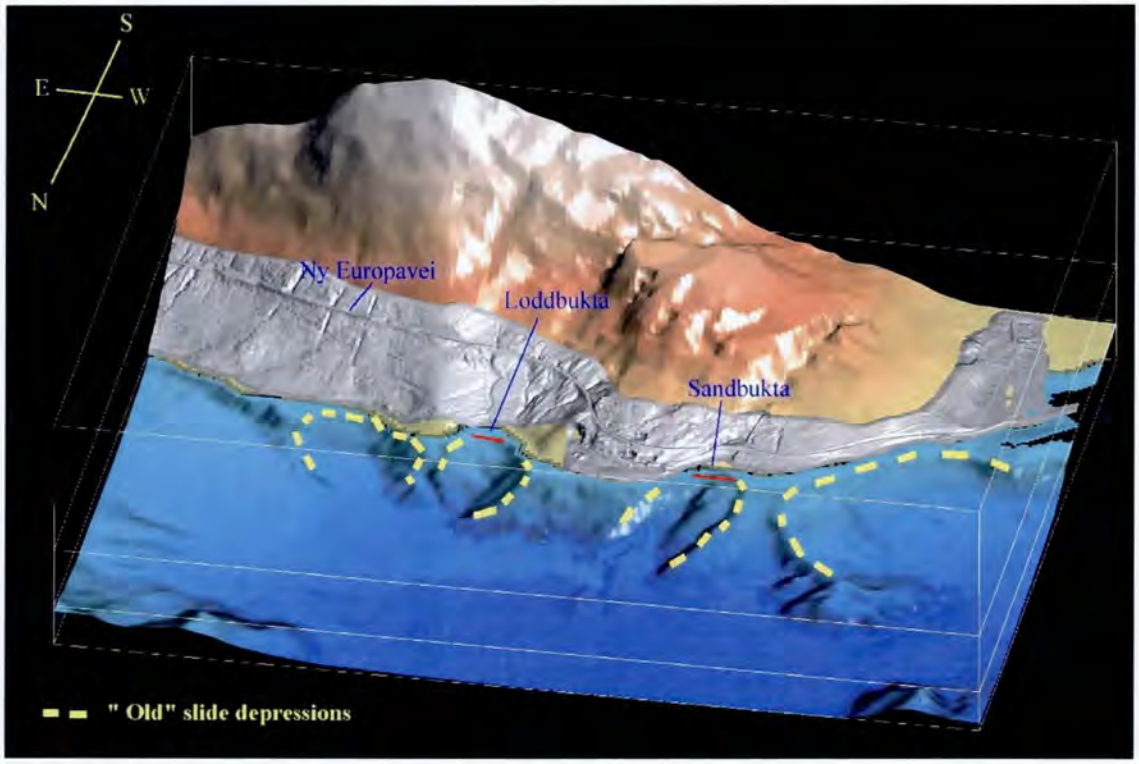

Fig. 4.3.11 Part of the southern side of Balsfjord. The "old" slide depressions marked by yellow stippled lines might have been formed by a palaeoseismic shock-induced collapse of fine-grained glaciomarine sediments.

4.3.6 Possible palaeoseismic triggering

The area in northern Troms from Balsfjord to Kåfjord is characterised by a high number of large-scale slope failures (Fig. 4.3.1). The distribution pattern of these different types of large gravitational-slope failures in the studied areas is to us a strong indication that palaeoseismic activity, either tectonic movement or high-magnitude seismic shocks could be the triggering mechanism for some of the observed features. This is due to their specific geographic distribution, the high number of large-scale events, their limited time-span occurrence and the low-angle sliding surface of the gravitational-bedrock failures. Through the northernmost area runs a postglacial normal fault, the Nordmannvikdalen fault (Dehls *et al.* in press), a fact which strengths our interpretation. The events occurred shortly after the deglaciation and seem to have been triggered by a few episodes.

Keefer (1984) studied 30 historical earthquakes and drew boundaries around all reported landslide locations. If we compare his area versus earthquake magnitude plot with the areas of mapped large-scale gravitational-slope features in Troms, it indicates that the potential large earthquakes could have magnitudes in the order of M 7 to 8.

4.3.7 Conclusions and further work

We tentatively propose that the triggering mechanisms for some of the observed gravitational-slope features are tectonic movements, or high-magnitude seismic shocks. We propose to classify the concentrations of events in the Balsfjord-Kåfjord area to be of grade B (probably neotectonics). We further propose to classify the less pronounced concentrations in the southern part of Troms county to be of grade C (possibly neotectonics).

An even more systematic work on mapping large-scale gravitational-slope features onshore Norway, including fjords, are still needed in order of getting a realistic spatial distribution pattern of such features. A dating program on such features in order of see if there are any age grouping will be of fundamental importance. Detailed studies in fjords are important to test a potential link of onshore features to the large-scale slides on the continental slope. It is our opinion that a better understanding of the evolution and history of large-scale gravitational-slope events since the last ice age is fundamental in order of evaluating possible palaeoseismic activity. Such data will be essential for the estimation of possible future seismic activity, including the possibility of getting high-magnitude earthquakes.

4.3.8 References

Bergstrøm, B. *Et al.* in press: Quaternary geological map Harstad 1332 IV M 1:50 000. Geological Survey of Norway.

Blikra, L.H. 1998: Rock avalanches, gravitational faulting and its potential palaeoseismic cause. In Dehls, J. and Olesen, O. (Eds.) Neotectonics in Norway, Annual Technical Report 1998. *NGU Report* 99.007, 88-92.

Corner, G. 1972: Rockslides in North Norway, Norway. Unpublished report Tromsø museum, 10 pp.

Dehls, J. F., Olesen, O., Olsen, L. and Blikra, L. H. in press: Neotectonic faulting in northern Norway: the Stuoragurra and Nordmannvikdalen postglacial faults. *Quaternary Science Reviews.*

Keefer, D.K. 1984: Landslides caused by earthquakes. *Geological Society of America Bulletin* 95, 406-421.

Longva, O., Blikra, L.H, Mauring, E., Thorsnes, T. and Reither, E. 1999: Testprosjekt Finneidfjord; integrert skredfarekartlegging – metodevurdering. *NGU Rapport* 99.051, 62 pp.

Sveian, H. *et al.* in prep: Løsmassekart Troms fylke M 1:250 000. Geological Survey of Norway.

Tolgensbakk, J. and Sollid, J.L. 1988: Kåfjord, Kvartærgeologi og geomorfologi 1:50 000, 1634 II. Geografisk institutt, Universitetet i Oslo.

4.4 SLIDES IN LOW-GRADIENT AREAS OF FINNMARKSVIDDA

By Kari Sletten, Lars Olsen and Lars H. Blikra, NGU

Vertical aerial photos covering approximately 40% of Finnmarksvidda have been studied in order to discover slides in low-gradient areas. This type of slides can probably not be explained by gravity forces alone, but must be seen in connection with earthquakes, probably with a magnitude higher than 6. Most of these slides may have their origin during formation of the Stuoragurra postglacial fault (magnitude 7-8 earthquake). Three slides of this kind have been discovered at Finnmarksvidda earlier, but a systematic study of aerial photos in order to recognise this type of slide scarps has never been carried out in the area.

Through this study, 45 localities were first pointed out as interesting with regard to possible postglacial slide activity initiated by tectonics. These were later grouped into the following three classes: class 1: very likely (7 localities + the earlier discovered 3 localities), class 2: possible (9 localities) class 3: not interesting (29 localities). Figure 4.4.1 gives an example of a slide of class 1.

The slides are situated in areas covered by glacial tills, and the features are characterised by well-defined scarps. However, the slide or debris flow deposits are difficult to distinguish on the aerial photos. The reason for this might be the fact that the sediments were totally liquefied and ran out without forming distinct features. Another more possible explanation might be that the lower areas were still covered by ice during the sliding event, and that the deposits were removed or disturbed by processes related to the deglaciation.

Eight class 1 slides lie within a relatively short distance from the Stuoragurra fault, and it is thus very likely that post-glacial tectonics have induced the slides (Fig. 4.4.2).

Further work should include a study of aerial photos from the remaining part of Finnmarksvidda, and also fieldwork at the most interesting localities. The slides should be mapped in detail and dated if possible.

Fig. 4.4.1 Example of a class 1 slide with slumping and debris flows. From map 1833 IV Mållejus. Aerial photo 2033 – G55 from Fjellanger Widerøe AS.

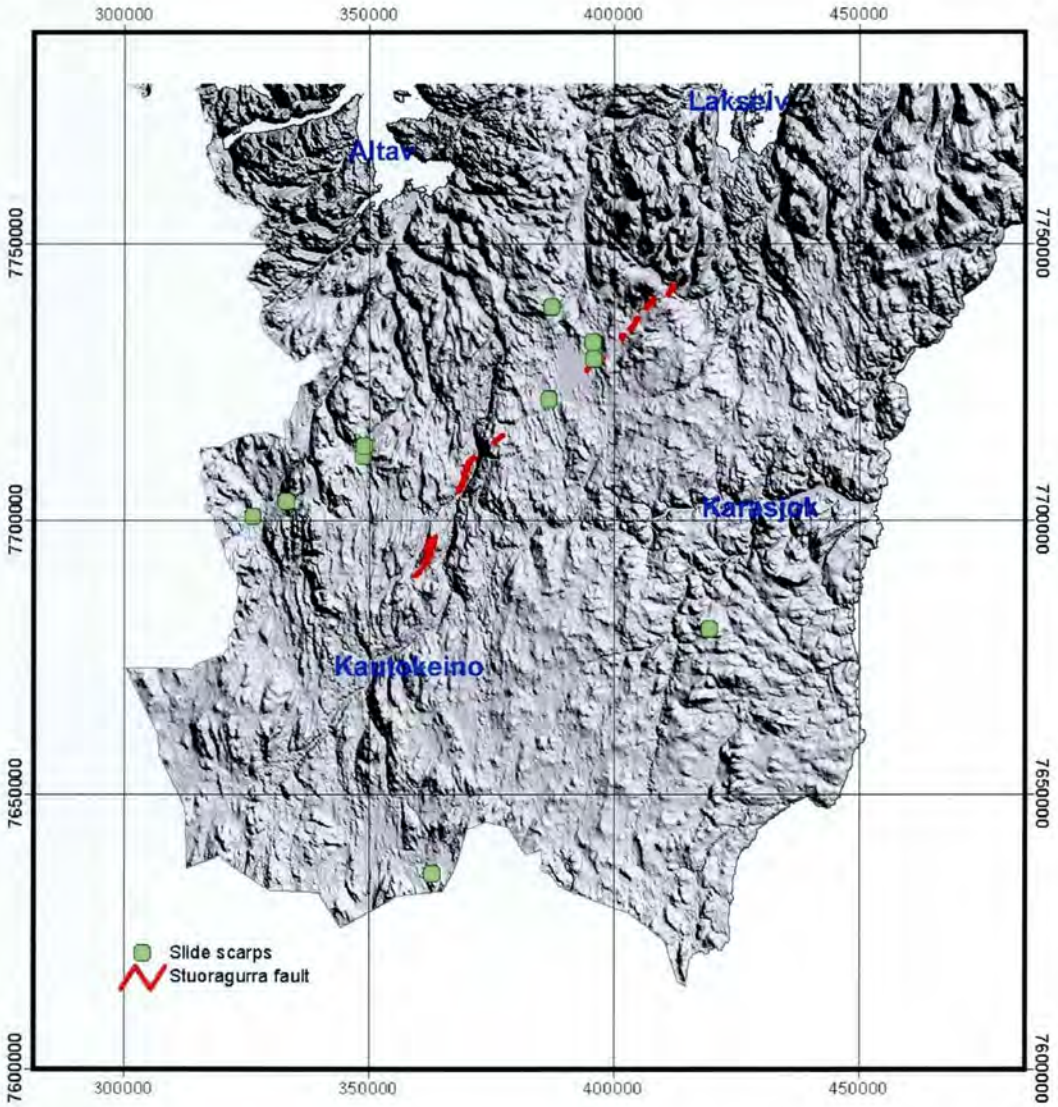

Fig. 4.4.2 Map of the study area at Finnmarksvidda. The Stuoragurra fault and slides of class 1 are marked. The line spaceing is 50 km.

4.5 QUATERNARY GEOLOGY AND TRENCHING OF THE BÅSMOEN FAULT

By Lars Olsen, NGU

4.5.1 Introduction

The Quaternary in Fennoscandia was characterised by repeated periods of ice growth followed by ice retreat. The glacial isostasy during these alternations had a considerable influence on ground stability. This was particularly well expressed during deglaciation periods, which were characterised by the frequent occurrence earthquakes and faulting in many areas (Kujansuu 1964, Lundqvist and Lagerbäck 1976, Olesen 1988). It is not known whether the Båsmoen Fault (Olesen *et al.* 1994, 1995) was active during the last deglaciation, but some liquefaction structures in sand along the fault zone suggest that earthquake-induced disruptions may have occurred during late-/postglacial time (Olesen *et al.* 1994, Olsen 1998).

The last deglaciation is dated to 9200 – 9500 ^{14}C-yr BP in the area around Mo i Rana (Fig. 4.5.1) (Blake and Olsen 1999). Excavations with trenching of the Båsmoen Fault at Båsmofjellet in 1995 revealed structures which indicate a reverse fault, where the hanging-wall block of the faulted rock has penetrated up to some 40-50 cm vertically through the till and sand cover of the lowermost part of the fault slope (Fig. 4.5.2). Observations of glacial striae on the hanging-wall block wall some 40 cm above ground surface along the fault some kilometres west of Båsmofjellet, led us to conclude that the postglacial vertical movement along the fault was no more than 30-40 cm.

In 1995 it was suggested that the colluvial sand complex both on the up-slope and down-slope sides of the exposed hanging-wall block might have been produced by postglacial slope processes (gravity mass movements) during severe climatic conditions (heavy rain storms, rapid and repeated freezing-thawing cycles, etc.). A re-evaluation of the deformation structures observed in 1995, followed by additional data from a new excavation in 1999 (Fig. 4.5.3), has lead to the conclusion that at least the oldest part of the colluvium, which is characterised by rip-up clasts of till matrix, was most likely induced by the last significant tectonic vertical movement of the fault.

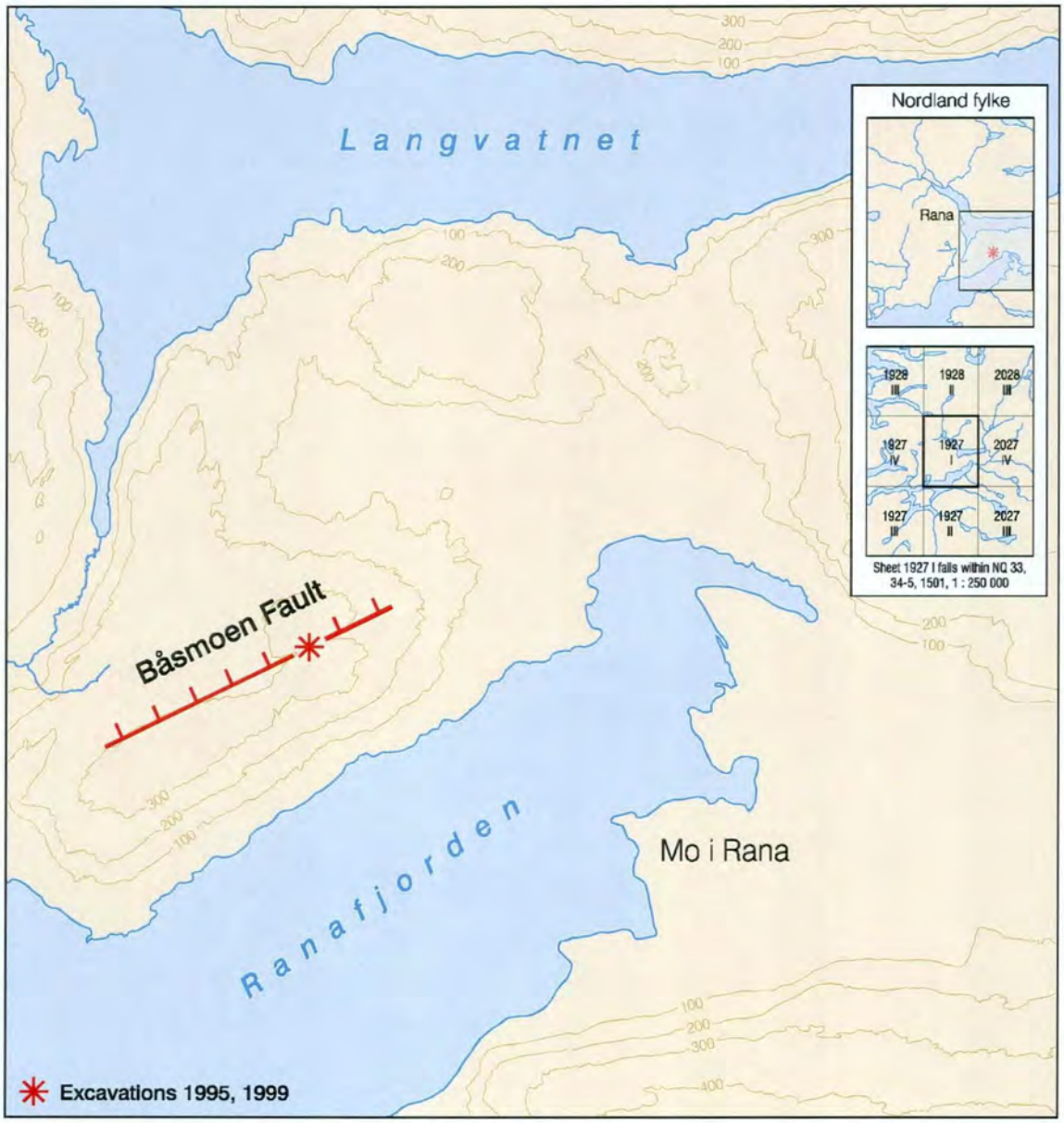

Fig. 4.5.1 Map with position of the Båsmoen Fault and the excavations 1995 and 1999 at Båsmofjellet, Rana area.

4.5.2 Radiocarbon dating of the Båsmoen Fault

The oldest part of the colluvial sand complex is underlain by peat A (Fig. 4.4.2) and overlain by peat B (Fig. 4.4.3). Samples of these organic units should give maximum and minimum ^{14}C-ages of the oldest part of the colluvium, and consequently the approximate age of the tectonic fault activity.

An estimated age of the last significant fault activity would be early to middle Holocene, i.e. about 5000 – 8000 ^{14}C-yr BP. To test this supposition samples from peat A and B have been radiocarbon dated, and the results achieved were 8695 +/- 55 (T-14433) and 3850 +/- 50 (T-14432) ^{14}C-yr BP, respectively.

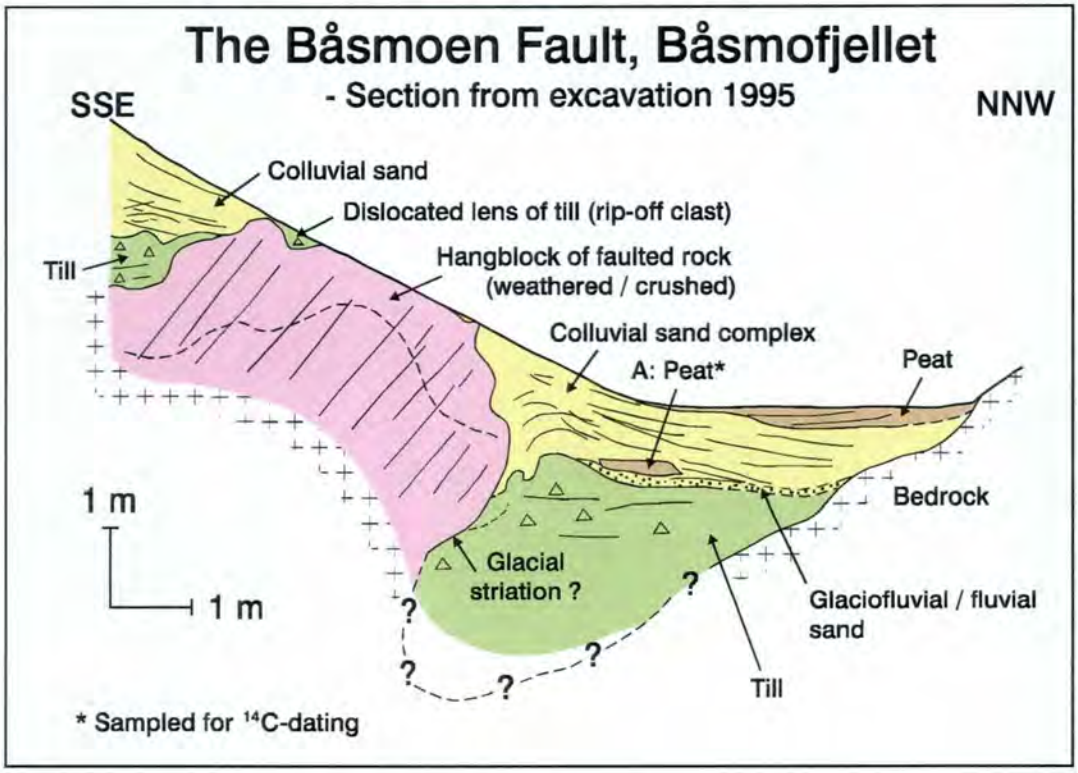

Fig. 4.5.2 Simplified sketch of the main section of excavation transverse to the Båsmoen Fault, 1995.

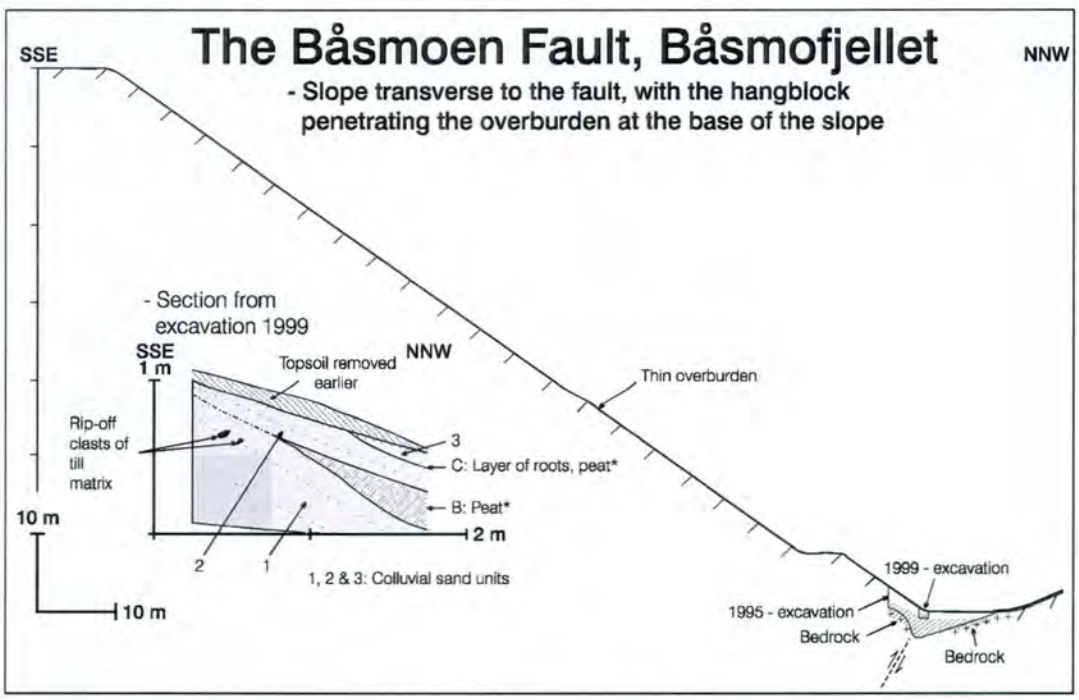

Fig. 4.5.3 Simplified sketch of a vertical profile transverse to the Båsmoen Fault at Båsmofjellet, including positions of the trenching through the fault in 1995 and 1999. A sketch of a vertical section from 1999 transverse to the fault is also included.

4.5.3 References

Blake, K. and Olsen, L. 1999: Deglaciation of the Svartisen area, northern Norway, and isolation of a large ice mass in front of the Fennoscandian Ice Sheet. *Norsk Geografisk Tidsskrift 53,* 1-16.

Kujansuu, R. 1964: Nuorista sirroksista Lapissa. Summary: Recent faults in Lapland. *Geologi 16,* 30-36.

Lundqvist, J. and Lagerbäck, R. 1976: The Pärve fault: A lateglacial fault in the Precambrian of Swedish Lapland. *Geologiska Föreningens i Stockhom Förhandlingar 98,* 45-51.

Olesen, O. 1988: The Stuoragurra Fault, evidence of neotectonics in the Precambrian of Finnmark, northern Norway. *Norsk Geologisk Tidsskrift 68,* 107-118.

Olesen, O., Gjelle, S., Henkel, H., Karlsen, T.A., Olsen, L. and Skogseth, T. 1994: Neotectonic studies in the Ranafjorden area, northern Norway. *NGU Report 94.073,* 43 pp.

Olesen, O., Gjelle, S., Henkel, H., Karlsen, T.A., Olsen, L. and Skogseth, T. 1995: Neotectonics in the Ranafjorden area, northern Norway. *Norges geologiske undersøkelse Bulletin 427,* 5-8 (Extended abstract).

Olsen, L. 1998: Quaternary studies mainly in the Sjona – Ranafjorden area with some additional information from other areas in northern Norway. *In* Dehls, J. and Olesen, O. (eds.): *Neotectonics in Norway, Annual Technical Report 1997. NGU Report 98.016,* 104-114.

4.6 REPORT ON FIELD ACTIVITIES, SUMMER 1999

By David Roberts, NGU

4.6.1 Introduction

Field support this year for the undersigned, in the NEONOR project, was restricted to 2½ days. This involved follow-up work in the Roan district of the Fosen Peninsula, Sør-Trøndelag, i.e., examining road-cuts for possible drillhole (borehole) offsets or axial fractures in drillholes which may provide evidence of neotectonic movements. A few additional examples of offsets were found, though in more or less the same area/locality as last year. In another district of Trøndelag, a brief examination of new road-cuts in the Snåsa Limestone revealed yet another rather fine example of offset (reverse-faulted) drillholes. Comparatively new, long road-cuts along the E6 in the Støren district were also examined late in the autumn. Although no offsets were found, many of the drillholes revealed axial fractures of quite consistent orientation. These various new or additional observations are described briefly below.

4.6.2 Roan district

Examples of drillholes that are clearly offset in a reverse-fault sense are to be found in road-cuts along the county road to Roan, south of Beskelandsfjorden, in the western part of the Fosen Peninsula. The bedrock is a comparatively massive, quartz-monzonitic granulite gneiss of Proterozoic age. One such offset drillhole was illustrated in the 1998 NEONOR report, and in a paper in press (Roberts in press). This showed a reverse-slip displacement of c. 3.5-4 cm on an east-dipping (008°/28°) master joint (fault) surface, the offset directed towards c. 295°.

Along a c.150 m stretch of nearly continuous road-cut at this same locality, four other reverse-slip offsets were recorded in separate drillholes. The road-cut is up to 8 metres in height and all the displaced drillholes measured occur in the lower, accessible part of the road-cut. Details of the measurements are as follows:-

(1) Offset of c. 2.5 cm towards 292° along a 026°/16° joint (slip) surface (Fig.4.6.1).

(2) Offset of 1-1.5 cm towards 288° along a 033°/25° joint (slip) surface.

(3) Offset of 1.5 cm towards 283° along a 038°/41° joint (slip) surface.

(4) Offset of c. 2.5 cm towards 268° along a 031°/22° joint (slip) surface.

The direction of displacement of these separate reverse-faulted drillholes is reasonably consistent. Indeed, the average displacement vector of the 5 recorded offset drillholes (i.e., the four recorded this year and the one from last year) is 285°. This would seem to indicate that the S_{Hmax} (maximum principal horizontal stress) in this particular area trends c. WNW-ESE. This orientation does, in fact, accord extremely well with contemporary, *in situ*, stress measurements reported from this district of Central Norway (Myrvang 1988) (Fig. 4.6.2).

Fig. 4.6.1 Reverse-faulted offset drillholes in Proterozoic granulite gneisses, along the road to Roan, south of Beskelandsfjorden (NE of Roan). Photograph taken looking SSW.

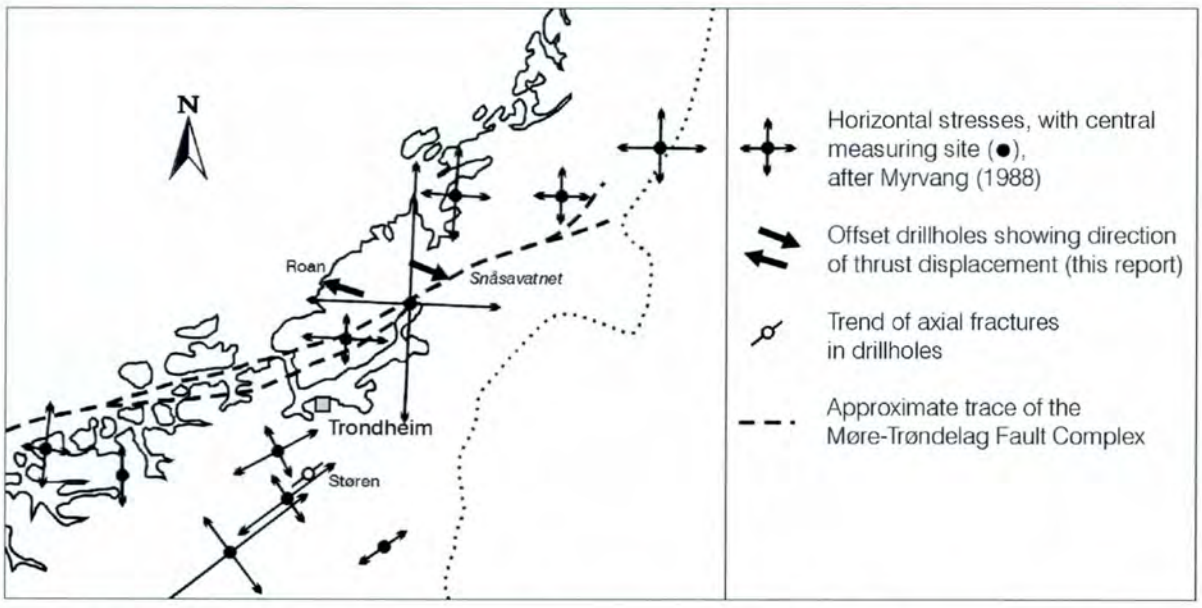

Fig. 4.6.2 Magnitudes and directions of contemporary, in situ, horizontal stress measurements in bedrock (crosses with arrowed terminations), Central Norway (after Myrvang 1988). For scale, 14 mm of the length of the arms of the crosses corresponds to 30 Mpa. The two localities with thrust-offset drillholes described in this report are indicated by the thick arrows (the localities are approximately at the tips of the arrowheads). The trend of axial fractures in drillholes from near Støren is an average value from 22 separate drillhole measurements over a 400 m-long road-cut.

Many other road-cuts were examined in the Roan district, but no other indisputable reverse-slip features were found. Two or three minor examples of normal dip-slip were encountered, but these drillhole displacements were clearly due to gravitational slippage of large blocks loosened by the blasting of the road-cuts. Drillholes were also examined for indications of near-vertical axial fracturing, and especially for signs of any consistency in trend of such fractures. Unfortunately, the granulite-facies rocks of the Roan district were not too helpful in this regard. Even road-cuts aligned normal to the WNW-ESE S_{Hmax}, where axial fracturing in boreholes might be expected to occur, did not disclose any regularity in occurrence of axial fractures. A reason for this might be that the massive granulitic rocks in this district are too coarse grained and isotropic; and that axial fractures may develop preferentially in finer grained, thinly bedded or laminated rocks carrying a penetrative continuous cleavage, as for example in the roofing slates of the Friarfjord area, Finnmark (see the 1998 NEONOR report; also Roberts, *in press*).

4.6.3 Snåsavatnet district

Stretches of the main E6 road on the northwest side of Snåsavatnet, Nord-Trøndelag, have been reconstructed in recent years, and this has provided several new road-cuts. One such new road-cut was examined briefly in the autumn while driving back to Trondheim from NGU fieldwork in Nordland, and reverse-faulted drillholes were observed in one locality. The precise locality is unfortunately uncertain, as I did not have the 1:50,000 topographic maps of this area in the car at that time. However, the road-cut is almost certainly in the eastern part of 1.50,000 map-sheet Steinkjer 1723 III, somewhere near the farms Haugan and Flekkstad, northwest of Veines.

The drillhole offsets can be seen along the north side of the E6, in a c. 5 m-high road-cut in the Middle Ordovician Snåsa Limestone. Displacement occurs along a 10-13 cm-thick shear (fault) zone with a strike/dip of 204°/13° (Fig. 4.6.3). Within this narrow shear zone, composed of crushed and gouged limestone, there are internal shear bands dipping northwest at 20° (strike 223°). The drillhole offsets are $\leq$ 7.5 cm, and the thrust direction is towards 105°. This is virtually the same trend for S_{Hmax} as in the case of the offset boreholes in the Roan district (Fig. 4.6.2). In the map of all horizontal stresses recorded in Central Norway (Fig. 4.6.2), taking the area north and south of Trondheimsfjorden it does appear as if the Møre-Trøndelag Fault Complex (MTFC) marks some sort of major divide in contemporary stress orientations; N-S/E-W to the northwest of the MTFC, and NE-SW/NW-SE to the southeast. More data are required, however, before we can say for sure if this changeover is truly significant.

If there are still funds available in the project, then a more detailed examination of all the new road-cuts in the Snåsavatnet district should provide more data on these comparatively rare stress relief features.

Fig. 4.6.3 Drillholes offset in a reverse-slip (thrust) sense along a comparatively flat-lying fault in the Snåsa Limestone, near Veines, Snåsavatnet, Nord-Trøndelag. Photograph taken looking north.

4.6.4 Støren area

New road-cuts along the E6 near Støren, Sør-Trøndelag, are of particular interest to bedrock geologists since they cut through pillowed metabasalts (greenstones) of the Støren ophiolite, and also metasedimentary rocks of the Gula Group. Because of traffic regulations (no stopping and no pedestrians), only a cursory examination was made of sections in Gula rocks on either

side of the new tunnel just southeast of Voll. These drillholes were of no particular value for our studies.

The c. 400 m-long road-cut in pillowed greenstones immediately to the north of Haga Bridge (3 km north of Støren) did, however, provide some interesting features. This road-cut is aligned roughly NW-SE. Although no drillhole displacements were seen, some 20-30% of the vertical or subvertical drillholes in the 6-10 m-high road-cuts displayed reasonably continuous, but partly irregular axial fractures. Measurements were made of the trends of these fractures – which are considered to be extensional, stress-relief fractures – only in cases where they exceeded 1 m in length, i.e., the fractures could be judged to be fairly continuous through the rock body from one lava 'pillow' to another. Twenty-two such measurements were recorded from separate drillholes over this 400 m-long stretch of road-cut; and they showed a reasonable consistency of trend from c. 030/210° to 060/240°, with an average value of 051/231°.

This average trend of the axial fractures occurring in vertical/subvertical drillholes at Støren, i.e., quite close to NE-SW, thus corresponds extremely well with the S_{Hmax} recorded in the region south of Trondheim by Myrvang (1988) (Fig. 4.6.2).

4.6.5 References

Myrvang, A. 1988. Rock stress measurements in Norway: recent results and interpretations. Report, Workshop on Nordic Rock Stress Data. SINTEF, Trondheim, 10 October 1988, 5 pp.

Roberts, D. in press. Reverse-slip offsets and axial fractures in road-cut boreholes in the Caledonides in Finnmark, northern Norway: neotectonic stress orientation indicators. Quaternary Science Reviews.

5 GEODESY (TASKS 5, 6 AND 7)

5.1 NORWEGIAN MAPPING AUTHORITY: REPORT FOR 1999

By Lars Bockmann and Leif Grimstveit, Statens Kartverk

5.1.1 General

Within the NEONOR project, repeated GPS campaigns were planned to be carried out in three areas, namely in Masi, Bremanger and Mo i Rana, where active faults are suspected. It was hoped that these campaigns would allow to detect particularly vertical movements or at least to give an upper limit for the deformation across the suspected faults. In addition to the GPS campaigns, precise levelling was carried out across the fault in Masi.

GPS measurements at Masi and Bremanger have so far been completed only once, and therefore no information is yet available concerning significant deformation. Indications of deformation will only begin to emerge once additional observations and computations are completed. The planned reobservations of these nets in 1999 were dropped due to higher priority of measurements in the GPS network of Mo i Rana. This net had been measured both in 1994 and 1997, thus providing more data sets covering a longer time span. Therefore, it could be expected that a new campaign on this net would allow detecting deformation in the area. However, after discussing the methodology lying behind the 94 and 97 campaigns and the quality of the available data, we are forced to reconsider these arguments. More details about this are given at the end of this section. To achieve the original goal, all the GPS-nets involved in the project have to be remeasured in a new future project or as a prolongation of NEONOR.

The data and a list of point descriptions as well as picture documentation are kept at the Norwegian Mapping Authority, Geodetic Institute.

5.1.2 Masi: Levellings across the Stuoragurra fault 1987-1999

At Stuoragurra, the elevation difference (DH) between benchmarks on both sides of the fault has been measured by precise levelling. Sundsby (1996, in Norwegian) reports the results of levellings at the Stuoragurra fault carried out in 1987, 1990, 1991, and 1996. All these levellings were done using Wild N3 precision spirit levels. On July 9, 1999 another relevelling was done, using two digital levels Zeiss DiNi11 simultaneously. The weather was very favourable for precise measuring work. 40 series of observations were performed, from 9.30 am to 4.30 pm. Each instrument was used on both sides of the fault. The precision of this series of measurements is expected to be roughly 0.1 mm. After having analysed the observations, no significant change of elevation difference across the Stuoragurra Fault in Masi can be detected since 1996. Earlier conclusions about a vertical displacement of 2.3 mm between 1987 and 1991 have to be reconsidered due to scepticism concerning the quality of the data from 1987. These questions are discussed below.

Fig. 5.1.1 Stuoragurra fault. Levelling across the marsh, seen from east to west.

At Stuoragurra, the elevation difference DH between benchmarks VI and ØI was monitored by repeated precise levelling. The marks are built in solid rock on the western and eastern side, respectively, of a potentially active fault. Computed results for DH are:

```
1987:      3.8599 m
1990:      3.8612 "
1991:      3.8622 "
1996:      3.8621 "
1999:      3.8617 "
```

The computed DH cannot be expected to be exactly the same from one year to another, as the readings are made to mm/100, and as each levelling includes a shot of nearly 90 m across a swamp. The apparent changes of DH should be statistically analysed to make conclusions concerning their significance.

To estimate the quality of a levelling, we routinely compute the misclosure, which is, for a levelling line, the difference between levelled DH forwards and backwards. For the shot across the swamp, sight lengths fore and back are very different, giving systematic error effects. This error will be eliminated when taking the mean of (or averaging) the fore and back levellings, if fore and back instrument setups are made at different ends of this line. However, the common misclosure check is then lost. Another check should be made, using results from two independent levellings, both fore and back.

From 1987 to 1991, the apparent change of DH was 2.3 mm. The standard deviation was estimated from the misclosures 1987, 1990, and 1991. In Sundsby (1996) it was concluded that 2.3 mm was a significant change on the 95%-level. It then was assumed that the 3 computed results as equally strong, considering the rather close absolute values of the misclosures.

Against this, one could object:

1) The 1987 and 1990 misclosures do not have the same quality as the corresponding 1991 and later results, as the fore and back levellings were each made only once.
2) The levelled line is very short, and gives no degrees of freedom for the adjustment. One should, possibly, use representative values of standard deviation, taken from extended levellings. Sigma is now computed from paired observations, fore and back.
3) Professor Arthur G. Sylvester makes objections to our earlier conclusion, strongly stressing the improbability of an active fault. Possibly, a significance level higher than 95% should be used. Using 95%, there is a risk of making a wrong conclusion in 1 case of 20.

5.1.3 Classical Observations: Monitoring of horizontal movements Yrkjevågen 1984 – 1997

There has been no activity in the field in 1999. The results of the vertical monitoring at Yrkje and Ølen are given in the NEONOR technical report from 1998 (Bockmann, 1999), and will not be repeated here. The computation of the horizontal monitoring in the so-called "Holsen-net" has, however, been going on and a final report is given below.

Fig. 5.1.2 There are 3 levelling crossings in the picture; left, middle and right side.

At Yrkjevågen, in the municipality of Tysvær, a local geodetic network was established in 1983, to monitor the local horizontal movements. Instruments may be stationed at 6 concrete pillars, and directions (angles) and/or distances may be measured between the pillars. Their relative positions may then be computed. The network and the pillars were designed by Professor Jon Holsen at the Technical University of Norway (Holsen 1986).

Professor Holsen measured the horizontal angles of this network 4 times: spring 1984, autumn 1984, autumn 1986, and autumn 1987, and he was the manager of another measurement of angles, spring 1993. Related to the NEONOR project, the Norwegian Mapping Authority has continued Holsen's work at Yrkjevågen. Until now, the network has been measured once by us, autumn 1997, with the precision distance meter Mekometer ME5000.

Generally, measurements have rounding errors and inevitable random errors. These errors being different from one measurement campaign to another, we always find apparent changes between the computed sets of results, when lots of ciphers are given. Such changes from 1984 to 1997 may be analysed statistically, in order to estimate the probability of the apparent movements of the pillars being real movements.

The statistical analysis may be performed in several different ways. We prefer the general linear hypothesis test for normally distributed observations. The original measurements are then used. Examining the reports from Holsen's work, we have, until now, found this material for spring 1984, only. Therefore, we have here analysed the apparent network changes from spring 1984 to autumn 1997, without regarding the other surveying campaigns.

The general linear hypothesis test is used to estimate the consequences of making conditions for the unknown parameters, when adjusting measurements according to method of least squares. The observations are then considered statistically independent and normally distributed. This assumption is commonly considered valid for surveying measurements.

We use the test, trying to answer the following three questions:

1) Have horizontal displacements occurred?

A null hypothesis H0 is made, that the pillars are not displaced, relatively to each other. The test may give a statistically justified reason for refusing H0. Two different common adjustments of the measurements spring 1984 + autumn 1997 are made: initially without demanding H0, then with H0 as conditions. From the results of these two adjustments, a test value is computed. Its value indicates acceptance or rejection of H0. In the Yrkjevågen case, the test value is much bigger than may be expected if the three above-mentioned conditions (independent observations, normally distributed observations, H0) are simultaneously met. Therefore, we conclude that the pillars have been internally displaced during the period spring 1984 – autumn 1997. The test is made with a 5% significance level, giving a probability of at least 0.95 for the conclusion being correct or at the most 0.05 for being wrong.

2) Which points have been disturbed?

This investigation is much more time consuming than 1). We have to make many adjustments, testing different hypotheses for the pillars' movements. The conclusion is that pillars 1 and 5 seem to have moved significantly, relatively to the others. Again, we use the 5% significance level.

3) Do we find a regularity for the displacements, and possibly which?

The network has 3 pillars on each side of the potential geological fault, and we initially test if these two groups of points also seem to move as groups. One may guess from conclusion 2) that such a regularity will be difficult to find. We have had lots of work testing different hypotheses, without being able to conclude at the 5% level that a grouped movement has occurred.

Additional thoughts:

- May the pillars 1 and 5 have moved relatively to the bedrock, locally? Professor Holsen monitored the pillars 3 and 5 individually, to check their stability. He found an apparent position change of 0.24 mm, maximally.
- Could there be a seasonal variation? Holsen found this being a tendency for his monitoring 1984-1993.
- Could it have some importance that the types of measurement were quite different in 1997 and 1984 (distances and directions, respectively)? For experiments, we routinely prefer the outer conditions being unchanged.

Fig. 5.1.3 A concrete pillar in the Holsen-net

5.1.4 Ranafjorden

In 1994, a GPS network with 18 points, numbered from 9401 to 9418, was established. The network was designed to measure the geological strain in the Ranafjord. The network has been measured by staff from the Department of surveying and mapping, NTNU, in 1994 and 1997.

In 1999 the network has been extended with two new points in Lurøy in the western profile, numbered 9919 and 9920. The GPS field observation was carried out in the period 16-15 June 1999 by Lars Bockmann and Knut Gjerde of the Norwegian Mapping Authority. Terje Skogseth, NTNU, participated also during the first two days of the campaign together with Arngrim Utskarpen, a student at NTNU. A total of 11 Ashtech Z-surveyor together with Dorne and Margolin choke ring antennas were used.

The standard specifications for such GPS observations followed within the Norwegian Mapping Authority, where different processing software packages are used, is that GPS observations are recorded continuously at each station for a minimum of two full days. Furthermore, whenever receivers have to be moved from station to station for different observational sessions, the various sessions must include at least two common stations where the receivers remain unmoved. As usual, GPS data were recorded at 30 second intervals, with all visible satellites over 10° elevation angle being tracked.

Unfortunately the instrument in point 9414 close to Nesna had stopped logging for instrumental reasons, so there is a reduced amount of data at this station. No observations were done in 9407, the most northern point in the eastern profile, due to lack of instruments. The point 9402 could not be occupied due to a site selection on a little rock in the fjord only accessible during low water. Instead another point was chosen close by and connected to 9402 through observation of the short link vector.

The data and a list of point description as well as picture documentation are kept at the Norwegian Mapping Authority, Geodetic Division.

Fig. 5.1.4 Observations in progress at station 94-09 Hemnesberget

GPS analysis and results

Single station point positioning solutions were produced for each day. Non-fiducial precise orbits, earth orientation parameters and satellite clocks from NASA's Jet Propulsion Laboratory (JPL) were used. The single station solutions for each day were adjusted and ambiguity resolution was carried out. Finally, the daily free-network solutions were transformed to the ITRF96 reference frame using transformation parameters from JPL. These daily transformation parameters were the same that JPL had estimated and used to transform their global free network solution to ITRF96.

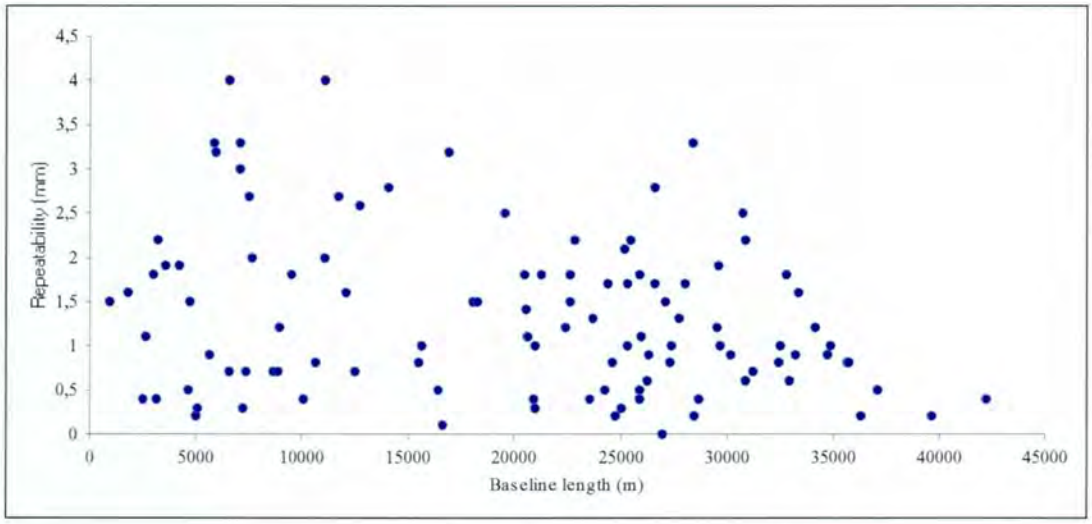

Fig. 5.1.5 Baseline repeatability versus baseline length.

Figure 5.1.5 plots the baseline length repeatabilities as a function of baseline length. The distance between the stations varies from 0.9 to 42.3 km, and the mean repeatability is 1.3 mm. Figure 5.1.6 plots the repeatability in north, east, and height. The mean repeatability is given in parentheses. The ITRF96 Cartesian coordinates with uncertainties are seen in Table 5.1.1, and the cartesian baseline vectors are seen in Table 5.1.2.

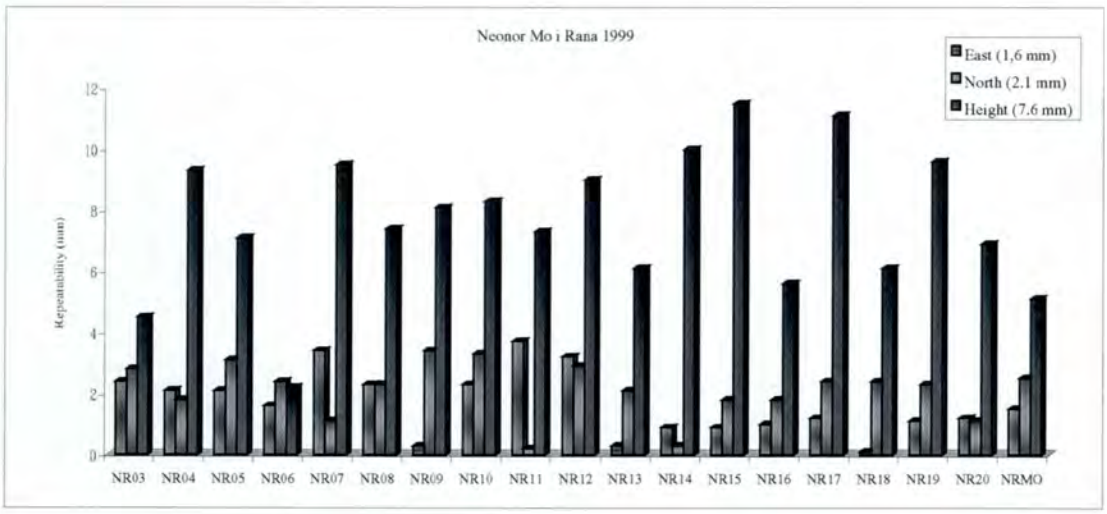

Fig. 5.1.6 Repeatability in east, north, and height. Mean repeatability is given in parentheses.

Table 5.1.1 ITRF96 cartesian coordinates with uncertainties for the stations.

	X $\pm \sigma_x$ (m)	Y $\pm \sigma_y$ (m)	Z $\pm \sigma_z$ (m)
NR01	2491342,7615 $\pm$ 0.0050	633121,6159 $\pm$ 0.0030	5817812,9502 $\pm$ 0.0082
NR03	2490262,3216 $\pm$ 0.0030	626192,4172 $\pm$ 0.0017	5818880,6830 $\pm$ 0.0047
NR04	2489451,4722 $\pm$ 0.0040	625993,8789 $\pm$ 0.0014	5819275,6307 $\pm$ 0.0087
NR05	2488214,8292 $\pm$ 0.0052	622778,0724 $\pm$ 0.0016	5820242,2642 $\pm$ 0.0059
NR06	2486880,8759 $\pm$ 0.0031	620175,6931 $\pm$ 0.0024	5821019,3968 $\pm$ 0.0024
NR08	2510226,3356 $\pm$ 0.0035	611137,1683 $\pm$ 0.0025	5811952,5484 $\pm$ 0.0069
NR09	2506257,1993 $\pm$ 0.0062	606361,4347 $\pm$ 0.0012	5814159,1652 $\pm$ 0.0062
NR10	2502377,1946 $\pm$ 0.0051	604513,1491 $\pm$ 0.0016	5815994,2717 $\pm$ 0.0075
NR11	2499753,3575 $\pm$ 0.0038	606039,2776 $\pm$ 0.0029	5816957,2466 $\pm$ 0.0067
NR12	2495617,7186 $\pm$ 0.0040	606407,8807 $\pm$ 0.0035	5818974,8973 $\pm$ 0.0085
NR13	2518844,5659 $\pm$ 0.0037	585176,6711 $\pm$ 0.0008	5810903,5102 $\pm$ 0.0051
NR14	2515889,6133 $\pm$ 0.0044	581476,6571 $\pm$ 0.0001	5812538,3348 $\pm$ 0.0090
NR15	2515302,9070 $\pm$ 0.0055	579135,9476 $\pm$ 0.0015	5813020,9678 $\pm$ 0.0102
NR16	2512633,4302 $\pm$ 0.0035	578059,8381 $\pm$ 0.0011	5814275,1880 $\pm$ 0.0047
NR17	2508921,7419 $\pm$ 0.0052	574315,1941 $\pm$ 0.0020	5816240,0759 $\pm$ 0.0099
NR18	2501206,3133 $\pm$ 0.0042	577402,7573 $\pm$ 0.0010	5819239,0416 $\pm$ 0.0049
NR19	2482498,0161 $\pm$ 0.0051	582886,0303 $\pm$ 0.0008	5826659,4997 $\pm$ 0.0085
NR20	2493593,0197 $\pm$ 0.0037	582319,9390 $\pm$ 0.0014	5821989,4063 $\pm$ 0.0059
NRMO	2491540,4938 $\pm$ 0.0012	627261,0979 $\pm$ 0.0012	5818227,6621 $\pm$ 0.0057

Table 5.1.2 Cartesian baseline vectors between the stations.

	Δx (m)	Δy (m)	Δz (m)	Δl (m)
NR03NR04	810,8496	198,5382	-394,9481	923,5142
NR03NR05	2047,4924	3414,3446	-1361,5819	4207,5978
NR03NR06	3381,4463	6016,7239	-2138,7139	7225,5963
NR03NR07	-1080,4395	-6929,1993	1067,7324	7093,7441
NR03NR08	-19964,0146	15055,2474	6928,1346	25946,5105
NR03NR09	-15994,8772	19830,9817	4721,5174	25911,323
NR03NR10	-12114,8709	21679,2678	2886,4107	25001,8422
NR03NR11	-9491,0357	20153,1394	1923,4359	22359,0785
NR03NR12	-5355,3962	19784,5334	-94,2191	20496,7536
NR03NRMO	-1278,1721	-1068,6809	653,0203	1789,4799
NR04NR05	1236,6428	3215,8065	-966,6337	3578,4183
NR04NR06	2570,5967	5818,1857	-1743,7658	6595,4508
NR04NR07	-1891,289	-7127,7375	1462,6805	7518,0483
NR04NR08	-20774,8642	14856,7093	7323,0827	26569,613
NR04NR09	-16805,7268	19632,4435	5116,4655	26344,7055
NR04NR10	-12925,7204	21480,7296	3281,3588	25283,6569
NR04NR11	-10301,8853	19954,6012	2318,3841	22576,3118

	Δx (m)	Δy (m)	Δz (m)	Δl (m)
NR04NR12	-6166,2458	19585,9953	300,729	20535,9255
NR04NRMO	-2089,0217	-1267,2191	1047,9684	2658,5886
NR05NR06	1333,9539	2602,3792	-777,1321	3025,8461
NR05NR07	-3127,9319	-10343,5439	2429,3143	11075,8488
NR05NR08	-22011,507	11640,9028	8289,7165	26243,7889
NR05NR09	-18042,3696	16416,6371	6083,0993	25140,3494
NR05NR10	-14162,3632	18264,9232	4247,9926	23499,4764
NR05NR11	-11538,5281	16738,7947	3285,0178	20594,0822
NR05NR12	-7402,8886	16370,1888	1267,3628	18010,887
NR05NRMO	-3325,6645	-4483,0255	2014,6021	5934,3226
NR06NR07	-4461,8857	-12945,9232	3206,4463	14063,6641
NR06NR08	-23345,4609	9038,5236	9066,8485	26625,4239
NR06NR09	-19376,3235	13814,2578	6860,2313	24765,6699
NR06NR10	-15496,3171	15662,5439	5025,1246	22598,739
NR06NR11	-12872,482	14136,4155	4062,1499	19545,846
NR06NR12	-8736,8425	13767,8096	2044,4948	16433,6532
NR06NRMO	-4659,6184	-7085,4048	2791,7342	8927,9776
NR07NR08	-18883,5752	21984,4468	5860,4022	29567,7125
NR07NR09	-14914,4378	26760,181	3653,785	30852,8424
NR07NR10	-11034,4314	28608,4671	1818,6783	30716,6186
NR07NR11	-8410,5962	27082,3387	855,7036	28371,1724
NR07NR12	-4274,9568	26713,7328	-1161,9515	27078,5691
NR07NRMO	-197,7326	5860,5184	-414,7121	5878,4998
NR08NR09	3969,1374	4775,7342	-2206,6172	6590,2086
NR08NR10	7849,1411	6624,0195	-4041,7232	11037,3084
NR08NR11	10472,9789	5097,8919	-5004,6986	12677,4918
NR08NR12	14608,6169	4729,2874	-7022,3492	16884,645
NR08NR13	-8618,2311	25960,4965	1049,0387	27373,7423
NR08NR14	-5663,2793	29660,5095	-585,7865	30202,0149
NR08NR15	-5076,5725	32001,2197	-1068,4192	32418,9939
NR08NR16	-2407,0956	33077,3291	-2322,6394	33246,0293
NR08NR17	1304,5925	36821,9737	-4287,5273	37093,7002
NR08NR18	9020,0211	33734,4106	-7286,493	35671,6164
NR08NR19	27728,3186	28251,1374	-14706,9509	42228,9098
NR08NR20	16633,3147	28817,2287	-10036,8576	34753,9687
NR08NRMO	18685,8425	-16123,9283	-6275,1143	25466,033
NR09NR10	3880,0064	1848,2861	-1835,1067	4673,1389
NR09NR11	6503,8415	322,1577	-2798,0814	7087,5242
NR09NR12	10639,481	-46,4482	-4815,7365	11678,6999
NR09NRMO	14716,7051	-20899,6626	-4068,4971	25883,0055
NR10NR11	2623,8352	-1526,1284	-962,9748	3184,4779
NR10NR12	6759,4759	-1894,7321	-2980,626	7626,5756
NR10NR13	-16467,3695	19336,4778	5090,7613	25903,4646
NR10NR14	-13512,4178	23036,4912	3455,9376	26929,7023
NR10NR15	-12925,7109	25377,201	2973,3033	28634,1905
NR10NR16	-10256,234	26453,3105	1719,0832	28423,9902
NR10NR17	-6544,5459	30197,955	-245,8048	30899,9674
NR10NR18	1170,8827	27110,3919	-3244,7704	27328,9746
NR10NR19	19879,1802	21627,1187	-10665,2283	31251,5786
NR10NR20	8784,1763	22193,21	-5995,135	24609,7942
NR10NRMO	10836,6987	-22747,9487	-2233,3904	25296,0717
NR11NR12	4135,6395	-368,6059	-2017,655	4616,3098
NR11NRMO	8212,8636	-21221,8203	-1270,4157	22791,0232

	Δx (m)	Δy (m)	Δz (m)	Δl (m)
NR12NR13	-23226,8466	21231,2076	8071,3834	32486,8867
NR12NR14	-20271,8953	24931,2204	6436,5596	32771,0968
NR12NR15	-19685,188	27271,9308	5953,9254	34157,1964
NR12NR16	-17015,7111	28348,0403	4699,7053	33395,1051
NR12NR17	-13304,023	32092,6848	2734,8173	34848,4816
NR12NR18	-5588,5944	29005,1218	-264,1483	29539,791
NR12NR19	13119,7031	23521,8485	-7684,6062	28008,162
NR12NR20	2024,6992	24087,9399	-3014,5129	24360,122
NR12NRMO	4077,2241	-20853,2143	747,2394	21261,2011
NR13NR14	2954,9519	3700,0136	-1634,824	5009,4402
NR13NR15	3541,6586	6040,7232	-2117,4579	7315,5526
NR13NR16	6211,1354	7116,8327	-3371,6781	10029,742
NR13NR17	9922,8236	10861,4772	-5336,566	15649,6981
NR13NR18	17638,2521	7773,9141	-8335,5317	21000,5421
NR13NR19	36346,5497	2290,6409	-15755,9896	39680,8508
NR13NR20	25251,5458	2856,7322	-11085,8963	27725,414
NR14NR15	586,7078	2340,7101	-482,6306	2460,9109
NR14NR16	3256,1836	3416,8192	-1736,8534	5029,3185
NR14NR17	6967,8727	7161,4644	-3701,74	10655,5479
NR14NR18	14683,301	4073,9006	-6700,7067	16646,1846
NR14NR19	33391,5983	-1409,3728	-14121,1649	36282,1232
NR14NR20	22296,594	-843,281	-9451,0699	24231,6312
NR15NR16	2669,4769	1076,1095	-1254,2201	3139,6157
NR15NR17	6381,1651	4820,754	-3219,1081	8620,9972
NR15NR18	14096,5936	1733,1909	-6218,0737	15504,2685
NR15NR19	32804,8911	-3750,0823	-13638,5316	35724,411
NR15NR20	21709,8872	-3183,991	-8968,4383	23704,2167
NR16NR17	3711,6882	3744,6445	-1964,888	5626,7021
NR16NR18	11427,1167	657,0815	-4963,8536	12476,0007
NR16NR19	30135,4143	-4826,1918	-12384,3115	32936,4007
NR16NR20	19040,4104	-4260,1004	-7714,2182	20980,8209
NR17NR18	7715,4285	-3087,5631	-2998,9656	8834,8558
NR17NR19	26423,7261	-8570,8363	-10419,4235	29668,787
NR17NR20	15328,7222	-8004,745	-5749,3302	18223,6238
NR18NR19	18708,2976	-5483,2732	-7420,4579	20859,767
NR18NR20	7613,2937	-4917,1819	-2750,3646	9471,2947
NR19NR20	-11095,0039	566,0913	4670,0933	12051,1137

All combinations $\Delta x = x_i - x_j$, $\Delta x = y_i - y_j$, $\Delta x = z_i - z_j$ and $\Delta l = \sqrt{\Delta x^2 + \Delta y^2 + \Delta z^2}$. Station i is the first station and j is the second. NR19NR20 means thatNR19 is i and NR20 is j.

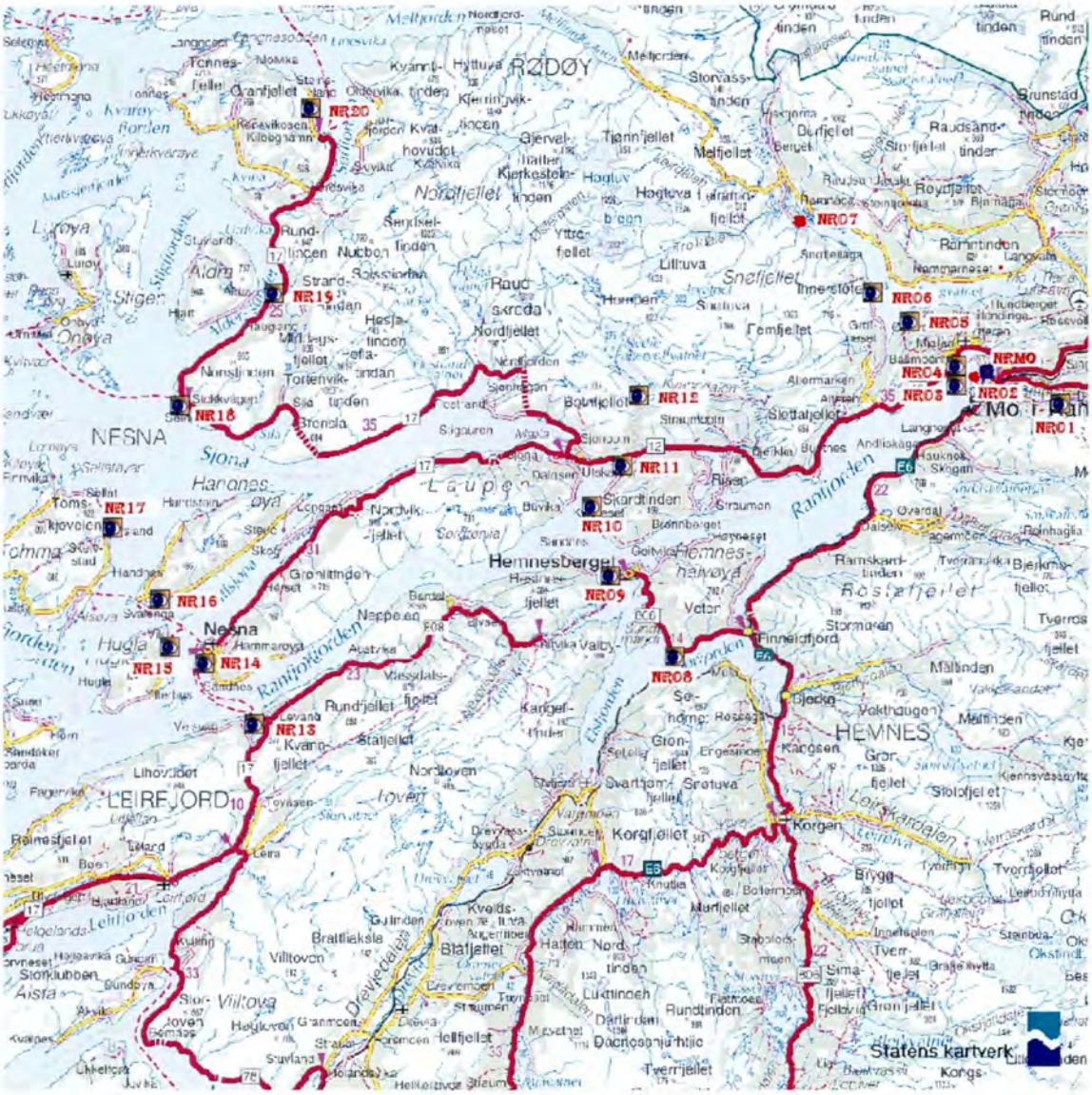

Fig. 5.1.7 The control points in Mo i Rana

5.1.5 Conclusions

The GPS observations in 1994 and 1997 were performed as standard vector observations. Vectors shorter than 10 km were measured for sessions of at least 1 hour while longer vectors were observed for about 3-4 hours. These session lengths are not sufficient for highest level of accuracy. The vectors give different results, depending on time of the day, varying by up to 1 cm or more. This is due to, among other things, the variations of the atmosphere, ionosphere and satellite geometry. In 1999 the stations were instrumented for at least 3 full days. GPS-data were analysed as single-point solutions with independent solutions for each day. The final coordinates are computed as means of the single-point solutions. In 1999 the GPS-instruments as well as the antennas had a better quality than earlier instrumentation.

By processing the 1999 data as vectors, in a similar way as in 1994 and 1997, it is again confirmed that results from short sessions depend on the time of the day as well as on the length of the sessions.

Consequently, it seems useless to compare the 1999 results for Mo i Rana with results from earlier campaigns. The risk of drawing wrong conclusions about geological strain is high. It would be, in fact, a waste of time and resources.

As reported in the technical report for 1998, in the MASI computations, the standard Ashtech reduction software was used for computing vectors for non-overlapping 4-hour sessions spanning at least three full days. The final vectors were means of these short session vectors and subsequently adjusted in a horizontal network by means of the Norwegian Mapping Authority's program "GUNDA". Based on the statistics from this adjustment, it could be concluded that the GPS observations can reveal horizontal and vertical deformations of 3 mm and 9 mm respectively, assuming again that systematic errors can be avoided, so that there is consistency from campaign to campaign.

Most likely the data from 1999 in Mo i Rana as well as the Bremanger and Masi measurements from 1997 have such a high precision that comparing these with future measurements may reveal significant information about the deformation going on. However, to achieve this, future field measurements have to be carried out in a similar way as the earlier ones, and the processing has to be realized in the same reference frame with use of the same programs.

Finally, it should be mentioned, that by use of more advanced analysis methods, as for example the computation of the full strain tensor, a more reliable detection of the three-dimensional deformation field from repeated GPS campaigns may be possible.

5.1.6 References

Holsen, 1986: Rapport om måling av jordskorpeforskyvelser i Yrkje, Rogaland. NTH, 24.11.86.

Sundsby, J., 1996: Nivellement over Stuoragurra-forkastninga i Finnmark 1996. Statens kartverk, report in Norwegian.

5.2 NEOTECTONICS IN THE RANAFJORDEN AREA, NORTHERN NORWAY: REPORT ON THE GPS CAMPAIGN IN 1997

By Terje Skogseth, NTNU

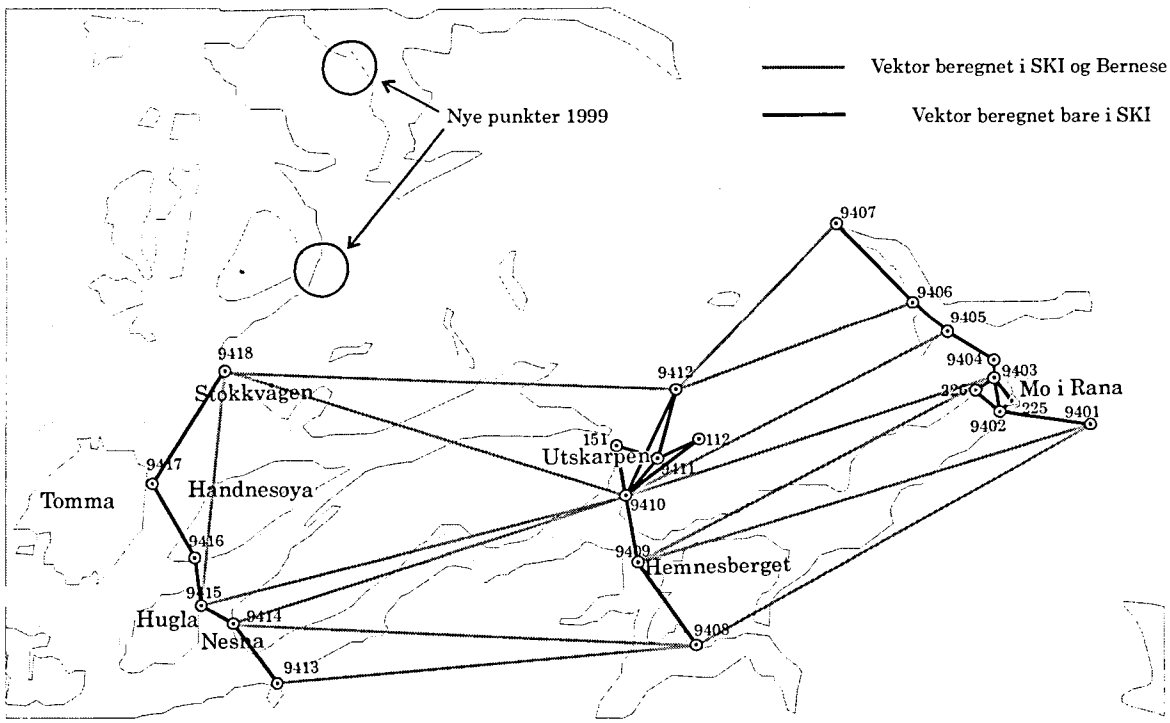

Fig. 5.2.1 GPS net with 18 control points (numbered 9401-9418)

5.2.1 Introduction

In summer and autumn 1999 the final calculations of the 1997 campaign, were carried out as a student project (MSc final thesis) by our student Arngrim Utskarpen. In the thesis the measured GPS baseline vectors were processed and the GPS network with 18 control points was adjusted.

A slightly shortened version of his thesis is included as Appendix 1 (in Norwegian). Results and figures in this report are mainly copied from the thesis of Utskarpen (1999).

The thesis is carried out at the Department of surveying and mapping, NTNU. It describes how GPS can be used in high precision tasks, such as detection of neotectonic movements. As a case study he used the measurements from 1997 in Ranafjorden in different computer programs. Fjellanger Widerøe AS (Morten Strand) helped us with the calculations using the Bernese software.

We have the complete set of all observations (raw data, baseline vectors and variances/covariances of the vectors) and the adjustments of the network stored at our department. A CD contains all the data files from 1997 as mentioned above.

5.2.2 About the network

A summary from last year's report describes the project and the measurements:

In 1994 a GPS network with 18 control points, numbered from 9401 to 9418, was established. The network was designed to measure the geological strain in the Ranafjord area.

The points in the network are situated in three profiles across the fjord. There are 7 points in the 22 km long eastern profile at Mo, 5 points in the 19 km long profile at Utskarpen and 6 points in the 25 km long western profile at Nesna. The distances between the profiles are approximately 25-30 km. See figure.

In 1997, the GPS network was measured for the second time. The fieldwork was carried out by staff from Department of surveying and mapping, NTNU. We used 4 GPS receivers: Leica SR9500 sensors with Leica CR344 controllers. Approximately 28 baseline vectors were measured. The network is built up by triangles and quadrangles, as the lines in the figure above shows. The measuring time for the short vectors within the three profiles were at least 1 hour (vectors shorter than 10 km), and the longer vectors between the profiles were measured for about 3-4 hours (vectors up to 30 km long.). We also connected our GPS network to the official national Norwegian network (SK network), established by Statens kartverk (the Norwegian Mapping Authority) by measuring between 4 points in the SK network and 4 points in our network at Mo and Utskarpen. One of the SK points we used, is a national point of first order. We therefore have exact absolute coordinates for the calculations of our GPS network. This is an important advantage when calculating the measured baseline vectors, as the accuracy of a vector is also dependent upon good absolute coordinates.

The 1999 campaign was carried out by Norwegian Mapping Authority.

5.2.3 Results of the calculations of the baseline vectors from 1997

The calculations indicate standard deviations (rms) of approximately 10 mm for the distance between the profiles and 4-5 mm between control points in the same profile. The corresponding standard deviations of the heights are about 50 % higher.

We carried out the final calculations with good coordinates of the orbits of the GPS satellites, they were loaded from Internet (Utskarpen 1999).

The GPS vectors were calculated by use of two different methods or computer programs.

- Bernese from the University of Bern in Switzerland. This is a program which gives the user wide possibilities of choosing the strategy and the parameters of the calculations. Bernese will therefore usually give better results than the more commercial software.
- Leica SKI is a standard computer program that is used in transferring field data, computing baseline vectors and adjust GPS network.

For the 1997 measurements we have used Bernese for the long GPS baseline vectors between the profiles, and we used SKI for the short GPS vectors within the three profiles, as the observation time for the short vectors were not long enough to take full advantage of the Bernese program.

Long vectors between the profiles

For the 1997 measurements we have used Bernese software for the long GPS baseline vectors between the profiles. Several of the long vectors between the profiles are also calculated in SKI. A comparison of the results is given in chapter 6 in (Utskarpen 1999).

The baseline vectors listed in the table are those which were chosen to be part of the adjustment of the whole GPS network.

Unit: meter

Coordinate type: Cartesian (geosentric coordinate system)

Reference ellipsoid: WGS 1984

From - to	ΔX	ΔY	ΔZ
9410-9418	-1170.9234	-27110.4058	3244.6861
9412-9403	-5355.3779	19784.5366	-94.1948
9412-9406	-8736.8370	13767.8218	2044.4804
9412-9407	-12185.0040	7788.8262	4162.6165
9418-9412	-5588.5949	29005.1260	-264.1145
9410-9418	-1170.8840	-27110.3922	3244.7504
9410-9414	13512.4160	-23036.4917	-3455.9785
9410-9415	12925.7155	-25377.1912	-2973.3067
9410-9418	-1170.8935	-27110.3997	3244.7246
9414-9418	-14683.3037	-4073.9051	6700.7120
9415-9418	-14096.6018	-1733.2064	6218.0358
9403-9409	15994.9248	-19830.9617	-4721.4633
9401-9408	18883.5735	-21984.4470	-5860.3825
9401-9409	14914.4844	-26760.1704	-3653.7315
9408-9414	5663.2729	-29660.5256	585.7942
9408-9413	8618.2361	-25960.5433	-1049.0173
9405-9409	18042.3984	-16416.6714	-6083.0956
9405-9410	14162.3639	-18264.9307	-4247.9994
9405-9408	22011.5084	-11640.9016	-8289.7116
9403-9410	12114.8563	-21679.2649	-2886.4173
9403-9411	9491.0151	-20153.1344	-1923.4434

Short vectors between the control points in a profile

The GPS vectors between the control points within the three profiles are calculated by use of the SKI computer program. The baseline vectors listed in the table are those which were chosen to be part of the adjustment of the whole GPS network.

Unit: meter

Coordinate type: Cartesian (geocentric coordinate system)

Reference ellipsoid: WGS 1984

From - to	ΔX	ΔY	ΔZ	Remarks
9402-9401	-640.4573	5925.9263	-226.9583	
9403-9402	1720.9061	1003.2896	-840.7705	
225-9402	442.7257	-65.3970	-187.7752	
225-9403	-1278.1805	-1068.6869	652.9973	
225-9403	-1278.1813	-1068.6858	652.9901	
9403-9404	-810.8478	-198.5216	394.9492	
9403-9404	-810.8452	-198.5236	394.9634	
9405-9404	1236.6438	3215.8130	-966.6447	
9403-9405	-2047.4886	-3414.3374	1361.5930	
9405-9406	-1333.9502	-2602.3812	777.1287	
9407-9406	3448.1935	5979.0127	-2118.1210	
9409-9408	3969.1170	4775.7306	-2206.6105	
9409-9408	3969.1235	4775.7336	-2206.6044	
9410-9409	3880.0189	1848.2903	-1835.1287	
9410-9411	-2623.8455	1526.1241	962.9535	
9411-9412	-4135.6273	368.6018	2017.6693	
9410-9412	-6759.4748	1894.7287	2980.6258	
9413-9414	-2954.9611	-3700.0181	1634.8117	
9414-9415	-586.7219	-2340.7034	482.6240	
9515-9416	-2669.4482	-1076.1121	1254.2244	
9418-9417	7715.4257	-3087.5649	-2998.9778	
9416-9417	-3711.6534	-3744.8004	1964.8448	Problems
9415-9418	-14096.6092	-1733.2223	6218.0075	

5.2.4 Results of the adjustments of the GPS network from 1997

The calculations indicate half axis of the 95% error ellipse (2D) of approximate 5-10 mm in a free net adjustment. The corresponding standard deviations of the heights (1D) are as expected higher.

See Appendix 1 for more details. As there were used different methods when measuring and in the calculations, the comparison of different campaigns (1997 and 1999) can be done by comparing the vectors between the control points. This adjustment is also a tool to mark outliers (gross errors) and test the quality of the GPS observations.

5.2.5 Eccentricity between bolt and antenna

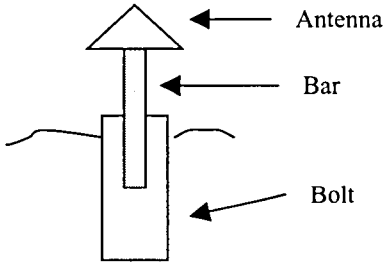

Fig. 5.2.2 The control points numbered 9401 to 9418 are permanently marked with aluminium bolts in rock. The antenna is mounted on a loose brass bar (each bar exactly of the same length), and the bar is mounted in a centric hole in the bolt when the measurements are carried out.

Eccentricity in height

The phase centre of the antenna type used in 1997, is (0,175 + 0,039 =) 0,214 m above the top of the bolt. In the calculations we entered 0,214 m as height of the antennas for the control points. The top of the bolt is therefore the reference for the heights of the control points in the calculations.

Eccentricity in the 2D-plane (ground plane)

The originally GPS base line vector is between the phase centres of the antennas, see figure. We usually want to define the baseline vector to be between the top centre of the two (permanently marked) bolts. If the bolt is not mounted exactly vertical, the phase centre will not be exactly vertical above the centre of the top of the bolt. This skew line must be corrected, if we want the final baseline vector to be defined between top centres of the bolts. We have measured this eccentricity for the bolts, thus we are able to correct the measured vector from the distance between antenna centres to the distance between the bolts.

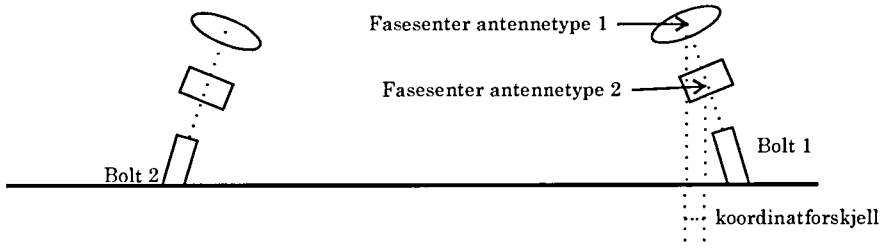

Fig. 5.2.3 Skew bolts showing phase centres, bolts and coordinate difference.

The eccentricities are measured by use of the optical plump of a theodolite. The optical plumb was centred at the top of the brass bar that is placed centric in the hole of the bolt of the control point. The bar was removed, and the bearing and the distance from centre of the hole of the bolt to the optical plumb, were measured by use of a compass and a tape.

The table shows the eccentricities (measured in 1994) measured from the bolt to the eccentric point. The eccentricity refers to a point 144 mm higher than (above) the top of the bolt.

Point	Bearing (gon/grads)	Distance (mm)	Remarks
9401	150	7	
9402	270	5	
9403	250	6	
9404	80	4	
9405	165	4	
9406	140	4	
9407	20	4	
9408	200	1	
9409	210	13	
9410	320	3	
9411	40	2	
9412	360	3	
9413	300	1	
9414	300	1	
9415	80	12	
9416	180	6	
9417	320	8	The brass bar is permanently mounted
9418	230	7	

5.2.6 Conclusions

When we compare results from different campaigns, we must be aware of:

- Different types of antennas have different heights from the top bolt to the phase centre
- The eccentricity in coordinates (2D) is also dependent of the height of the antenna

The calculations in Appendix 1 are not corrected for the eccentricity in the ground plane (2D). The main (and the most difficult) calculations are to decide the base line vector. The corrections because of the eccentricities in height and in ground plane must be carried out in such a way that two campaigns with different measuring equipment can be compared.

Comparisons between campaigns

1994 campaign

The control network was established in 1994 and the first measurements were carried out at the same time. Due to some serious problems (at the field work carrying out both the setting out and the measurements within the planned time limit, and later disc crashes and other problems at the office), we have not been able to, and we considered it too difficult and time consuming to, restore the data and do any further calculations.

1997 and 1999 campaigns

As reported by Mr Lars Bockmann, Norwegian Mapping Authority (Statens kartverk), a new method was introduced in the 1999 campaign; three or six days of observations in each control point, combined with advanced software (GIPSY) when calculating. This approach gives absolute coordinates and heights of the control points with a very high precision. The 1999 campaign uses methods that are significant better than the methods available (within the cost and time limits) for the 1997 measurements, where we only are able to calculate relative values.

The change of methods makes it more difficult to compare the 1997 and the 1999 measurements, but the great advantage of changing to a more precise method, makes it easier to detect smaller size of neotectonic movements in the future. Methods:

- 1997: Baseline vectors and adjusted network
- 1999: Absolute coordinates and heights

One way of comparing the results of the 1997 and the 1999 campaigns, is to compare the measured baseline vectors from 1997 with vectors calculated from the coordinates and heights of the control points in the 1999 campaign.

There are some points to take into consideration when doing this comparing:

- Different GPs receivers and antennas are used
- Different measuring techniques are used (absolute vs relative positions)
- The standard deviations of the vectors will be much better for the 1999 vectors
- Different heights of the antennas. See chapter 5 about eccentricity between bolt and antenna.

Suggested method of comparing 1997 and 1999 is to use hypothesis tests, where we test the baseline vectors and use their standard deviations to find out if there are any significant difference for one vector at 95% level between two control points.

An assumed standard deviation of a short GPS vector of approximately 5 mm in 1997 and 1 mm in 1999 means we have an uncertainty of ± 10 mm for a vector from 1997 and ± 2 mm for a vector from 1999. These uncertainties indicate that we must have a movement of about 15-20 mm at least, before we can state that there is a significant difference of the lengths between two control points.

Compared to the assumed values of neotectonic movements in the Rana area, we assume we cannot detect any movements so far, the uncertainties of the baseline vectors considered. Partly for this reason a detailed comparison between 1997 and 1999 has not yet been carried out.

The 1997, and especially the 1999 campaign, will give a very good foundation for further surveying of the movements in the GPS network. The time horizon to detect movements for this neotectonic area is considered to be longer than the time limit of the NEONOR project.

5.3 LEVELLING OF SHORELINES IN NORTH-ØSTERDALEN

By Morten Thoresen, NGU

5.3.1 Background and purpose of the study

Based on detailed levelling of shoreline features from glacial dammed lakes in North-Østerdalen, Holmsen (1916b) postulated that the presence of gabbro massifs could have influenced the isostatic uplift in the region. The mountain of Tron in Alvdal is one of the areas where Holmsen, according to his measurements, recorded irregular isobase orientation (Fig. 5.3.1). The purpose of this study has been to investigate Holmsen's postulates and look at possible neotectonic movements in this area.

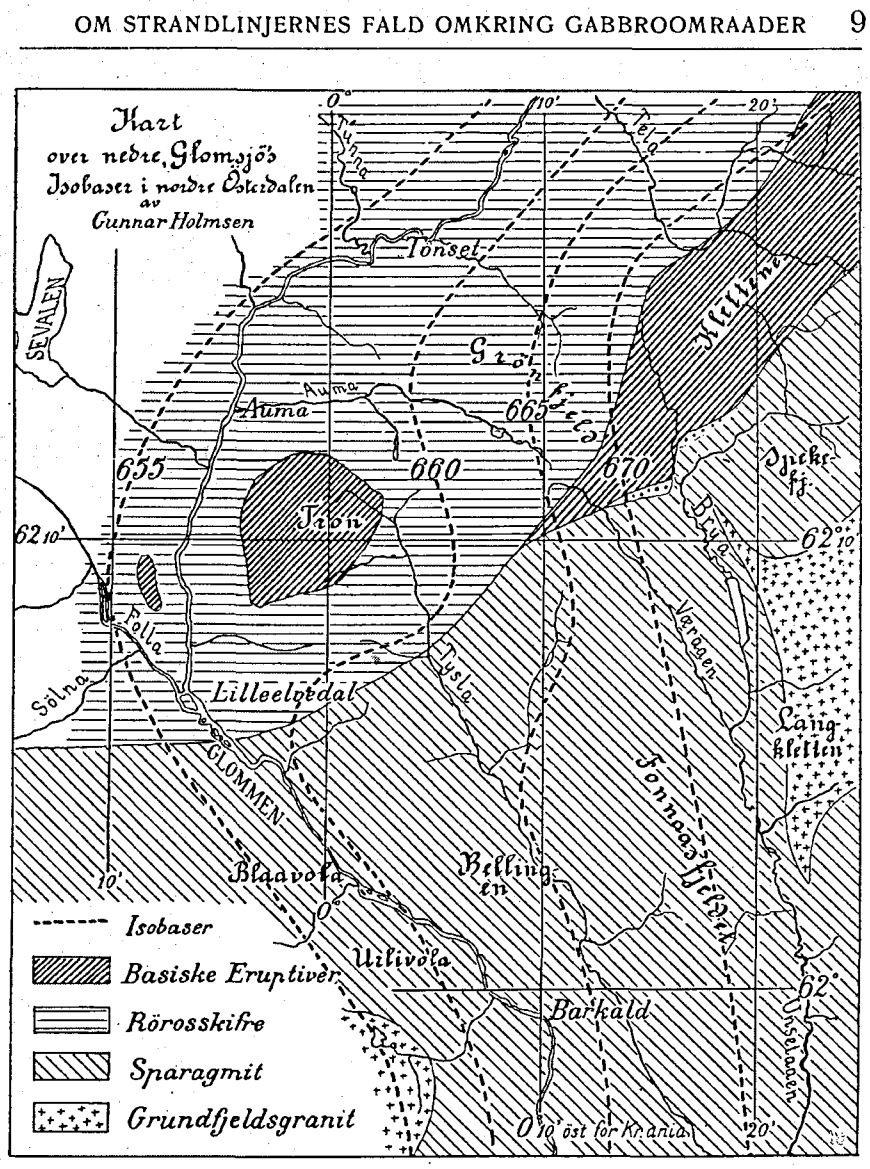

Fig. 5.3.1 Original figure from Holmsen (1916b).

5.3.2 Field method

Differential GPS (Global Positioning System) has been used with a base-point near Alvdal municipality centre (WGS – 84: 6887779, 5865600, height 565,443 m a.s.l.).

A geological evaluation was also needed to choose the right localities to get comparable sites and measurements. The measurements are mainly focused on The Lower Glåmsjø (Holmsen 1915) level (about 660 m a.s.l.) and a few from Upper Glåmsjø (about 720 m a.s.l.). These lakes drained to Rugeldalen and Kvikne during the deglaciation of the area about 10.000 years ago. The lake levels appear as different landforms:

- Lateral terraces along the valley sides (Fig. 5.3.2) (mostly erosional)
- Gravel and sand terraces deposited out in the lake as glaciofluvial fans and deltas
- Beach ridges deposited along the borders of the glacial dammed lake (Fig. 5.3.3)

Fig. 5.3.2 Typical lateral terrace at Brenna (1005 5).

Fig. 5.3.3 Beach ridges at Ripan appear as small but distinct ridges on top of other deposits and are light in colour because they are dry.

5.3.3 Registrations

The measurements are recorded in three periods in autumn 1999 and 33 sites are measured (Table 5.3.1).

Table 5.3.1 GPS measurements in the Alvdal region. corr. level is based on correction for measure equipment height. Geological deposition: S – lateral terrace, V – beach ridge, T – glaciofluvial terrace.

Fieldnr	Geological evaluation	North	East	Height m a. s. l.	Std. Deviation	Corr. m a. s. l.	Geological deposit
1004s002	Less good	6888494.23910	586193.36519	657,95149	0,150	656,17	S – lateral level
1004s005	OK, innerlevel	6888169,71526	586192,95576	656,96751	0,043	656,12	S
1004s006	Good	6887920,97009	586220,64066	658,93826	0,380	658,09	S
1004s009	Less good	6891001,08386	585327,66614	656,51968	0,408	656,52	S
1004s011	Good	6890692,22051	585461,44623	657,43656	0,796	656,84	S
1004s014	Good	6890644,83255	585518,97824	657,51875	0,265	656,82	S
1004s015	Very good	6890552,07170	585676,58172	658,40784	0,205	657,95	S
1004s017	Good	6896934,98007	574778,36876	662,00033	0,808	661,70	T - terrace
1004s018	Good	6885456,40545	580254,11162	661,60918	0.081	660,90	V - beach ridge
1005s002	OK	6885454,97891	58026,29518	661,40575	0,161	660,70	V
1005s003	OK	6889820,03101	579985,85088	654,62687	0,078	653,93	S
1005s004	Less good?	6889635,84702	579700,39279	713,86963	0,096	713,37	S
1005s005	Good	6890372,26111	586020,91403	657,80611	0,516	657,81	S
1005s006	Very good	6899252,38773	587951,49276	662,75624	0,240	661,96	V
1005s007	OK	6899271,34492	587949,29094	661,80464	0,195	661,00	V
1005s008	OK ? innerlevel	6898799,50987	587319,94772	662,56541	0,542	662,56	T/S
1005s009	OK ?	6899207,42932	587745,64986	656,65422	0,302	655,85	T/S
1005s010	Good	6899119,95324	588791,75769	720,02408	0,603	719,22	T
1005s011	OK ?	6900007,94946	589761,67509	658,80626	0,686	658,06	T
1005s012	Less good	6900137,40449	589829,10260	669,11295	0,346	668,31	T
1005s013	Very good	6902079,42276	589509,63420	666,63420	0,451	665,83	V
1005s014	Good	6902094,16577	589506,22502	665,22502	0,291	664,53	V
1005s015	Good	6902101,67089	589507,54593	664,54593	0,458	663,75	V
1007s001	Very good	6886955,64629	583546,05026	656,80113	0,088	656,05	S
1007s002	Less good	6898092,72929	587265,50382	712,97330	0,086	712,97	S
1007s003	Good	6899529,49902	580474,04767	654,30485	1,674	653,50	S/T
1007s004	Good	6911406,48423	598149,59956	671,19476	0,789	670,69	S(B)
1007s005	Good	6911414,76882	598148,81292	671,05946	0,827	670,26	S
1007s006	Good	6905862,82095	602070,89227	671,88755	0,215	671,28	V
1007s007	OK	6905857,42069	602092,08487	670,98818	0,814	670,19	V
1007s009	OK, small remnant	6893423,98293	591949,31344	666,09641	0,231	665,45	S(T)
1007s010	Good	6888816,38141	592906,43918	661,25938	0,098	660,66	S
1007s011	OK ?	6876689,47822	599237,16629	665,34134	0,160	664,64	S

5.3.4 Results and discussion

Based on the geological evaluation and the results from the measurements the recorded values give a picture of the isostatic uplift (after 9200 BP), but they also point out that the geological explanation of the phenomena is complicated.

The erosional levels (lateral terraces) give a picture of an uplift centre in the east (Norwegian/Swedish border?), with the lowest values west of Alvdal. The measurements also point out that these landforms were deposited during the same time interval. They do not indicate a special situation around the mountain of Tron (see 1004 2-15, 1005 9).

If we on the other hand look upon the terraces and the beach ridges, they both show a different picture and they do not coincide with the lateral forms. This is clearly justified if we compare 1005 3 with 1004 18 and 1005 2. The two latter ones are from a beach ridge on Brennbakkmoen west of Alvdal, a ridge 4-10 m wide on the edge of the glaciofluvial terrace behind it. Point 1005 3 is from a very distinct level on a lateral terrace at Lian, 4-5 km north of Brennbakkmoen. According to both Holmsen's and my measurement, these localities should lie on the same isobase curve with a similar uplift, but the difference is about 7 meters (653,93 and 660,90). This is also the same for other localities where measurement are done on both beach ridges and lateral terraces, e.g. at Auma 1005 6-7, Ripan 1005 13-15 and also in Gammeldalen (1007 6-7). At Auma the landforms support this interpretation, and the ridges (1005 6-7) lie higher than the lateral level (1005 9). The phenomena at Brennbakkmoen/Lian is not due to different uplift, but clearly demonstrates that the ridge is deposited in another environment and during another time period than the lateral level. The critical factor for this kind of study seems to be to measure the right localities with regard to both type of and time of deposition. This has to be looked upon in the light of new Quaternary hypotheses of the deglaciation history of this area.

Some points of interest:

- Are the lateral levels subglacial rather than lateral deposits (this hypothesis is supported by other Quaternary investigations (B.A. Follestad pers. com)
- Do the lateral levels represent the exact level of the glacial dammed lake, or could they represent a level formed some meters below the lake level?
- How far above the lake level are the beach ridges formed?
- What could be explained by fluctuations in lake level during the deglaciation?

These questions have to be considered during a more detailed Quaternary study of the area.

5.3.5 References

Holmsen, G. 1915: Brædæmte sjøer i nordre Østerdalen. Nor. geol. unders. nr. 73.

Holmsen, G. 1916a: Rendalens bræsjø. Nor. geol. unders. Aarbog 1916.

Holmsen, G. 1916b: Om strandlinjernes fald omkring gabbroområder. Norsk Geol. Tidsskr. IV.

Thoresen, M. and Follestad, B. A. 1999: ALVDAL Kommune, Kvartærgeologisk kart i M 1:60,000. Norges geologiske undersøkelse.

6 SEISMICITY (TASK 10)

6.1 SEISMIC INSTALLATIONS IN RANA AND BREMANGER

By Erik Hicks, NORSAR

6.1.1 Summary

The seismic network installed in June 1997 in the Rana area was originally planned to be demobilized during 1998, but a continued presence was considered beneficial in light of the excellent results from the first year of operation. It was possible to maintain a network of four stations at minimal cost by installing a remote data acquisition system at the central station.

A six-station network was installed in the Bremanger area in September/October 1998 by NORSAR, using a similar remote data acquisition system to Rana. This has reduced the substantial transmission costs of the first year to next to nothing. There has been several hardware problems with the equipment in Bremanger, which has required several field trips in order to carry out repairs. This has unfortunately reduced the effective operating time of the Bremanger network.

6.1.2 Technical installations

Rana and Bremanger seismic networks

There are currently two networks operated under the NEONOR project, the reduced network in the Ranafjord area, now consisting of four stations (Fig. 6.1.1), and a six-station network in the Bremanger/Nordfjord area in Western Norway (Fig. 6.1.2). Both networks are based on the Seislog remote data acquisition system from the Institute of Solid Earth Physics (IFJF) at the University of Bergen (available free of charge). This is the same system used to operate the national Norwegian seismic network.

The systems run on standard Intel PC's, using the QNX UNIX operating system. The PCs used by NEONOR are old 486 machines that were donated by NORSAR and upgraded with AMD K6-2 processors and 2.5 GB hard disks. Data transmission to NORSAR is via modem (Rana) or ISDN (Bremanger),

The PCs have a diskloop containing approximately 10 days of continuous data, in addition to space for a minimum of around 5,000 events.

The Bremanger network has experienced numerous problems over the last 15 months, with various parts of the equipment comprising the network malfunctioning. Among others there has been problems with amplifiers, radio transmitters and receivers, modem/ISDN router, power supplies and the Telenor ISDN line. This is strange considering the equipment is identical to the Mo i Rana network, which has been operating without major problems for close to two and a half years.

Fig. 6.1.1 The current Mo i Rana seismic network (inverted black triangles). The two stations dismantled in September 1998 are shown by the green inverted triangles. The NNSN seismic station (MOR8) is shown by the triangle. The surface trace of the Båsmoen fault is also shown (black line).

6.1.3 Data analysis

The Seislog system detects events by continuously monitoring the value of the short term average over long term average for bandpass filtered data for each station (Utheim and Havskov, 1997). The short term and long term time windows, as well as filter parameters and trigger/detrigger thresholds are adjustable via remote login through the modem/internet, so fine-tuning is possible after installation. A minimum number of station triggers within a set time limit is considered an event detection, and a detection is entered into the detection database and data are saved to disk.

The detections and data are downloaded into a temporary database at NORSAR, where the data can be evaluated, and the event discarded or copied to the NEONOR database for analysis. This is all done from within the Seisan program package (Havskov, 1997), also from IFJF.

Fig. 6.1.2 The seismic network in the Bremanger area (inverted triangles).

6.1.4 System response

Since the sensors, amplifiers, gain and filter settings and digitizers are identical for all stations in both Mo i Rana and Bremanger, the same system response can be used. System response is calculated from sensor, filter and digitizer parameters, thus including all factors of influence on the signal. The Seisan program package includes a program for calculating system response, and creates a parameter file used directly by other Seisan programs during analysis, to calculate ground motion from the signal. This is necessary for calculation of magnitudes and synthetic waveform modelling. A system displacement response curve is shown in Fig. 6.1.3.

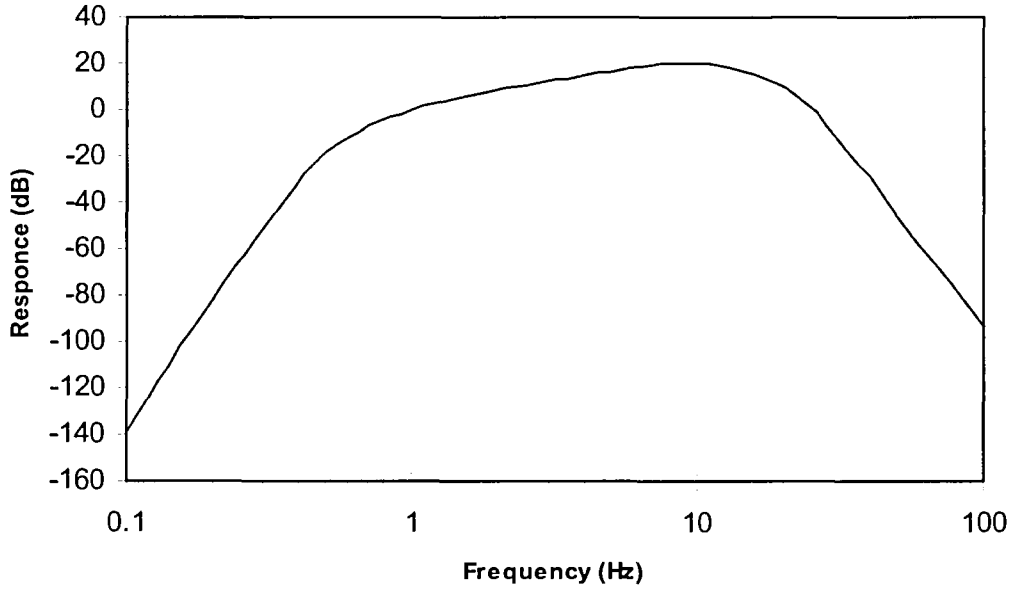

Fig. 6.1.3 System displacement response for the NEONOR seismic stations.

6.1.5 References

Havskov, J., (1997): *The Seisan earthquake analysis software*, Institute of Solid Earth Physics, University of Bergen, 236 pp.

Utheim, T. and J. Havskov, (1997): *The Seislog data acquisition system*, Institute of Solid Earth Physics, University of Bergen, 101 pp.

6.2 SEISMIC ACTIVITY IN THE RANA AND BREMANGER AREAS

By Erik Hicks, Hilmar Bungum and Conrad Lindholm, NORSAR

6.2.1 Introduction

During a total of 29 months operation (July 1997 – November 1999), the seismic network in the Ranafjord area has been used to detect and locate a total of almost 450 seismic events, of which around 350 are local earthquakes. The activity in 1999 has been somewhat lower than in 1997 and 1998, with only around 70 local quakes located. Almost all were within the previously defined area of high activity in the western parts of the network. One new focal mechanism has been determined, which shows the same inversion of the stress field as the earlier solutions.

The Bremanger network has experienced a number of technical problems since its installation in October 1998, which have reduced the effective time of operation. However, the data that are available from November 1998 to November 1999 have been analysed, the locations of the approximately 100 local earthquakes do not show any clear pattern of distribution in space and time. A number of quite large earthquakes have been located, the largest having a magnitude of M_L 3.9, the largest is this area for over 10 years. Five other earthquakes with magnitudes larger than M_L 2.0 have also been located. Earthquake focal mechanism solutions have been determined for a total of five of the largest earthquakes.

6.2.2 Results, Rana

As of December 1, 1999, 62 new local earthquakes have been located in 1999, bringing the total to 317. An additional 65 seismic events in total have been located by the network at greater distances (50 to 200 km from the network), and are outside the main area of interest. A total of 71 events have been classified as probable local explosions, and therefore removed from the maps. These explosions mainly originate from a talc mine a few km northwest of Mo i Rana, and from Storforshei Gruber around 40 km east of Mo i Rana.

The level of seismic activity has been significantly lower in 1999 than 1998 and the last half of 1997, probably a reflection of the cyclic nature of the seismic activity.

Event locations

The majority of the 1999 earthquakes are located within the active areas surrounding the Sjona fjord in the western part of the network. Fig. 6.2.1 shows the earthquakes from 1999 plus the older quakes. It is readily apparent that it is the same areas that are active, with a large number of the earthquakes occurring within the groups defined by earlier activity.

Focal mechanisms and derived crustal stress

One new focal mechanism solution has been determined in the Rana area using waveform modelling, bringing the total to ten. All solutions are listed in Table 6.2.1 (one composite- and eight individual solutions).

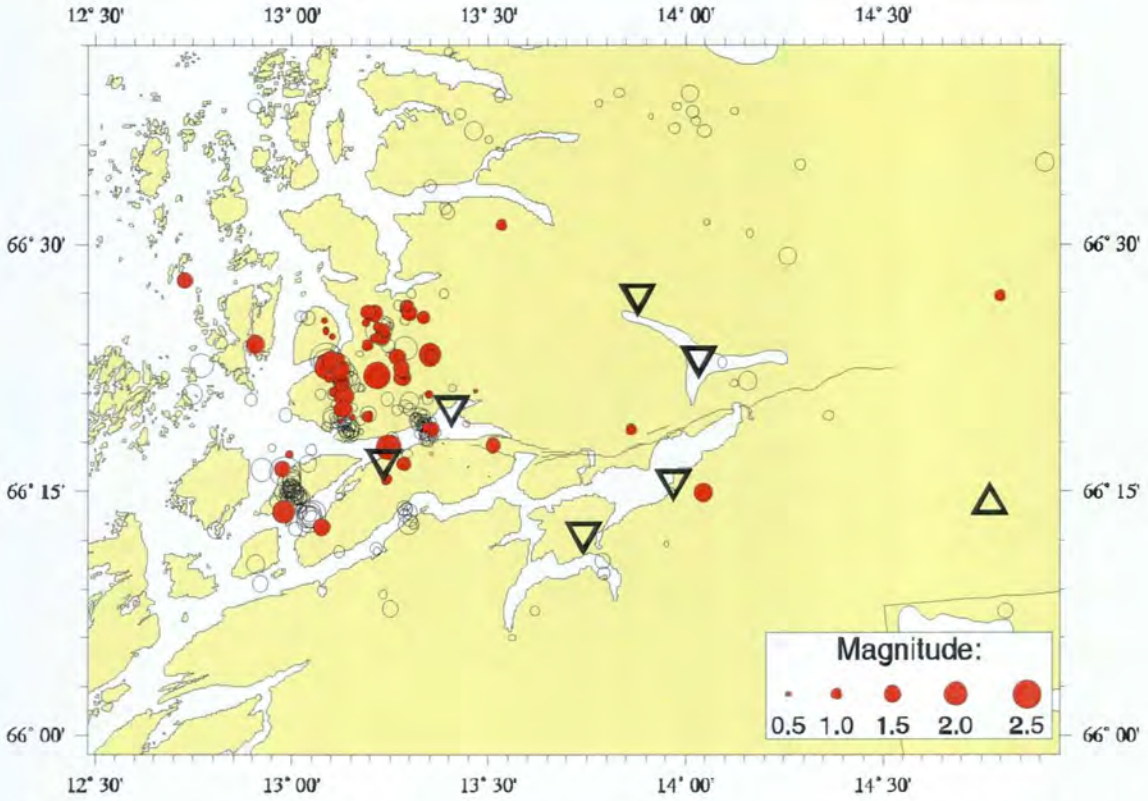

Fig. 6.2.1 Local earthquakes located by the NEONOR network in 1999 (red circles). Earthquakes located by the network in 1997 and 1998 are shown as open circles.

Table 6.2.1 Earthquake focal mechanism solutions determined using data from the NEONOR seismic network in Rana. The composite solution is determined by first motion polarities only, the other eight are determined by first motion polarities combined with full waveform modeling. P-trn, P-plng, T-trn and T-plng are the trend and plunge for the P (compression) and T (tension) axis respectively.

Date	Lat.	Lon.	Depth	Mag.	P-trn	P-plng	T-trn	T-plng
Comp.1	66,31	13,32	5 km	N/A	167	48	270	11
97.11.21	66,41	13,22	7 km	2,3	208	29	302	7
97.11.25	66,52	12,40	11 km	2,7	77	29	343	7
97.11.28	66,32	13,14	11 km	1,7	74	58	299	23
97.11.28	66,32	13,15	11 km	1,7	74	58	299	23
97.12.26	66,33	13,11	11 km	1,8	176	1	268	67
98.01.08	66,37	13,13	13 km	2,2	27	33	284	19
98.02.09	66,39	13,10	11 km	2,8	351	22	257	11
98.03.09	65,85	13,53	7 km	2,8	118	13	228	57
99.04.09	66,39	13,35	8 km	2,0	357	58	258	6

The new focal mechanism solution was determined by waveform modelling (using Herrmann's code, Havskov, 1997), using the first motion polarities to constrain possible solutions. All eight focal mechanism solutions within the network (seven old and one new) show a

rotation with regard to the regional stress field, while the focal mechanism for the earthquake further west has a maximum horizontal compressive stress direction that is closer to the regional trend. The M_L 2.8 earthquake further south has a compressive stress direction that complies more or less exactly with the regional stress field.

Magnitude and depth distributions

The magnitude distribution plot shown in Fig. 6.2.2 indicates that the detection threshold is around magnitudes (M_L) of 0.9. The detection threshold in the active areas near the Sjona fjord is most likely unchanged by the removal of two stations in October (further described in Section 6.1.2), due to the fact that the two closest stations have been retained. The effect on location precision should be similarly small.

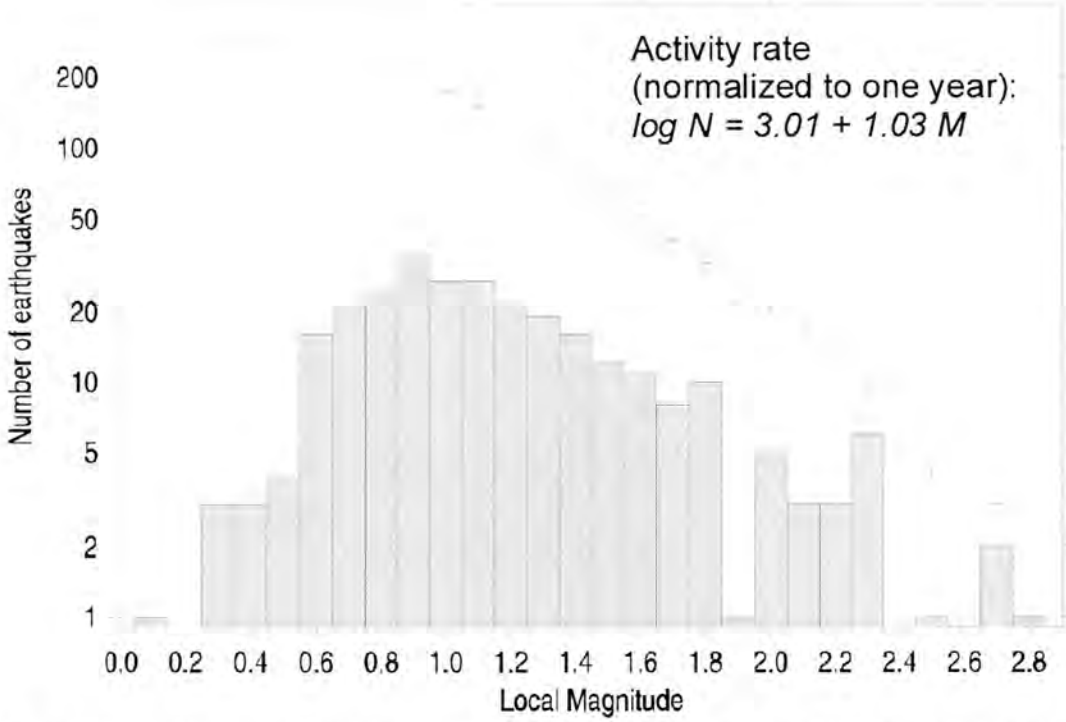

Fig. 6.2.2 Magnitude distribution for the earthquakes in the Ranafjord area determined by the NEONOR network (probable explosions removed). Note that the threshold of detection drops sharply below magnitudes around M_L 0.9. Crosses represent the cumulative number of earthquakes. The activity rate shown determined using the magnitude range M_L 1.0 to 2.8, and is normalised to one year.

A fundamental scaling relationship for earthquakes says that for a given region over a given period of time, the relation between number of earthquakes N of magnitude equal to or greater than M is given by:

$$\log N = a - bM$$

The *a* and *b* values have been estimated from the available date from the NEONOR network, giving values of a=3.30 and b=1.08. This gives a return period of 10.5 years for earthquakes of magnitude M_L 4 or larger, 126 years for M_L 5 and just over 1500 years for M_L 6. Although M_L

is not properly defined at the level of magnitude 6, it still gives a ballpark indication of the activity level in this area.

Fig. 6.2.3 shows a plot of the depth distribution within the network. The activity observed to the north and west of the Sjona fjord appears to have somewhat less shallow foci, with depths around 8-12 km. The approx. 50 earthquakes comprising the group by Handnesøya had hypocenter location depths around 7-9 km, but the witness reports of loud cracking and banging noises in conjunction with the earthquakes implies a shallower depth. These events have therefore been placed in the 3-5 km bin in Fig. 6.2.3. This illustrates the uncertainty in the depth determination of earthquake hypocenters, although a local network may provide epicenter locations within a few km, the hypocenter depths may still have errors of 5 km.

It should be noted that most of the depths observed (2-6 km) are very shallow compared to what is generally the case in Norway (5-30 km), and the slightly deeper earthquakes to the west and north of the Sjona fjord (8-12 km) would also be considered shallow in this sense. Shallow seismic activity appears not to be atypical for coastal areas in northern Norway where earthquake swarms have been studied, such as in Meløy (Bungum *et al.*, 1979) and in Steigen (Atakan *et al.*, 1994).

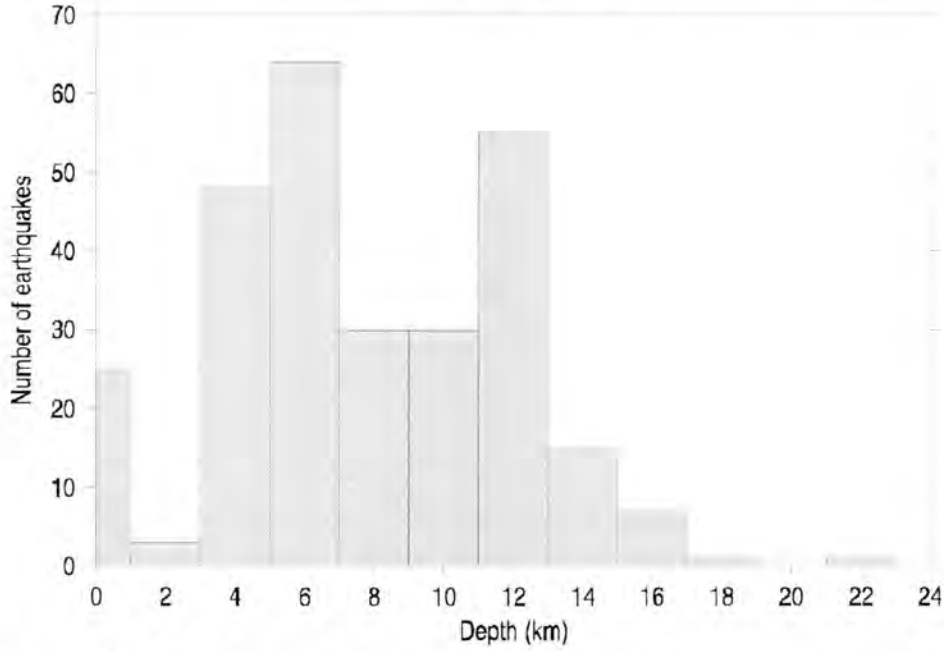

Fig. 6.2.3 Depth distribution of the earthquakes within the network (probable explosions removed).

6.2.3 Results, Bremanger

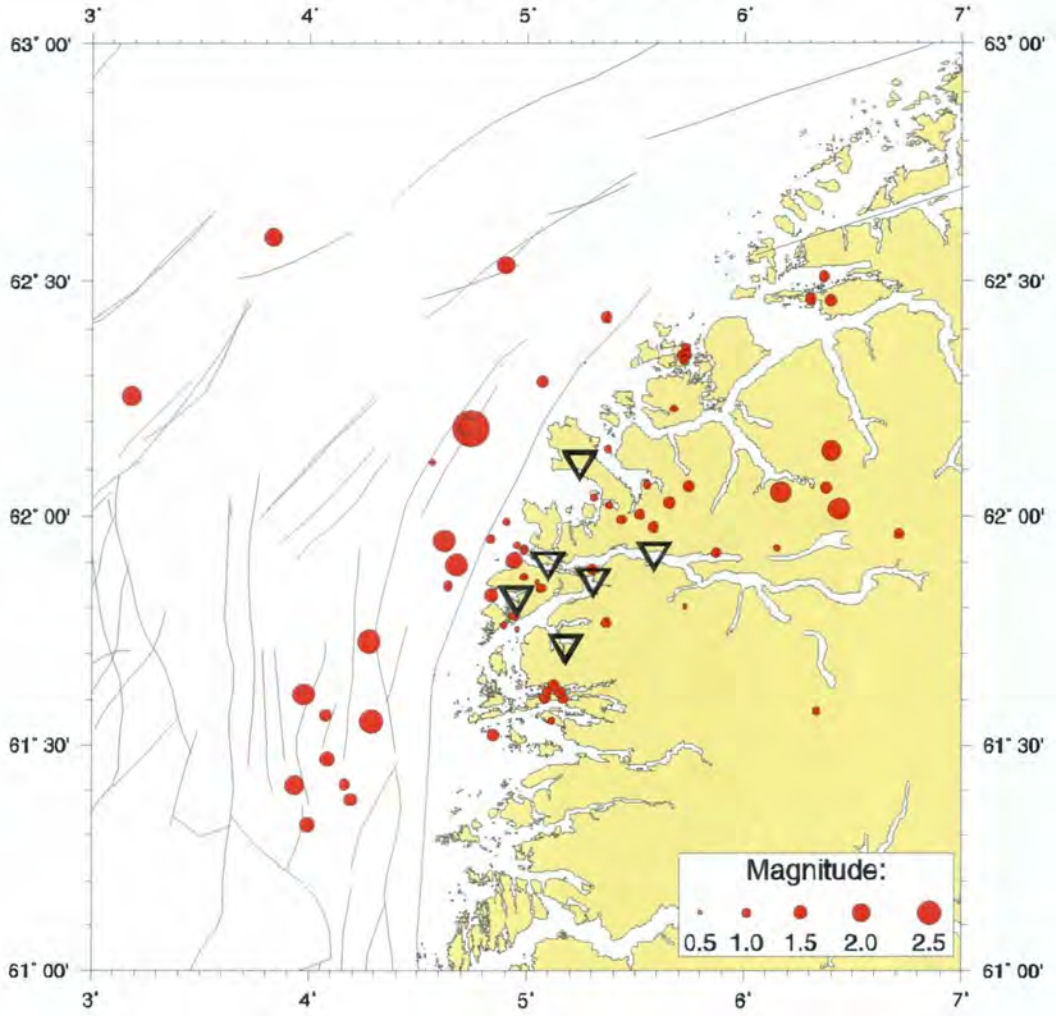

Fig. 6.2.4 Probable earthquakes located using data from the Bremanger network. The most certain explosions have been removed, but some of the smaller events on the map could also be explosions. The larger onshore events and all offshore events are most likely earthquakes.

A total of 113 seismic events were located in the vicinity (within ~200 km) of the Bremanger network. 22 of the events appear to be explosions, from the locations it is probable that they originate from Olivin AS, a large open-pit quarry east of Stadtlandet. The rest appear to be earthquakes, with magnitudes mainly in the M_L 1.0 to 2.3 range, although it is hard to be certain with events of such low magnitude. The earthquakes are shown in Fig. 6.2.4.

The 29. May 1999 ML 3.1 earthquake

The largest earthquake in the North Sea since 1989 occurred on May 29, just offshore from the network. This quake had a magnitude of M_L 3.9, and was felt over most of northern Sogn and Fjordane and the Møre coast. Depth was fairly shallow at around 10 km. The close proximity to the network meant that the signal was saturated (clipped), rendering the data unusable for further source studies of this earthquake. This is in part due to a relatively high gain used in order to enable the location of microearthquakes. However, it would most likely be impossible to avoid saturating the signal from an earthquake of this magnitude at this distance with the

equipment used in the NEONOR networks. This would require 24-bit digitizers at each station, with either digital transmission or data logging at each station, which would have been far beyond the budget of the NEONOR project. Nevertheless, first-motion polarities could be identified and used in the determination of a focal mechanism solution for this quake.

Focal mechanisms and derived crustal stress

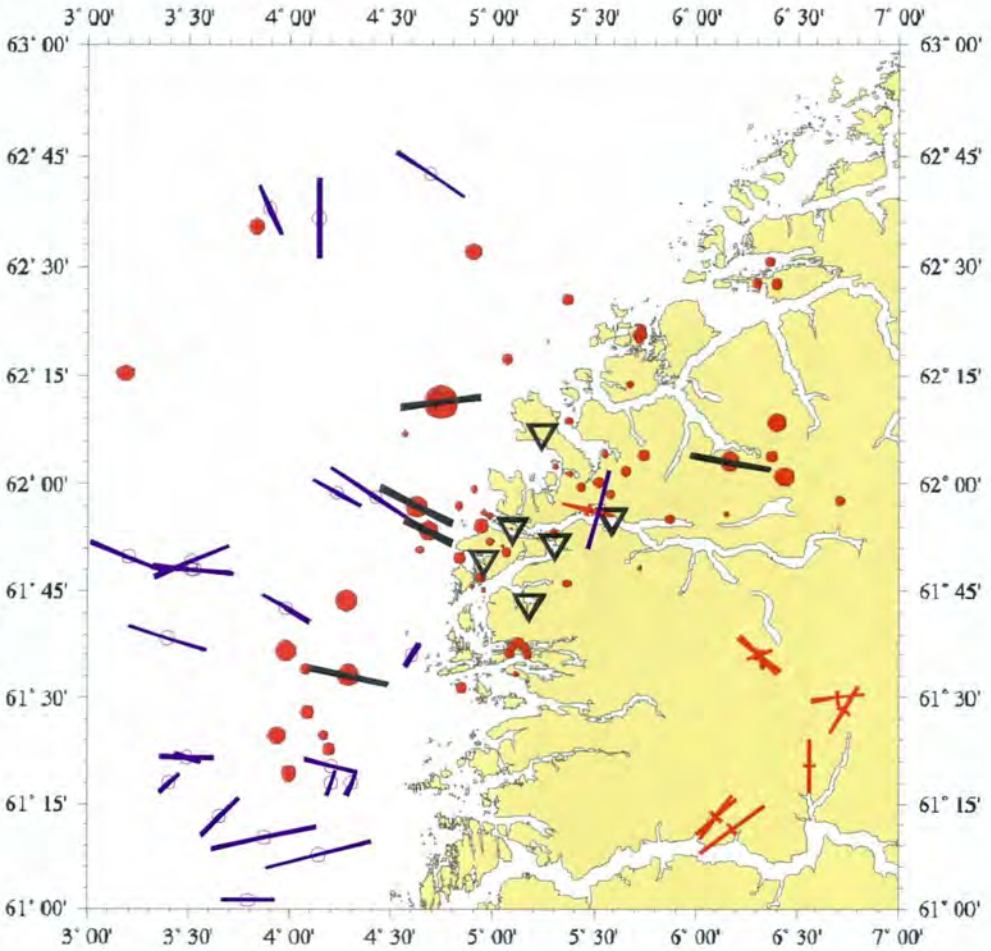

Fig. 6.2.5 Horizontal compressive stresses from new earthquake focal mechanism solutions (black bars), previous focal mechanism solutions (blue bars/circles) and in situ (overcoring) measurements (red bars).

Earthquake focal mechanism solutions could be determined for a total of five earthquakes in the Bremanger area, four offshore and one onshore. Four of the solutions vary from reverse to reverse/strike-slip, while the fifth is a normal/strike-slip solution. The onshore focal mechanism solution does not appear to differ from the offshore solutions in terms of mode of faulting or horizontal stress directions. All five solutions comply well with the regional WNW-ESE stress tensor of tectonic origin ('ridge push'), as shown in Fig. 6.2.5, with previous stress measurements included (earthquake focal mechanisms and *in situ* measurements).

*Table 6.2.2 Earthquake focal mechanism solutions determined using data from the NEONOR seismic network in Bremanger. The solutions with a * after the date are determined by first motion polarities only, the others are determined by first motion polarities combined with full waveform modeling. The 99.08.23 earthquake is the earthquake in Nord-Trøndelag described in section 6.2.4. P-trn, P-plng, T-trn and T-plng are the trend and plunge for the P (compression) and T (tension) axis respectively.*

Date	Lat.	Lon.	Depth	Mag.	P-trn	P-plng	T-trn	T-plng
99.05.29*	62,19	4,74	10	3,9	262	15	144	46
99.06.15	61,95	4,62	13	2,4	272	65	35	14
99.08.02*	61,55	4,29	24	2,5	283	15	67	72
99.08.07*	62.05	6,17	10	2,2	111	36	10	16
99.09.02	61,89	4,68	21	2,3	296	5	45	74
99.08.23¤	65,10	11,75	15	3,1	143	68	257	9

6.2.4 Other earthquakes

Two other significant earthquakes of regional interest were detected by the NEONOR networks in 1999, a M_L 3.1 earthquake in the coastal areas of Nord-Trøndelag in August, and the M_L 3.9 quake north of Tromsø in October.

The Nord-Trøndelag quake occurred close to the Leka island near the border between Nord-Trøndelag and Nordland on August 7. The quake was detected by both NEONOR networks, in addition to several stations in the national network. All available stations were used in the location, and a focal mechanism solution could be determined using available first-motion polarities only. The mechanism is an almost pure normal fault, with approximately EW-extension. This is similar to the observed stresses further north in Nordland (Rana, Meløy, Steigen), although Nord-Trøndelag and south Nordland have very low levels of seismic activity. The solution is included in Table 7.2.2.

On October 17, an earthquake was felt over large areas in Troms and Finnmark. The quake was detected by the Rana network and the national network stations in northern and central Norway. The hypocenter location is in the vicinity of the Senja FZ north of Tromsø. The azimuthal station coverage is quite scarce, so a focal mechanism solution has, as of yet, not been determined. The hypocenter depth is uncertain for the same reason.

6.2.5 Conclusions

Rana

The Rana area has long been known as one of the seismically most active regions in Norway (e.g., Byrkjeland, 1996). Local stress sources certainly play an important role in controlling the seismic activity in the Rana area, as evidenced by the change in the stress tensor from the plate tectonic derived coast-normal compression on the continental margin, to coast-normal extension indicated by the new focal mechanism solutions. (Bungum *et al.*, 1991; Hicks, 1996; Hicks *et al.*, submitted). The majority of the earthquakes used to determine the regional stress field in mid Norway are located on the margin (Byrkjeland, 1996; Hicks 1996), so it may be inferred that seismic activity is to a large degree controlled by local second and third order sources of stress (density inhomogenities, flexural stresses, topographic loads, geological features, etc.) rather than first order (plate motion related) effects. This is also indicated both by the Meløy (Bungum *et al.*, 1979) and the Steigen earthquake sequences (Atakan *et al.*,

1994). Byrkjeland *et al.* (in press) point in this respect to a possible correlation between topography and earthquakes on a larger scale along the Trøndelag and Nordland coastal areas, as the coastal areas adjacent to the most elevated provinces also have the highest levels of seismic activity. However, using the data from the current NEONOR network, it seems likely that postglacial rebound plays an important role in controlling the seismicity along the Nordland coast, although some more local stress sources should also be considered, given the concentrated areas of seismic activity (Hicks *et al.* in press).

The consistency of the NNW-SSE lineations observed in the five main groups of earthquakes on the local scale in the western parts of the network is remarkable, although the geological connection is at present uncertain, and should receive further attention both from a seismological and geological viewpoint.

Bremanger

Although the Bremanger network has been plagued by technical problems, the data obtained provide some insight into the seismic activity in the area. The onshore earthquakes tend to be somewhat shallower (<15 km) than the earthquakes offshore (>15 km). There does not appear to be any systematic distribution of activity as observed in the Rana area, but the volume of data is also much smaller due to the technical problems.

The stress tensor in this area appears to be quite stable and controlled by the ridge push force from the Mid-Atlantic spreading ridge, although there are a few previous earthquake focal mechanism solutions offshore that show a 90° rotation of the direction of horizontal compression. This indicates that some significant local stress source(s) could be in effect.

6.2.6 References

Atakan, K., Lindholm, C. D. and Havskov, J. 1994: Earthquake swarm in Steigen northern Norway: an unusual example of intraplate seismicity. *Terra Nova*, 6, 180-194.

Bungum, H., Alsaker, A., Kvamme, L.B. and Hansen, R.A. 1991: Seismicity and seismotectonics of Norway and surrounding continental shelf areas. *J. Geophys. Res.*, 96, 2249-2265.

Bungum, H., Hokland, B.K., Husebye, E.S. and Ringdal, F. 1979: An exceptional intraplate earthquake sequence in Meløy, Northern Norway. *Nature*, 280, 32-35.

Bungum, H. and Lindholm, C. 1997: Seismo- and neotectonics in Finnmark, Kola Peninsula and the southern Barents Sea. Part 2: Seismological analysis and seismotectonics. *Tectonophysics*, 270, 15-28.

Byrkjeland, U. 1996: *Seismotectonics of the Norwegian Continental Margin, 62°-71°N.* Cand. Scient thesis in applied geophysics, University of Oslo, Norway, 146 pp.

Byrkjeland, U., Bungum, H. and Eldholm, O. in press: Seismotectonics of the Norwegian continental margin. Journal of Geophysical Research.

Fejerskov, M., Lindholm, C.D., Bungum, H., Myrvang, A., Bratli, R.K. and Larsen, B.T. 1996: *Crustal stress in Norway and adjacent offshore regions*, Final report for the IBS-DNM project, Topic 1.3 "Regional stress field".

Havskov, J. 1997: *The Seisan earthquake analysis software*, Institute of Solid Earth Physics, University of Bergen, 236 pp.

Havskov, J., Kvamme, L.B., Hansen, R.A., Bungum, H. and Lindholm, C.D. 1992: The northern Norway seismic network: Design, operation and results. *Bull. Seism. Soc. Am.*, 82, 481-496.

Hicks, E. C. 1996: Crustal stresses in Norway and surrounding areas as derived from earthquake focal mechanisms and *in situ* stress measurements. Cand. Scient thesis in applied geophysics, University of Oslo, Norway, 163 pp.

Hicks, E.C., Bungum, H. and Lindholm, C.D. submitted: Stress inversion of earthquake focal mechanism solutions from onshore and offshore Norway. Nor. Geol. Tidsskr.

Hicks, E.C., Bungum, H. and Lindholm, C.D. in press: Seismic activity, inferred crustal stresses and seismotectonics of the Rana region, Northern Norway. QSR.

Muir Wood, R. 1989: The Scandinavian earthquakes of 22 December 1759 and 31 August 1819. *Disasters*, 12, 223-236.

Olesen, O., Gjelle, S., Henkel, H., Karlsen, T.A., Olsen, L. and Skogseth, T. 1994: Neotectonics in the Ranafjorden area, northern Norway. NGU Report No. 94.073, 33 pp.

6.3 THE 1999 FINNMARK SEISMIC FIELD EXPERIMENT

By J. Schweitzer, F. Krüger, G. Richter, E. Hicks, C. Lindholm and H. Bungum

6.3.1 Introduction

As is well known and documented, the seismicity of Finnmark is relatively low at present (Bungum *et al.*, 1991; Bungum and Lindholm, 1997). It is also well known, however, that a series of large reverse faults have ruptured the bedrock near the center of the former Fennoscandian icecap in response to the last glacial unloading (Lundquist and Lagerbäck, 1976; Olesen, 1988; Muir Wood, 1989). If single earthquakes have been responsible for the dislocations, as proposed by Bäckbom and Stanfors (1989) and Dehls and Olesen (1998; 1999), these earthquakes should have been in the range M 7.4-8.2 (Arvidsson, 1996; Bungum and Lindholm, 1997). If the seismicity was largely suppressed when the icecap was in place (Johnston, 1987), then the buildup of elastic strain from the entire last ice age would have been released over a relatively short time period since the onset of deglaciation (Muir Wood, 1989, Johnston *et al.*, 1998).

In fact, these faults may still be active, including the Stuoragurra fault in Finnmark. Based on existing data from the national networks, Bungum and Lindholm (1997) showed that a number of small reverse faulting earthquakes lined up along a relatively wide zone parallel to the fault, and at a variety of depths. However, the relatively poor station coverage did not allow any precise locations.

The original NEONOR plans included the Masi region as a place for a third microearthquake network in addition to Rana and Bremanger. This could not be realised as planned because of limited resources. The solution then came with an initiative from the University of Potsdam, Germany, who informed us that they had a set of 13 mobile seismic stations that would be available for such an experiment during the summer of 1999. By mobilising additional funding, NORSAR then joined in the planning of the field experiment MASI-1999, as a cooperative effort between the two institutions.

Besides the local seismicity, additional motivation for this experiment came from the need to calibrate the ARCES array in Finnmark, which is an important station in the IMS (International Monitoring Station) network for monitoring of the Comprehensive Test Ban Treaty (CTBT). There are two main purposes here, to use the new data in investigations of the crustal and upper mantle structure of this area, and to study the wave field from local and regional events using many stations distributed over the whole area, giving a better understanding of the characteristics of local and regional wave propagation. In addition the University of Potsdam wants to use the new data in further studies of sources of microseismic disturbances, as originating in oceanic and coastal areas (Krüger, 1998).

6.3.2 Field experiment and recorded data

During the time period May 18-27, 1999, 13 Lennartz MARSlite data loggers equipped with three-component LE-3D/5s seismometers were installed in Finnmark. These instruments have an eigenperiod of 5 seconds. The station locations are shown in Fig. 6.3.1 and the coordinates of the seismometer sites are given in Table 6.3.1.

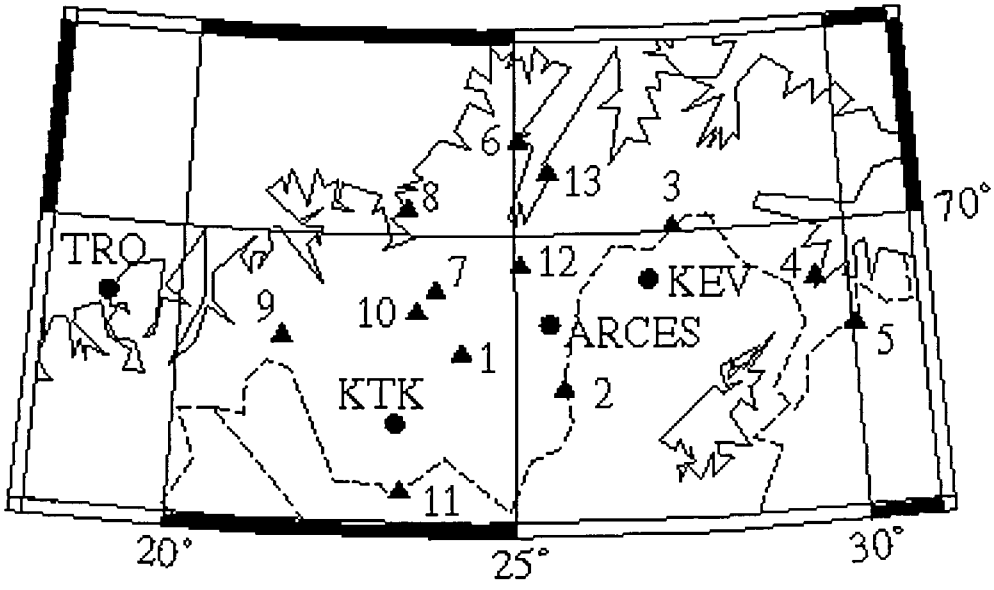

Fig. 6.3.1 Map of all 13 MASI-1999 stations in Finnmark (triangles). The dots show the positions of the permanent stations ARCES, KEV, KTK, and TRO in the same area. The station MA00 was located at ARCES.

Table 6.3.1 Coordinates and recording times of the MASI-1999 mobile station experiment in Finnmark.

Station	Lat [°]	Lon [°]	Elev [m]	Start	Stop
MA00	69.5346	25.5056	403	18-05	01-10
MA01	69.3752	24.2122	315	18-05	30-09
MA02	69.1875	25.7033	160	19-05	29-09
MA03	70.0210	27.3962	95	19-05	01-10
MA04	69.7127	29.5059	20	19-05	01-10
MA05	69.4533	30.0391	30	20-05	16-08
MA06	70.4813	25.0610	50	21-05	28-09
MA07	69.7050	23.8203	265	21-05	29-09
MA08	70.1278	23.3736	15	22-05	29-09
MA09	69.4566	21.5334	90	22-05	27-09
MA10	69.5875	23.5274	375	23-05	30-09
MA11	68.6595	23.3219	390	24-05	30-09
MA12	69.8349	25.0824	75	24-05	29-09
MA13	70.3161	25.5156	30	25-09	29-09
GP03	69.99	24.94	20	18-05	24-05

During the installation phase, one station (MA00) was running in parallel at the ARCES array site ARA0 to check the compatibility of data from the mobile stations and the ARCES array. At all sites, continuous data were recorded and written on hard disks. With the chosen sampling rate of 125 samples per second, these hard disks were filled up after about two months.

Therefore, two maintenance visits including disk changes were necessary during the deployment time of the mobile stations. In the middle of August, during the last disk change visit, the station MA05 was moved to the ARCES array site ARA0, to have a continuous data stream available also during a subsequent ARCES refurbishment and upgrading in September, 1999.

The field experiment was finished during the last days of September, when all stations were dismantled and sent back to Germany. The last available data records from the mobile stations were from October 1, 1999. The performance of the 13 stations was very good, as only three stations had recording outages due to technical problems.

All data from the mobile stations were stored continuously on recordable CDs together with all available data from the permanent stations in and around Finnmark: ARCES, KEV, KTK, and TRO (see Fig. 6.3.1). The data from the Kevo station (KEV) are, except for some minor outages, continuously available. We included in our database the output of the broadband 80 Hz sampled Guralp CMG-3T instrument at KEV. The short period data from the stations Kautokeino (KTK) and Tromsø (TRO) are unfortunately triggered data, so that these stations contribute little to the database. All data from the ARCES array (i.e. all short period array channels and the channels from the ARCES broadband site ARE0) were copied into the data base. However, due to the ARCES upgrading work, the ARCES array was out of operation for about three weeks. The data from both the mobile MARSlite stations and the other stations were reformatted into a common GSE2.0 format (double differences, 6-bit compression).

The whole database as described above has been copied to CDs, to have all data easily available by direct access. One CD usually contains the data for a half day. In addition, all available bulletins were copied to the CDs, i.e. the automatically produced listings of NORSAR's data processing for ARCES and Apatity (detection lists, location lists, and bulletins), the preliminary Scandinavian bulletin produced at the University of Helsinki, and bulletins from the (prototype) International Data Center (pIDC) for the CTBT. For backup, the contents of all CDs were copied in addition onto EXA-BYTE tapes.

This very extensive data handling work was finished in mid November, 1999, and as soon as possible, the data base will be copied to a second set of CDs at the University in Potsdam such that both partners can work with the data in their research programs.

6.3.3 Data examples

Because the field experiment and the production process of the recordable CDs ended very recently, only some preliminary data examples of this campaign can be shown. Because one main topic of this experiment was the detection and analysis of possible neotectonic movements in northern Scandinavia, a first screening of the data concentrates on local and regional events which cannot be associated with known sources of man-made seismic sources like the northern Swedish (Kiruna) iron mines or the mines and the many quarries on the Kola peninsula, Russia.

Unfortunately, a felt earthquake in the north-east of the Stuoragurra fault system (March 30, 1999) occurred just before the mobile stations were installed, and the largest earthquake in recent years offshore of Tromsø (October 17, 1999) occurred two weeks after demobilization of the stations. Even though we missed these two very interesting events in this way, we did still record some local seismicity.

Up to now, the data until the end of June, 1999, have been preliminarily searched. During this time at least three smaller, non-felt events could be found and located, two on the Stuoragurra fault and one at the end of the Porsanger Fjord. In addition, on August 22, 1999, an M_L 2.6 event occurred near Masi on the Stuoragurra fault, large enough to be felt locally.

Fig. 6.3.2 shows vertical-component seismograms of the small event at the end of the Porsanger Fjord on May 24, 1999. All seismograms shown were recorded in a 1° to 2° epicentral distance range. This event with M_L 1.9 was not observable at all stations and shows a relatively low signal-to-noise ratio. However, with the MASI-1999 stations the epicenter could be well located (see Table 6.3.3). For estimating the depth of this event, which presumably occurred relatively close to the surface, a better S velocity model of the region is needed.

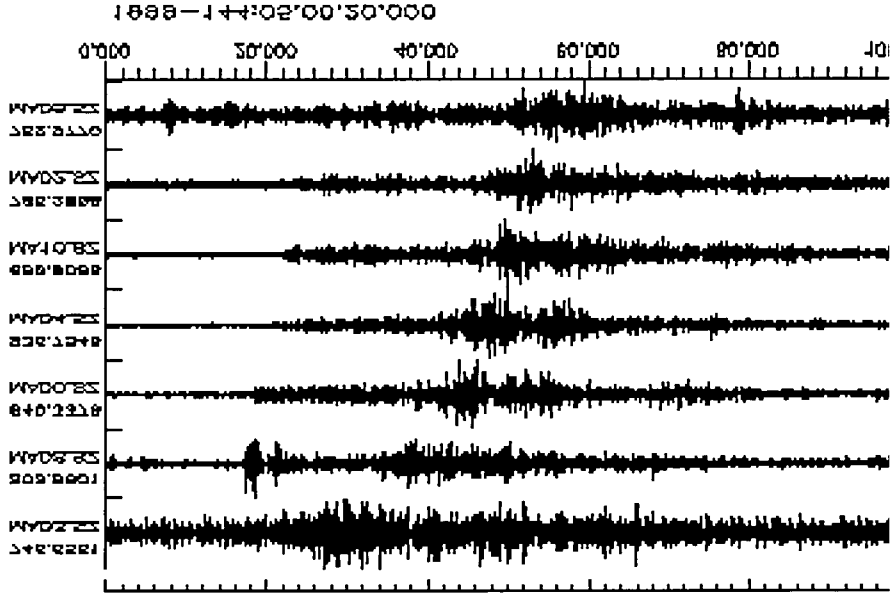

Fig. 6.3.2 Vertical component seismograms of the M_L 1.9 event on May 24, 1999 (see Table 3). The seismograms were band-pass filtered between 3 and 9 Hz, the epicentral distances to the stations are between 1° and 2°.

Table 6.3.2 Epicentral parameters of local events, which were observed with the MASI-1999 stations For the events on May 24, 1999 and August 22, 1999, data are shown in Figs. 6.3.2-5.

Date	Time	Lat.	Long.	Depth (km)
May 24,1999	05:00:12.8	70.91	26.53	0 (fixed)
June 04, 1999	12:22:38.9	70.26	22.73	0 (fixed)
June 08, 1999	01:22:19.6	69.12	23.70	8
June 10, 1999	02:50:55.7	69.43	23.98	15
August 22, 1999	02:08:47.9	69.27	23.70	11

Fig. 6.3.3 shows a map with unfiltered records at all temporary seismic stations (vertical components) of the felt event from August 22, 1999, south of Masi on the Stuoragurra Fault.

Fig. 6.3.4 shows the same records as single seismograms, while Fig. 6.3.5 shows the same data highpass filtered above 40 Hz. Note the low attenuation for the high frequently energy in this region. A preliminary location of the event is listed in Table 6.3.3.

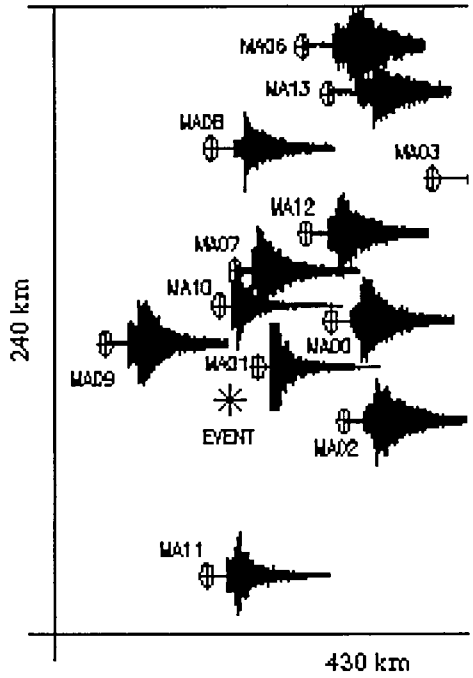

Fig. 6.3.3 Geographical distribution of observed seismograms with respect to the felt event of August 22, 1999. Unfiltered vertical-component traces. Note that the seismogram at station MA01 is clipped, and the different amplitude ratio between P and S onsets.

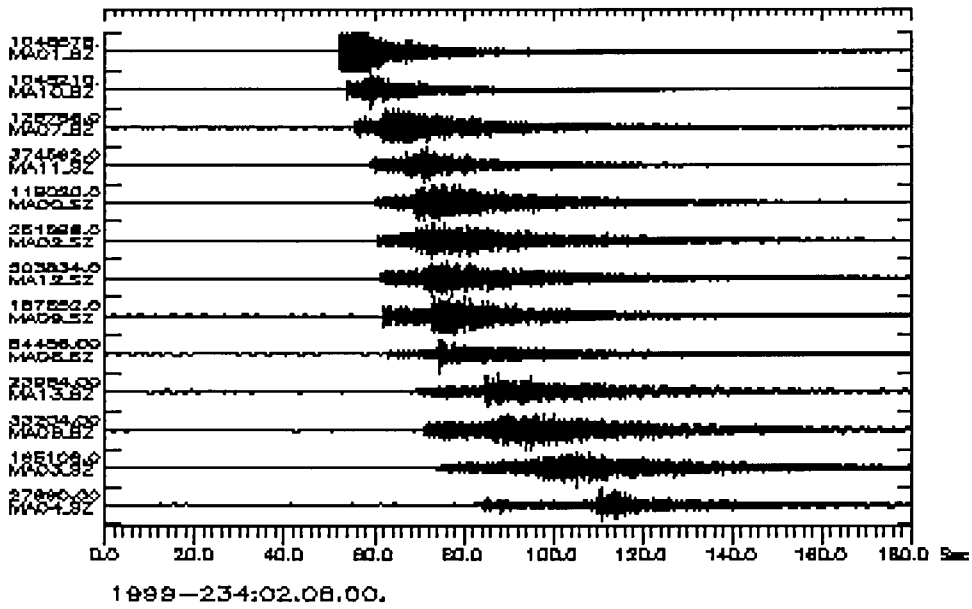

Fig. 6.3.4 The unfiltered vertical-component records at all MASI-1999 stations of the August 22, 1999 M_L 2.6 event at the Stuoragurra fault. The stations observed the event in epicentral distances between 0.2° and 2°. The closest station MA01 was clipped.

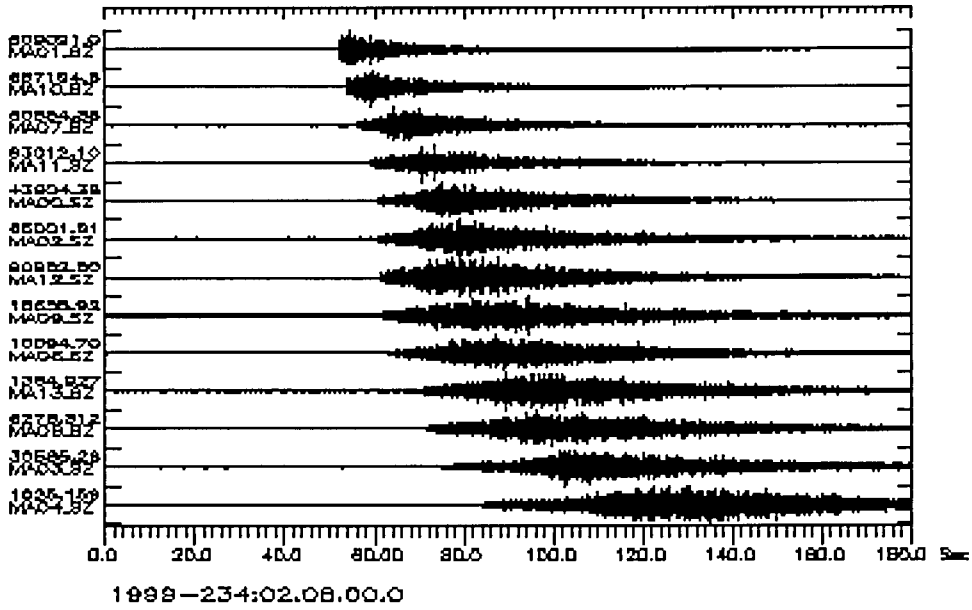

Fig. 6.3.5 The same data as in Fig. 6.3.4., now filtered with a Butterworth high-pass at 40 Hz. Note the high-frequency scattered energy, which is an indication for a relative high Q structure in the Finnmark area.

On August 17, 1999, a mining induced event occurred near Lovozero on the Kola peninsula. The event was the strongest earthquake observed during the last years in this area and was well recorded with the MASI-1999 stations. Fig. 6.3.6 shows the raw data and Fig. 6.3.7 the broadband filtered (8-20 s) data, where a dominant Rayleigh wave is visible. Using these Rayleigh observations we have obtained a surface wave magnitude estimate of M_S 4.3. The traditional IASPEI M_S formula was applied by measuring amplitudes at shorter dominant periods for the 2° to 5° distance range (e.g. see Willmore, 1979). The measured magnitude is consistent with Kværna *et al.* (1999), who used NOA and ESDC broadband data to derive an M_S of 4.2 for this event.

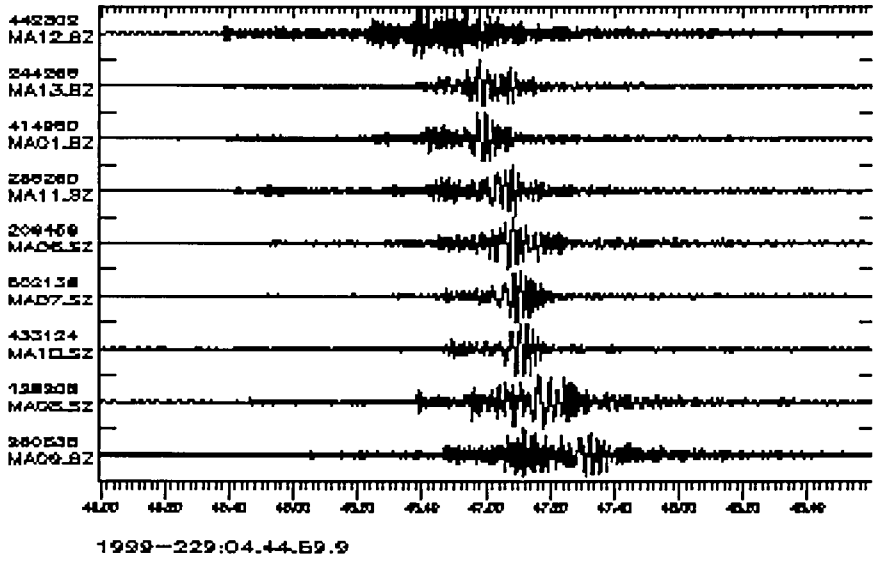

Fig. 6.3.6 The raw seismograms of the Lovozero event August 17, 1999 as observed at some of the MASI-1999 stations.

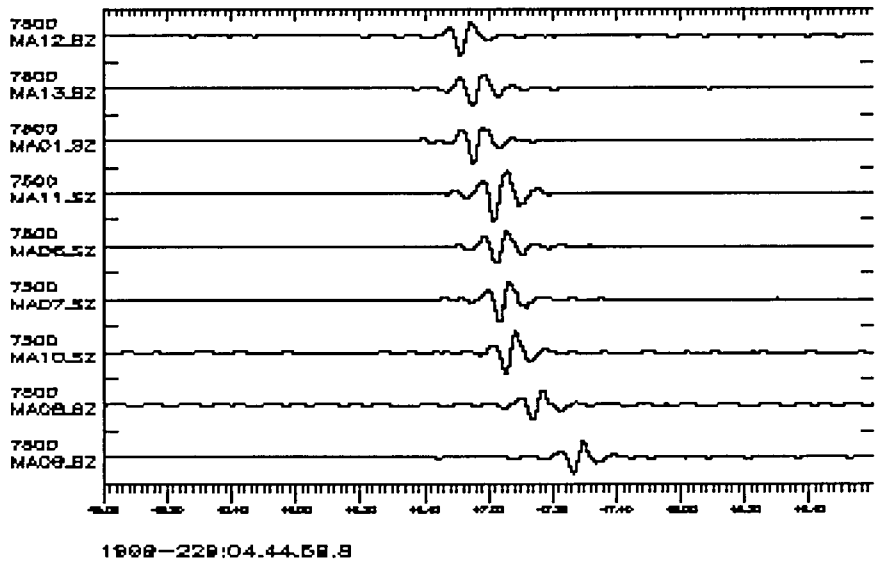

Fig. 6.3.7 Seismograms of the Lovozero event August 17, 1999, filtered with a band-pass filter at 8-20 seconds. The amplitude scale was normalised to the maximum amplitude. From these data the M_S value 4.3 was determined.

A focal mechanism has been determined for the 22. August M_L 2.6 earthquake, showing an oblique reverse/strike-slip movement. The focal mechanism is included in Fig. 8, which also shows the background seismic activity from Bungum and Lindholm (1996) as open circles. The new local earthquakes are shown as red filled circles, with no magnitude scaling. Although the new focal mechanism solution does not appear to have any direct connection with the Stourragurra fault, it is important to bear in mind that the magnitude for this event is significantly lower than the M_L 4.0 earthquake in January 1996, which had one nodal plane closely following the fault strike, and one should expect more variance in the mode of faulting. The direction of compressive stress is consistent with the other focal mechanism solutions on Finnmarksvidda (NW-SE).

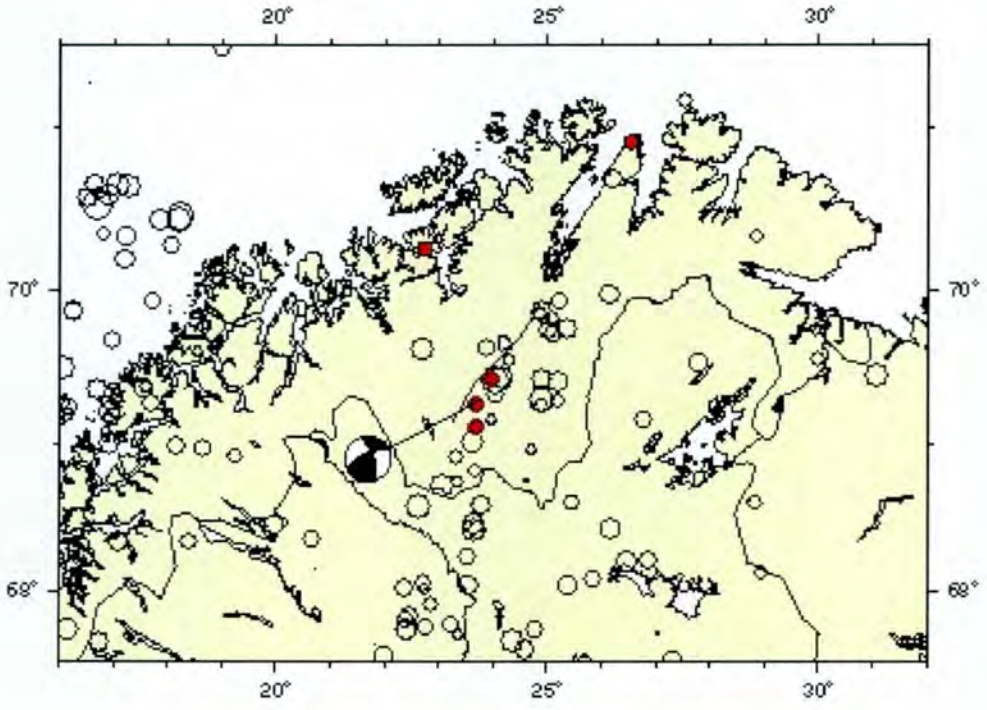

Fig. 6.3.8 Previous earthquakes in Finnmark as compiled from Bungum and Lindholm (1996) (1979-1992), NORSAR (1993-1996) and felt earthquakes 1996-1999, shown as open circles. Preliminary locations from this study are shown as filled circles. Note that magnitudes are not yet available for the new earthquakes. The focal mechanism for the 22. August M_L 2.6 earthquake is shown.

6.3.4 Further work

The examples shown indicate that the records of the MASI-1999 experiment are usable to address further a number of interesting scientific issues:

- Seismicity of Finnmark in general and contemporary movements on the Stuoragurra Fault in particular.
- Fault plane solutions for the best observed events in this area.
- Improved travel-time tables for local and regional P- and S-phases.
- Moho depth measurements in this region with receiver function studies.
- Local and regional amplitude attenuation curves by observing the same event at different distances.
- Anelastic attenuation (Q) for local regional Lg and Sn phases.
- Improved S-phase understanding in northern Scandinavia by analysing the 3C data.
- Crustal structure by inversion of local/regional surface waves.

- Source studies of the ocean generated microseisms.
- Relative locations of seismic events in the different mining areas.

6.3.5 References

Arvidsson, R. 1996: Fennoscandian earthquakes: Whole crustal rupturing related to postglacial rebound. *Science*, 274, 744-746.

Bäckbom, G. and Stanfors, R. 1989: *Interdisciplinary study of postglacial faulting in the Lensjärv area, northern Sweden 1986-1988*, SKB Tech. Rep. 89-31, Swed. Nucl. Fuel and Waste Mange. Co., Stockholm.

Bungum, H., Alsaker, A., Kvamme, L.B. and Hansen, R.A. 1991: Seismicity and seismotectonics of Norway and surrounding continental shelf areas. *J. Geophys. Res.*, 96, 2249-2265.

Bungum, H. and Lindholm, C. 1997: Seismo- and neotectonics in Finnmark, Kola, and the southern Barents Sea, part 2, Seismological analysis and seismotectonics. *Tectonophysics*, 270, 15-28.

Dehls, J. F. and Olesen, O. 1998: NEONOR: Neotectonics in Norway: Annual technical report 1997, Rep. 98.016, Norges Geol. Undersøkelse, Trondheim, 149 pp.

Dehls, J. F. and Olesen, O. 1999: NEONOR: Neotectonics in Norway: Annual technical report 1998, Rep. 98.007, Norges Geol. Undersøkelse, Trondheim, 206 pp.

Friedrich, A., Krüger, F. and Klinge, K. 1998: Ocean-generated microseismic noise located with the Gräfenberg array. *J. of Seismology,* 2, 47-64.

Johnston, A.C. 1987: Suppression of earthquakes by large continental ice sheets. *Nature,* 330, 467-469.

Kværna, T., Taylor, L., Schweitzer, J. and Ringdal, F. 1999: Continious assesment of upper limit M_S. *Semiannual Technical Report 1 April - 30 September 1999.* NORSAR Sci. Report 1-99/00, Keller, Norway.

Lundquist, J. and Lagerbäck, R. 1976: The Pärve fault, A late-glacial fault in the Precambrian of Swedish Lapland. *Geol. Fören. Stockholm Förh.*, 98, 45-51, 1976.

Muir Wood, R. 1989: Extraordinary deglaciation reverse faulting in northern Fennoscandia. *In* S. Gregersen and P.W. Basham (eds.): *Earthquakes at North-Atlantic Passive Margins: Neotectonics and Postglacial Rebound*, NATO ASI Ser., 266, 99. 141-174.

Olesen, O. 1988: The Stuoragurra fault, evidence of neotectonics in the Precambrian of Finnmark, northern Norway. *Norsk Geologisk Tidsskrift,* 68, 107 - 118.

Willmore, P. L. 1979: Manual of seismological observatory practice. World Data Center A for Solid Earth Geophysics, Report SE-20, reprinted 1982, 165 pp.

6.4 STRESS INVERSION OF EARTHQUAKE FOCAL MECHANISM SOLUTIONS FROM ONSHORE AND OFFSHORE NORWAY

By Erik C. Hicks, Hilmar Bungum and Conrad D. Lindholm, NORSAR

6.4.1 Introduction

Earthquakes contribute essentially in two different ways to the understanding of the seismotectonic conditions in any particular region, firstly through analysis of individual earthquakes (single sources), such as location, size, mode of faulting, rupture characteristics, etc., and the way the event may fit into the seismic cycle, and secondly through various ensemble analyses, essentially spatio-temporal characteristics as expressed through recurrence behaviour, seismic lineations, etc. Both types of analyses are important when the goal is to improve our understanding of lithospheric seismo-dynamics, provided that such information is properly tied in to structural geologic and geodetic observations.

The earthquake activity in and around Norway has been documented through a number of detailed studies, and for comprehensive analyses and reviews we refer to Bungum *et al.* (1991) and to Byrkjeland *et al.* (in press). It is concluded there that while the stress field along the margin is generally consistent with the ridge push force, regional (such as sedimentary loading) and local (such as topography) stress enhancement factors are also essential for explaining the earthquake activity along and near the Norwegian continental margin. The potentials for earthquakes, including structural reactivation, is therefore most likely tied to a mixture of platewide, regional and local stress, in combination with existing weakness zones and faults, without any single factor being dominant.

The purpose of the present paper is twofold, firstly to provide a comprehensive and consistent overview of all (112) available earthquake focal mechanism solutions for both onshore and offshore Norway, including some (7) new and unpublished solutions, and secondly to analyse these solutions in search for regionally consistent stress patterns, using the stress inversion method of Gephart and Forsyth (1984). Six regions are covered in this way (Northern North Sea, Offshore Mid Norway, Onshore Mid Norway, Onshore West Norway, Oslo Rift Zone and Finnmark) and in addition we have covered two more regions using *in situ* stress data (Western Barents Sea and Southern North Sea).

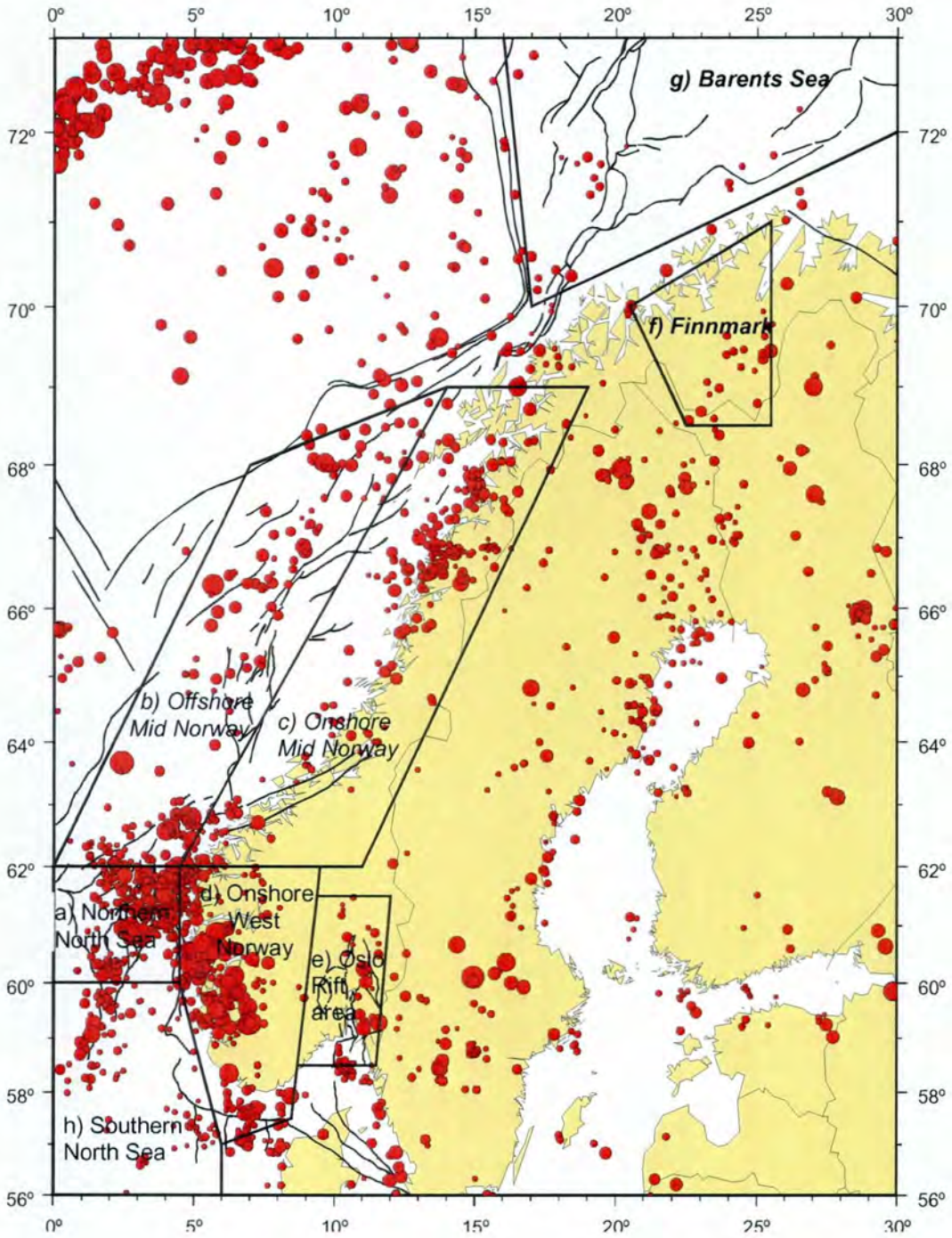

Fig. 6.4.1 Earthquakes in Norway and surrounding areas for the time period 1980-1999, for magnitudes greater than or equal to 2.0 (symbol size proportional to magnitude). Note the areas of higher seismic activity in the northern North Sea and onshore in western Norway, separated by the Horda Platform but coming together in the Sogn Graben area. In northern Norway there is a similar separation in that a more or less aseismic Vøring Shelf (Trøndelag Platform) is separating the seismic activity along the continental margin (Møre and Vøring Basins) from that along the Nordland Coast, coming together in the Lofoten region. The Oslo rift appears to have a higher level of seismic activity than the surrounding basement. The zones (with names) used in the stress inversion are shown.

6.4.2 Focal mechanism determination

First motion polarities

The classical and most widely used method for determining an earthquake focal mechanism solution is to use P-wave first-motion polarities in sampling sense of motion in different ray directions from the source, thereby defining the two nodal planes, delineated in a (usually lower hemisphere) stereographic plot. To do this with a sufficient precision, a good station coverage of azimuths and distances is needed, a condition which quite often is not met when analysing the seismicity in and around Norway. However, some earthquakes are located close to or within denser local networks, and many of the larger earthquakes also have an adequate signal-to-noise ratio to allow first-motion determination at a sufficient number of stations for a solution to be determined in this manner. Two of the seven new earthquake focal mechanism solutions published for the first time in this paper were determined using first motion polarities only, as both of these are located close to a six-station local seismic network in western Norway, operated under the Neotectonics of Norway (NEONOR) project (Dehls at al. 1998; 1999). In addition, these earthquakes were of sufficiently large magnitude to also have readable first-motion polarities at several of the permanent stations within the Norwegian seismic network, giving a coverage sufficient to allow for reasonably reliable focal mechanism solutions. The actual solutions are developed by performing a simple grid search, allowing for a systematic comparison between data and model.

Waveform modelling

For earthquakes that do not have a large enough number of available first-motion polarities, it is possible to use full waveform modelling to select a focal mechanism solution, or at least to support indications from first-motion data. This is the case for the other five of the seven new mechanisms, one of which is located close to a local network in mid Norway. The permanent Norwegian network has few stations in this area, so the available first motions were only able to provide a rough constraint on the focal mechanism solution. One earthquake, although large enough (M_L 3.1) to normally provide a useful station coverage, was located in an area with low station coverage. The final three earthquakes were located close to the network in western Norway, but first motions alone were insufficient to determine a solution with sufficient precision in these cases.

After reading all available first-motion polarities for these five earthquakes, possible focal mechanism solutions were determined using the same grid search method as used in the first-motion only determinations. Subsequently, synthetic seismograms for the possible focal mechanism solutions were generated for selected stations with good data quality, using the Herrmann code (e.g. Herrmann 1978; 1979; Wang and Herrmann 1980). The algorithm uses discrete wavenumber integration to consider the complete wave field of a point source, this requires a large amount of computational power and is thus quite computer-time consuming. However, once this step has been performed for an earthquake location and defined stations, the actual synthetic seismogram for various source focal mechanisms can be generated much more quickly. In comparing synthetic seismograms for the possible focal mechanism solutions with observed data the main emphasis is on the relative amplitudes for the P and S phases, whereupon the solution giving the best correlation for the modelled stations is selected.

6.4.3 Data

The list of earthquake focal mechanism solutions is compiled from a number of published sources, and updated with the new solutions determined under the NEONOR project. A com-

prehensive list of all solutions is given in Table 6.4.1. Solutions outside the inversion regions are also included, mainly comprising seven solutions in the oceanic crust of the Norwegian Sea and the Mohns ridge, and six solutions in and around Svalbard. The date, location, depth and magnitude are given (composite solutions have magnitudes of -1.0), while the focal mechanism solution is given by trend (trn) and plunge (plg) of the T (tension) and P (compression) axes. An 'm' in the comment (Com.) field implies that a waveform modelling approach has been utilized in determining the solution. The quality (Qual.), maximum horizontal compressive stress (σ_{Hmax}) and stress regime (Reg.) are according to criteria defined in the World Stress Map project (e.g. Zoback, 1992). The maximum horizontal compressive stress directions from all available stress data (earthquake focal mechanism solutions and *in situ* data) are plotted in Fig. 6.4.2, with colour code differentiating on stress regime. In Fig. 6.4.2 we have also indicated the eight regions (boxes) within which we have been inverting for a common (dominating) stress region, where the ones farthest south (southern North Sea) and north (western Barents Sea) contain only *in situ* data (borehole breakouts).

The seven new earthquake focal mechanism solutions are shown in Fig. 6.4.3, with derived directions of maximum horizontal compressive stress (σ_{Hmax}) indicated by black bars. Two of the new solutions are located close to the coast in mid Norway (99.04.09 and 99.08.23). They both show a normal fault movement, have an approximately N-S orientation of σ_{Hmax}. The other five solutions are from western Norway, the solution from the 99.08.02 earthquake is located in the Northern North Sea inversion box, the other four fall into the Onshore West Norway box. The five solutions comprise one normal fault, two reverse and one strike-slip and one oblique reverse/strike-slip. The σ_{Hmax} directions range from E-W to NW-SE.

Table 6.4.1 Complete list of earthquake focal mechanism solutions in Norway. T-trn, T-plg, P-trn and P-plg are trend and plunge for the T (tension) and P (compression) axes, respectively. An 'm' in the comment field refers to a waveform modelling approach used in determining the solution. Quality ratings, σHmax direction and stress regime are determined according to the criteria defined in the World Stress Map project (e.g. Zoback 1992). References: 1 - Lazareva and Misharina (1965), 2 - Savostin and Karasik (1981), 3 - Bungum and Fyen (1979), 4 - Bungum and Kristoffersen (1980), 5 - Bungum et al. (1979), 6 - Vaage (1980), 7 - Kibsgaard (1985), 8 - Mitchell et al. (1990), 9 - Chan and Mitchell (1985), 10 - Havskov and Bungum (1987), 11 - Hansen et al. (1989), 12 - Lindholm and Havskov (1989), 13 - Bungum et al. (1991), 14 - Bungum and Lindholm (1996), 15 - Engell-Sørensen (pers. comm. 1994), 16 - Lindholm et al. (1995), 17 - Fejerskov et al. (1996), 18 - Hicks (1996), 19 - Atakan et al. (1994), 20 - Inst. of Solid Earth Phys., Univ. of Bergen, 21 - Hicks et al. (in press), 22 - This paper.

Date	Lat	Lon	Depth	Mag	T-trn	T-plg	P-trn	P-plg	Ref.	Com.	Qual	Hmax	Reg.
Com.-78	66.80	13.65	9	-1.0	258	11	164	18	6		C	164	SS
Com.-78	66.80	13.80	6	-1.0	132	15	255	64	5		C	36	NF
Com.-81	77.70	17.00	4	-1.0	315	90	270	0	8		?	270	TF
Com.-82	80.20	21.70	4	-1.0	15	0	285	0	9		B	285	SS
Com.-82	80.10	20.00	4	-1.0	187	45	298	20	9		B	298	U
Com.-82	80.30	20.00	4	-1.0	180	0	270	0	9		B	270	SS
Com.-86	61.00	2.50	19	-1.0	270	65	90	25	12		?	90	TF
Com.-92	67.77	14.88	10	-1.0	337	6	77	55	19		B	243	NF
Com.-97	66.31	13.25	5	-1.0	270	11	167	48	22		C	0	NS
1959.01.29	70.90	7.30	33	5.8	310	20	220	10	1		?	220	SS
1959.03.01	74.80	8.10	33	5.4	120	0	25	30	1		?	210	SS
1968.01.03	72.22	1.55	33	5.2	86	1	354	46	2		C	176	NS

Date	Lat	Lon	Depth	Mag	T-trn	T-plg	P-trn	P-plg	Ref.	Com.	Qual	Hmax	Reg.
1970.10.21	74.62	8.56	33	5.5	82	3	349	39	2		D	172	SS
1971.05.31	72.21	1.09	20	5.5	264	1	356	49	2		C	354	NS
1971.07.19	60.72	10.73	31	1.4	227	11	127	42	3		B	317	NS
1973.11.23	60.55	11.47	23	1.7	229	3	137	26	3		D	319	SS
1975.01.20	71.70	14.20	24	5.0	59	14	156	25	2		C	149	SS
1976.01.18	77.79	18.34	4	5.5	333	9	243	2	4		?	243	SS
1977.12.11	60.94	10.89	22	2.0	95	25	259	64	3		D	2	NF
1979.03.29	60.79	10.99	11	2.2	86	13	320	69	13		A	180	NF
1979.06.14	60.38	11.32	17	2.7	204	9	113	12	7		B	113	SS
1980.11.18	60.96	11.34	30	2.2	37	53	185	32	7		B	185	TF
1981.06.22	65.70	0.20	15	4.0	161	55	309	31	13		D	309	TF
1981.06.07	60.54	11.16	19	1.3	227	10	125	49	7		B	317	NS
1981.09.03	69.62	13.68	12	4.7	49	38	301	22	13	m	C	301	U
1982.07.29	60.40	2.00	17	4.3	55	12	320	25	10		C	145	SS
1982.10.18	60.96	11.58	20	2.1	218	80	102	4	13		A	102	TF
1983.03.08	59.70	5.40	15	4.6	6	46	267	9	10		B	267	TS
1983.03.08	60.53	10.69	15	1.4	246	4	340	44	7		B	336	NS
1984.03.01	60.55	10.73	17	0.7	46	12	313	15	7		B	313.	SS
1985.01.25	61.22	3.65	33	3.1	295	45	46	20	15		C	46	U
1985.05.16	60.94	3.41	33	2.5	104	3	205	74	15		C	13	NF
1985.09.08	61.30	3.40	19	3.1	319	8	227	14	10		D	227	SS
1985.10.27	61.30	4.30	15	2.8	293	12	30	32	10		D	203	SS
1985.10.01	61.30	4.20	15	3.0	109	8	200	9	10		D	200.	SS
1985.11.30	61.60	4.60	6	3.0	99	28	212	36	10		D	212	U
1986.02.05	62.71	4.69	20	4.9	198	55	303	10	11	m	B	303	TF
1986.10.26	61.83	3.20	14	4.5	305	78	112	12	13	m	B	112	TF
1986.12.16	60.61	11.02	11	1.9	69	30	281	56	13		B	168	NF
1987.04.04	67.25	8.03	15	3.6	17	75	118	3	13		D	118	TF
1987.09.04	61.45	2.95	33	3.0	213	69	326	9	15		C	326	TF
1987.10.31	61.13	4.14	20	3.4	345	12	248	32	13		A	255	SS
1987.12.26	59.81	6.55	12	2.4	21	4	286	47	13	m	B	111	NS
1988.01.31	68.03	9.58	20	4.3	92	24	329	51	13		C	329	U
1988.06.30	61.12	9.97	20	1.9	36	21	176	64	13		B	300	NF
1988.06.02	62.09	2.20	29	3.1	37	64	306	1	13		B	306	TF
1988.08.08	63.68	2.44	25	5.3	31	77	277	5	11		B	277	TF
1988.10.27	66.89	8.88	25	3.9	191	83	300	2	13		D	300	TF
1988.10.20	59.91	6.36	11	3.5	166	14	273	49	13		A	256	NS
1989.01.20	57.93	8.46	29	3.1	216	28	96	43	13		C	96	U
1989.01.23	61.97	4.42	26	5.1	239	72	124	8	11	m	A	124	TF
1989.01.29	59.64	6.02	7	4.2	201	15	90	54	13		A	301	NF
1989.01.09	69.56	24.30	12	1.4	182	71	329	16	14	m	C	329	TF
1989.02.14	61.17	3.87	11	2.9	348	4	81	31	13	m	A	258	SS
1989.04.10	60.61	11.40	22	1.9	35	42	303	3	13		A	303	TS
1989.07.13	69.74	24.87	8	2.1	245	52	351	12	14	m	C	351	U
1989.09.01	61.34	4.20	33	2.6	340	63	103	16	16		C	103	TF
1989.09.02	61.36	3.49	33	2.2	16	35	109	5	16		D	109	SS
1989.09.02	61.36	3.49	33	2.5	359	48	92	3	16		C	92	TS
1989.09.20	59.11	6.01	10	2.7	210	24	97	41	13		A	97	U
1989.11.02	60.68	11.54	33	1.3	20	35	281	12	13		B	281	SS
1989.11.16	68.83	23.67	12.5	1.6	45	0	135	0	14		D	135	SS

Date	Lat	Lon	Depth	Mag	T-trn	T-plg	P-trn	P-plg	Ref.	Com.	Qual	Hmax	Reg.
1990.02.26	57.67	6.91	6.4	3.4	252	39	139	26	18		C	139	U
1990.05.16	66.04	6.26	30	3.4	225	1	135	10	18		C	135	SS
1991.04.13	69.33	24.02	9.7	1.8	19	69	279	4	14	m	C	279	TF
1991.09.01	79.02	3.59	10	5.0	84	0	174	0	17		C	174	SS
1991.12.31	61.98	4.23	15	3.3	210	5	30	85	17		C	120	NF
1991.12.16	67.91	9.97	10	2.4	193	5	291	60	18		C	100	NF
1992.02.19	59.27	10.88	10	3.6	258	9	160	39	18		C	348	SS
1992.04.14	59.50	5.66	12	3.0	202	30	292	0	18		B	292	SS
1992.06.30	60.88	11.53	12	2.8	299	5	182	78	18		B	30	NF
1992.08.14	67.89	12.85	17	3.7	159	23	293	58	18	m	B	60	NF
1993.01.20	64.75	4.81	15	3.5	175	90	285	0	17		C	285	TF
1993.06.26	62.61	4.14	17	3.9	280	37	180	12	18		B	180	SS
1993.09.13	66.37	5.72	20	3.9	7	9	246	72	18		B	99	NF
1993.10.18	64.99	5.19	10	3.3	49	10	299	62	18		D	144	NF
1993.12.27	61.25	2.84	20	3.3	0	58	121	18	18		?	121	TF
1994.07.27	62.63	3.90	10	3.7	66	2	334	30	17		C	156	SS
1994.08.01	60.38	9.89	5	2.1	6	57	117	13	18		C	117	TF
1994.11.19	60.17	11.06	13	3.5	185	18	68	54	18		B	286	NF
1995.02.06	59.84	6.51	10	3.0	6	19	115	44	18		?	96	NS
1995.06.20	61.71	3.98	10	2.9	31	0	300	40	18	m	C	300	U
1995.11.13	60.02	11.06	18	3.4	239	12	343	47	18	m	B	329	NS
1996.01.21	69.42	24.04	10	4.2	25	70	281	5	18		B	281	TF
1996.02.08	61.05	2.9	24	2.7	277	52	37	21	20		C	37	U
1996.03.03	60.74	11.64	32	1.9	62	58	299	19	18		B	299	TF
1996.03.17	60.23	5.18	7	2.4	26	16	281	42	20		C	116	NS
1996.04.16	61.94	5.52	13	2.8	105	24	312	63	20		B	15	NF
1996.06.07	59.84	5.13	12	1.9	172	79	289	5	20		D	289	TF
1996.06.25	61.64	3.39	17	3.2	192	12	288	27	20		B	288	SS
1996.10.31	61.80	3.51	15	3.9	184	3	276	40	20		B	94	U
1996.10.31	61.82	3.51	15	3.9	157	19	266	44	20		B	67	NS
1996.10.31	61.80	3.52	15	3.7	6	3	273	40	20		B	96	U
1996.12.16	61.02	3.79	20	3.0	180	0	270	60	20		C	90	NF
1997.05.13	60.97	3.72	19	3.1	346	2	254	30	20		C	76	SS
1997.11.21	66.41	13.22	7	2.3	302	7	208	29	21	m	B	212	SS
1997.11.25	66.50	12.40	11	2.7	343	7	77	29	21	m	B	73	SS
1997.11.28	66.32	13.14	11	1.7	299	23	74	58	21	m	C	200	NF
1997.11.28	66.32	13.15	11	1.8	299	23	74	58	21	m	C	200	NF
1997.12.08	59.82	6.65	12	2.7	43	29	137	7	20		C	137	SS
1997.12.26	66.32	13.11	11	1.8	268	67	176	1	21	m	C	176	TF
1998.01.08	66.37	13.13	13	2.2	284	19	27	33	21	m	B	14	SS
1998.02.03	66.39	13.09	11	2.8	257	11	351	22	21	m	B	347	SS
1998.03.09	65.85	13.53	7	2.8	225	57	115	13	21	m	B	115	TF
1998.11.28	60.35	5.867	10	2.8	358	57	248	13	20		C	248	TF
1999.04.09	66.39	13.35	8	2	258	6	357	58	22	m	C	164	NF
1999.05.29	62.19	4.74	9	3.9	144	46	262	15	22	m	B	262	TS
1999.06.15	61.95	4.62	13	2.4	35	14	272	65	22	m	B	130	NF
1999.08.02	61.55	4.29	24	2.5	67	72	283	15	22		B	282	TF
1999.08.07	62.05	6.17	10	2.2	10	16	111	36	22		B	100	SS
1999.08.23	65.10	11.75	15	3.1	257	9	143	68	22	m	B	350	NF
1999.09.02	61.89	4.68	21	2.3	45	74	296	5	22	m	C	296	TF

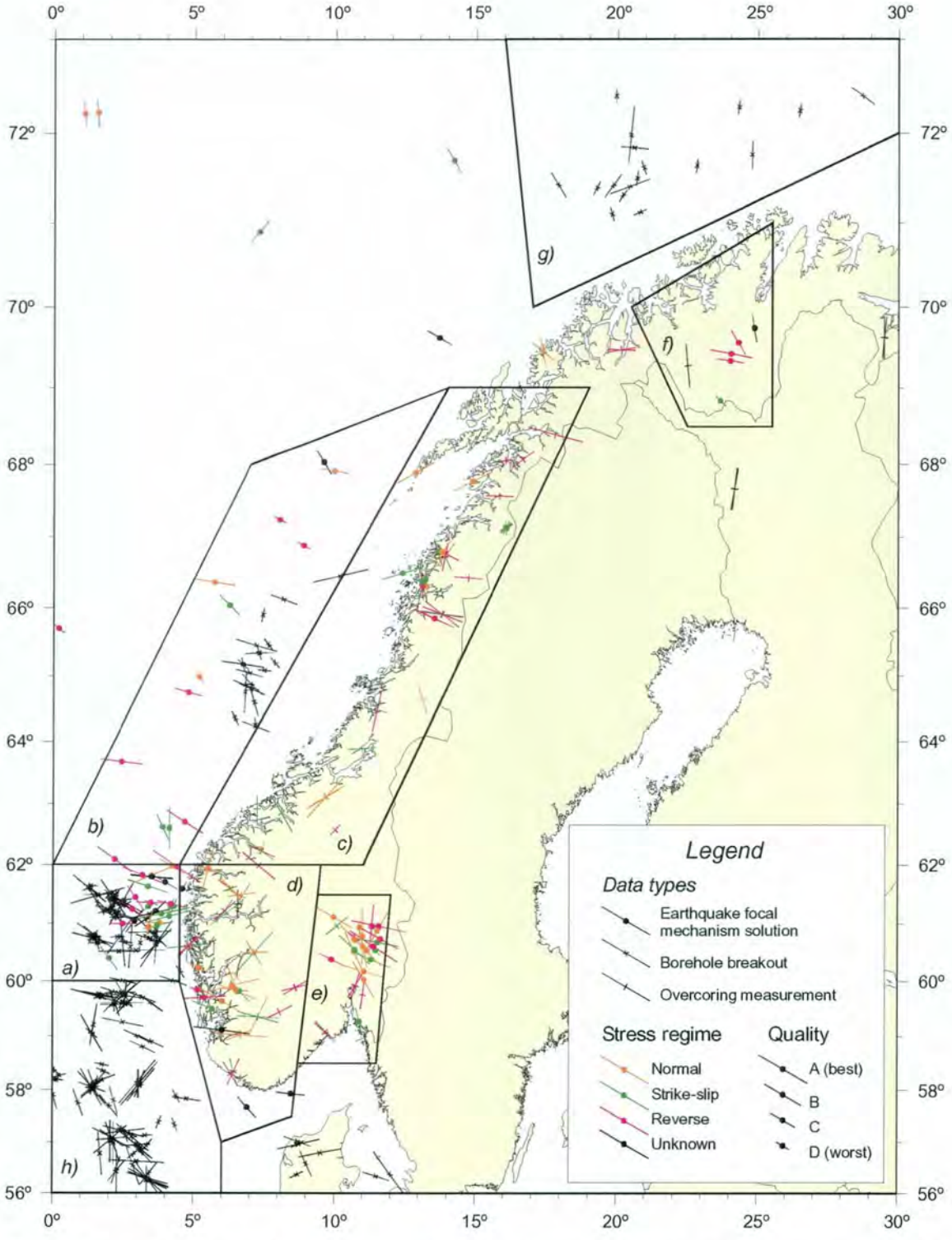

Fig. 6.4.2 Directions of maximum horizontal compressive stress and stress regime by colour for the individual data. Circles represent earthquake focal mechanism solutions, crossbars are overcoring measurements and crosses are borehole breakouts. The length of the bars reflect the World Stress Map (WSM) quality rating of the data (Zoback et al., 1992).

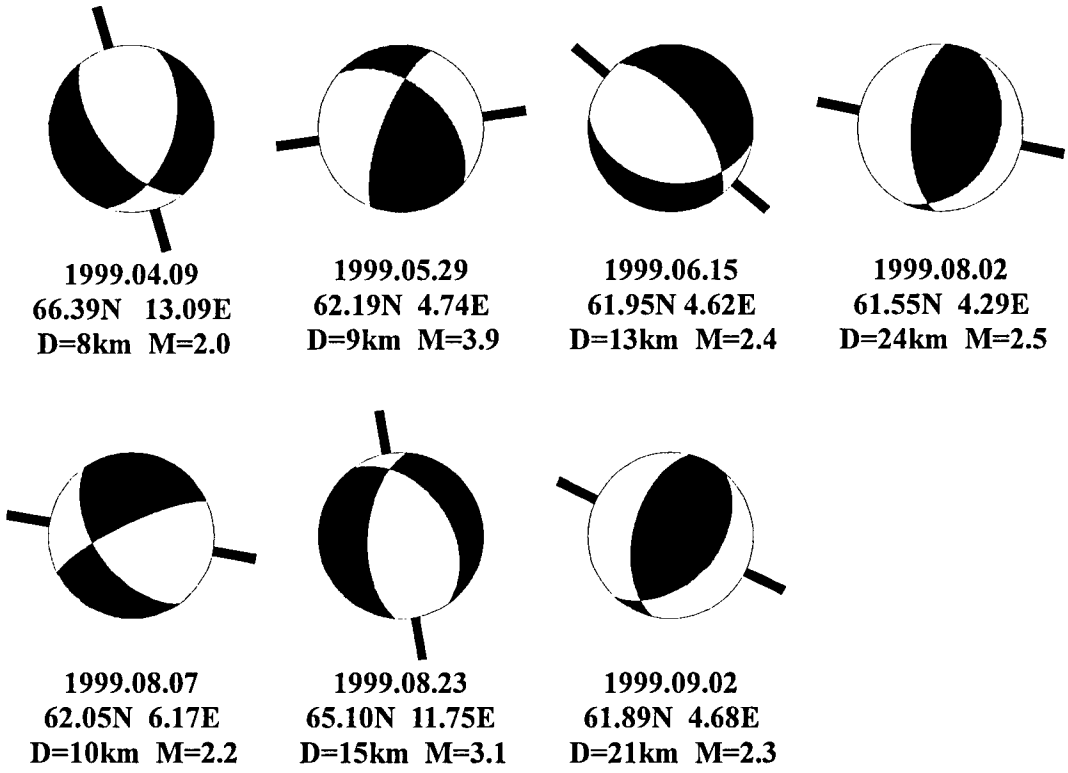

Fig. 6.4.3 The seven previously unpublished earthquake focal mechanism solution used in this study. The direction of maximum horizontal compressive stress (σ_{Hmax}) is shown by black bars behind the focal mechanisms. Two of the solutions, 1999.04.09 and 1999.08.23, are from mid-Norway, both showing a clear rotation of the σ_{Hmax} direction compared to the solutions from western Norway, which comply fairly well with the expected WNW-ESE direction of the 'ridge push' force.

6.4.4 Stress inversion of focal mechanism solutions

Principles of analysis

The P and T axes as derived from focal mechanism solutions are normally assumed also to represent the orientations of the primary stress axes that result in the highest shear stress on the two nodal planes. However, this will rarely be the case in practice, with rupture occurring at varying angles to σ_1, thus introducing a large uncertainty in the principle stress orientation for single focal mechanism solutions. Inversion is one method of reducing this uncertainty, by considering groups of focal mechanisms assumed to derive from a common stress tensor.

Stress inversion of the available focal mechanisms was done using the FMSI (Focal Mechanism Stress Inversion) package by John Gephart (Gephart 1990a), based on procedures described by Gephart and Forsyth (1984) and Gephart (1990b). The principle involved defines the misfit of a given mechanism with regard to a stress model as the minimum rotation axes required to bring each nodal plane into compliance with the stress model (Fig. 6.4.4). The plane with the smallest angle is regarded as the fault plane, unless one plane has been uniquely identified as the fault plane. The nodal plane best corresponding with a given model is thus selected. This procedure allows for errors both in fault plane orientation and slip direction. The stress models and confidence limits are determined through a simple grid search, which is

a reliable, albeit computation intensive, approach to achieve convergence for nonlinear problems.

For each stress model tested, the rotation magnitudes are summed for all data, resulting in a single measure of misfit for each model. The model with the smallest misfit value has the best fit to the combined data for that inversion.

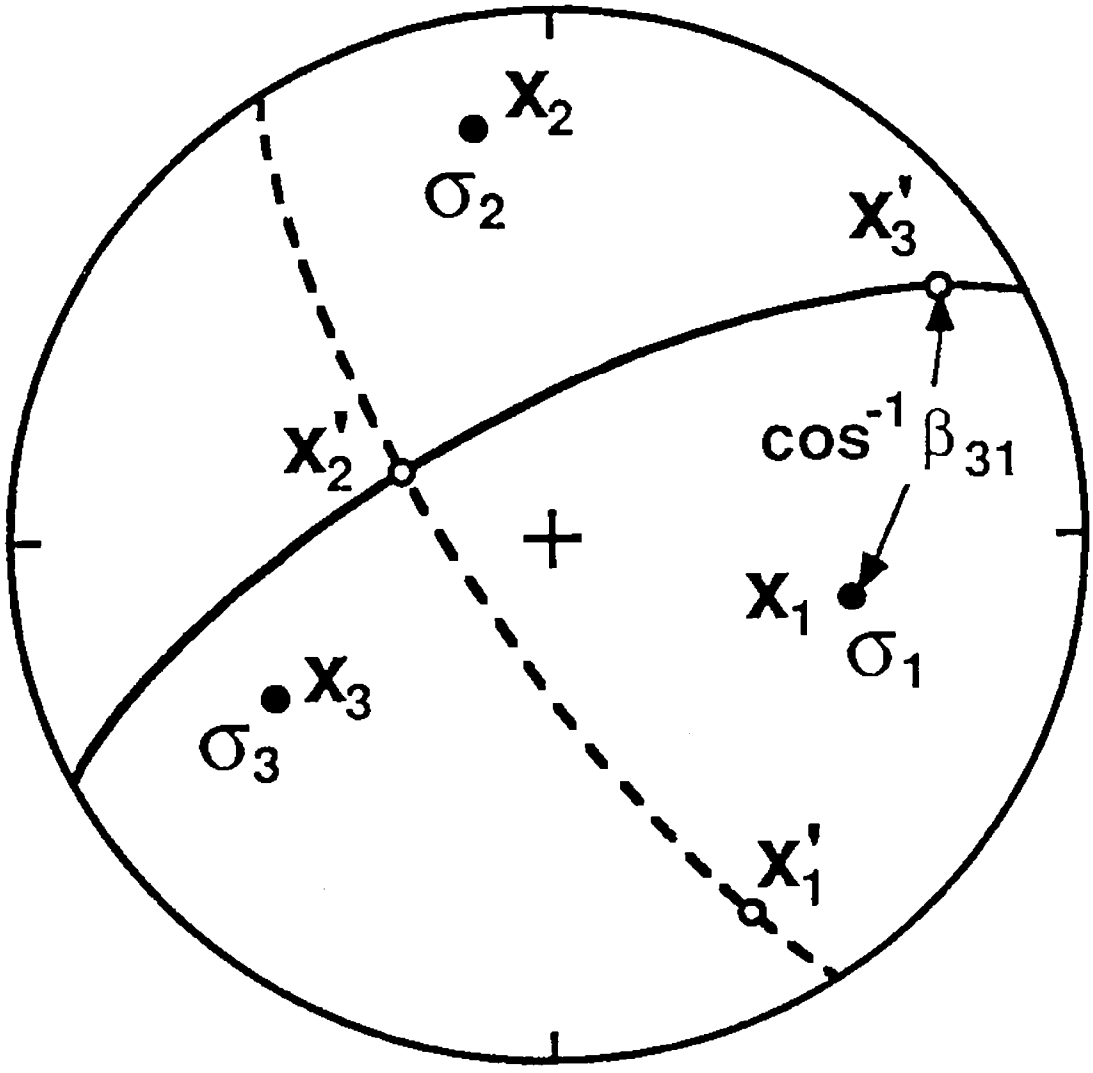

Fig. 6.4.4 The two Cartesian coordinate systems used, where x_i are principal stress axes. Fault geometry axes (x_i') are fault pole, B axis and slip direction. Solid great circle is fault plane, dashed is auxiliary plane. Transformation matrix ij = cos(xii ^ xj). After Gephart (1990a)

Method of analysis

The available earthquake focal mechanism solutions were separated within the inversion boxes shown in Fig. 6.4.2, and the P and T axes checked for orthogonality as a quality check against possible data input or conversion errors. As the solutions have quality designations from A (best) to D (worst) according to the World Stress Map (e.g. Zoback, 1992), these quality designations were used. The A, B, C and D quality data have been assigned weights of

2.0, 1.66, 1.33 and 1.0, respectively. The inversion was performed on the solutions from each area using FMSI (Gephart 1990a), calculating the misfit value for a total of 2880 stress models with σ_1 directions covering the entire hemisphere at intervals of approximately 10°. The lowest misfit values (representing the best model for each inversion) for each σ_1 direction were extracted from the result tables, gridded, and plotted stereographically. Since the misfit values have a non-uniform distribution, it is non-trivial to calculate meaningful statistical confidence values. However, to indicate the stability of the selected model within each zone, the area covered by the best 5%, 10% and 30% of the misfit values for each inversion are plotted. A small, well defined 5% area indicates a stable solution, while a large 5% area implies that there is a relatively large number of models with misfit values almost identical to the best solution. This is typically seen in regions with little data, as a large number of stress models then will give similar misfit values.

6.4.5 Crustal Stresses inferred from earthquake data

The crustal stresses for each of the eight regions are discussed based on available data. The regions have been selected based on data availability, seismic activity and crustal regime, and are of sufficient size that the first and second order stresses (continental and regional scale, cf. Table 6.4.2) should be reflected in the inversion results, while the third order (local) stresses should be reduced as they are of a more random nature. Table 6.4.2 lists some stress generating mechanisms for the different scale stresses (Fejerskov and Lindholm in press; see also Byrkjeland *et al.* in press).

For each of the six regions a) to f) in Figs. 6.4.1-2, all containing a sufficient number of earthquakes, the individual observations are shown in three different ways. In Fig. 6.4.5 the individual P and T axes are plotted stereographically with different symbols, in Fig. 6.4.6 the directions of the P axes are shown in terms of rose diagrams, properly weighted with respect to quality, and in Fig. 6.4.7 the actual focal mechanisms are shown on tripartite plots where the three principal modes of faulting are connected to different corners in the triangles using the technique of Frolich and Apperson (1992). The last type of presentation is particularly useful in that the degree of obliqueness is so well facilitated.

Table 6.4.2 Overview of stress generating mechanisms (after Fejerskov and Lindholm in press).

Stress field	Lateral endurance	Stress generating mechanisms
1. order Continental	>1000 km	Plate tectonic forces • Ridge push • Basal drag • Slab pull
2. order Regional	100-1000 km	Large-scale density inhomogeneities • Continent-ocean boundary Flexural stresses • Deglaciation • Sediment loading Wide topographic loads
3. order Local	<100 km	Topography • Fjords • Mountain ranges Geological features • Faults • Hard and soft inclusions

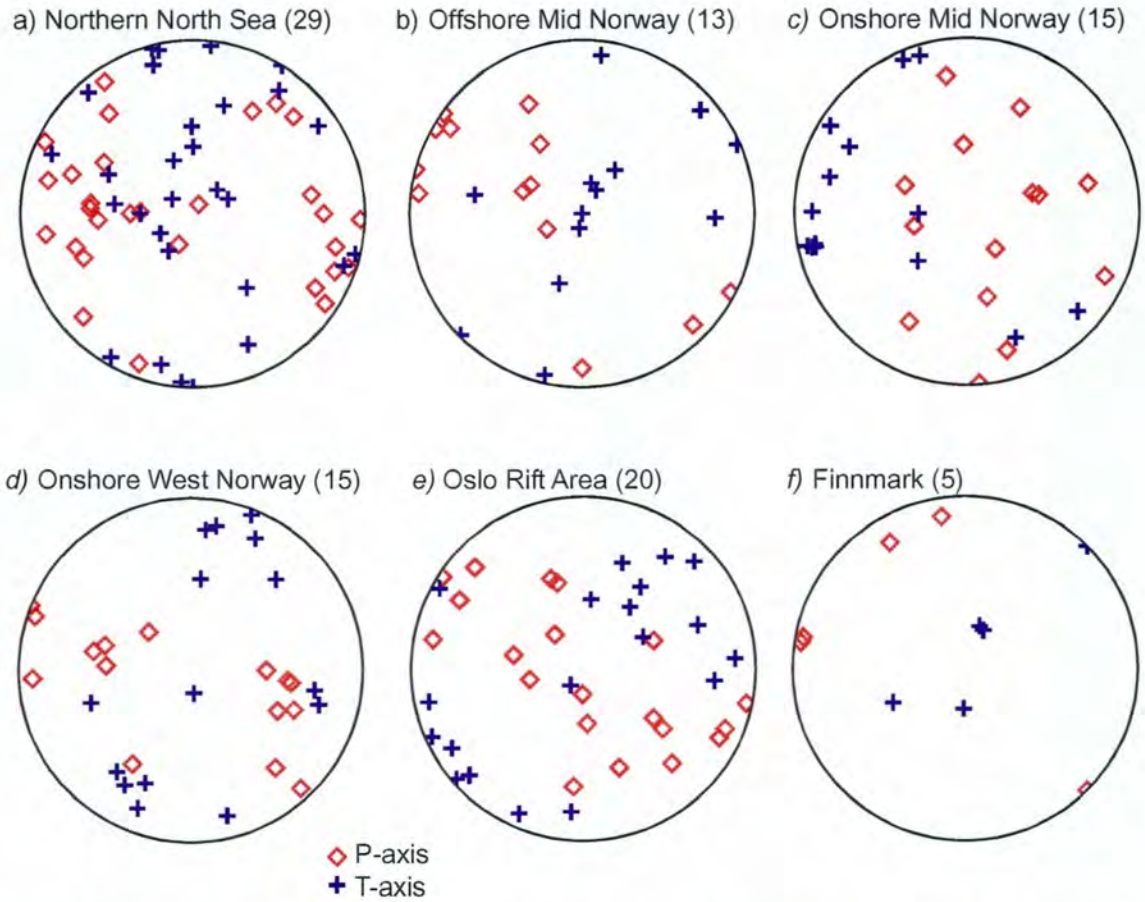

Fig. 6.4.5 Stereographic plots of P (compression) and T (tension) axes from all the earthquakes within each inversion area (defined in Fig. 6.4.1), shown as diamonds and crosses, respectively. The number of solutions in each area is given in parenthesis.

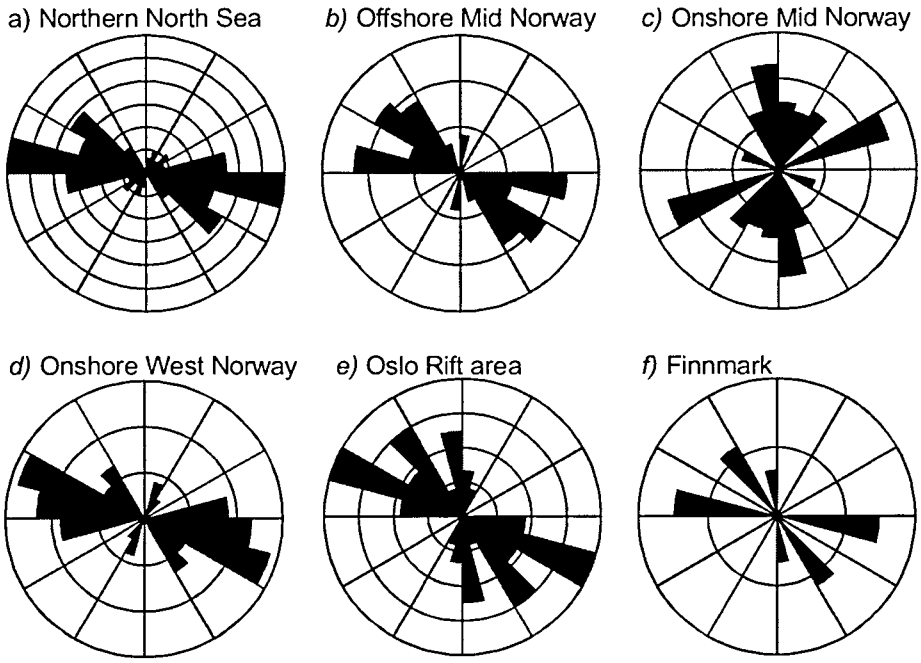

Fig. 6.4.6 Directions of maximum horizontal compressive stress as derived from the earthquake focal mechanism solutions for each inversion area (defined in Fig. 6.4.1). Each concentric circle represents one WSM 'A' quality solution (weight 2.0) or two 'D' quality solutions (weight 1.0). 'B' and 'C' quality solutions have weights of 1.66 and 1.33, respectively.

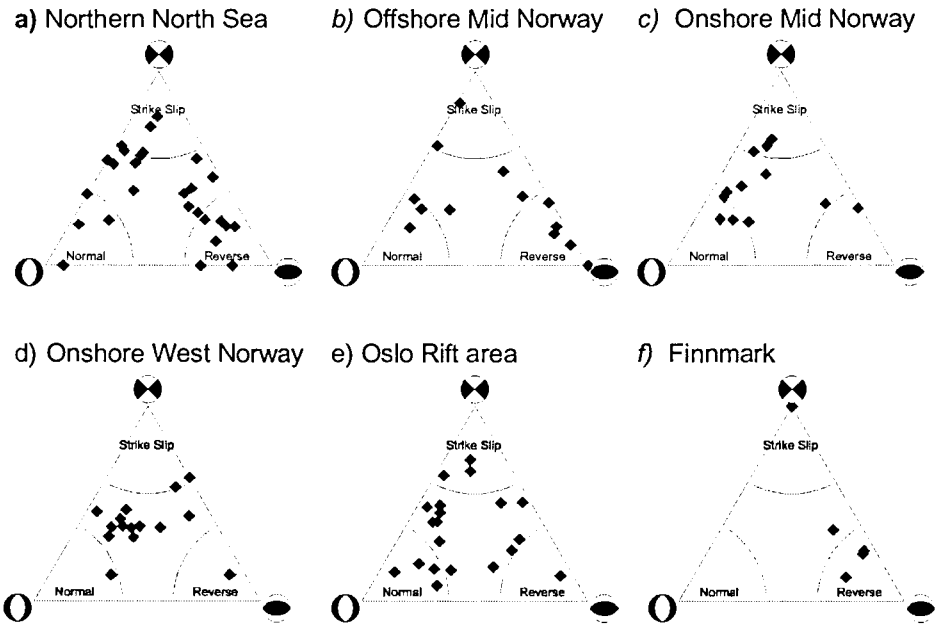

Fig. 6.4.7 Triangle plots (Frolich and Apperson, 1992) of fault regime distribution of the earthquake focal mechanism solutions for the six areas. The corners represent mechanisms where the B axis is oriented vertically (P and T axes horizontal), corresponding to pure normal, reverse and strike-slip mechanisms, respectively. The arcs represent 60° dips of the B axis, defining within each triangle the area that for practical purposes could be considered to contain "pure" solutions. The solutions located elsewhere, i.e. within the central parts of the triangles, would thereby be considered to represent oblique faulting.

The results of the inversions for each of the six areas are shown in Fig. 6.4.8, also plotted stereographically, and with indications of the resolution in each particular case. It is seen there that the only really difficult area is Finnmark, tied to the small number of events, and in spite of the fact that there are only reverse faulting mechanisms there. For the other areas the solutions are a lot more scattered while at the same time complying reasonable well with one common stress field orientation. What this first of all demonstrates is that the focal mechanism is reflecting the interaction between a regional stress field and the local conditions where the earthquake occurs, primarily existing zones of weakness.

For each of the six areas, supplemented by the western Barents Sea (area g) and the southern North Sea (area h), we also show available *in situ* stress measurements. Finally, in Fig. 6.4.10, we present a summary of the inversion results, directly based on Fig. 6.4.8, together with the two extra *in situ* areas. We now proceed to a discussion of each of the six areas in more detail.

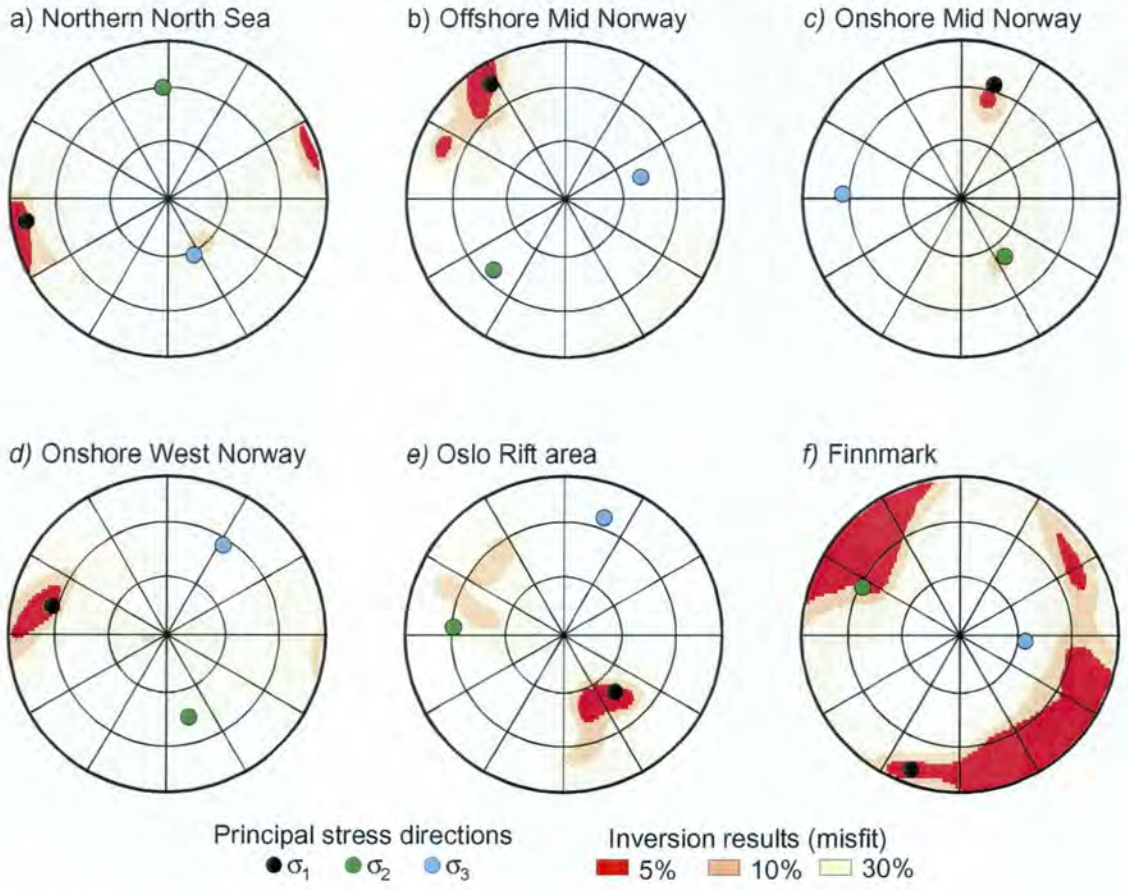

Fig. 6.4.8 Results from inversion of the earthquake focal mechanism solutions, plotted stereographically. The best stress model is shown for each area. The colored areas represent the corresponding best percentage (defined below) of the inversion results, which gives an indication of the stability of the best selected stress model. Note that most areas have a well defined, limited area covered by the best 5%, indicating a stable result. The Finnmark area is an exception, as the low number of available mechanisms give an uncertain result there, but a weak NW-SE trend is still apparent.

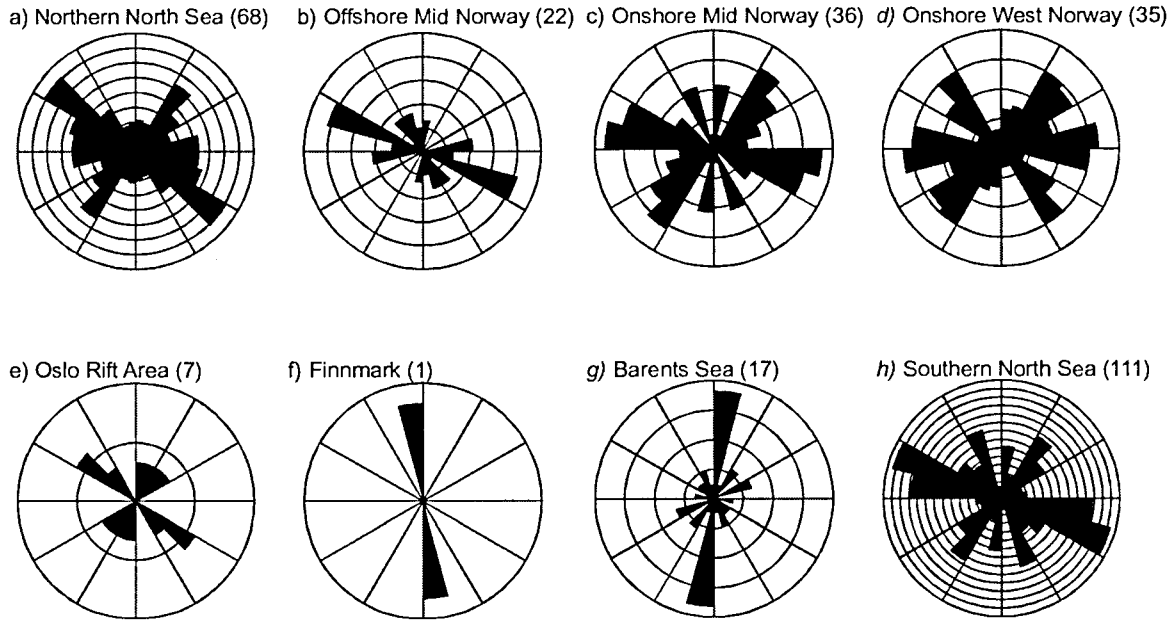

Fig. 6.4.9 Directions of maximum horizontal compressive stress from in situ measurements for each of the six earthquake inversion areas, in addition to data from the western Barents Sea and the southern parts of the North Sea. The measurements consist of borehole breakouts offshore and overcoring measurements onshore. The weighting is the same as for Fig. 6.4.6.

Table 6.4.3 Earthquake focal mechanism stress inversion results for the six areas. For each geographical area (Figs. 6.4.1 and 6.4.9) the table gives number of focal mechanisms, relative misfit number (see main text), and trend and plunge of the three orthogonal stress axes of the stress tensor.

Area	No. of F.M.s	FMSI misfit	σ1		σ2		σ3	
			trend	plunge	trend	plunge	trend	plunge
a) Northern North Sea	29	9.997	261	10	357	30	155	58
b) Offshore Mid Norway	13	5.251	327	14	225	37	74	49
c) Onshore Mid Norway	15	6.397	16	26	143	52	272	26
d) Onshore West Norway	15	6.676	284	26	165	45	32	34
e) Oslo Rift area	20	7.519	138	50	274	31	19	23
f) Finnmark	5	0.517	200	10	296	32	95	56

Table 6.4.4 Summary of the eight areas within which stress inversions are performed. The seismic activity levels used in the table are relative for Fennoscandia. Focal depths are denoted 'deep' when the bulk of earthquakes occur below 15 km, and 'shallow' when most of the earthquakes have depths less than 15 km. Similar principles are applied for stress regimes and stress directions.

Area	Tectonic regime	Seismic activity level	Focal depths	Modes of faulting	σHmax direction
Northern North Sea	Triassic-Cretaceous rifted margin	Very high	Deep	Reverse to oblique-reverse Normal to strike-slip	E-W
Offshore Mid Norway	Cretaceous-Paleocene volcanic rifted margin	High	Deep	Reverse to oblique-reverse Normal to strike-slip	NW-SE
Onshore Mid Norway	Caledonian thrust belts	High in northern parts. Earthquake swarms	Shallow	Normal to strike-slip	NNE-SSW
Onshore West Norway	Precambrian shield, thrust belts to the north	High	Shallow	Oblique at the normal to strike-slip side	ESE-WNW
Oslo Rift Zone	Permian rift	Intermediate	All	Normal (shallow) Reverse to s-s (deeper)	E-W
Finnmark	Precambrian basement, thrust belts near coast	Low	Shallow	Reverse	NW-SE
Western Barents Sea	Jurassic-Tertiary rift with later uplift	Very low			N-S
Southern North Sea	Triassic-Cretaceous rifted margin	Low	Deep	Unknown	ESE-WNW

Northern North Sea (area a)

The northern part of the North Sea is one of the most seismically active areas in Norway, and a large number of earthquake focal mechanism solutions exist for this area (29). As can be seen in Fig. 6.4.5a, there is a quite large scatter in the distribution of the P and T axes, although a trend is visible in an WNW-ESE direction for the P axes, with five outliers having an almost 90° rotation of P axis trend. This WNW-ESE trend is more visible in the rose diagram (Fig. 6.4.6a) for the maximum horizontal compressive stress (σ_{Hmax}) directions as derived from the individual earthquake focal mechanism solutions. The faulting mechanisms in this area (Fig. 6.4.7a) seem to be organized in two groups, reverse to oblique-reverse and normal to strike-slip.

The inversion results for this area (Fig. 6.4.8a) show a σ_1 axis with a fairly shallow plunge, and a trend close to E-W (see also Table 6.4.3), which is comparable to the main trend of individual σ_{Hmax} directions visible in Fig. 6.4.6a. The *in situ* σ_{Hmax} data from borehole breakouts shown in Fig. 6.4.9a is more scattered, however, but also there with a weak trend in the E-W to NW-SE direction. An WNW-ESE direction of maximum compressive stress is compatible with the expected direction of the ridge-push force in this area (Bungum *et al.* 1991).

The are a number of earthquake focal mechanism solutions from the Sogn Graben area that show a 90° rotation of σ_{Hmax} to a NNW-SSE direction, compared to the stress tensor determined by the FMSI program, and also compared to the rose diagrams of the individual σ_{Hmax} directions. The *in situ* data also has a number of measurements with a similar orientation, but these are not confined to the Sogn Graben area. This implies that a more local source of stress is active in this area, in addition to the regional scale stress sources.

Offshore Mid Norway (area b)

As seen from Fig. 6.4.1, the mid-Norwegian margin has a band of relatively high seismic activity running roughly parallel to the shelf edge through the East Vøring Basin, where evidence suggests that the prominent Plio-Pleistocene glacial wedge may be one of the main factors influencing the stress field responsible for this activity (Byrkjeland *et al.*, in press). The offshore activity here is separated from the coastal activity by the more or less aseismic Trøndelag Platform. The depth estimates for these earthquakes are uncertain due to the large hypocentral distances, but available evidence, based in part on waveform modelling (NORSAR and NGI, 1998) suggests that most of the earthquakes occur deeper than 15 km. There are 13 available earthquake focal mechanism solutions in this area. The trend of the P axes shown in Fig. 6.4.5b is quite consistent, as all but one of the focal mechanism solutions lie in a NW-SE trending band. This is also seen in the rose diagram in Fig. 6.4.6b, with all the σ_{Hmax} directions but one being confined to a 60° segment with a E-W to NW-SE trend. Fig. 6.4.7b shows that the modes of faulting in this area are organized more or less in the same way as in area a) further south in the northern North Sea, with a balance between reverse and normal.

The FMSI inversion (Fig. 6.4.8b) shows a best fitting stress tensor with a shallow plunging σ_1 axis in the NW direction. There a fewer *in situ* measurements in this area (Fig. 6.4.9b), but they also have a quite clear NW-SE trend. It would appear that the offshore areas of mid Norway have a fairly stable stress field, given the consistency of the data in this area, also between different data types. While the direction of maximum horizontal compressive stress is compatible with the expected direction of the ridge-push force in this area also, it also happens to be perpendicular to the orientation of the glacial wedge and to the continental margin itself, with significant lateral crustal inhomogeneities (cf. Byrkjeland *et al.* in press).

Onshore Mid Norway (area c)

The onshore parts of mid Norway have a noticeable pattern of seismic activity in that the southern parts are almost completely aseismic while the northern parts have significantly higher levels of seismic activity, having experienced several shallow (depth less than 12 km) earthquake swarms in recent years (Bungum *et al.* 1979; Atakan *et al.* 1994, Hicks *et al.* In press). The largest onshore earthquake know from historical times in Norway, the 31 August 1819 Rana earthquake with a magnitude of M_S 5.8-6.2 (Muir Wood 1989), also occurred in this area.

The P and T axes for the 15 available earthquake focal mechanism solutions in this area are quite scattered (Fig. 6.4.5c), although there does appear to be a weak trend for the P axes to have azimuths in an approximately N-S band. Similarly, the tension axes have a weak tendency towards a NW-SE orientation. This is the exact opposite of the offshore areas to the west (Fig. 6.4.5b). This trend is not readily apparent in the σ_{Hmax} rose diagram (Fig. 6.4.6c), but his is due the single WSW-ENE bin containing three solutions. The five bins from NNW-SSE to NE-SW contain a total of 11 solutions, so there is a very real trend of compressional stress centred around a N-S orientation visible in the earthquake focal mechanism solution data. Fig. 6.4.7c shows that the faulting is predominantly in the normal to strike-slip range, as reflected also in the noted differences in T axis orientations.

This FMSI inversion results (Fig. 6.4.8c) show a similar picture to the individual solutions, with the σ_1 axis is dipping around 25° in a northerly direction. The σ_3 axis has an approximate E-W orientation, so the stress tensor for the seismically active parts of onshore mid Norway appears to be rotated nearly 90° with respect to the expected direction of the ridge push force from the Mohns ridge in the North Atlantic. Recent compilations of postglacial uplift data

(Olesen *et al.* 2000; Hicks, in press) indicate that the contemporary uplift in this area is not necessarily as uniform as previously thought to be the case. There appear to be fairly large variations (on the order of several mm/yr) over relatively short wavelengths of less than 100 km, which certainly is a possible local stress source in the affected areas.

The *in situ* data (Fig. 6.4.9c), which consists of overcoring measurements mainly taken in or near mines are more scattered. There appears to be two trends, one sub-parallel to the coast (NE- SW) and the other roughly normal to the coast (WNW-ESE), but there does not appear to be any systematic distribution of the two main σ_{Hmax} trends with location. If the rotation just seen in the earthquake P axis directions was due to a systematic regional crustal source of stress, we should have expected to see a σ_{Hmax} rotation also in the *in situ* data in the seismically active northern areas, but this does not appear to be the case. However, one would always expect more scatter in *in situ* data, and from overcoring measurements in particular, in particular the shallow measurements are influenced by local effects (Table 6.4.2) to a much higher degree than the earthquake focal mechanism solutions.

Onshore West Norway (area d)

The onshore areas of western Norway are located in close proximity to the high seismicity levels in the northern North Sea, revealing a similarly high seismic activity (Fig. 6.4.1). The 15 earthquake focal mechanism solutions available in this area appear to be quite consistent in terms of P and T axis distribution (Fig. 6.4.5d), with the P axes aligning in an WNW-ESE direction and with the T axes oriented at 90°. This is reflected by the σ_{Hmax} directions in the rose diagram in Fig. 6.4.6d, and with a consistency that is quite striking. Almost all of the available focal mechanism solutions here are oblique (Fig. 6.4.7d), but clustered in the normal to strike-slip region.

The stress inversion results do not contradict this, as the σ_1 axis has an azimuth of 284° and with a 26° plunge (Fig. 6.4.8d). Compared to the northern North Sea to the west, this represents a small (~20°) rotation of the σ_1 axis, however the σ_2 and σ_3 axis have exchanged places, i.e. the stress tensor is rotated ~90° around the σ_1 axis compared to the offshore areas to the west. This implies a different dominant faulting regime, which is observable in the raw data. The onshore focal mechanism solutions tend to be normal faulting, while strike-slip and reverse faulting is more predominant offshore. There is a quite distinct hypocenter depth difference as well, with the onshore earthquakes generally having shallower hypocenter depths (<15 km) as compared to the greater depths (>15 km) encountered offshore.

The *in situ* data, consisting of overcoring measurements, appear to have a near random distribution, again implying that the shallow measurements are strongly influenced by local (third order) stress generating mechanisms (Table 6.4.2).

Oslo Rift area (area e)

The Permian Oslo rift has intermediate levels of seismic activity, somewhat higher than the surrounding basement areas. Due to the location of the NORSAR seismic array in this area, the number of available earthquake focal mechanism solutions is quite high (20), while the magnitudes for the solutions are generally somewhat lower.

The hypocenter depths range through the entire crust, from shallow (<5km) to more than 30 km. The P and T axes for the individual focal mechanism solutions appear to be quite systematic (Fig. 6.4.5e), with the P axes aligned in a NW-SE trending band. The rose diagram of the focal mechanism σ_{Hmax} directions (Fig. 6.4.6e) also shows a similar trend, although somewhat more scattered than for the data from western Norway. The faulting mechanisms here

(Fig. 6.4.7e) seem to be organized mostly as for onshore Mid-Norway, mostly normal to strike-slip, but some also towards the reverse side. There does, however, appear to be some variation of faulting regime with depth in the Oslo Rift zone, with the shallow (<13 km) earthquakes being of predominantly normal faulting while the deeper earthquakes are dominated by strike-slip and reverse faulting (Hicks 1996).

The FMSI inversion gives a best fitting stress model with a fairly steeply plunging σ_1 axis (50°), trending towards the SE (Fig. 6.4.8e; Table 6.4.3). This is a significant rotation compared to the adjacent area in western Norway, probably related to a second order stress generating mechanism, possibly the rift structure itself. Only seven *in situ* measurements are available for this area, so no significant information can be inferred from this. However, based on the generally large scatter in overcoring measurements in western and mid Norway, it does not appear as if overcoring measurements can offer much meaningful data on regional or continental scale stresses in any case.

Finnmark (area f)

Finnmarksvidda is an area that is, in general, considered to have low levels of seismic activity. A relatively large earthquake occurred in 1996, with a magnitude of M_L 4.0, the largest in this region in 60 years (Bungum and Lindholm 1996; Hicks 1996). This earthquake, and five others with magnitudes ranging from M_L 1.4 to 3.3 all have shallow hypocenter locations within 10 km southeast of a large, postglacial fault striking NE-SW (Olesen 1988; Bungum and Lindholm 1996).

With only five focal mechanism solutions available in this area, one can not normally expect to be able to infer a stress model with any significant certainty, however it is apparent from Fig. 6.4.5f that all five solutions have near-horizontal P axes in an approximately NW-SE direction. The rose diagram (Fig. 6.4.6f) of the σ_{Hmax} directions is similar, although the data is to scarce for any more detailed trends to be apparent. The mechanisms (Fig. 6.4.7f) are almost all purely reverse in this case, fully consistent with the strong neotectonic observations from this area (Olesen, 1988).

Due to the low number of data points, the inversion results seem to be quite unstable (Fig. 6.4.8f; Table 6.4.3). The best fitting stress model has an orientation in a NNE-SSW direction, but with the best 5% of the misfit values covering a large area ranging from E-W to NNE-SSW. However, based on the individual data the σ_1 axis has a most likely azimuth around NW-SE, with a shallow plunge. This is a direction that is compatible with the expected direction of horizontal compression from the mid-Atlantic spreading ridge.

6.4.6 Crustal stresses inferred from *in situ* data

Western Barents Sea (area g)

The western Barents Sea has very low levels of seismic activity, which combined with the fact that the distance to any seismic station is large, means that there are no earthquake focal mechanism solutions available. However, the 17 available borehole breakouts are surprisingly consistent in σ_{Hmax} directions (Fig. 6.4.9g), with nearly 2/3 of the data lying within the same 15° bin with a N-S trend. The boreholes are scattered over a large area in the southern parts of the western Barents Sea, so it would appear that this is a real trend.

Southern North Sea (area h)

The southern parts of the North Sea have, in contrast to the regions to the north, low to intermediate levels of seismic activity. This means that there are currently no earthquake focal mechanism solutions available. However, due to extensive hydrocarbon exploration in this area, a large number of borehole breakouts area available (111). Although the σ_{Hmax} directions are quite scattered, there is a fairly consistent trend in the WNW-ESE direction (Fig. 6.4.9h). The low seismic activity of this area suggests that there are no dominant stress generating mechanisms capable of inducing the differential stresses required for higher levels of seismic activity, but the *in situ* data suggests that there is a compressive force in the WNW- ESE direction, quite possible originating from the mid-Atlantic ridge.

These results from the southern North Sea are in a clear contrast to similar *in situ* results reported from further south in the Central Graben (Ask 1998), where the stress data are much more scattered, essentially random. The difference here is expected to be somehow related to a difference in the ability of the sedimentary rocks in the two regions to support regional stress propagation (Bjørlykke 1995; Bjørlykke and Høeg 1997).

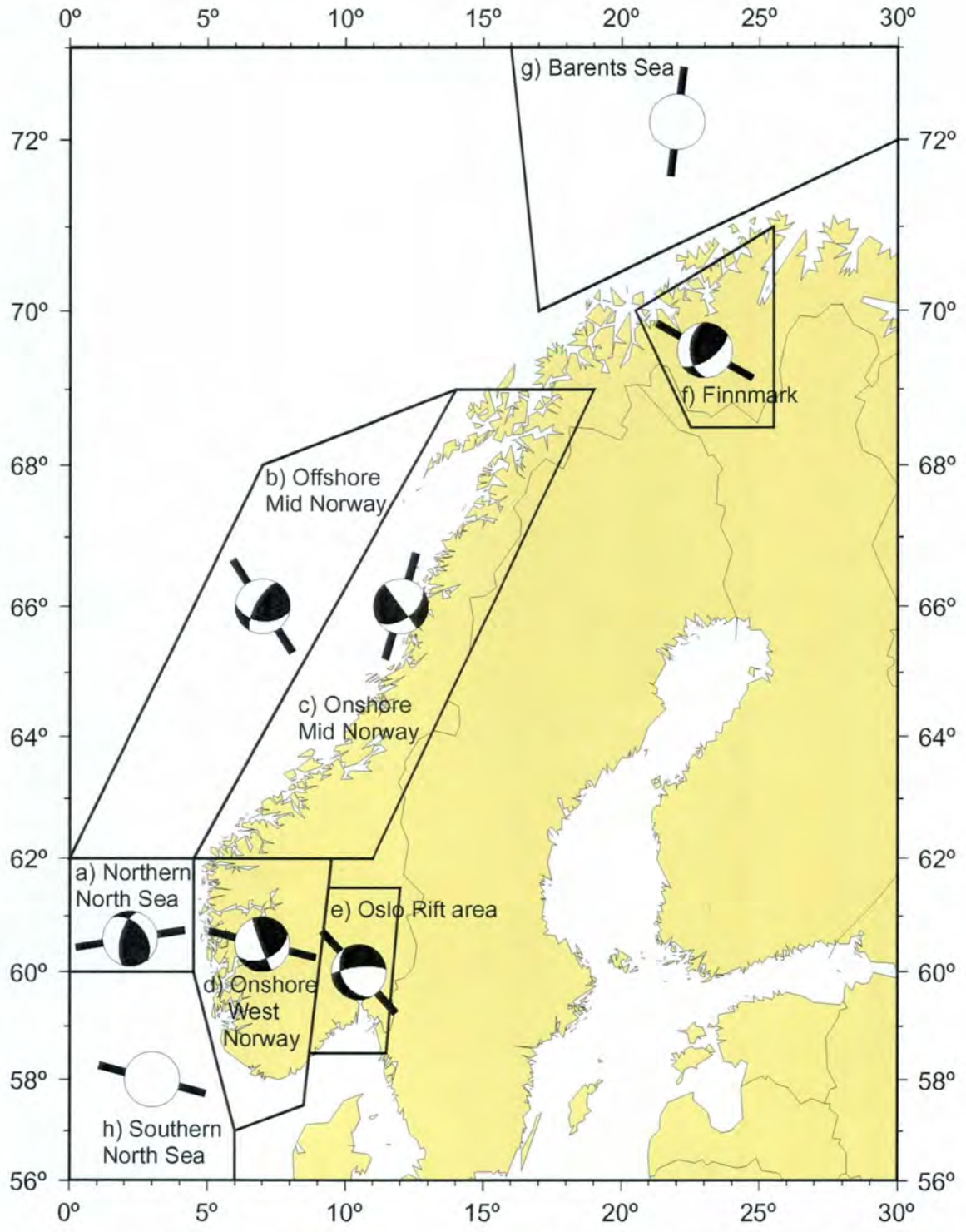

Fig. 6.4.10 Composite focal mechanism solutions derived from the inversion results for each area. The solution in Finnmark is rotated with regard to the inversion result to reflect the consistent σ_{Hmax} direction in the data, as the inversion in this case appears to be unstable due to the low number of solutions in this area. The western Barents Sea and southern North Sea areas are plotted as pure strike-slip solutions, as the only available data there are borehole breakouts with σ_{Hmax} values only.

6.4.7 Concluding remarks

The results as obtained through the earthquake stress inversions for the six regions in southern, central and northern Norway are summarized in Table 6.4.4 and Fig. 6.4.10, complemented with two regions (southern North Sea and western Barents Sea) from where only *in situ* stress measurements are available. The regional differentiation in terms of modes of faulting as shown in Fig. 6.4.7 reflects a considerable scatter, but at the same time interesting systematic differences, and the main observation here is a (albeit weak) tendency for reverse to strike-slip faulting in offshore areas (a-b) and normal to strike-slip in onshore areas (c-e), as discussed in more detail elsewhere (e.g., Stein *et al.*, 1979; Byrkjeland *et al.*, in press). The quality and resolution of these observations are, however, considerably improved in the present study as compared to what has been documented earlier.

The inversion results basically show stress directions which comply quite well with the directions expected from the plate-wide, first-order gravitational force from the mid-Atlantic spreading ridge (Fejerskov and Lindholm in press). This is the so-called ridge push, which by definition should be perpendicular to the spreading ridge (and not necessarily following the flow lines for the spreading, which is often assumed). The different direction in the western Barents Sea is not really an exception here since the ridge push force there should be expected to be different both in direction and strength, reflecting the change both in direction, morphology and rheology as one moves from the Mohns Ridge and into the Knipovich Ridge.

This coincidence between observed and predicted stress directions, also clearly seen globally (Zoback *et al.* 1992), is a strong indication of an acceptable physical mechanism. However, it is not necessarily enough to unequivocally conclude that what we see is a ridge push domination within all sub-regions in our study. The reason for this is that for some of these sub-regions we have second order sources of stress (cf. Table 6.4.2) which should be expected to be oriented in the same direction, first of all large-scale density inhomogeneities across the continental margin and farther into the Fennoscandian shield. Even more locally, third order sources of stress are expected to come into play. In an extensive review of this problem Byrkjeland *et al.* (in press) have concluded, from a combined study of seismicity distribution, inferred stress and stress modelling, that such higher order sources of stress are in fact needed in order to explain the seismicity in our study region. Another support for a reflection of more local effects in our focal mechanisms is the difference in mode of faulting between onshore and offshore areas, showing a tendency for normal (and also more shallow) faulting onshore and strike-slip and reverse faulting offshore, as also expected theoretically (Stein *et al.* 1979).

One of the most interesting observations in the available focal mechanism data base presented here is the 90° rotation of σ_{Hmax} in the Sogn Graben/Tampen Spur area and in the coastal parts of Nordland (Rana), demonstrating significant local stress variations as well as the importance of local stress sources. Such a rotation was noted for the first time by Bungum *et al.* (1991) and has been commented on often since then (Lindholm *et al.* 1995; 1999; Hicks *et al.* In press; Byrkjeland *et al.* in press), but explained generally only as an interchange of σ_H and σ_h (the largest and smallest horizontal stress components) which more easily can been achieved when the $\sigma_H/\ \sigma_h$ ratio is not far from unity. This would most easily be feasible in thrust-faulting regimes where σ_3 is vertical and in normal-faulting regimes when σ_1 is vertical, allowing σ_H and σ_h to be close to each other. An example here is an *in situ* measurement from 100 m depth in Bidjovarre, Finnmark (Dehls *et al.* 1999), where σ_1 and σ_2 both were of the order of 15-17 MPa and σ_3 was 12-13 MPa.

Another possible explanation for stress axis rotation as seen in our data has been suggested recently by Nick Barton (pers. comm. 1999), based on the fact that dilation accompanying

rock failure and weakness zone shearing introduces a component of shear strain that is no longer parallel to the assumed direction of shearing. Principal stresses are transformed to their shear and normal stress components along the wrong surface, following Mohr theory, and result in incorrect magnitudes of both the shear and normal components due to ignorance of the mobilized dilatation angle (Barton, 1986). The dilation angle in turn is dependent on fault roughness and compression strength, and it is easily seen that this effect also may significantly affect the balance between the stress components. The normal and shear stress changes that accompany dilatant shearing can radically alter the principal stress components that caused the event to occur, thereby potentially rotating major principal stresses, as apparently observed.

6.4.8 References

Arvidsson, R. and Kulhanek, O. 1994: Seismodynamics of Sweden deducted from earthquake focal mechanisms. *Geophysics Journal International 116*, 366-292.

Ask, M.V.S., 1988: *In situ* stress breakouts in the Danish sector of the North Sea. *Mar. Petr. Geol.*, 14, 231-243.

Ask, M.V.S., Mueller, B. and O. Stephansson, O. 1996: *In situ* stress determination from breakouts in the Tornquist Fan, Denmark. *Terra Nova 8*, 575-584.

Atakan, K. Lindholm, C. D. and Havskov, J. 1994: Earthquake swarm in Steigen northern Norway: an unusual example of intraplate seismicity. *Terra Nova 6*, 180-194.

Barton, N.R. 1986: Deformation phenomena in jointed rock. *Géotechnique 36*, 147-167.

Bjørlykke, K., 1995: Fracturing and brittle/ductile properties of sedimentary rocks in relation to diagenesis and *in situ* stress. *In* Fejerskov, M. and Myrvang, A.M. (eds.), *Proceedings of the Workshop: Rock Stresses in the North Sea*, pp. 64-75, Univ. of Trondheim, Norway.

Bjørlykke, K. and Høeg, K. 1997: Effects of burial diagenesis on stresses, compaction and fluid flow in sedimentary basins. *Mar. Petr. Geol. 14*, 267-276.

Bungum, H., Alsaker, A., Kvamme, L. B. and Hansen, R. A. 1991: Seismicity and seismotectonics of Norway and nearby continental shelf areas. *Journal of Geophysical Research 96*, 2249-2265.

Bungum, H. and Fyen, J. 1979: Hypocentral distribution, focal mechanisms and tectonic implications of Fennoscandian earthquakes, 1954-1978. *GFF 101*, 261-271.

Bungum, H., Hokland, B., Husebye, E. S. and Ringdal, F. 1979: An exceptional intraplate earthquake sequence in Meløy, northern Norway. *Nature 280*, 32-35.

Bungum, H. and Kristoffersen, Y. 1980: A microearthquake survey of the Svalbard region, Final report, Phase I. *NORSAR Tech. Rep. 1/80*, NTNF/NORSAR, Kjeller, Norway, 28pp.

Bungum, H. and Lindholm, C. 1996: Seismo- and neotectonics in Finnmark, Kola and the southern Barents Sea, part 2: Seismological analysis and seismotectonics. *Tectonophysics 270*, 15-28.

Byrkjeland, U., Bungum, H. and Eldholm, O. in press: Seismotectonics of the Norwegian continental margin. *Journal of Geophysical Research.*

Chan, W. W. and Mitchell, B. J. 1985: Intraplate earthquakes in northern Svalbard. *Tectonophysics 114*, 181-191.

Dehls, J. and Olesen, O., 1998: NEONOR: Neotectonics in Norway: Annual technical report 1997, Rep. 98.016, 149 pp., Norges Geol. Undersøkelse, Trondheim.

Dehls, J. and Olesen, O. 1999: NEONOR: Neotectonics in Norway: Annual technical report 1998, Rep. 98.007, 206 pp., Norges Geol. Undersøkelse, Trondheim.

Fejerskov, M. and Lindholm C.D.: Crustal stress in and around Norway; An evaluation of stress generating mechanisms. *Geological Society of London, Spec. Publ*, in press.

Fejerskov, M., Lindholm, C. D., Bungum, H., Myrvang, A., Bratli, R. K. and Larsen, B. T. 1996: Crustal stresses in Norway and adjacent offshore regions, Final report for the IBS-DNM project, topic 1.3 "Regional Stress Field", Norwegian Institute of Technology, Trondheim, Norway, 29 pp.

Frolich, C. and Apperson K.D. 1992: Earthquake focal mechanisms, moment tensors, and the consistency of seismic activity near plate boundaries. *Tectonics 11*, 279-296.

Gephart, J. W. and Forsyth, D. W. 1984: An improved method for determining the regional stress tensor using earthquake focal mechanism data: Application to the San Fernando earthquake sequence. *Journal of Geophysical Research 89*, 9305-9320.

Gephart, J. W. 1990a: FMSI: A FORTRAN program for inverting fault/slickenside and earthquake focal mechanism data to obtain the regional stress tensor. *Computers and Geosciences 16*, 953-989.

Gephart, J. W. 1990b: Stress and the direction of slip of fault planes. *Tectonics 9*, 845-858.

Hansen, R. A., Bungum, H. and Alsaker, A. 1989: Three recent larger earthquakes offshore Norway. *Terra Nova 1*, 284-295.

Havskov, J. and Bungum, H. 1987: Source parameters for earthquakes in the Northern North Sea. *Norsk Geologisk TIdsskrift 67*, 51-58.

Herrmann, R.B. 1978: A note on causality problems in the numerical solution of elastic wave propagation in cylindrical coordinate systems. *Bulletin of the Seismological Society of America 68*, 117-124.

Herrmann, R.B. 1979: SH-wave generation by dislocation sources - a numerical study. *Bulletin of the Seismological Society of America 69*, 1-15.

Hicks, E. C. 1996: Crustal stresses in Norway and surrounding areas as derived from earthquake focal mechanism solutions and *in situ* stress measurements. Cand. Scient thesis, University of Oslo, Norway, 164 pp.

Hicks, E.C., Bungum, H. and Lindholm, C.D.: Seismic activity, inferred crustal stresses and seismotectonics in the Rana region, Northern Norway. *Quaternary Science Reviews*, in press.

Kibsgaard, A. 1985: Focal mechanism studies of P to SV amplitude ratio. Cand. Scient thesis, University of Oslo, Norway, 115 pp.

Lazareva, A. P. and Misharina, L. A. 1965: Stresses in earthuqake foci in the Arctic seismic belt. *Inv. Earth. Phys. Ser. 2*, 5-10 (translated).

Lindholm, C. D., Bungum, H., Bratli, R. K., Aadnøy, B. S., Dahl, N., Tørudbakken, B. and Atakan, K. 1995: Crustal stress in the northern North Sea as inferred from *in situ* measurements and earthquake focal mechanisms. *Terra Nova 7*, 51-59.

Lindholm, C.D., Bungum, H., Hicks, E. and Villagran, M. 1999: Crustal stress and tectonics in Norwegian regions determined from earthquake focal mechanisms. *Geol. Soc. Spec. Publ.*, in press.

Lindholm, C. D. and Havskov, J. 1989: Final report on evaluation of Statfjord OBS data, A detailed study of the seismicity in northern North Sea. *Progress report 11*, University of Bergen, Norway, 34 pp.

Mitchell, B. J., Bungum, H., Chan, W. W. and Mitchell, P. B. 1990: Seismicity and present-day tectonics of Svalbard. *Geophysics Journal International 102*, 139-149.

Muir Wood, R. 1989: The Scandinavian earthquakes os 22 December 1759 and 31 August 1819. *Disasters 12*, 223-236.

NORSAR and NGI, 1998: Seismic Zonation for Norway, Rep., 188 pp., Norwegian Council for Building Standardization (NBR), Oslo.

Olesen, O. 1988: The Stuoragurra fault, evidence of neotectonics in the Precambrian of Finnmark, northern Norway. *Norsk Geologisk Tidsskrift 68*, 107-118.

Savostin, L. A. and Karasik, A. M. 1981: Recent plate tectonics of the Arctic basin and of northeastern Asia. *Tectonophysics 74*, 111-145.

Stein, S., Cloetingh, S., Sleep, N.H. and Wortel, R. 1979: Passive margin earthquakes, stresses and rheology. In: Gregersen, S. and Basham, P.W (eds.): *Earthquakes at North-Atlantic Passive Margins: Neotectonics and Postglacial Rebound*, NATO ASI Ser., 266, 231-259.

Vaage, S. 1980: Seismic evidence of complex tectonics in the Meløy earthquake area. *Norsk Geologisk Tidsskrift 60*, 213-217.

Wang, C.E. and Herrmann, R.B. 1980: A numerical study of P-, SV-, and SH-wave generation in a plane layered medium. *Bulletin of the Seismological Society of America 70*, 1015-1036.

Zoback, M.L. 1992: First and Second-Order Lithospheric Stress Patterns. *Journal of Geophysical Research 97*, 11703-11728.

6.5 SEISMIC ACTIVITY, INFERRED CRUSTAL STRESSES AND SEISMOTECTONICS IN THE RANA REGION, NORTHERN NORWAY

By Erik C. Hicks, Hilmar Bungum and Conrad D. Lindholm, NORSAR

6.5.1 Introduction

The Fennoscandian Shield has long been recognized as an ideal natural laboratory for studies of lithospheric and asthenospheric response to glacial loading and unloading, on the basis of its history of glaciations and deglaciations, including an uplift rate today of 7mm/year in the Bothnian Bay region (e.g., Ekman, 1996; Fjeldskaar, 1994; 1997). The last deglaciation, which occurred approximately 8-10,000 years ago, was rapid but also most likely irregular (e.g., Denton and Hughes, 1981), in time as well as in space. As late as in the 1970's (Lundquist and Lagerbäck, 1976), strong manifestations of sudden crustal response to this deglaciation (Johnston, 1987) were found as prominent Lappland neotectonic faults indicating the early Holocene occurrence of several M7+ earthquakes in this region (Muir Wood, 1989; Bungum and Lindholm, 1997). While a broad range of research efforts on these topics were initiated in Sweden in the 1980's (e.g., Bäckblom and Stanfors, 1988), more recent neotectonic research on the Norwegian side has further contributed to our understanding of this phenomenon (e.g., Dehls and Olesen 1998; 1999; Dehls *et al.*, 1999).

The seismicity and seismotectonics along the continental margin and the coastal region of mid and northern Norway (Fig. 6.5.1) is well documented. Byrkjeland *et al.* (in press) and Fejerskov and Lindholm (in press) have recently studied the seismotectonics of this region in relation to possible stress generating mechanisms, and have concluded that even though the first-order regional compressive stress field most likely is connected to plate boundary related ridge push forces, the ridge push stress effects in themselves are not considered sufficient for releasing earthquakes. These authors therefore claim that other regional and local stress factors, such as flexural stresses from sedimentary loading, together with favorably oriented and sufficiently weak faults, have to be invoked in order to explain the occurrence and distribution of earthquakes in this region.

It is the seismicity along the coastal region of northern Norway which is the main subject of the present study. The main data used in pursuing this have been obtained from a local network of six short-period vertical-component stations which were installed in the Rana region in July 1997, extending about 40 km E-W and 25 km N-S (Fig. 6.5.2), and reduced to a four-station configuration in September, 1998. The purpose of this paper is to report the main results and to analyze and discuss them in a wider neo- and seismo-tectonic context.

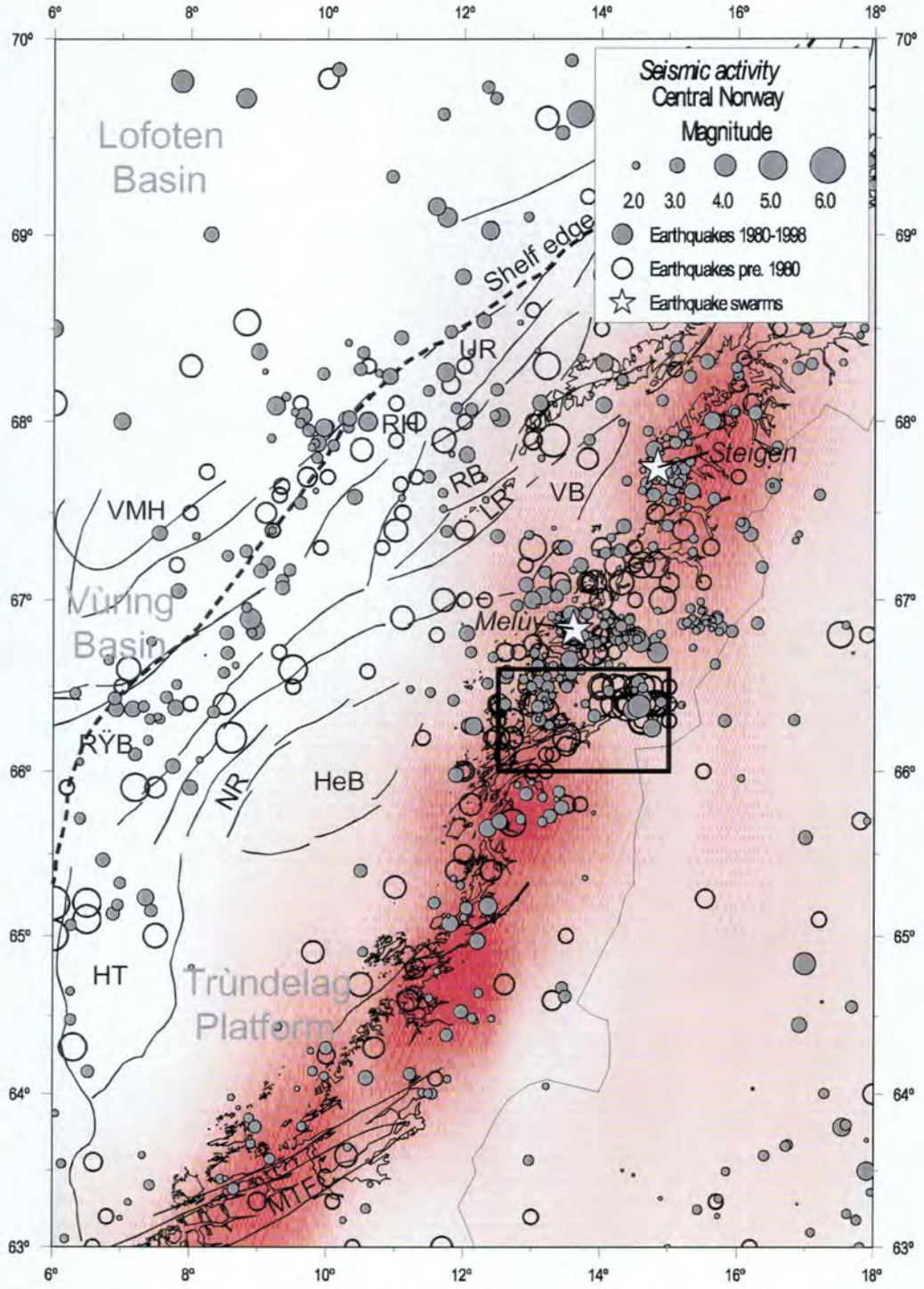

Fig. 6.5.1 Regional seismic activity from pre 1980 (open circles) and 1980 to 1998 (grey circles), from the NORSAR catalog (NORSAR and NGI, 1998). The black rectangle indicates the Rana area studied in this paper. The Meløy (Bungum et al., 1979) and Steigen (Atakan et al., 1994) earthquake swarms are shown by white stars. The uplift gradients calculated from a rather coarsely filtered grid (100 km lowpass) are shown in red, where dark red indicates a high uplift gradient. Structural information from Byrkjeland et al. (in press). HeB= Helgeland Basin, HT= Halten Terrace, LR= Lofoten Ridge, MTFC= Møre-Trøndelag Fault Complex, NR= Nordland Ridge, RB= Ribban Basin, RH= Røst High, RåB= Rås Basin, UR= Utrøst Ridge, VB= Vestfjorden Basin, VMH - Vøring Marginal High.

6.5.2 Seismo-geological setting

Regional and local seismicity

The seismicity distribution as shown in Fig. 6.5.1 has been established using a combination of field-based historical data (Muir Wood and Woo, 1987) and more recent instrumental data from the country-wide network of seismic stations. In going westward towards the coast, Byrkjeland *et al.* (in press) have concluded that the oceanic crust is mostly aseismic apart from areas that have experienced rapid glacial loading since 2.6 Ma, notably in the East Lofoten and East Norway basin provinces. Here, thick sediment loads and high deposition rates are considered to be responsible for local flexures and corresponding earthquake activity. The Vøring marginal high and the adjacent basins that experienced rifting and crustal thinning prior to the Early Tertiary continental breakup are almost entirely aseismic, suggesting that the crustal thickening and underplating resulting from the igneous breakup event have strengthened the crust in these regions.

Along the shelf edge (shown on Fig. 6.5.1), the seismicity is significant again, revealing a spatial correlation with a late Pliocene-Pleistocene glacial wedge that suggests that rapid sediment loading here has led to rejuvenation of Late Jurassic-Early Cretaceous faults. East of the main glacial wedge most of the seismic activity is found along the coast. Even if the postglacial rebound is small in the coastal region, the relative subsidence west of the hinge line makes the coastal region an area of high postglacial rebound gradients, which implies high strains and increased seismicity.

NEONOR, a 1997-1999 neotectonics research project (Dehls and Olesen, 1998; 1999; Olesen et al. 2000) selected the Rana area for an in-depth study of a smaller region. Among the reasons for this was the fact that for a long time this region has revealed a relatively high, constant level of seismic activity, including the largest known historical earthquake in northwestern Europe, an M 5.8- 6.2 earthquake in 1819 (Muir Wood, 1989a), and that this region contains the prominent EW trending Båsmoen fault, which has been considered to be likely neotectonic (Olesen *et al.*, 1994; Dehls and Olesen, 1998).

The seismicity map in Fig. 6.5.1 shows, besides the seismicity along the shelf edge (which should be expected to relate to other stress generating mechanisms), that there also is a clear coastal trend, with the majority of the activity concentrated between 66° and 68° N. It is also seen from Fig. 6.5.1. that also the postglacial uplift gradients are highest along the coast.

Local geological setting

The geology of the Rana area is dominated by the exotic terranes of the upper parts of the Caledonian thrust belts, emplaced towards the end of the Caledonian orogeny around 400 Ma, with smaller windows of Precambrian basement (Fig. 6.5.2). The nappes consist mainly of fairly high-grade mica schist/gneiss and marble, and large, mostly granitic intrusions. The lower units (lower and upper Rødingfjell nappes) occur to the north and west of the Rana area, and contain large marble bodies and moderately large granitic intrusions. The uppermost unit (Helgeland nappe) is found to the southwest of the Rana fjord, and is dominated by batholitic scale granitic intrusives. The visible Precambrian basement areas northwest of the Rana and Sjona fjords are mostly composed of granitic gneisses.

Deglaciation of the Rana area occurred around 11000-9000 BP, constrained by mapping of moraine ridges (e.g. Blake and Olsen, 1999). The Vega glacial limit (~12200 BP) (Rasmussen, 1981; Gjelle *et al.* 1995) is only encountered offshore on islands west of the mainland, while the moraines associated with the Tjøtta glacial event (11200-10400 BP) can be followed across the mainland north of the Sjona fjord, across the Handnesøya and Hugla islands, and

continue south of the Rana fjord (Andersen, 1975, Andersen *et al.*, 1982, 1995). The Nordli (10200-10100 BP) moraines are located around 20 km east of the Tjøtta moraines (Andersen *et al.*, 1982). The Preboreal moraines are quite poorly constrained between the Rana fjord and the Svartisen glacier, but several segments are mapped south of the Rana fjord that have been constrained in two groups that are correlated with the Narvik II and Rombak events (Bergstrøm 1994, Olsen *et al.*, 1996). The outer Preboreal moraine group consists of Narvik II (9600±200 BP) south of the Svartisen glacier, (Andersen, 1975, Andersen *et al.*, 1995) and is located around 15-20 km east of the Nordli moraines. The inner Preboreal moraine group, the Rombak moraines (9300±200 BP) is located east of the Svartisen glacier to the north, and appears to pass quite close to Mo i Rana (Andersen, 1975, Andersen *et al.*, 1995).

The Båsmoen fault is a southward dipping reverse structure, from which the surface trace can be followed as a marked topographic lineament for approximately 50 km on the north side of the Rana fjord (Olesen *et al.*, 1994). Studies performed as part of the NEONOR project concluded that the fault most likely has experienced postglacial movement on the order of 30-40 cm, confined by C14 dating from layers directly above and below the tectonic indicators to between 8780 (±80) and 3880 (±75) years BP.

Sources of stress

For the region under study there are three main sources of stress to be considered, namely the ridge push effect, density differences (including topography) and flexural stresses (loading/unloading). In oceanic lithosphere, the ridge push force is considered capable of giving rise to stresses of the order of 20-30 MPa, dependent on (increasing with) age (Dahlen, 1981; Bott and Kusznir, 1984). Since the magnitude of stress is inversely proportional to the crustal thickness, one should expect lower values (~10-20 MPa) in thicker continental crust (Bott, 1991; Fejerskov and Lindholm, in press), albeit dependent on possible subcrustal density differences. However, it is generally accepted (e.g., Byrkjeland *et al.*, in press) that the ridge push force in itself is not sufficient to explain the seismicity along the continental margin. This follows from the observation that the seismic activity is unevenly distributed, and follows tectonic features (including the margin itself, sedimentary depocenters, failed continental rifts, and the coast line). This identifies these structures as important. In addition, the inferred stress directions (Lindholm *et al.*, 1995; Hicks *et al.*, submitted) reveal significant deviation from the expected ridge push direction in the vicinity of the margin (shelf edge) and the coast, stabilizing again to that direction farther into the continent (Bungum *et al.*, 1991; Gregersen, 1992; Zoback *et al.*, 1992).

Among second-order sources of stress (Fejerskov and Lindholm, in press) are lateral density contrasts, topography and its possible compensation at depth, changes in crustal thickness, and flexural loading and unloading. Loading effects may induce large flexural stresses (>100 MPa), perturbing the regional stress field at wavelengths that depend on the lateral extent of the load (e.g., Walcott, 1970; McNutt and Menard, 1982). The density contrast across the continent-ocean boundary causes extension normal to the margin within the continental lithosphere, and margin-normal compression in the oceanic lithosphere (Bott and Dean, 1972; Fejerskov and Lindholm, in press), which is difficult to separate from the ridge push effect. At marginal highs, crystalline basement blocks should be expected to introduce tensional stresses within the high and compressive stresses on either side. Second-order stress effects of these kinds are therefore quite complicated and sensitive to local geological conditions.

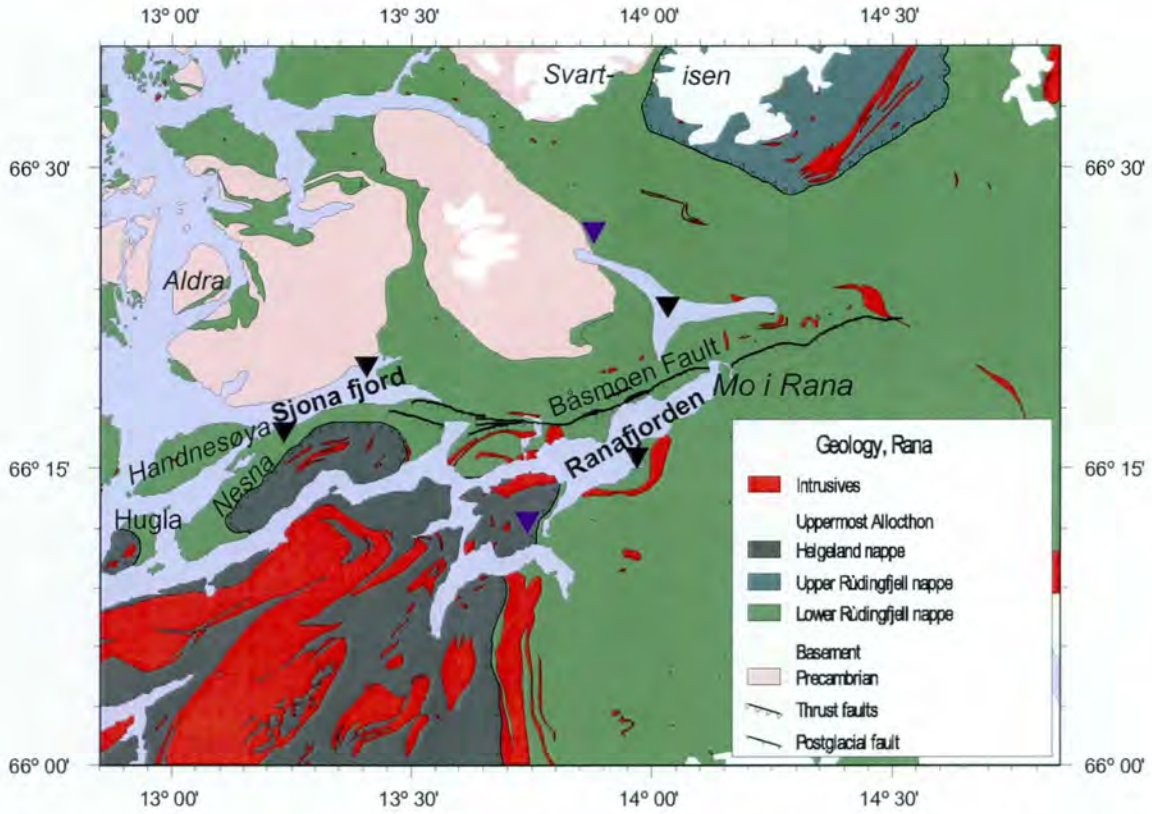

Fig. 6.5.2 Geological map of the Rana area, with seismic stations in the new local network included (inverted triangles). The two stations shown in blue were dismantled in September 1998. The Caledonian trust belts in the Rana area are part of the Uppermost Allochton, consisting mainly of mica schist/gneiss, marble and granitoid intrusions. The Precambrian basement mostly consists of granitic gneisses.

While it is accepted that sediment loading may create large stresses (~100 MPa) on passive margins (Frohlich, 1982; Stein *et al.*, 1989), albeit with strong influence from the geometry of the load (e.g., Muir Wood, 1993), the residual effects of glacial loading and unloading are more disputed (cf. Stephansson, 1988; Stein *et al.*, 1989; Johnston *et al.*, 1994). Essential parameters are the boundary conditions determined by the glacial loading history and in particular the plate relaxation time, where there are important differences between the models of Stephansson (1988) and Stein *et al.* (1989). The latter model is predicting deglaciation flexure with continental extension and oceanic compression, of the order of 10 MPa, and some support for this is found from the fact that observations indicate a change from somewhat more normal faulting toward land as compared to somewhat more thrust faulting seaward both on the Norwegian and Canadian margins (Adams and Basham, 1991; Hicks *et al.* submitted). To further complicate these considerations, however, there are indications that the response to glacial loading/unloading may be quite sensitive to the overburden conditions (Wu and Hasegawa, 1996), while Johnston *et al.* (1998) points to the importance of the lateral extent of the Fennoscandian ice sheet.

The regional characteristics of the Fennoscandian postglacial uplift over time as well as at present is fairly well known. Much less is known, however, about local tectonic responses to this regional uplift. There is direct geodetic evidence that the spatial pattern of uplift may be more irregular than previously assumed (Olesen, 1988; Muir Wood, 1993; Dehls and Olesen, 1999), and it is likely that the present-day seismicity is particularly sensitive to crustal irregularities

(such as density differences, topography and weakness zones), as suggested by recent seismotectonic research concerned with this region (Fejerskov and Lindholm, in press; Byrkjeland *et al.*, in press). Even though the passive continental margin in itself is important, as evidenced by global comparisons (Johnston and Kanter, 1990), the seismicity variation both along and across the margin is such that regional and local factors must have significant importance, including but not limited to the regional postglacial uplift. Other factors of great importance are zones of weakness, including shear zones and preexisting faults with favorable orientations with respect to the stress field, a situation which in turn is complicated by a poorly known distribution of crustal fluids (Sibson, 1985).

Our understanding of the seismicity of Norway has developed gradually in parallel with an improved instrumental coverage of the region (Havskov *et al.*, 1992). The coastal areas of central Norway, particularly the northern parts, have long been known to exhibit relatively high levels of seismic activity, including several earthquake swarms. This is discussed in more detail below.

6.5.3 New microseismicity results

Between July 1997 and January 1999 a total of 373 seismic events (309 earthquakes) have been located using data from the new microseismicity network in Rana. 42 of the located events occurred within distances of 50 to 200 km from the network, and are thus outside the main study area. A total of 64 events have been classified as probable explosions, essentially on the basis of their time-of-day distribution and/or their occurrence in known areas of industrial activity, and therefore removed from the maps. The explosions mainly originate from a talc mine (Altermark mine) a few km northwest of Mo i Rana, and from Storforshei mines around 30 km east of Mo i Rana (mines in the area are shown in Fig. 6.5.5). This leaves 267 probable local earthquakes as a basis for this analysis. Fig. 6.5.3 shows the distribution of these earthquakes in and around the Rana fjord area.

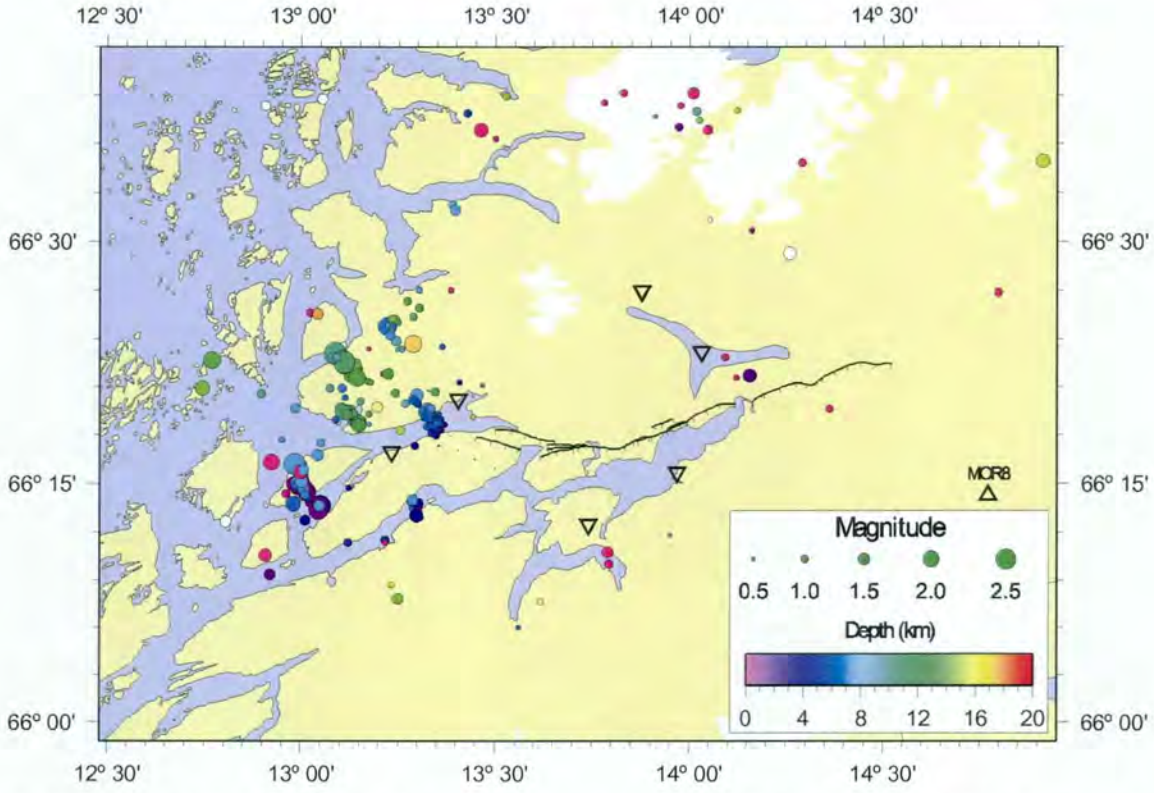

Fig. 6.5.3 Earthquakes located by the network August 1997 - January 1999, plotted with symbol size proportional to magnitude (ML) and color according to depth. Note the five main groups in the western parts of the map. These five groups include a majority of the earthquakes in the Rana area. The MOR8 station in the eastern part of the map is part of the Norwegian national seismic network, data from this station have been used in the locations where available.

Earthquake locations

There are five major groups of earthquake epicenters to be seen in Fig. 6.5.3, all in the western part of the network, and all with similar NNW-SSE trending distributions of epicenter locations. Even though there are no mapped faults that these earthquakes easily can be tied to, there are morphological lineaments in that direction.

The group located under the eastern part of the Sjona fjord consists of 59 small earthquakes (magnitudes up to ML 1.6, using the scale of Alsaker *et al.*, 1991) with the bulk of the activity in August to October, 1997. There has been only sporadic activity since then. The focal depths in this group are among the shallowest observed, mainly between 4 and 6 km. The group in the western part of the Sjona fjord (31 earthquakes) occurred mainly during November and December, 1997. The magnitudes are slightly higher here than in the first group, up to ML 1.8, and the earthquakes occur at slightly greater depths, 8-12 km.

The group further north, just south of the Aldra island (north of the Sjona fjord) was active mainly in January and February, 1998, although there was some sporadic activity also in 1997. 27 earthquakes make up this group, including the largest earthquake within the network during the period of operation, with a magnitude of ML 2.8. The hypocenter depths in this group lie in the 10-12 km range. A somewhat smaller group is located north of the three previous groups, containing two earthquakes with magnitudes of ML 2.1 and 2.3, in addition to 18 smaller earthquakes (magnitudes up to ML 1.2).

The fifth group consists of 51 earthquakes that occurred close to Handnesøya in October and December, 1998. The largest earthquake in this group had a magnitude of ML 2.7, and several of the larger events were felt by local inhabitants associated with banging/cracking noises. This implies very shallow hypocenter depths, of the order of only a few kilometers. The event locations yield hypocenter depths between 6 and 8 km.

The remaining local epicenters are quite scattered, with some of the largest ones being located under the Rana fjord on the southern side of the Nesna peninsula. There are also a few relatively large events further west, and a number of events are moreover located near the Svartisen glaciers north of Mo i Rana. There was also a single 'large' (ML 2.8) earthquake about 30 km south of the network, in an otherwise quiet area.

Focal mechanisms and inferred crustal stress

Of the 267 local earthquakes detected and located within the study area, a total of eight were of a quality which allowed the determination of focal mechanisms using data from the network. In addition, one composite solution using first motion polarities from 10 earthquakes in the eastern Sjona fjord group has been determined. The other eight solutions were determined using waveform modeling (Herrmann and Wang, 1985; Herrmann, 1987), which was essentially used to select a final solution after constraining the solution using available first motion polarities. All nine solutions are listed in Table 6.5.1 and shown in Fig. 6.5.4, where all solutions are also plotted together in terms of P and T axes, and as a rose diagram for the directions of the P axes, trending NNE-SSW, and in terms of their faulting regime in a triangle plot (Frohlich and Apperson, 1992). It is seen there that all solutions except for two are found on the normal to strike-slip side. Fig. 6.5.4 finally shows an example of a real and the matching synthetic waveform for one of the focal mechanism solution (97.12.26, ML 1.8).

Table 6.5.1 Earthquake focal mechanism solutions. The composite solution is based on first- motion polarities from ten earthquakes (ML 0.9 - 1.6). All eight single-event solutions are determined from waveform modelling constrained by first motion polarities. P-trnd P-plng, T-trnd and T-plng are trend and plunge of P (compression) and T (tension) axes respectively. The earthquakes dated 97.11.25 and 98.03.09 have locations outside the network. The modes of faulting (N= normal, NO= normal oblique, R= reverse, RO= reverse oblique, SS= strike-slip) correspond to the locations of the solutions in the triangle plot in Fig. 6.5.4, where pure normal, reverse and strike-slip (indicated circle sectors) requires a plunge of at least 60° of the P, T and B (null) axes, respectively.

Date	Lat.	Lon.	Depth (km)	Mag. (M_L)	P trnd	P plng	T trnd	T plng	Mode of faulting
Comp.1	66.31	13.32	5	N/A	167	48	270	11	N to SS
97.11.21	66.41	13.22	7	2.3	208	29	302	7	SS
97.11.25	66.50	12.40	11	2.7	77	29	343	7	SS
97.11.28	66.32	13.14	11	1.7	74	58	299	23	NO
97.11.28	66.32	13.15	11	1.8	74	58	299	23	NO
97.12.26	66.32	13.11	11	1.8	176	1	268	67	R
98.01.08	66.37	13.13	13	2.2	27	33	284	19	SS to N
98.02.09	66.39	13.09	11	2.8	351	22	257	11	SS
98.03.09	65.85	13.53	7	2.8	115	13	225	57	RO

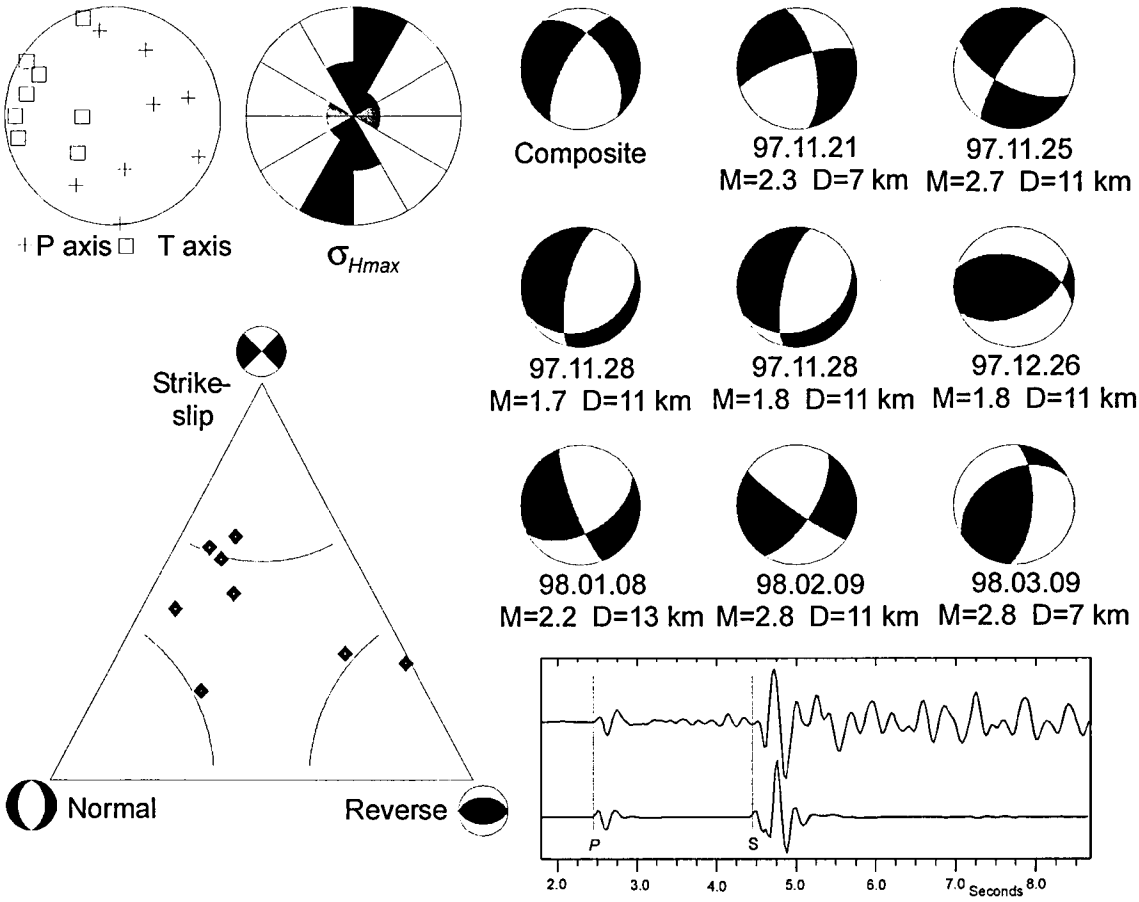

Fig. 6.5.4 The nine new earthquake focal mechanism solutions determined using data from the network. The composite solution uses first-motion polarities from 10 earthquakes, the other eight solutions were determined using waveform modelling constrained by available first-motion polarities. The P (compression) and T (tension) axis for all solutions are plotted stereographically (upper left), showing that the T axes (equivalent to s3; the minimum principal stress direction) are more consistent than the P axes (corresponding to s1; the maximum principle stress). The directions of maximum horizontal compressive stresses are plotted in the rose diagram (central left), showing a consistent NNE- SSW direction of horizontal compression. The two solutions outside the network (97.11.25 and 98.03.09) have clearly different sHmax directions, and are plotted in grey. The actual focal mechanisms are shown on tripartite plots (lower left) where the three principal modes of faulting are connected to different corners in the triangle using the technique of Frohlich and Apperson (1992). At the bottom is shown a sample real (upper) and synthetic (lower) seismogram from one station, used in deriving the focal mechanism solution for the December 26, 1997, ML 1.8 earthquake. The P (compressional wave) and S (shear wave) phase arrivals are shown. The station was at a distance of 13 km from the earthquake hypocenter.

The maximum horizontal compressive stress directions (σHmax) inferred from the focal mechanisms are plotted in Fig. 6.5.5, along with available *in situ* stress measurements from the region (Fejerskov *et al.*, 1996). Even though a focal mechanism solution does not necessarily represent the true (precise) stress tensor (see e.g., McKenzie, 1969), it is well known that the stress directions derived from earthquake focal mechanism solutions generally comply well with other observed stress indicators and measurements, and also that they tend to be quite consistent on a regional scale (e.g., Bungum *et al.*, 1991; Lindholm *et al.*, 1995).

The most significant observation in Figs. 6.5.4 and 6.5.5 is that the directions of the largest horizontal compressive stress component are aligned subparallel to the coastline, which is close to a 90° rotation with respect to the regional 'ridge push' dominated trend. However, to describe these results in terms of maximum compressive stress is deceptive since Fig. 6.5.4 shows (see also Table 6.5.1) that the solutions are predominantly normal to oblique normal/strike slip, and therefore are better described by the tensional stress component, running perpendicular to the coast. For this reason, the direction of horizontal tension is shown for the solutions with this classification in Fig. 6.5.5. Another important point is that the tensional component is much better constrained by this type of stress regime (Hicks *et al.*, submitted), while the compressional axis is properly determined only in terms of its horizontal direction (as seen from Fig. 6.5.4), since its plunge may rotate more or less randomly, with a corresponding variation in the significance of the horizontal component. In conclusion, the data show a predominance of normal to strike-slip faulting in this region, with the tension axis oriented normal to the coast, the same direction as the compression axis in other areas.

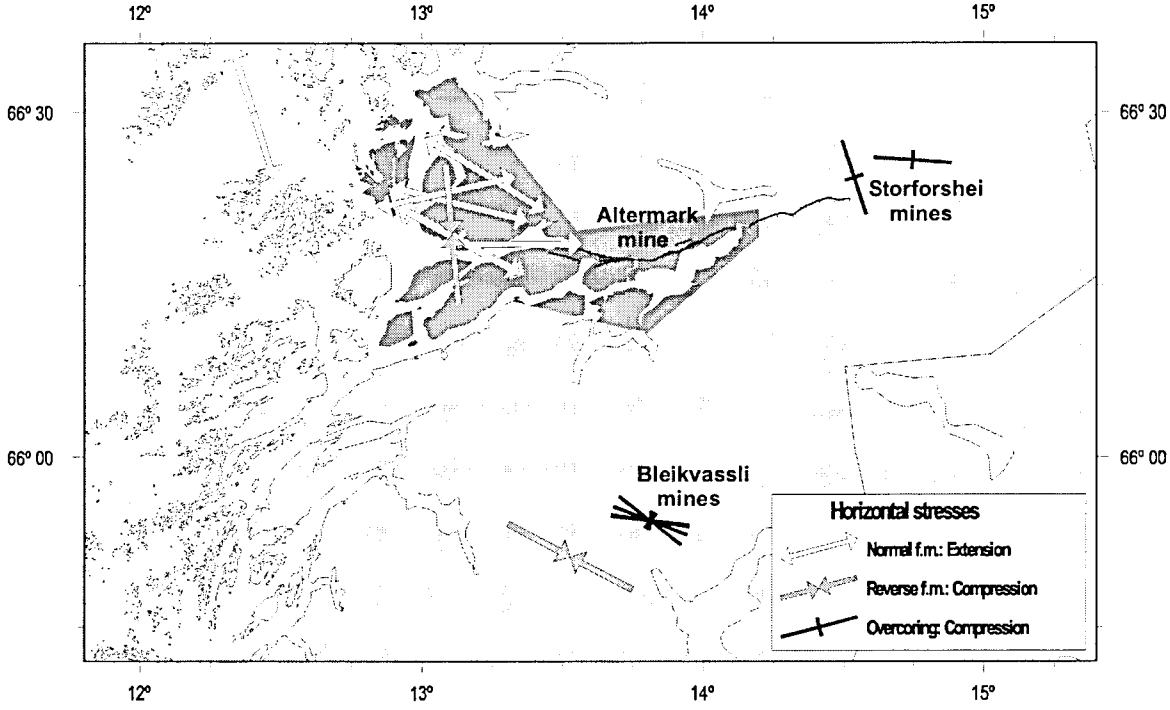

Fig. 6.5.5 Horizontal stresses from earthquake focal mechanism solutions and overcoring measurements in the Rana area. Normal faulting focal mechanism solutions are plotted as arrows in the direction of horizontal tension, while reverse solutions are plotted as arrows in the direction of horizontal compression. The overcoring measurements have the direction of maximum horizontal compression indicated by the symbol's long axis. The darker grey shaded area represents the spatial extent of reported secondary ground effects (seiches, rockfalls, landslides, difficulties standing) from the 1819 Ms 5.8-6.2 earthquake.

A similar reversal of the main horizontal compressional axis has also been found in parts of the northern North Sea (Bungum *et al.*, 1991; Lindholm *et al.*, 1995; in press; Hicks *et al.*, submitted), in a region with very complex tectonics. In this case, however, the mode of faulting is more mixed and the reversal is also less prominent. It is important to note here that a switching of sH and sh (the largest and smallest horizontal stress component, respectively) is fairly easy to achieve when the sH/sh ratio is close to unity, and it should be understood that this is therefore not as dramatic as is may appear at first. In this respect it is interesting to

check this against *in situ* data, although the only available *in situ* data for this area are overcoring measurements from two mines (Storforshei mines and Bleikvassli mines, Fig. 6.5.5) taken at depths down to 400m (Fejerskov *et al.*, 1996). As for all *in situ* measurements, in this case especially due to the shallow depth of the measurements, the relation to the stress field at anything above the most local scale is uncertain. The horizontal stress anisotropy values of 1.1 for the Storforshei mines and four values between 1.2 and 1.7 for the Bleikvassli mines are not particularly close to unity, however, the measured anisotropy values are still low compared to many other mine overcoring measurements on the Norwegian mainland, where values above 2 are common.

A low horizontal stress anisotropy also raises the possibility that dilation effects (Barton, 1986) could have contributed to the observed stress rotation (Hicks *et al.*, submitted). Such effects are based on the fact that dilation accompanying rock failure and weakness zone shearing introduces a component of shear strain that is no longer parallel to the assumed direction of shearing. The normal and shear stress changes that accompany dilatant shearing can radically alter the principal stress components that caused the event to occur, thereby potentially rotating major principal stresses (Nick Barton, pers. comm. 1999).

Magnitudes and depth distributions

The magnitude distribution as shown in Fig. 6.5.6 indicates that the detection threshold is about ML 0.9. The detection threshold in the active areas near the Sjona fjord was most likely unchanged by the removal of two stations in October 1998 (see Fig. 6.5.2), due to the fact that the two closest stations were retained. The effect on location precision should be small, for the same reason.

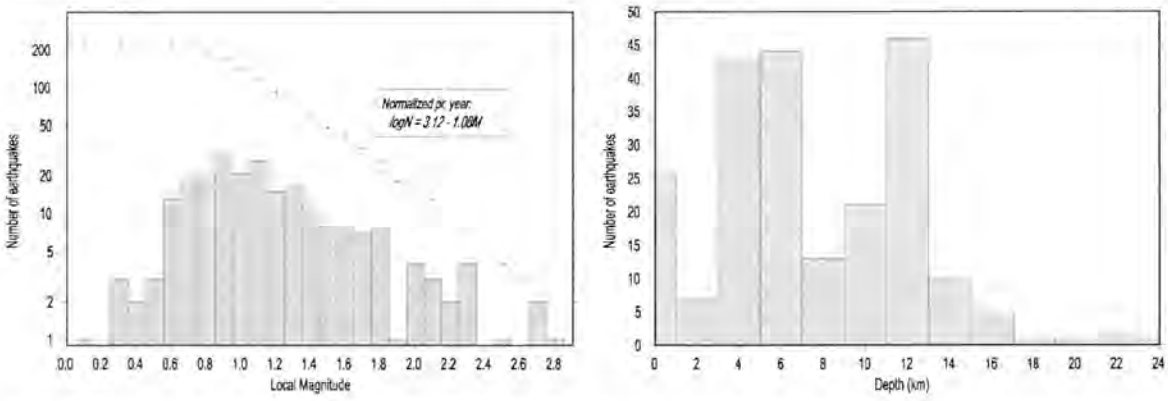

Fig. 6.5.6 Left: Magnitude distribution for local events in the Rana area. Crosses represent the cumulative number of earthquakes. The activity rate (straight line) is defined using the magnitude range ML 1.0 to 2.8. Right: Depth distribution of earthquakes within the network. The majority if the events have hypocenter depths in the 3-7 km range, but with a large number also in the 9-13 km range. Note that the earthquakes with 0 km depths are due to insufficient data quality due to low magnitude and/or great distance, and should not be considered real.

The Gutenberg-Richter scaling relationship for earthquakes says that for a given region over a given period of time, the relation between number of earthquakes N of magnitude equal to or greater than M is given by

$$\mathrm{Log}N = a - bM$$

where the parameters a and b describe the activity level and the ratio between smaller and larger events, respectively. This has been applied to the local earthquake data to quantify the activity and magnitude scaling. The a and b values have been estimated as shown in Fig. 6.5.6, giving annual values of a=3.12 and b=1.08 (the latter being close to the commonly observed value of 1.0). This corresponds to a return period of 16 years for earthquakes of magnitude ML 4 or larger, 190 years for ML 5 and just under 2300 years for ML 6. Even though this is an excessive extrapolation, and ML is not properly defined at the level of magnitude 6, it still provides a gives a rough indication of the activity level in this area. These values could be compared to the regional activity levels as taken from a major seismic zonation study (NORSAR and NGI, 1998) developed for earthquake design purposes, which shows, albeit based on moment magnitudes, activity rate values a=3.0 and b=1.05 for a larger zone covering onshore Norway 66°N to 68°N. This zone has return periods for magnitudes 4, 5 and 6 of 16, 180 and 2000 years, respectively. This implies that the microearthquake activity in the Rana area, recorded only over 18 months, is quite consistent with the long term (~100 years) average. If taken literally (that is, extrapolated linearly), these results indicate that the Rana area has a significant amount of the total seismic activity in onshore northern Norway.

The distribution of focal depths within the network is shown both in Fig. 6.5.3 and in Fig. 6.5.6. The activity observed to the north of the Sjona fjord appears to have somewhat deeper hypocenter locations, with depths of about 8-12 km. The 51 earthquakes comprising the group by Handnesøya were located with hypocenter depths of about 6-8 km, but the witness reports of loud cracking and banging noises in conjunction with the earthquakes may indicate even shallower depths. As a consequence of the macroseismic reports, these events have been placed in the 3- 5 km bin in Fig. 6.5.6, a depth range that is consistent with what has been found further north, in the Meløy region (Bungum *et al.*, 1979).

It should be noted that most of the depths observed (2-6 km) are shallow compared to what is generally the case in Norway with offshore regions, and the slightly deeper earthquakes to the west and north of the Sjona fjord (8-12 km) are still considered shallow. Shallow seismic activity appear to be common for coastal areas in northern Norway where earthquake swarms (albeit with fairly normal b-values around 1.0) have also been observed earlier, notably in Meløy (Bungum *et al.*, 1979; 1982) and in Steigen (Atakan *et al.*, 1994), as further discussed below. However, such swarms are not known from coastal areas further south.

It is interesting to note that similar swarms have also been documented in NW Scotland (Assumpção, 1981), on the Greenland margin (Gregersen, 1979; 1989; Chung and Gao, 1997), at Svalbard (Bungum *et al.*, 1992; Mitchell *et al.*, 1990), and at many locations in the Canadian Arctic, in particular the Sverdrup Basin (Smith *et al.*, 1968, Basham *et al.*, 1977; Wetmiller and Forsyth, 1978; Adams and Basham, 1991).

6.5.4 Discussion and conclusions

The local NEONOR network used in this study represents a significant improvement in terms of earthquake surveillance capability for this part of northern Norway. Even though a regional network has been in operation since 1987, with one station actually in the Rana region (MOR8 in Fig. 6.5.3), around 20% of the 267 local earthquakes analyzed here have been reported by the regional network. That network needs three stations to be detecting in order to report an event (Havskov *et al.*, 1992), and has a detection threshold around ML 2.0 in the Rana area. Even then, the results found during these 18 months of operation are consistent with the more long-term seismicity models available, as suggested by the simple activity rate comparisons above.

The Rana area is the site of the largest historical earthquake known in Fennoscandia (and most likely also in northwestern Europe), namely the August 31, 1819 MS 5.8-6.2 earthquake (Muir Wood, 1989a). This event created widespread ground effects in the Rana area, shown by the shaded area in Fig. 6.5.5, including standing waves (seiches) in the fjords, numerous rockfalls and landslides, and reports of people having difficulties standing. It is notable that a large number of these effects were reported from the western parts of the present network (even though the villages were distributed fairly evenly along the Rana fjord), which is also where most of the present day seismic activity takes place. The exact location of the 1819 earthquake is, in spite of this, fairly poorly known, with estimates varying from the coastal region in the west to the Swedish border in the east. These locations are, however, mostly estimated from the isoseismal contours that extend throughout Fennoscandia (Muir Wood and Woo, 1987). The problem with using the local secondary ground effects as indicated in Fig. 6.5.5 (as compared to the more distant isoseismal contours) in locating the event, is that the population density is more dispersed east of Mo i Rana than farther west. Nevertheless, we believe that the local ground effects are strong evidence that the epicenter was in the area covered by the present study.

Is the Rana region a persistent zone of enhanced seismic activity? Fig. 6.5.7 shows the spatial pattern of the instrumental earthquake locations from 1980 to 1997, and the new locations made using data from the NEONOR network. The instrumental locations between 1980 and 1997 are concentrated mainly in the western parts of the network, consistent with the new data. In contrast, a number of larger historic earthquakes (pre 1980) shown in Fig. 6.5.1 (a mix of macroseismic and instrumental locations) have locations further east, in an area just north of Mo i Rana. However, the location uncertainty for most of these earthquakes are of the order of 30-50 km (NORSAR and NGI, 1998), and some of these errors could also be systematic. In spite of these quality problems, however, the new data confirms that the Rana region as a whole is an area of continuosly elevated seismic activity.

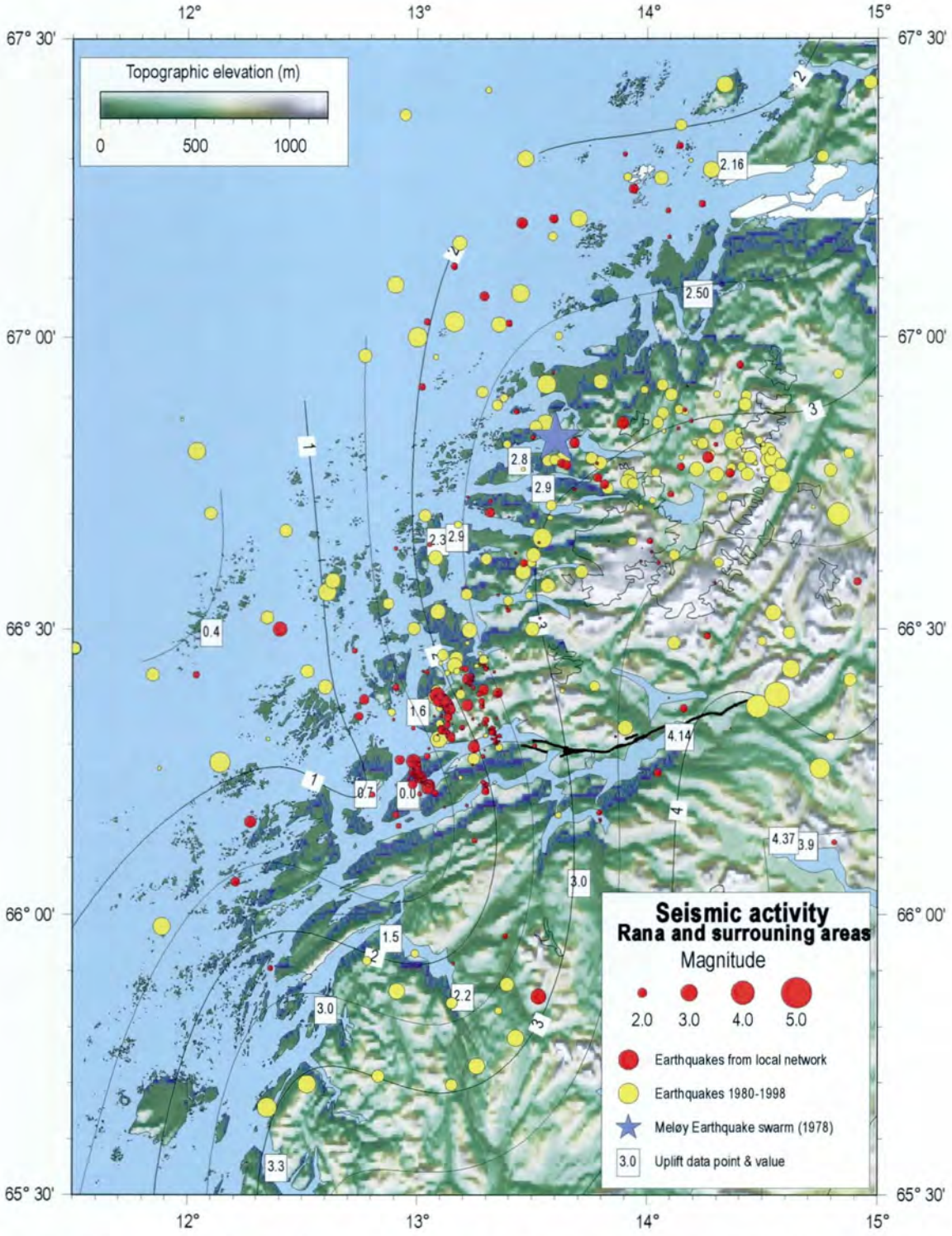

Fig. 6.5.7 New (August 1997 to January 1999 - red) and instrumental (1980 to 1997 - yellow) earthquakes in northern central Norway. Contour lines for present-day uplift rates (mm yr-1)are included, showing a clear anomaly in the western parts of the Rana fjord area. Data points and values used in the uplift grid are shown. The location of the Meløy earthquake swarm (Bungum et al., 1979) is given by the blue star. The 1819 earthquake has been located to the northwest of Mo i Rana (Muir Wood, 1989a), based on the large scale isoseismal intensity contours. However, due to the results presented in this paper, the epicenter is most likely located somewhat further west.

Geodynamic implications

Given the relatively large seismic activity in the Rana area, it is surprising that none of this activity at present is directly connected to the Båsmoen fault itself (Dehls *et al.*, 1998). However, this does not exclude the possibility that the fault has been active on a Holocene or historical time scale, even though the latter possibility is less likely than earlier assumed. It is also uncertain if the large 1819 earthquake can be linked to any of the more N S oriented structures that today's activity seems to define (cf. Fig. 6.5.3). In this respect it is worth noting that a magnitude 6 earthquake should normally be expected to nucleate deeper than the presently located shallow microearthquakes.

Local stress sources appear to play an important role in controlling the seismic activity in the Rana area, as shown by the apparent 90° rotation of the principal horizontal compression stress direction from the regional stress direction, which is commonly accepted to be related to plate tectonics (Zoback, 1992; Hicks, 1996; submitted). In this region, the orientation of the maximum horizontal compressive stress, as derived from earlier available onshore earthquake focal mechanism solutions, is more or less parallel to the coast (Byrkjeland *et al.*, in press). The focal mechanisms further west on the margin, however, have a NW-SE sH orientation which is in compliance with the 'ridge push' direction. The majority of the earthquakes used to determine the regional stress field in mid Norway are located on the margin. It may be inferred that such earthquakes are, to a large degree, reflecting local second and third order sources of stress (density inhomogeneities, flexural stresses, topographic loads, geological features, etc.) rather than first order (plate-motion related) effects. This local control is also indicated by studies of the Meløy (Bungum *et al.*, 1979) and the Steigen earthquake sequences (Atakan *et al.*, 1994).

Several of these second order sources of stress should be expected to generate stress perpendicular to the margin, to the coastline, and to the uplift trend, with potentials for both constructive and destructive interference. The fact that sediment flexure may create stresses one order of magnitude above those from ridge push, continental margin spreading and deglaciation flexure (Stein *et al.*, 1989) means that this effect may dominate completely for offshore areas, as also concluded by Byrkjeland *et al.* (in press). Onshore this situation is different, however. What looks like a 90° rotation of the sH direction in reality reflects normal-faulting mechanisms where the main tectonic significance is tied to the tensional axes, as discussed above and as plotted in Fig. 6.5.5. A tendency for more shallow normal-faulting earthquakes is also found onshore in southwestern Norway (Hicks *et al.*, submitted).

As already noted, continental-side extension can result from sediment flexure, density difference and spreading across continental margins, and from deglaciation flexure. The two former sources of stress should, however, be expected to be of less importance in coastal areas, well into crystalline basement. This is also exactly where the postglacial uplift gradients are at their highest (Fig. 6.5.1), suggesting that the former source is more important than the latter two. The two other well-documented coastal earthquake swarms in northern Norway (Meløy in 1978 and Steigen in 1992) also show similar patterns of shallow normal faulting with coast-normal extension. The geologic and tectonic setting for these swarms is similar to the Rana area. The main Meløy swarm (cf. Figs. 6.5.1 and 6.5.7) in 1978 consisted of around 10,000 earthquakes up to a magnitude of ML 3.2 during a ten-week period (Bungum *et al.*, 1979), based on temporary stations. The observed effect of the earthquakes by the local populace are also similar to those observed from the Handnesøya swarm in Rana, indicating similarly shallow depths. The Steigen swarm (cf. Fig. 6.5.1) consisted of 207 earthquakes in 1992 (Atakan et al, 1994) in several pulses. Hypocenter depths in this swarm are on the order of 8-11 km, again similar to some of the groups in the Rana area.

The two composite focal mechanism solutions available from the Meløy swarm show normal (Bungum *et al.*, 1979) and strike-slip faulting (Vaage, 1980), the normal mechanism with coast-normal extension, and the strike-slip solution with the direction of horizontal compression around 45° to the coast. The focal mechanism solution (composite) available from the Steigen swarm is normal with coast-normal extension. The similarities between these two swarms and the seismic activity in the Rana area are striking, in terms of geologic setting, hypocenter depths, modes of faulting and postglacial uplift gradients. There is also a single-event focal mechanism solution from an earthquake under the Lofoten Islands to the northwest (Hicks *et al.*, 1996), indicating normal faulting with extension in the same direction as the Rana, Meløy and Steigen swarms. This argues that the stress sources responsible for the continuous high levels of seismic activity along the coast of northern Norway are effective on a scale of several hundred km, with postglacial uplift being the most likely candidate. It is important to note in this context that the maximum postglacial uplift gradients follow the coast quite closely (Fig 1), adding further credibility to this hypothesis. Nevertheless, some influence of shorter wavelength effects, such as topography and crustal inhomogeneities should also be considered due to the spatial concentration of the seismic activity. However, given the scarce nature and variable quality of the available seismic data in northern Norway, and also since many of the *in situ* stress orientations (albeit mostly from mines) show a NW-SE sH axis, these problems call for further and strengthened investigations based on future acquisition and analysis of seismicity and stress data from the whole coastal region.

Conclusions

Given that the seismicity along the continental margin and in oceanic crust offshore Norway seems to be related to a combination of ridge push forces, sedimentation flexure and density differences and spreading across the margin, the region along the coast of northern Norway seems to behave differently seismically. This is shown by the following conclusions that we can draw from the present study:

The Rana area has long been known as one of the more seismically active regions in Norway. The study confirms the continuous high level of seismic activity in this area, as the local seismic network has identified of the order of several hundred earthquakes within a limited area, with magnitudes up to ML 2.8. This is high for onshore Baltic shield areas.

The E-W oriented Båsmoen fault did not reveal any seismic activity during the 18 month study period, which weakens, but certainly does not exclude, the possibility that this fault has been active during or after the last deglaciation. The consistency of the NNW-SSE lineations in the swarm-like activity in the five main groups of earthquakes in the western parts of the network, including a systematic change of depth, is significant, although the geological connection here is at present uncertain.

The tensional stress orientation perpendicular to the coastline combined with shallow foci leaves postglacial uplift as a viable explanation for this seismicity, further supported by other earthquake source mechanisms farther north. Nevertheless, the very concentrated zones of activity are among the reasons why local sources of stress also could be influencing the occurrence of earthquakes in this region.

6.5.5 References

Adams. J. and Basham, P.W. 1991. Chapter 14 In Slemmons, D.B., Engdahl, E.R., Zoback, M., and Blackwell, D. (eds.): Neotectonics of North America, Decade of North American Geology volume DMV-1, pp. 261-276.

Alsaker, A., Kvamme, L.B., Hansen, R.A., Dahle, A. and Bungum, H. 1991: The ML scale in Norway. Bull. Seism. Soc. Am., 81, 379-398.

Andersen, B.G. 1975: Glacial geology of northern Nordland, North Norway. Norges Geol. Unders., 320, 1-74.

Andersen, B.G., Bøen, F., Rasmussen, A., Rokoengen, K. and Vallevik, P.N. 1982: The Tjøtta glacial event in southern Nordland, North Norway. Nor. Geol. Tidsskr., 62, 39-49.

Andersen, B.G., Mangerud, J., Sørensen, R., Reite, A., Sveian, H., Thoresen, M. and Bergstrøm, B. 1995: Younger Dryas ice-marginal deposits in Norway. Quat. Int., 28, 147-169.

Atakan K., Lindholm, C.D and Havskov, J. (1994). Earthquake swarm in Steigen, northern Norway: an unusual example of intraplate seismicity. Terra Nova, 6, 180-194.

Assumpção, M. 1981: The NW Scotland earthquake swarm of 1974. Geophys. J. R. Astr. Soc., 67, 577-586.

Bäckblom, G. and Stanfors, R. 1988: Interdisciplinary study of postglacial faulting in the Lensjärv area, northern Sweden 1986-1988. SKB Technical Report 89-31.

Basham, P.W., Forsyth, D.A. and Wetmiller, R.J. 1977: The seismicity of northern Canada. Can.J. Earth. Sci., 14, 1646-1667.

Bergstrøm, B. 1994: ERLSFJORD. Kvartærgeologisk kart 1927 III - M 1:50000, med beskrivelse (Quaternary geology map with description). Norges Geol. Unders.

Blake, K.P. and Olsen, L. 1999: Deglaciation of the Svartisen area, northern Norway, and isolation of a large ice mass in front of the Fennoscandian Ice Sheet. Nor. geogr. Tidsskr., 53, 1-16.

Bott, M.H.P. 1991: Ridge push and associated plate interior stress in normal and hot spot regions. Tectonophysics, 200, 17-23.

Bott, M.H.P. and Kusznir, N.J. 1984: The origin of tectonic stress in the lithosphere. Tectonophysics, 105, 1-13.

Bungum, H., Alsaker, A., Kvamme, L.B. and Hansen, R.A. 1991: Seismicity and seismotectonics of Norway and surrounding continental shelf areas. J. Geophys. Res., 96, 2249-2265.

Bungum, H., Hokland, B.K., Husebye, E.S. and Ringdal, F. 1979: An exceptional intraplate earthquake sequence in Meløy, Northern Norway. Nature, 280, 32-35.

Bungum, H. and Lindholm, C. 1997: Seismo- and neotectonics in Finnmark, Kola Peninsula and the southern Barents Sea. Part 2: Seismological analysis and seismotectonics. Tectonophysics, 270, 15-28.

Bungum, H., Mitchell, B.J. and Kristoffersen, Y. 1982: Concentrated earthquake zones in Svalbard. Tectonophysics, 81, 175-188.

Bungum, H., Vaage, S. and Husebye, E.S. 1982: The Meløy earthquake sequence, northern Norway: Source parameters and their scaling relations. Bull. Seism. Soc. Am., 72, 197-206.

Byrkjeland, U., Bungum, H. and Eldholm, O. in press. Seismotectonics of the Norwegian continental margin. J. Geophys. Res.

Chung, W.-Y. and Gao, H. 1997: The Greenland earthquake of 11 July 1987 and postglacial fault reactivation along a passive margin. Bull. Seism. Soc. Am., 87, 1058-1068.

Dahlen, F.A. 1981: Isostasy and the ambient state of stress in the oceanic lithosphere. J. Geophys. Res., 86, 7801-7807.

Dehls, J. and Olesen, O. 1998: Neotectoncs in Norway, Annual Technical Report 1997, NGU (Norges Geologiske Undersøkelse) Report 98.016, 149 pp.

Dehls, J. and Olesen, O. 1999: Neotectoncs in Norway, Annual Technical Report 1998, NGU (Norges Geologiske Undersøkelse) Report 99.007.

Dehls, J., Olesen, O., Olsen, L. and Blikra, L.H. in press: Neotectonic faulting in northern Norway: the Stuoragurra and Nordmannvikdalen postglacial faults. Quaternary Science Reviews.

Denton, G. H. and Hughes, T.J. 1981: The last great ice sheets. John Wiley and Sons.

Ekman, M. 1996: A consistent map of the postglacial uplift of Fennoscandia. Terra Nova, 8, 158-165.

Fejerskov M. and Lindholm, C. in press: Crustal stress in and around Norway; An evaluation of stress generating mechanisms. Geol. Soc. Lond., Spec. Publ.

Fejerskov, M., Lindholm, C.D., Bungum, H., Myrvang, A., Bratlie, R.K. and Larsen, B.T. 1996: Crustal stress in Norway and adjacent offshore regions. Final report for the IBS-DNM project, Topic 1.3 "Regional stress field".

Fjeldskaar, W. 1994: Viscosity and thickness of the astenosphere detected from the Fennoscandian uplift. Earth Plan. Sci. Lett., 126, 399-410.

Fjeldskaar, W. 1997: Flexural rigidity of the Fennoscandia inferred from the postglacial uplift. Tectonics, 16, 596-608.

Frohlich, C. 1982: Seismicity of the central gulf of Mexico. Geology, 10, 103-106.

Frohlich, C. and Apperson, K.D. 1992: Earthquake focal mechanisms, moment tensors, and the consistency of seismic activity near plate boundaries. Tectonics, 11, 279-296.

Gjelle, S., Bergstrøm, B., Gustavson, M., Olsen, L. and Sveian, H. 1995: Geology and landscape around the Arctic Circle in Norway. Wennebergs trykkeri AS, Trondheim. 128 pp.

Gregersen, S. 1979: Intraplate earthquake swarms in Greenland and adjacent continental regions. Nature, 281, 661-662.

Gregersen, S. 1989: The seismicity of Greenland. In S. Gregersen and P.W. Basham (eds.): Earthquakes at North-Atlantic passive margins: Neotectonics and Postglacial Rebound, NATO ASI Series, Vol. 266, pp. 345-353.

Gregersen, S. 1992: Crustal stress regime in Fennoscandia from focal mechanisms. J. Geophys. Res., 97, 11821-11827.

Havskov, J. 1997: The Seisan earthquake analysis software. Institute of Solid Earth Physics, University of Bergen, 236 pp.

Havskov, J., Kvamme, L.B., Hansen, R.A., Bungum, H. and Lindholm, C.D. 1992: The northern Norway seismic network: Design, operation and results. Bull. Seism. Soc. Am., 82, 481-496.

Hasegawa, H.S. 1977: Focal parameters of four Sverdrup Basin, Arctic Canada, earthquakes in November and December of 1972. Can. J. Earth Sci., 11, 2481-2494.

Herrmann R. B. 1987: Computer programs in seismology, Vol. I-VII. Saint Louis University, St. Louis, Missouri.

Herrmann R.B. and Wang C.Y. 1985: A comparison of synthetic seismograms. Bull. Seism. Soc. Am., 75, 41-56

Hicks, E. C. 1996: Crustal stresses in Norway and surrounding areas as derived from earthquake focal mechanisms and *in situ* stress measurements. Cand. Scient thesis in applied geophysics, University of Oslo, Norway, 163 pp.

Hicks, E., Bungum, H. and Lindholm, C. submitted: Stress inversions of earthquake focal mechanism solutions from onshore and offshore Norway. Nor. Geol. Tidsskr.

Johnston, A.C. 1987: Suppression of earthquakes by large continental ice sheets. Nature, 330, 467-469.

Johnston, A.C., Coppersmith, K.J., Kanter, L.R., and Cornell, C.A. 1994: The earthquakes of stable continental regions, Tech. Rep., EPRI TR-102261s-V1-V5, Electr. Power Res. Inst., Palo Alto, Cal., 1994.

Johnston, A.C. and Kanter, L.R. 1990: Earthquakes in stable continental crust. Scientific American, March 1990, 42-49.

Johnston, P., Wu, P. and Lambeck, K. 1998: Dependence of horizontal stress magnitude on load dimension in glacial rebound models. Geophys. J. Int., 132, 41-60.

Kinck, J. J., Husebye, E. S. and Larsson, F.R. 1983: The Moho distribution in Fennoscandia and the regional tectonic evolution from Archaean to Permian times. Precambrian Research, 64, 23-51.

Lindholm, C.D., Bungum, H., Hicks, E. and Villagran, M. in press: Crustal Stress and tectonics in Norwegian regions determined from earthquake focal mechanisms. Geol. Soc. Lond., Spec. Publ.

Lindholm, C., Bungum, H., Bratlie, R.K., Aadnøy, B.S., Dahl, N., Tørudbakken. B. and Atakan, K. 1995: Crustal stress in the northern North Sea as inferred from *in situ* measurements and earthquake focal mechanisms. Terra Nova, 7, 51-59.

Lundquist, J. and Lagerbäck, R. 1976: The Pärve fault, A late-glacial fault in the Precambrian of Swedish Lapland. Geol. För. Stockh. För., 98, 45-51.

McKenzie, D.P. 1969: The relation between fault plane solutions for earthquakes and the directions of the principal stresses. Bull. Seism. Soc. Am., 59, 591-601.

Mitchell, B.J., Bungum, H., Chan, W.W. and Mitchell, P.B. 1990: Seismicity and present-day tectonics of the Svalbard region. Geophys. J. Int., 102, 139-149.

Muir Wood, R. 1989a: The Scandinavian earthquakes of 22 December 1759 and 31 August 1819. Disasters, 12, 223-236.

Muir Wood, R. 1989b: Extraordinary deglaciation reverse faulting in northern Fennoscandia. In Earthquakes at North-Atlantic passive margins: Neotectonics and Postglacial Rebound, edited by S. Gregersen and P.W. Basham, NATO ASI Series, pp. 141-174.

Muir Wood, R. 1993:. A review of the seismotectonics of Sweden. EQE International, Report: 43-01-R-001, Revision 2, 1993.

Muir Wood, R. and Woo, G. 1987: The historical seismicity of the Norwegian Continental Shelf. ELOCS (Earthquake Loading on the Norwegian Continental Shelf) Report 2-1, Norwegian Geotechnical Institute, Oslo.

NORSAR and NGI 1998: Seismic Zonation for Norway. Report prepared for the Norwegian Council for Building Standardization (NBR), 188 pp.

Olesen, O. 1988: The Stuoragurra fault, evidence of neotectonics in the Precambrian of Finnmark, northern Norway. Nor Geol. Tidskr., 68, 107-118.

Olesen, O., Hjelle, S., Henkel, H., Karlsen, T.A., Olsen, L. and Skogseth, T. 1994: Neotectonics in the Ranafjorden area, northern Norway. NGU (Norges Geologiske Undersøkelse) Report No. 94.073, 33 pp.

Olsen, L., Sveian, H. and Blikra, L.H. 1996: KORGEN 1927 II - M 1:50000, Kvartærgeologisk kart med beskrivelse (Quaternary geology map with description). Norges Geol. Unders.

Olesen, O., Dehls, J., Bungum, H., Riis, F., Hicks, E., Lindholm, C., Blikra, L.H., Fjeldskaar, W., Olsen, O., Longva, O., Faleide, J.I., Bockmann, L., Rise, L., Roberts, D., Braathen, A. and Brekke, H. 2000: NEONOR Final Report. NGU Report 2000.002.

Rasmussen, A. 1981: The deglaciation of the coastal area NW of Svartisen, Northern Norway. Norges Geol. Unders., 369, 1-31.

Smith, W.E.T., Whitham, K., and Piche, W.T., 1968: A microearthquake swarm in 1965 near Mould Bay, Northwest Territories, Canada. Bull. Seis. Soc. Am., 58, 1991-2011.

Sibson, R.H. 1995: A note on fault reactivation. J. Struct. Geol., 7 (6), 751-754.

Stein, S., Cloetingh, S., Sleep, N.H. and Wortel, R. 1989: Passive Margin Earthquakes, Stresses and Rheology. In S. Gregersen and P.W. Basham (eds.): Earthquakes at North- Atlantic passive margins: Neotectonics and Postglacial Rebound, NATO ASI Series, Vol. 266, pp. 231-259.

Stephansson, O. 1988: Ridge push and glacial rebound as rock stress generators in Fennoscandia. Bull. 14, pp. 39-48, Geol. Inst., Univ. of Uppsala, Sweden.

Vaage, S. 1980: Seismic evidence of complex tectonics in the Meløy earthquake area. Nor. Geol. Tidsskr., 60, 213-217.

Wetmiller, R.J. and Forsyth, D.A. 1978: Seismicity of the Arctic, 1908-1975. Publs. Earth Physics Br. 45, 15-24.

Wu, P., and Hasegawa, H. 1996: Induced stresses and fault potential in eastern Canada due to a realistic load: a preliminary analysis. Geophys. J. Int., 127, 215-229.

Zoback, M. L 1992: First- and second-order patterns of stress in the lithosphere: The World Stress Map Project. J. Geophys. Res., 97, 11703-11728.

7 MODELLING (TASK 11)

7.1 POST-GLACIAL UPLIFT, NEOTECTONICS AND SEISMICITY IN FENNOSCANDIA

By Willy Fjeldskaar, RF, Conrad Lindholm, NORSAR, John F. Dehls, NGU and Ingrid Fjeldskaar, UiB

7.1.1 Introduction

In historic time the rate of uplift along the coasts of Fennoscandia has been so high that its effects were easily observed within one generation. Since the 18th century the cause and the rate of displacement have been intensively discussed. At first the phenomenon was variously explained in terms of global changes in sea level, changes in the earth's rotation or elevation of the crust. It was not until the middle of the 19th century that the theory of an Ice Age was presented, and Jamieson (1865) was the first to see the Fennoscandian uplift as an evidence for a deformation of a non-rigid earth by an ice cap - glacial isostasy.

The seismicity in Fennoscandia is remarkably high for an interior plate region, with high seismicity concentrated in regional areas. The mechanism for the seismic activity has been debated for many years. Kolderup (1930) presumed that the seismicity, to a large extent, was due to the post-glacial uplift, Kvale (1960) on the other hand, argued against this explanation. Muir-Wood (in press) found that the observed seismicity favours a model with alternating quadrants of seismicity and aseismicity around the former forebulge and rebound dome. Gudmundsson (1999) has modelled the doming to improve our understanding of the associated stress field, with relation to Fennoscandia in particular. He found that one might expect strike-slip or reverse faulting in the marginal parts, as a consequence of the postglacial uplift. Rohr-Torp (1994) substantiated the dome uplift and the predicted stresses of Fennoscandia with ground water flow measurements. Wu *et al.* (1999) find that the post-glacial rebound is probably the cause of the large post-glacial thrust faults observed in Fennoscandia, and that the ice load history has large effects on the onset time of earthquakes and the magnitude of fault instability.

The aim of this paper is to search for a possible neotectonic component in the post-glacial uplift, to locate it and quantify it by means of movement direction.

7.1.2 Earthquake activity

The earliest historical records of large ground shaking were written in documents intended for other purposes (parish records etc.) and are of limited scientific value. The felt earthquakes were first recorded in a more systematic way at the end of the 19th century and in the 1980s Norway installed the first sensitive electromagnetic seismographs focussed on the detection of microearthquakes (earthquakes not felt by people). Sweden, Finland and Denmark made installations around the same years. With the low seismic activity of Scandinavia this means that our mapping of the microseismicity (and thereby our understanding of the Fennoscandian earthquake activity) is largely based on 20 years of microseismic data. Fig. 7.1.1 shows how the Fennoscandian earthquake activity is clearly concentrated in certain regions:

- Western Fennoscandia, offshore Norway.

- The highest activity offshore Norway is found in a belt offshore mid Norway; and in the northern end of the North Sea. These areas regularly exhibits larger earthquakes (M=4 to 5).
- The largest historical earthquakes (Rana, Nordland 1819 and Oslo 1904) occurred in areas that have been relatively quiet the past 20 years.
- Onshore activity is characterized by lower activity and smaller magnitudes. These areas are the Nordland coast, western Norway coast, Oslofjord area, Vänern area, the Swedish coast of the Gulf of Bothnia and northwards towards Finnmark, and the zone in mid Finland.

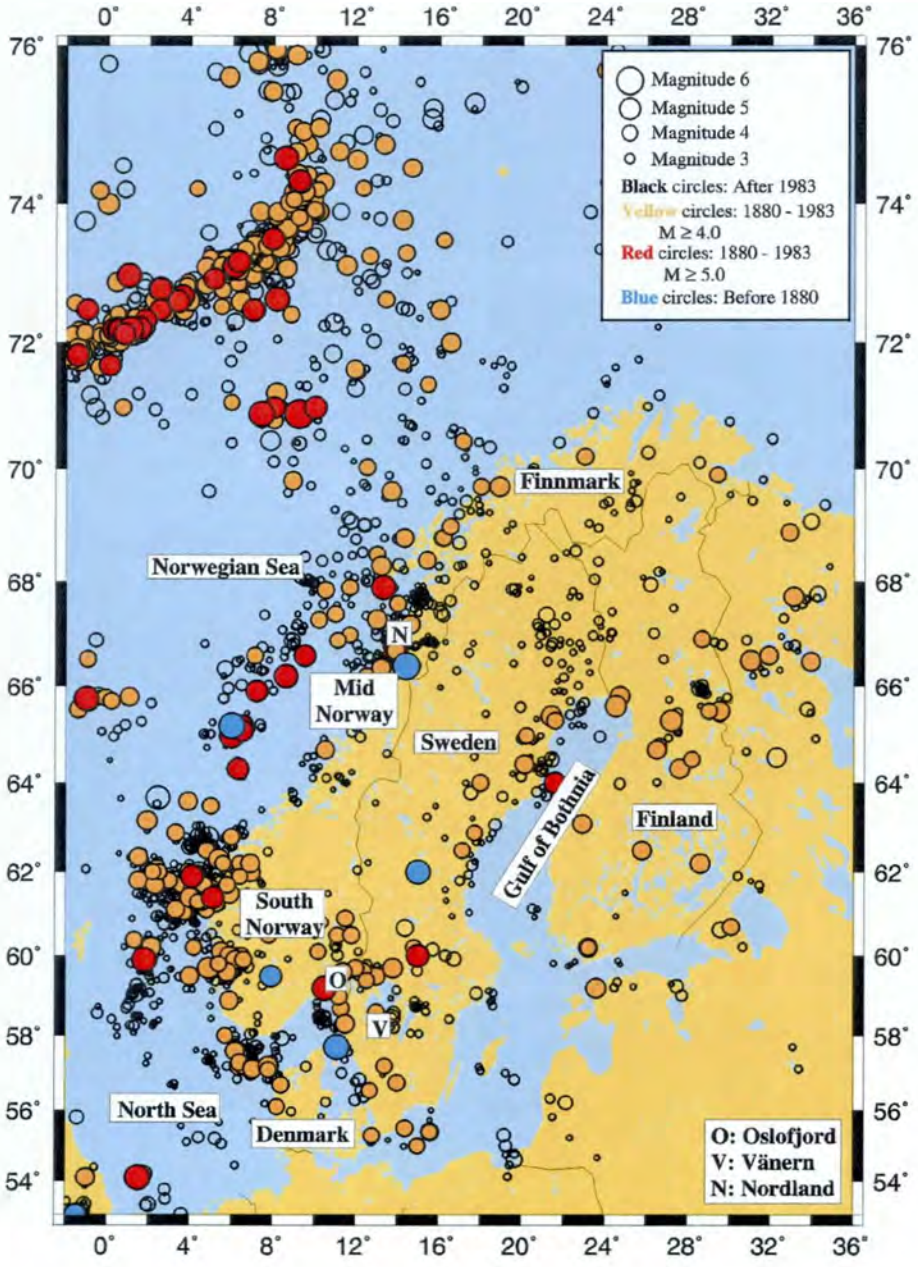

Fig. 7.1.1 Earthquakes in Fennoscandia during different periods of observation.

7.1.3 Earthquake focal mechanisms: Stresses and mode of faulting

The earthquake focal mechanism resolves the main stress directions and mode of deformation. An earthquake is generated through stress build-up and subsequent release, and if regional stress generating mechanisms dominate, this should be visible in the focal mechanisms. However, there is a range of local features (crustal strength, local stress deviation etc.) that may influence the individual earthquake rupture. By grouping many focal mechanisms we attempt to reduce the impact of local features and conversely enhance the regional stress imprint and the regional tectonism.

Over the last years more seismic stations could be deployed allowing for improved resolution and more detailed analysis. One of the major advances through this deployment is the increasing number of focal mechanisms that could be compiled, and as of 1999 more than 120 mechanisms have been computed for Norway and Sweden.

Fig. 7.1.2 provides a synthesis of the compressional stress directions obtained from the individual focal mechanisms. As seen from Fig. 7.1.2 the regional stress consistency is generally good, and regionally consistent stresses are the only viable explanation for this data. This consistency is also reflected in the *in situ* data (Fejerskov and Lindholm, in press).

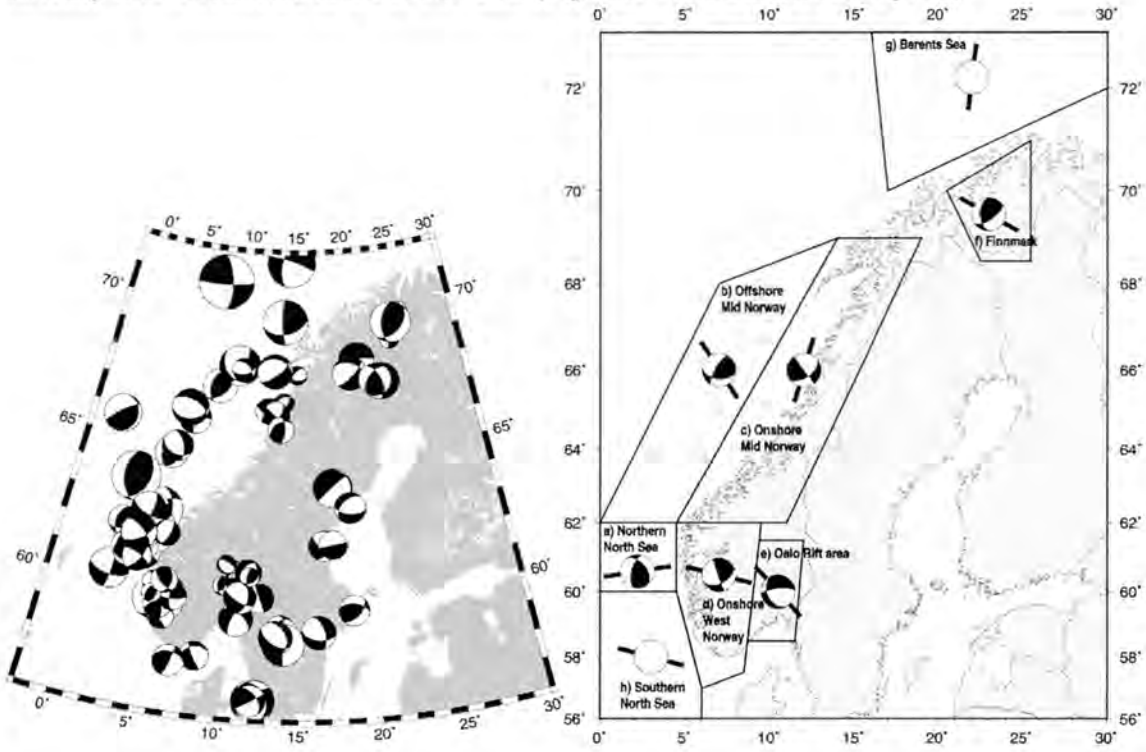

Fig. 7.1.2 a) Earthquake focal mechanisms in Fennoscandia. Complete for Norwegian regions only, only selected from Sweden. b) Directions of horizontal compression synthesised for selected Norwegian areas.

7.1.4 Stress generating mechanisms and observed horizontal stress

The forces acting on the crust cause the observed stresses, and these may be differentiated with respect to origin and lateral extent (Sykes and Sbar, 1974; Engelder, 1994). According to Zoback (1992) the general situation is that the observed stress is composed of plate wide continental stress overprinted by regional and local effects. For Scandinavia there may be a number of stress generating mechanisms that act together which can be grouped into classes re-

flecting their lateral extension (following Fejerskov and Lindholm, in press). The first order stresses in Fennoscandia are generally attributed to forces at the plate margins under the assumption of an elastic lithosphere in which stresses can propagate. The nearest plate margin is the mid Atlantic ridge, and the dominance of NW - SE compression sub-normal to the mid Atlantic ridge is found throughout Scandinavia (e.g. Stephansson, 1988). The second order stresses are more limited in extent (covering Scandinavia as a maximum), whereas the third order stresses relate to local features and rarely extend beyond ~100 km.

Fejerskov and Lindholm (in press) modelled the ridge push force based on elevation of the ridge and age of the crust, and compared stress magnitudes from this source with stress magnitudes originating from glacial rebound, crustal flexures and topographic effects. The results indicated the first order plate margin stresses (ridge push) to be of major importance. However, sediment loading (offshore) and topography may also be important secondary stresses. The modelling did not indicate high stress magnitudes from deglaciation flexures. However, the lateral extent of this mechanism combined with the Zatsepin and Crampin (1997) model, which allow deformations at very small deviatoric stress levels, may again increase the recognition of this stress source.

Fig. 7.1.3 synthesises the main trends of Figs. 7.1.1 and 7.1.2 in terms of seismic activity, type of faulting and direction of horizontal compression. Where the amount of data is large, as offshore western Norway the synthesis in Fig. 7.1.3 is quite reliable, however, in areas of lower seismic activity or offshore far from the seismic stations, the synthesis drawn in Fig. 7.1.3 is more tentative. From Fig. 7.1.3 some remarkable trends can be seen:

- The deep earthquakes occur mainly offshore. They are dominated by reverse faulting and reflect stress directions that can be attributed to the mid Atlantic ridge push (NW - SE).
- The shallow earthquakes occur predominantly onshore. Normal faulting (extentional deformation) is dominant and the direction of horizontal tension is largely coast perpendicular (for Norway).

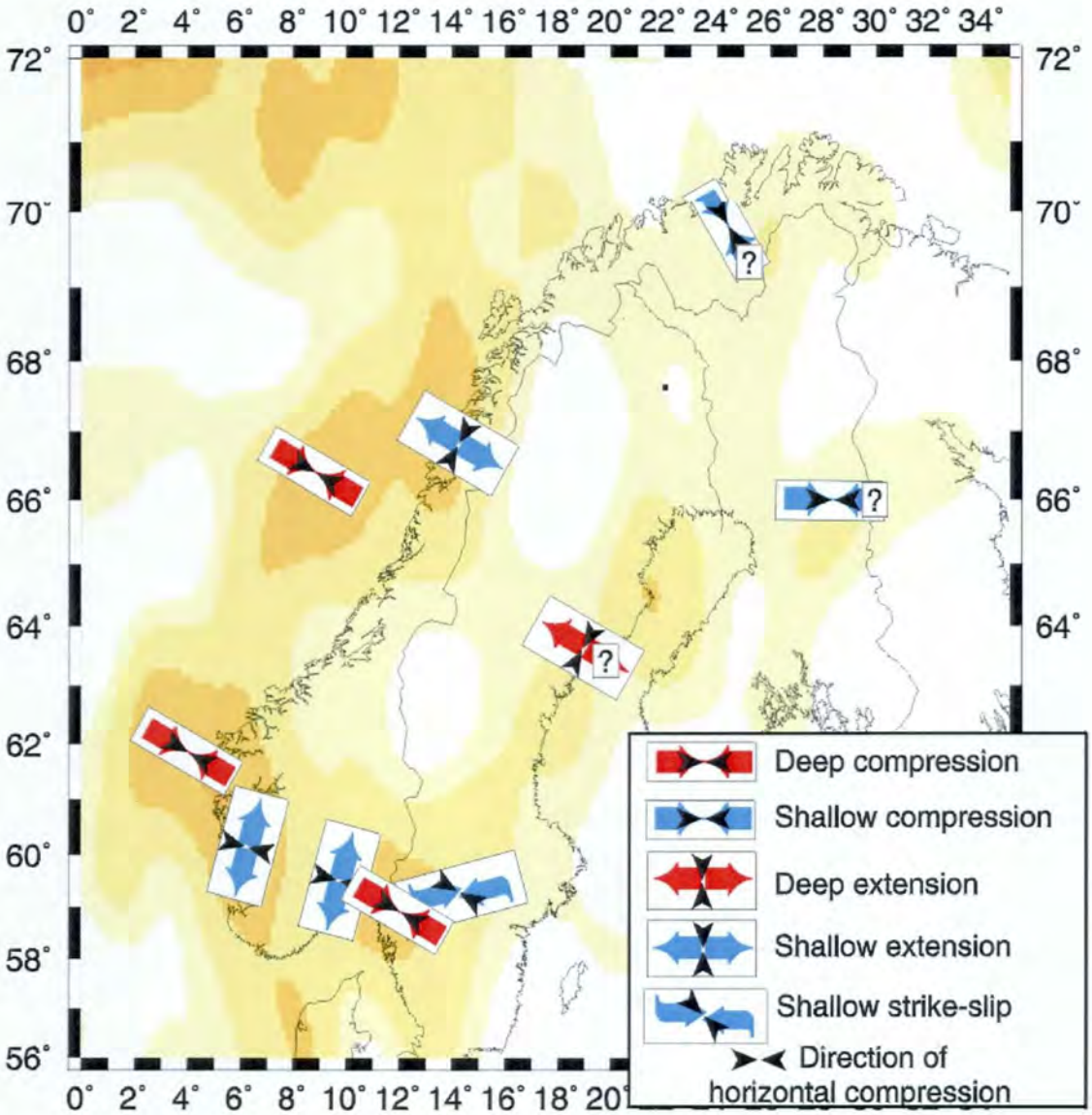

Fig. 7.1.3 Stress directions, type of faulting and focal depths synthesized from earthquake focal mechanisms and in situ stress measurements. Areas of less data are indicated with question marks. Intensity of yellow indicates intensity of seismicity (from Hicks et al., in press).

7.1.5 Post-glacial uplift and model parameters

Data on the uplift can be grouped in two: i) present rate of uplift and ii) shoreline tilts versus time. These observations are mainly results of the movements of the solid Earth, they are scarcely affected by movements of the sea level. The movements of the solid Earth are assumed here to have a glacial isostatic origin connected to the melting of the last ice sheets. It is, however, not unreasonable to assume that there is a neotectonic component in the uplift rate and the paleao-shoreline gradients. The general pattern of the uplift is believed to be a result of glacial isostasy, but there may be local disturbances to this general pattern caused by tectonic processes.

The dome-like present rate of uplift in Fennoscandia is now generally explained in terms of glacial isostasy. In previous papers Fjeldskaar (1994; 1997) modelled the isostatic response to deglaciation in Fennoscandia using an Earth model with a layered mantle viscosity overlain by an elastic lithosphere. The modelling is based on the mapped deglaciation. The melting history used previously, is compiled by B.G. Andersen and presented in Denton and Hughes (1981). The modelling was further based on a spatial resolution of approximately 50 by 50 km.

The modelled tilting of palaeo-shorelines at particular locations peripheral to the former ice load and the pattern of present rate of uplift are consistent and suggest a low-viscosity asthenosphere. It is suggested that the asthenosphere has a thickness less than 150 km and viscosity less than 7.0×10^{19} Pas beneath the lithosphere. The mantle viscosity below the asthenosphere has been set to 10^{21} Pas.

The most likely glacier thickness model gives a flexural rigidity of 10^{23} Nm ($t_e \approx 20$ km) at the Norwegian coast, increasing to above 10^{24} Nm ($t_e \approx 50$ km) in central parts of Fennoscandia.

7.1.6 Present rate of uplift

The present rate of uplift in Fennoscandia was calculated using data from tide-gauges, precise levelling, GPS and gravity measurements. Uplift rates calculated from repeated precise levelling along roads throughout Norway, Sweden and Finland make up the bulk of the data. Levelling results from the northern part of Finland have been used, together with the 1st , the 2nd , and a few lines from the 3rd precision levelling of Sweden. Data from all available Norwegian precision levelling lines were used, including the lines measured by surveyors from the Norwegian Railways (Danielsen, pers. comm.). The levelling lines are tied to tide-gauges along the coast. Additional tide gauge records from around the Baltic Sea (Ekman, 1998) helped constrain the regional uplift pattern. Between 1966 and 1984, repeated precise gravity measurements were performed on three lines across Norway, Sweden and Finland to determine the rate of uplift (Mäkinen *et al.*, 1986). Permanent GPS stations located in Sweden and Finland have also provided measurements of uplift rate (Ekman, 1998).

Uplift data from all sources were combined and gridded using a minimum curvature method. The resulting high-resolution grid shows areas of local disturbances (Fig. 7.1.4). The rate of uplift is close to zero along the Norwegian coast, increasing up to 7 mm/yr in central parts of the Baltic Sea.

It is, however, not unreasonable to assume that there is a neotectonic (non-glacial-isostatic) component in the uplift rate and the palaeo shoreline gradients. The general pattern of the uplift is here believed to be a result of glacial isostasy, but there may be local disturbances to this general pattern caused by tectonic processes.

The model that best fits with the observations is expected to give a good regional image of the glacial isostatic process. There will, however, be local areas with significant differences between the observations and the calculated uplift. One of the basic assumptions in this study is that these anomalous areas are today subject to vertical deformations of non-glacial-isostatic origin.

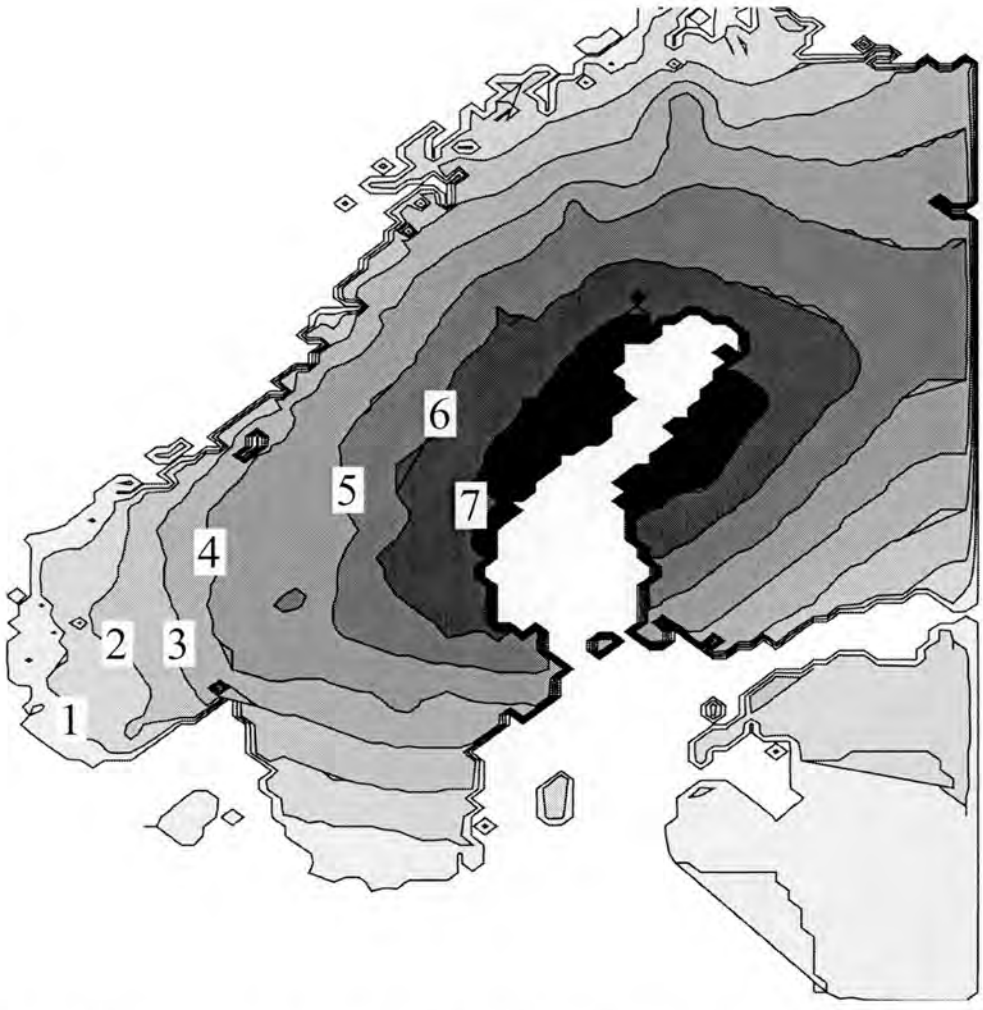

Fig. 7.1.4 Observed present rate of uplift. Contour interval is 1 mm/yr.

7.1.7 Neotectonics

A new model based on the above concepts was constructed, but with higher spatial resolution, approximately 20 by 20 km. A modified ice model for 20 000 BP was developed (Fig. 7.1.5), partly based on data from Svendsen *et al.* (1999), and the present topography in Scandinavia was also taken into account in the modelling (Fig. 7.1.6).

The net glacier thicknesses for various glacial times were the ice models of Fig. 7.1.5 minus the palaeo topography. The palaeo topography is calculated as the present topography modified by the glacial isostasy at the various time steps, calculated by the Earth rheology parameters mentioned above. The calculated uplift history for different times is shown in Fig. 7.1.7. Note the development of the forebulge offshore mid Norway. The resulting palaeo topography is shown in Fig. 7.1.8. The calculated present rate of uplift in Fennoscandia is shown in Fig. 7.1.9, which is the model that best fits the observations.

The uplift residuals are calculated only for land areas, and for Norway and Sweden, only. The areas with significant positive deviations (>1.0mm/yr) between the observations and the calculated uplift are shown in Fig. 7.1.10, where it is seen that almost the entire Norwegian land area has abnormal uplift rates. The most significant residuals (>1.5mm/yr), however, are located in the mountainous areas onshore southeastern Norway and northern part of western

Norway. These areas correspond largely with the areas of high Plio-Pleistocene (last 2.5 million years) erosion (Riis and Fjeldskaar, 1992). The Plio-Pleistocene erosion is assumed to be of glacial origin. Even though the estimated erosion is expected to have been largest in the early part of the Plio-Pleistocene (because the earliest ice ages were the biggest), a significant part of the subsequent uplift may seem to take place up to present. If this is correct, the mountain building process in Norway is a slow process, possibly connected to phase boundary migration (Riis and Fjeldskaar, 1992).

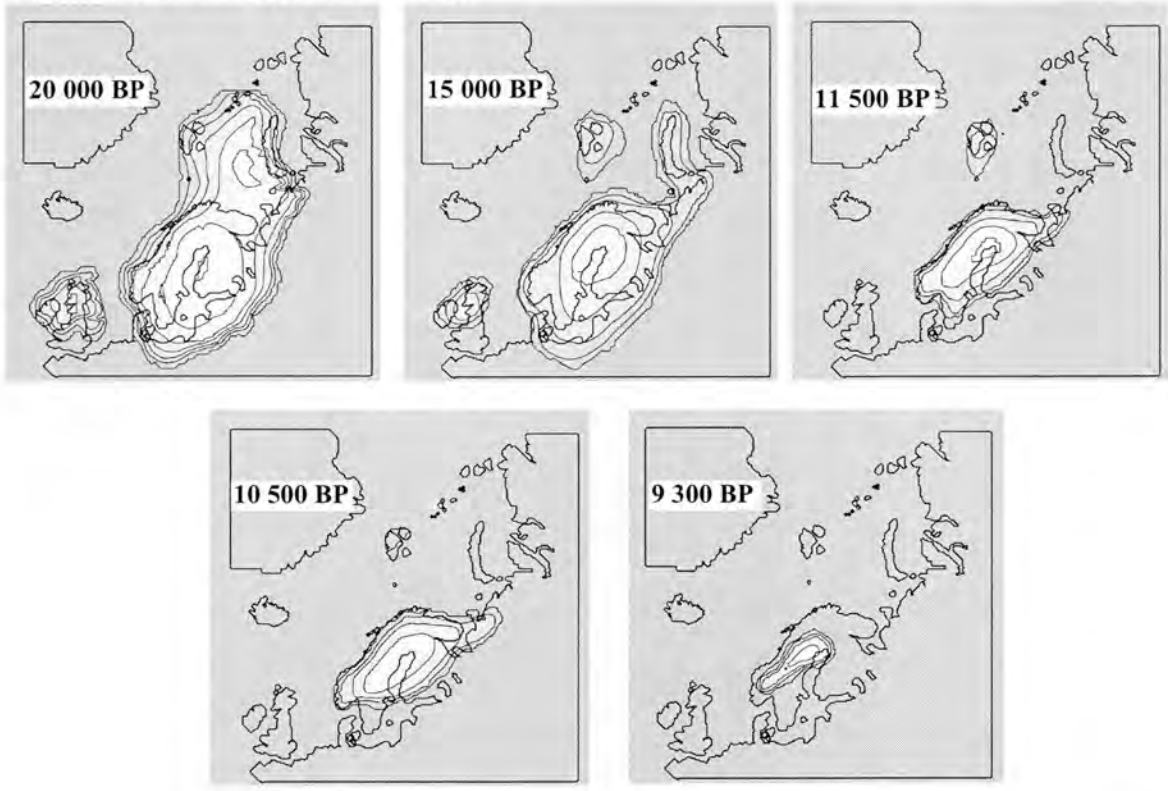

Fig. 7.1.5 The extent and thickness of the ice sheet during the deglaciation in Northern Europe partly based on Denton and Hughes [1981]: (a) 20,000 years BP, (b) 15,000 years BP, (c) 11,500 years BP, (d) 10,500 years BP, and (e) 9,300 years BP Contour interval is 500 m, except for (e), where the contour interval is 200 m.

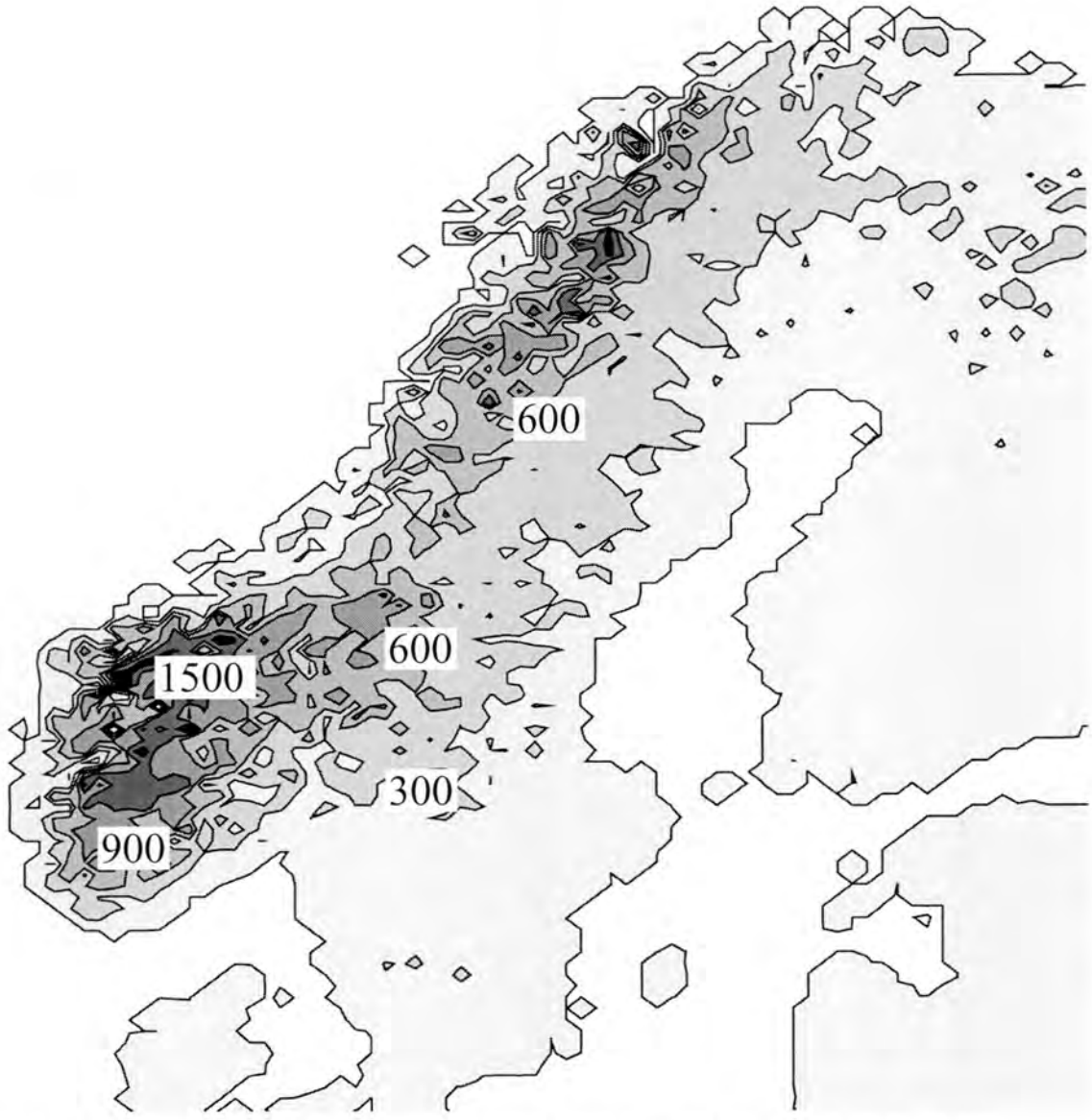

Fig. 7.1.6 Present day topography in Scandinavia (spatial resolution 20 by 20 km).

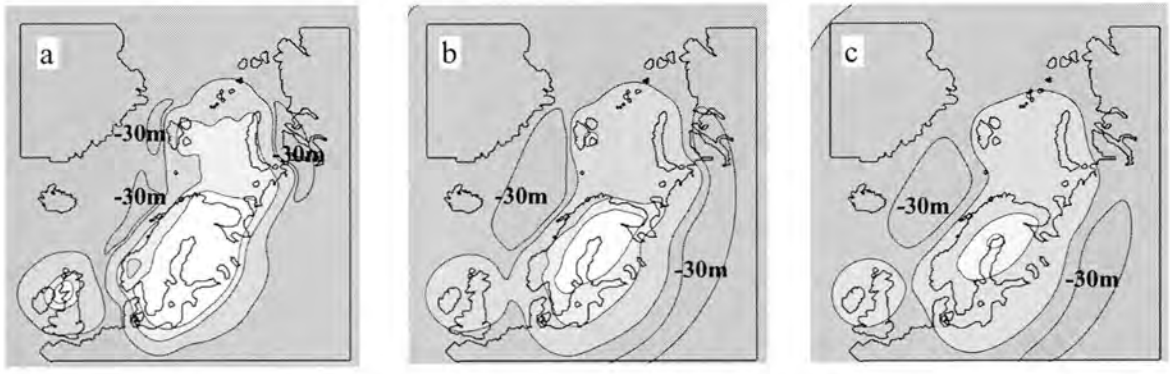

Fig. 7.1.7 Theoretical uplift response in meters for glacial and post-glacial time. Contours are given for –30m (forebulges), 0m, 300m, 500m and 1000m.

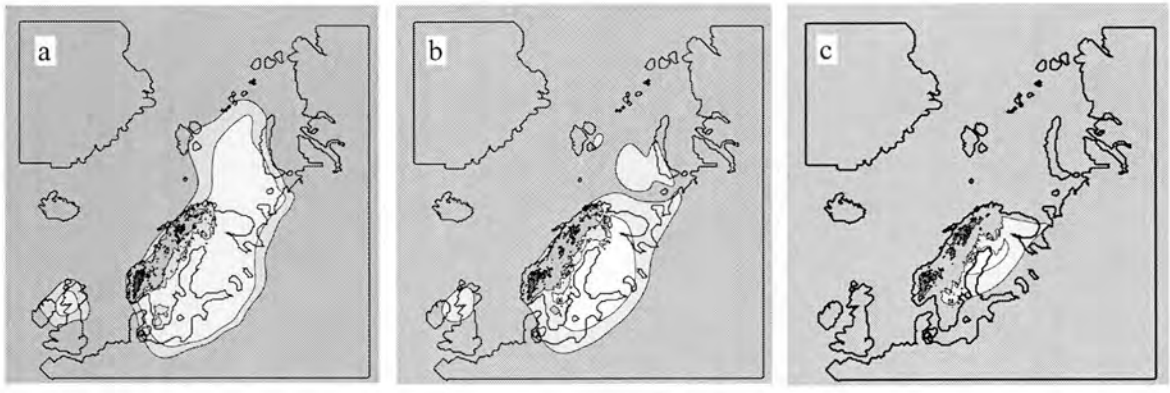

Fig. 7.1.8 *Calculated palaeo-topography is assumed to be the present topography modified by glacial isostasy for the various time steps. The glacial isostasy is calculated with the earth parameters mentioned above. Light areas indicate areas from 0 to 300 m below present sea level, dark areas more than 300 m above present sea level.*

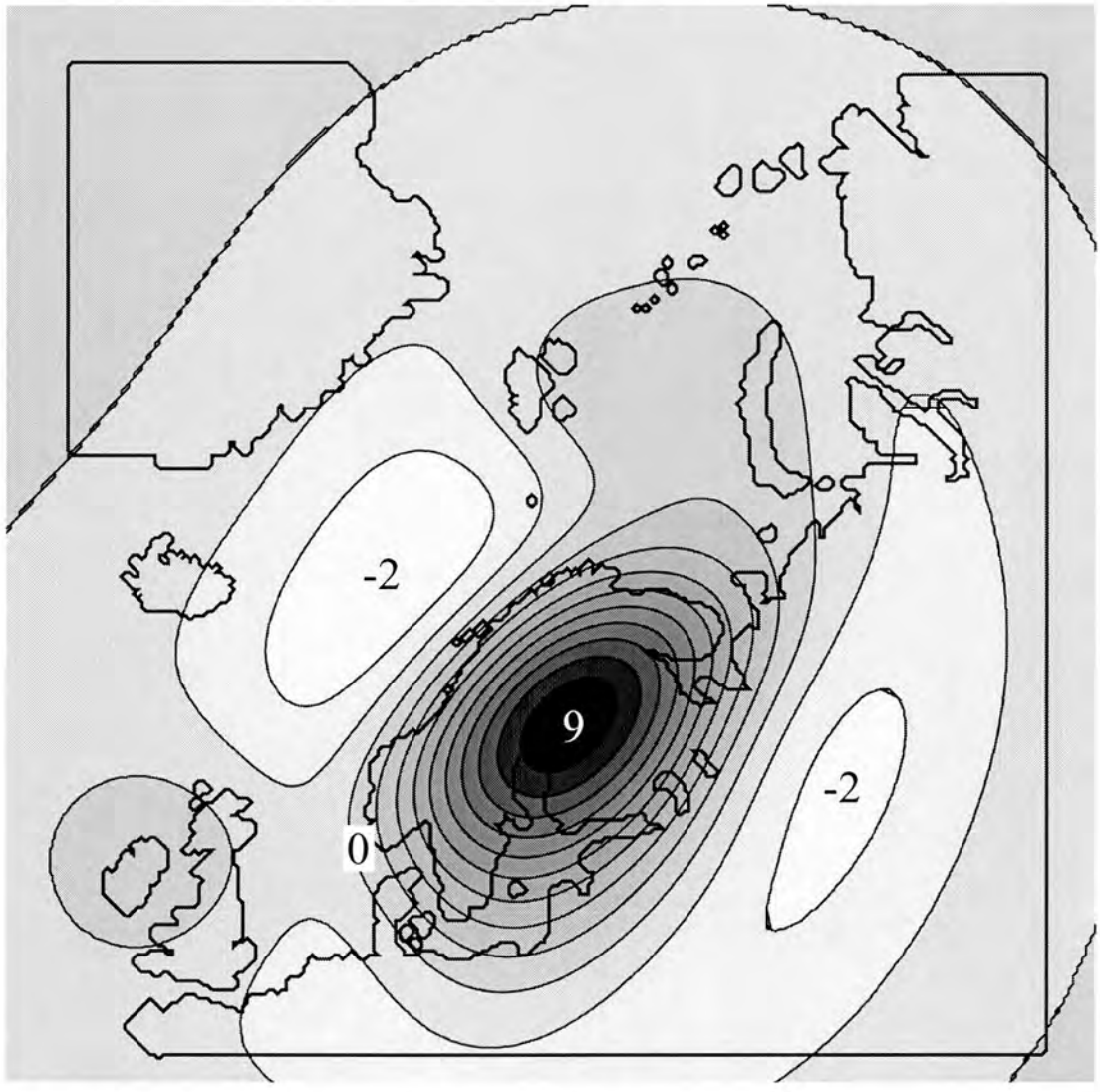

Fig. 7.1.9 Theoretical present rate of uplift in Fennoscandia.

Fig. 7.1.10 Areas with significant positive deviations (>1.0 mm/yr) between the observations and the calculated glacial isostatic uplift.

Fig. 7.1.11 shows that there is an area of significant negative (>0.5 mm/yr) residuals onshore northern part of the Baltic Sea, and, less pronounced, southwards on the eastern coast of Sweden. This area corresponds to an area of no Plio-Pleistocene erosion (Riis and Fjeldskaar, 1992). The Baltic Sea area constitutes a bulge area during the uplift of the surrounding land areas, because of the concentric erosional pattern of a central depression, marginal highs and huge sedimentary wedges made by continental ice sheets, as pointed out by White (1972).

There are three areas of significant anomalies in Scandinavia, relative to regionally predicted glacial rebound: onshore mid Norway, onshore western Norway including the zone from western to southeastern Norway, and the onshore area around the Gulf of Bothnia.

Fig. 7.1.11 Areas with significant negative deviations (>1.0mm/yr) between the observations and the calculated glacial isostatic uplift.

7.1.8 Discussion

The neotectonic movements resulting from the above calculations are based on several factors. Firstly, it is assumed that the observed present rate of uplift is mainly a postglacial phenomenon caused by isostatic adjustments following the melting of the Late Weichselian ice sheet. This is the most critical assumption, and not necessarily a correct one. Mörner (1979) proposed that the observed post-glacial uplift consists of two different components, one linear and one exponential. The linear component is assumed to have a tectonic origin and the exponential is assumed to be of glacial isostatic origin. He argues that the present rate of uplift is not a glacial isostatic phenomenon, but rather a tectonic process, with linear uplift rate. The arguments are based on an inferred change from exponential to linear uplift with time. However, the time resolution and precision of these curves are relatively low, and the arguments of Mörner are hence disputed.

The basis for this study is that present rate of uplift is mainly of glacial isostatic origin. The reason for this assumption is the consistent picture given by the observations of the deglaciation, palaeo-shoreline tilts and present rate of uplift. It is highly unlikely that a tectonic process would give a maximum present rate of uplift in the same geographical location as predicted from the observations of the deglaciation. It has been shown previously (e.g. Fjeldskaar, 1997) that the best-fitting parameters for palaeo-shoreline tilts also is the best-fitting parameters for the present rate of uplift.

Fig. 7.1.9 shows the uplift over the larger Fennoscandia including the forebulge offshore western Norway. The modelling predicts the transition zone between uplift and subsidence to be located just offshore, and in this zone the bending (stress) of the crust will be at its maximum. The high seismic activity offshore mid Norway may reflect this maximum bending with horizontal compression in a NW-SE direction. Additionally the horizontal compression originating at the mid-Atlantic ridge gives rise to similar stress directions. Finally the observation of shallow normal faulting earthquakes along the coast in the onshore areas are also in accord with expectations from the isostatic rebound model.

We have in this paper assumed that 100% of the regional part of the uplift is of glacial isostatic origin. This may be wrong. However, a sensitivity test shows that if only 80% of the regional uplift dome has a glacial isostatic origin, we would still have the same anomalies (=neotectonic movements) in the regions.

The quality and density of empirical data is crucial in any investigation: The uplift data, from which the uplift curves are constructed, are unevenly distributed, stemming from different methods and varying (and sometimes large) uncertainties. The possible incorrectness of these data or the synthesised uplift curves inevitably will affect the modelling results. The overall fit indicates that the data are reliable on the Fennoscandian scale, but it is presently not possible to resolve whether some of the deviations between model and observation reflect poor data.

7.1.9 Conclusions

We have demonstrated that the Earth's response to the deglaciation in Fennoscandia can be modelled using a layered viscous model overlain by an elastic lithosphere, and that the model response to the ice load is able to explain the regional uplift pattern to a considerable degree. The modelling has depicted certain areas with anomalous uplift rates in the order of 1.0 mm/yr (southern Norway, along the coast of northern Norway and in the Bothnian Bay). One interpretation is that the glacial isostatic uplift in these areas is overprinted by a weak tectonic uplift component.

The seismicity in Scandinavia, which is the highest in northwestern Europe, is largely concentrated in a few zones. In particular the offshore seismicity zones west of Norway correspond to zones where the uplift model predicts forebulges (compression), and this NW - SE compression would act constructively with ridge push generated compression. Furthermore, the shallow onshore (but coastal) normal faulting closely follows the Younger Dryas ice margin (10,500 BP), thereby indicating the importance of the deglaciation for present day seismicity, and in full accord with the glacial isostatic rebound model. In conclusion the findings support the idea that the stresses in western Scandinavia have two important components that interact constructively: post-glacial uplift and ridge push.

One idea supported by this investigation is that the Scandinavian peninsula is subject to a tilting with uplift to the west and subsidence to the east. The model anomalies reveal a zone of relative subsidence along the eastern Swedish coast and northwards which geographically coincide with the weak seismicity zones in Fig. 7.1.3. However, the quality of the horizontal

compression with depth (both magnitude and direction) in these areas is too uncertain to allow sound conclusions.

The apparent tilting may be a consequence of the Plio-Pleistocene erosional pattern, which is of glacial origin. The erosion has supposedly a maximum (marginal highs) in the mountainous areas of Norway (southern and northern Norway), and there will be a pronounced central depression in the Gulf of Bothnia. This is supported by the present investigation, both in terms of seismicity and calculated uplift residuals.

7.1.10 References

Crampin, S. 1994: The fracture criticality of crustal rocks. Geophys. J. Int., 118, pp. 428- 438.

Denton, G. H. and Hughes, T.J. 1981: *The last great ice sheets*. John Wiley and Sons.

Ekman, M., 1998: Recent postglacial rebound of Fennoscandia; a short review and some numerical results. GeoResearch Forum, 3-4, pp. 383-392.

Engelder, T. 1994: Stress regimes in the lithosphere, Princeton University Press

Fejerskov, M. and Lindholm, C. in press: Crustal stresses in and around Norway; An evaluation of stress generating mechanisms. Geol. Soc. London.

Fjeldskaar, W. 1994: Viscosity and thickness of the asthenosphere detected from the Fennoscandian uplift. Earth Planet. Science Lett. 126, 399-410.

Fjeldskaar, W. 1997: The flexural rigidity of Fennoscandia inferred from the post-glacial uplift. Tectonics vol. 16, no. 4, 596-608.

Fjeldskaar, W. in press: What about the asthenosphere viscosity? Geophys. Journ. Int.

Gudmundsson, A., 1999: Postglacial crustal doming, stresses and fracture formation with application to Norway. Tectonophysics, 307, pp. 407-419.

Hast, N. 1958: The measurement of rock pressure in mines. Swedish Geol. Survey Ser. C., No 560.

Hicks E., Bungum, H. and Lindholm, C. submitted: Stress inversion of earthquake focal mechanisms from onshore and offshore Norway. Submitted to Norsk Geologisk Tidsskrift.

Jamieson T.F. 1865: On the history of the last geological changes in Scotland, Geol. Soc. London Quart.J., 21, 161-203.

Kolderup, C.F. 1930: Jordskjelv i Norge 1926-1930. Bergens Museum Årbok, no. 6, 40 pp.

Kvale, A. 1960: Norwegian earthquakes in relation to tectonics, Universitetet i bergen Årbok, Matematisk-naturvitenskapelig serie, 10, 17 pp.

Lindholm, C., Bungum, H., Hicks, E. and Villagran, M. in press: Crustal stress and tectonics in Norwegian regions determined from earthquake focal mechanisms. Geol. Soc. London.

Mäkinen, J., Ekman, M., Midtsundstad, Å and Remmer, O. 1986: The Fennoscandian land uplift gravity lines 1966-1984. Reports of the Finnish Geodetic Institute, 85:4, 195 pp.

Mörner N.A. 1979: The Fennoscandian uplift and Late Cenozoic geodynamics: geological evidence, Geo Journal, 33, 287-318.

Muir-Wood, R, in press: Deglaciation Seismotectonics: a principal influence on intraplate seismogenesis at high latitudes?

Riis, F., and Fjeldskaar, W. 1992: On the magnitude of the Late Teriary and Quaternary erosion and its significance for the uplift of Scandinavia and the Barents Sea. In: Larsen, R.M., H. Brekke, B.T. Larsen and E. Talleraas (eds): Structural and Tectonic Modelling and its application to Petroleum Geology, NPF Special Publication 1, pp. 163-185. Elsevier, Amsterdam.

Rohr-Torp E. 1994: Present uplift rates and ground water potential in Norwegian hard rocks. Bull. Nor. Geol. Unders., 426, pp. 47-52.

Stephansson, O. 1988: Ridge push and glacial rebound as rock stress generators in Fennoscandia. Bulletin of the Geol. Inst. of the Univ. of Uppsala, Sweden, 14, pp. 39-48

Svendsen, J.I., Astakhov, V.I., Bolshiyanov, D.Y., Demidov, I., Dowdeswell, J.A., Gataullin, V., Hjort, C., Hubberten, H.W., Larsen, E., Mangerud, J., Melles, M., Möller, P., Saarnisto, M., and Siegert, M. 1999: Maximum extent of the Eurasian ice sheets in the Barents and Kara Sea during the Weichselian. Boreas, vol. 28, 234-242.

Sykes, L. R. and Sbar, M. 1974: Intraplate earthquakes, lithospheric stresses, and the driving mechanism of plate tectonics. Nature, 245, pp. 298-302

White, W.A. 1972: Deep erosion by continental ice sheets. Geol. Soc. Am. Bull., 83,p. 1037-1056.

Wu, P. Johnston, P. and Lambeck, K. 1999: Postglacial rebound and fault instability in Fennoscandia. Geophys. J. Int., 139, pp. 657-670.

Zatsepin, S. and Crampin, S. 1997: Modelling the compliance of crustal rock -I. Response of shear-wave splitting to differential stress. Geophys. J. Int., 129, pp. 477-494

Zoback, M. 1992: First and second order patterns of stress in the lithosphere; The world stress map project. J. Geophys. Res., 97, pp. 11703-11728.

8 APPENDIX 1: MSC THESIS OF ARNGRIM UTSKARPEN, NTNU

Fieldwork for this thesis was financed by the NEONOR project.

NTNU
Norges teknisk-naturvitenskapelige universitet

Institutt for kart og oppmåling
N-7491 Trondheim

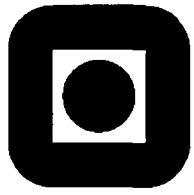

Arngrim Utskarpen

GPS

brukt til nøyaktig stedsbestemmelse

– som deteksjon av jordskorpebevegelser

Hovedoppgave høsten 1999

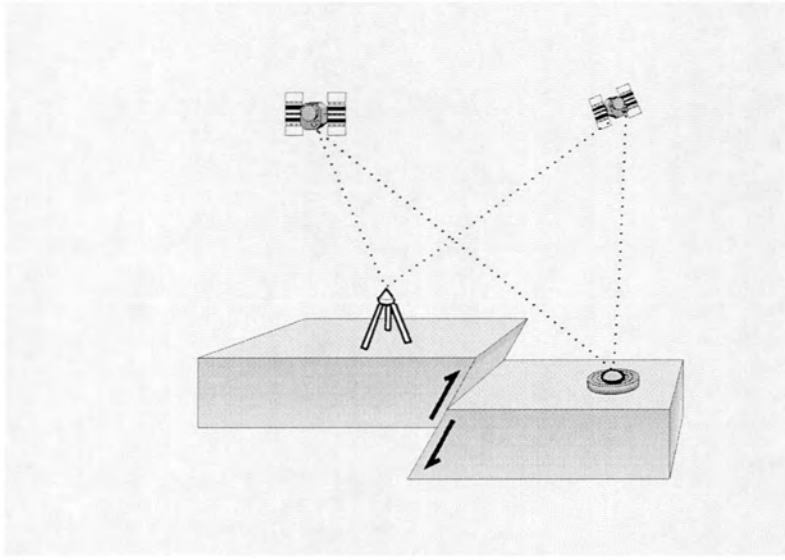

8.1 SAMMENDRAG

Denne oppgaven går ut på å beskrive hvordan GPS-metoder kan brukes til å detektere jordskorpebevegelser. Som et «case» har jeg brukt målinger fra 1997 av tektoniske forskyvninger ved Ranafjorden i Nordland.

Disse målingen fra 1997 er foreløpig de eneste det foreligger resultater fra, slik at det fremdeles ikke er detektert faktiske forskyvninger. I år (1999) ble det imidlertid målt på nytt i det samme området.

Nøyaktigheten for resultatet av 1997-målingene ligger i størrelsesorden rund 0,5-1,0 cm i 95%-konfidensintervallet, noe som betyr at det skal store forskyvninger til før man kan si tilsvarende sikkert om de har skjedd. Hvis man ikke stiller fullt så strenge krav til konfidens og går ned til 68,5%, så skulle det være mulig å detektere forskyvninger også mellom 1997 og 1999 gitt at de er store nok / forkastningen er aktiv (nok). Man må da imidlertid være oppmerksom på sjansen øker for feilaktig å fastslå forskyvning.

Oppgaven inneholder beskrivelse av forskjellige programmer og beregningsmetoder som er benyttet i tillegg til en kort presentasjon av lignende prosjekter andre steder.

8.2 INNLEDNING

Norges Geologiske Undersøkelser (NGU) driver som en del av samleprosjektet NEONOR med detaljert geologisk kartlegging av utvalgte steder i Norge. Denne aktiviteten er konsentrert der hvor det er funnet antatt aktive forkastninger, blant annet i Rana, Beiarn, Kåfjord og Masi. Flere disipliner og organisasjoner er involvert i denne kartleggingen, både geologi, geodesi og geofysikk er representert. I denne oppgaven er det metoder innen geodesien som står i sentrum med særlig vekt på GPS anvendt for å detektere bevegelser i forkastningsområdet i Rana.

For det aktuelle området i Rana har Institutt for kart og oppmåling ved NTNU fram til 1999 vært involvert i planlegging og utførelse av GPS-målinger.

I 1994 ble det satt ned bolter til et nett med 18 punkter fordelt på tre profiler som går på tvers av Ranafjorden, hovedsakelig i retning nord-sør. Det innerste profilet går fra Mofjellet, passerer Mo i Rana og går videre i retning nordvest. Et midtre profil går over Hemnesberget og Utskarpen mens det ytterste dekker Nesna og noen av øyene utenfor. Kartet nedenfor viser nettets beliggenhet i regionen med ekstra markering av de ytterste punktene i hvert av de tre profilene. Se også større kart senere i besvarelsen (i kapittel 4).

Nettets beliggenhet:

I 1997 ble nettet målt av Institutt for kart og oppmåling med metoden «klassisk statisk». Det er dataene fra disse målingen som utgjør grunnlaget for denne oppgaven. Nettet ble også målt like etter at det ble opprettet i 1994, men på grunn av dataproblemer den gangen er det ikke tatt med noen resultater fra disse målingene.

I år (1999) ble nettet målt på nytt igjen av Statens kartverk, som har overtatt ansvaret for denne delen av NEONOR-prosjektet. Denne gangen ble metoden «absoluttbestemmelse» benyttet og det ble også etablert 2 nye punkter på det ytterste profilet. Ved leveringsfristen for denne oppgaven foreligger det ennå ikke resultater fra disse målingene, men ut i fra måleopplegget og utstyret som ble benyttet er det rimelig å anta at nøyaktigheten vil bli bedre enn for målingene fra 1997.

Hvorvidt det vil bli mulig å si sikkert om det har skjedd forskyvning eller ikke i løpet av disse to årene kommer an på om den eventuelle forskyvningen overstiger tilfeldige målefeil eller ikke.

Videre i denne oppgaven kommer først en generell beskrivelse av GPS og målemetoder. Deretter kommer en presentasjon av målingene fra 1997 og sammenlikning av forskjellige beregningsstrategier og programmer.

8.3 GENERELT OM GPS

GPS står for Global Positioning System og er et satellittbasert navigasjonssystem utviklet og eid av det amerikanske forsvars-departementet.

Det finnes flere metoder i bruk som degraderer signalene for sivile brukere slik at de gir lavere nøyaktighet. De viktigste er Selective Availability (SA) og Anti-Spoofing (A-S).

Atomklokkene ombord i GPS-satellittene er nøkkelen til systemets nøyaktighet ettersom det er disse som genererer grunnfrekvensen f_0. Satellittene sender på to frekvenser L1 og L2. som er heltalls multipler av denne grunnfrekvensen. SA går ut på at det innføres feil på klokken, noe som virker inn på disse frekvensene. Som del av SA innføres også unøyaktigheter i de kringkastede banedataene.

GPS-satellitt

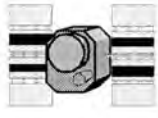

Frekvenser

f_0 =10,23 MHz

L1 = 1575,42 MHz

L2 = 1227,60 MHz

Signalene som sendes ut er påmodulert to slags koder: C/A kode, (Coarse/Acquisition) og P-code (Precision). C/A-koden, som finnes bare på L1-frekvensen gir lavest nøyaktighet mens P-koden, som finnes på begge frekvensene (L1 og L2) gir den høyeste nøyaktigheten som kan fås med kodemålinger alene. Når A-S er slått på er P-koden erstattet av den krypterte Y-koden som bare militære brukere har tilgang til. Dette har vært tilfelle mer eller mindre permanent siden 1994.

I frekvensplanet har GPS-signalene karakter av spredt spektrum signal, dette for å gjøre dem mindre utsatt for jamming, både tilsiktet og ikke tilsiktet.

8.3.1 Kodemålinger

Ved kodemålinger utnyttes den påmodulerte koden til signalet for å finne avstanden mellom satellitt og mottaker. Dette foregår ved at mottatt kodesekvens sammenlignes med en tilsvarende kodesekvens generert av mottakeren. I og med at satellittens atomklokke og mottakerklokken ikke går likt, vil dette imidlertid ikke bli den «sanne» avstanden. Av den grunn snakker vi om pseudoavstandsmålinger.

Ved måling mot 4 satellitter eller mer samtidig kan imidlertid denne klokkefeilen løses ut som en av de ukjente. Kodemålinger er den mest robuste metoden for posisjonering ved hjelp av GPS, men gir mindre nøyaktighet enn fasemålinger, som går ut på å måle endringen av fasen over tid.

8.3.2 Fasemålinger

Dette er den mest nøyaktige metoden og den som benyttes ved høypresisjonsberegninger. Ved å bruke fasen til signalet som observert størrelse går det an å få mer nøyaktig stedsbestemmelse enn ved kodeobservasjoner. L1-fasen er tilgjengelig via C/A-koden mens det benyttes forskjellige kodeløse teknikker for å rekonstruere L2 når P-koden ikke er tilgjengelig (gjelder så å si alle sivile brukere).

Ved fasemålinger blir avstanden mellom mottaker og satellitt bestemt som et helt antall N bølgelengder + fasen på mottatt signal ved tidspunkt t. Ulempen er at det kreves kontinuerlige observasjoner over et visst minimum av tid for å bestemme disse heltallene (N), som er ukjente til å begynne med. (Jfr. figuren.)

Prinsippet for fasemålinger:

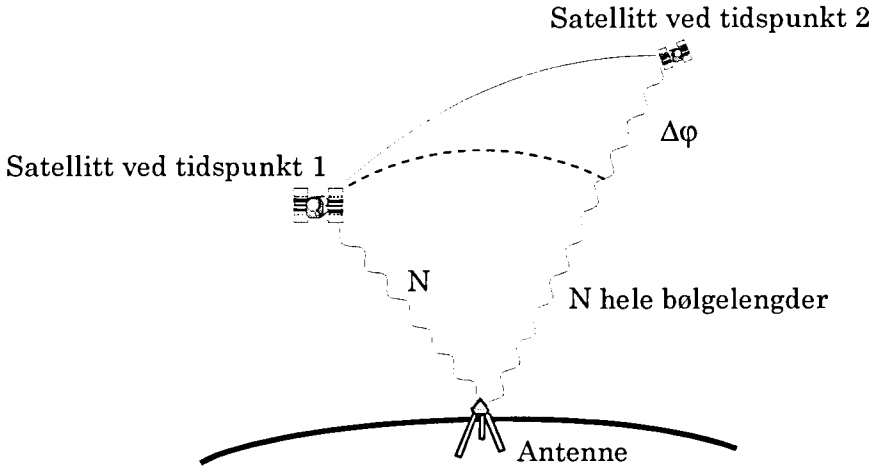

8.3.3 Banedata

For å kunne utlede de størrelsene vi er interesserte i fra GPS-målingene, er vi avhengige av å kjenne til satellittenes posisjoner til ethvert tidspunkt t i et gitt koordinatsystem.

GPS-satellittene følger som andre himmellegemer Keplers lover, og i et ideelt tilfelle vil de da gå i ellipsebaner med jordsenteret i det ene brennpunktet.

Figuren viser 1 baneplan med 1 satellitt. For det fullt utbygde GPS-systemet finnes 6 baneplan med 4 satellitter i hvert plan + reserver.

Følgende størrelser inngår i figuren:

i inklinasjon. Denne er *ca.* 55 grader for dagens GPS-satellitter, som er av Block II-typen.

ω er vinkelen mellom oppstigende knute og perigeum.

Ω er vinkelen mellom oppstigende knute og vårjevndøgnspunktet. For GPS-satellittene er denne verdien omtrent lik ±30, ±90 og ±150 (6 baneplan.)

v beskriver satellittens plassering i banen ved et gitt tidspunkt: $v(t)$. I den utenlandske litteraturen kalles størrelsen gjerne for «true anomaly».

Baneelementer:

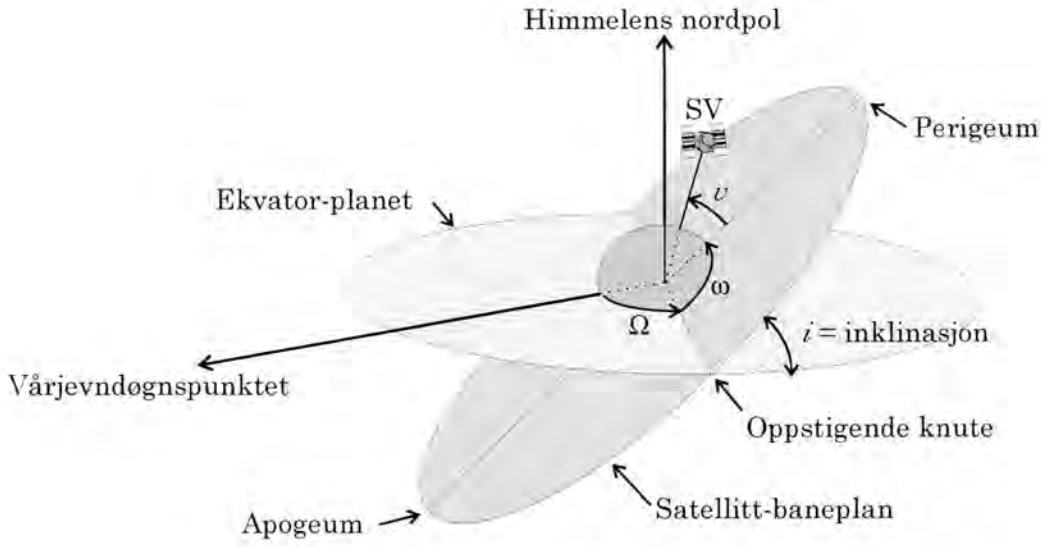

I virkeligheten flytter både vårjevndøgnspunktet og himmelpolene seg på grunn av presesjonen og nutasjonen. Dette kan tolkes som svingninger med forskjellige perioder som er overlagret hverandre.

Disse fenomenene fører til at satellittbanene i forhold til jorda også endrer seg over tid. I tillegg endrer de seg på grunn av polbevegelser, som konkret går ut på at omdreiningsaksen ikke «stikker ut» av jorda på nøyaktig samme sted hele tiden.

Satellittbanene avviker fra ellipsen blant annet på grunn av påvirkning fra måne og planeter samt uregelmessigheter i jordas tyngdefelt. Det er samtidig disse tingene som forårsaker presesjon og nutasjon slik at det på en måte blir to sider av samme sak. Det hele er i grunnen ganske komplekst, og for den som er ute etter detaljkunnskaper om emnet finnes det i litteraturen.

I resultatutskriften fra Bernese-programmet går det f.eks. an å se at den beregnede inklinasjonen ikke er 55 grader akkurat for noen av satellittene, slik som i den ville vært i et ideelt tilfelle.

For å bestemme banedata med høyeste nøyaktighet, må man altså ta med endringer i jordrotasjonen i beregningene. Til å overvåke disse endringene brukes VLBI (Very Long Baseline Interferometry) og SLR/LLR (lasermålinger mot satellitter og månen). I dag har vi mer nøyaktige verdier for slike uregelmessigheter enn tilfelle var for bare få år tilbake takket være disse teknikkene. Dette er metodene som brukes for vedlikehold og kontinuerlig oppdatering av presisjonsdatumet ITRF.

IERS

IERS – International Earth Rotation Service – tar imot VLBI og laserdata fra bidragsytere rundt om i verden og sammen med blant andre IGS – International GPS Geodynamics Service –beregner og tilbyr de verdier for disse størrelsene (jordrotasjonsparamtre) som utgjør grunnlaget for transformasjon mellom WGS-84 og ITRF.

NGS og SP3-formatet

Det amerikanske National Geodetic Survey (NGS) er ansvarlig for et verdensomspennende nettverk av permanente GPS målestasjoner som fungerer som tillegg og supplement til det offisielle tracking- og kontrollnettverket. Noen av disse stasjonene er også VLBI/SLR-stasjoner og det blir beregnet presise banedata for satellittene i ITRF-systemet. Disse dataene kan ha nøyaktighet rundt 10 cm, men er tilgjengelige først i ettertid.

Nøyaktigheten til de kringkastede banedataene begrenser seg til 5-20 m avhengig av nivået på S/A og hvorvidt AS er på eller ikke. Dette virker ikke inn på nøyaktigheten til de presise dataene.

Presise og kringkastede banedata:

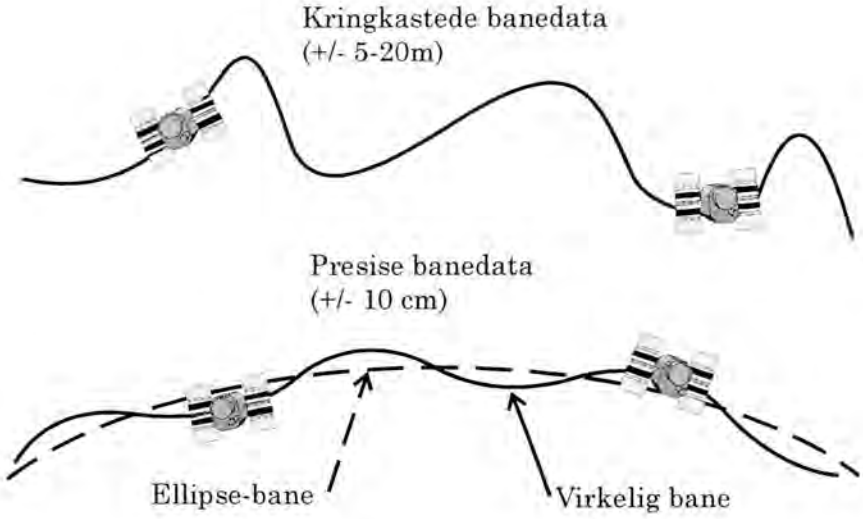

De presise banedata fra NGS kan fritt lastes ned forskjellige steder på Internett. Dataene finnes på forskjellige binær og tekstformater men det vanligste i dag er kanskje SP3-formatet. Dette er Ascii-filer som har listet posisjon og klokkekorreksjon til alle satellittene for hvert 15. eller 40. minutt. Posisjonene er oppgitt som kartesiske koordinater i gjeldende versjon av ITRF-systemet. For målingene fra september 1997 er dette ITRF 94.

Eksempel på en SP3-filer finnes på CDen under \banedata..

8.3.4 Andre forstyrrende faktorer

For GPS brukt til høypresisjonsformål er det en hel rekke forstyrrende faktorer å ta hensyn til. Dette kapittelet inneholder korte beskrivelser av noen av de viktigste.

Ikke alle disse fenomenene har noen betydning for metoder som lokal relativposisjonering og vektorberegninger. Brukervennlige programpakker som er kommersielt tilgjengelige tar da heller ikke hensyn til alt som er listet her. Dette gjelder Leicas SKI-program. For tyngre beregningsprogrammer som Bernese og GIPSY derimot, har mye av det relevans.

Tidejord

De varierende tiltrekningskreftene fra sol og måne samt jordrotasjonen er det som forårsaker tidevannet, og ettersom jordkloden selv er elastisk og deformerbar virker disse kreftene også inn på det som ikke er vann, bare i noe mindre grad.

Denne deformasjonen av jorda virker inn på retningen av vertikalen og tyngdekraftens verdi. Det var dette man målte med bl.a. pendler og gravimetre for å utforske fenomenet før VLBI og andre moderne metoder ble tatt i bruk. Av samme grunn kan tidejord være systematisk feilkilde ved presisjonsnivellement.

Ifølge *[Vanícek m.fl. 1982]* og andre kilder befinner tidejordsfenomenet seg i en størrelsesorden på noen desimeter og da er det klart at man også må ta hensyn til det ved globale høypresisjonsløsninger av GPS.

Troposfære, ionosfære

GPS-signaler som går gjennom atmosfæren, vil brytes og endre frekvens på grunn av ulik brytningsindeks i de forskjellige lagene. Dette påvirker observasjonene og det er nødvendig å gå inn med modeller som forsøker å korrigere for dette. Det finnes ingen klar grense mellom de forskjellige lagene i atmosfæren, men for modellering av effektene som virker inn på GPS-signalet er det vanlig å dele inn i troposfære og ionosfære.

Refraksjon i atmosfæren:

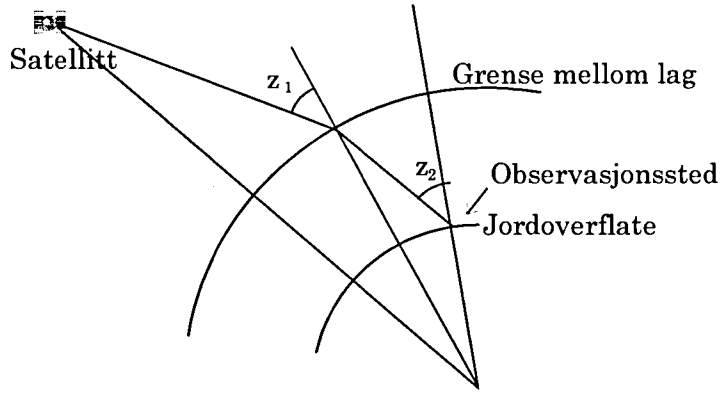

Ionosfæren inneholder ioner og frie elektroner og tettheten varierer både gjennom døgnet og året og med den 11-årige solsyklusen. Den mest effektive metoden for å løse ut virkningen av ionosfæren er å bruke to signaler med forskjellig frekvens og dette skal være hovedgrunnen til at GPS-systemet er konstruert med to frekvenser.

Troposfæren kan deles inn i våt og tørr del. Det finnes forskjellige modeller for å estimere den, hovedsakelig som en funksjon av høyden. De mest kjente er Hopfield og Saastamoinen.

Flerveisinterferens

Flerveisinterferens eller multipath er når et signal består av reflekterte signaler i tillegg til det direkte signalet. For TV-sendinger vises dette som «ghost image» eller spøkelsesbilde. GPS er heller ikke forskånet fra fenomenet. Signalkarakteristikken endres og det virker forstyrrende inn på pseudoavstandsmålingene.

For GPS-signalet er de største syndebukkene ting som nettinggjerder eller bygninger med metallkledning i nærheten av antennen. Flerveisinterferens vil imidlertid alltid forekomme til en viss grad selv om man prøver å unngå disse tingene.

Flerveisinterferens:

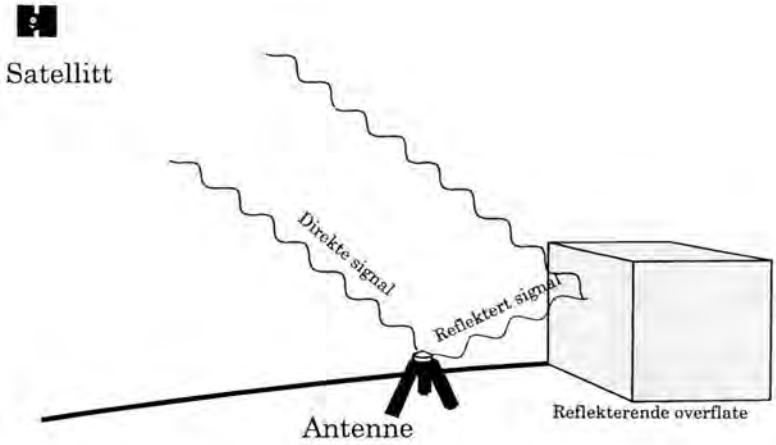

Forskjellige måter å konstruere antenner på tar sikte på å redusere effekten av fenomenet. I dag representerer antenner med chokering etter alt å dømme den beste løsningen på problemet. I tillegg har måten signalet blir prosessert på i mottakeren en viss betydning.

Chokering antenne:

EUREF Central Bureau (CB) anbefaler antenner av denne typen med Dorne-Margolin element og chokering for stasjonene som bidrar med data. Tilsvarende antennetype ble brukt av Statens kartverk under stamnettmålingene i 95-96 og under målingene i Rana-nettet i 1999 ble det også benyttet slike antenner. Under målingene i 1997 ble det derimot benyttet «vanlige» antenner.

Eksentrisk skjev bolt

Observasjonene som blir gjort med GPS referer seg til fasesenteret i antenna, mens det vi er interesserte i er koordinater for et fast punkt som f. eks. toppen av en bolt.

I landmålingspraksis kan slike bolter ofte være noe skjeve, da det å få dem 100% rette koster uforholdsmessig mye tid og penger. Det er mer kostnadseffektivt å bare måle skjevheten og korrigere for dette etterpå.

Skjev bolt:

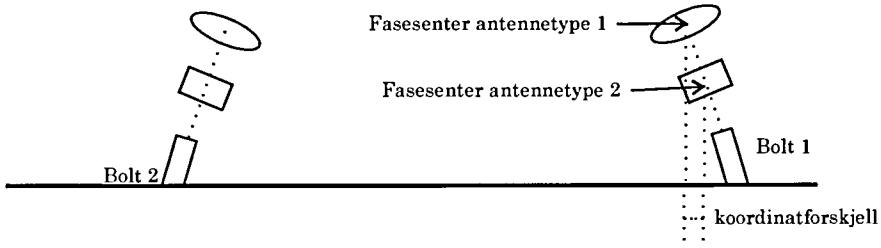

Ved stativoppstillinger er det vanlig å senke eller heve stativet mellom hver gang når det måles i flere perioder /«sessions» og prøve å få et hint om sentreringsnøyaktigheten på den måten. Boltene som Rana-nettet består av er av en type som tillater direkte montering av antennen på bolten, såkalt tvangssentrering. Problemet med sentreringsnøyaktighet skulle med dette være løst.

Ettersom også enkelte av disse boltene er skjeve er det imidlertid en teoretisk mulighet for at måling med ulike antenner fra år til år kan virke inn på koordinatbestemmelsene ved at avstanden fra skrue til fasesenter ikke er den samme for alle antenner.

I beregningene jeg har gjort i denne oppgaven er imidlertid alle boltene regnet som rette, og det kan av den grunn likevel være verdt å ofre problemstillingen litt oppmerksomhet hvis det senere skal sammenlignes med andre målinger.

8.4 MÅLINGENE FRA 1997

I 1997 ble nettet målt med 4 GPS-mottakere i løpet av 6 dager fra 8. til 13. september. Mottakerne var 12-kanals tofrekvente av typen Leica SR9500. Antennene som ble benyttet har betegnelsen LEICA AT302-GP – «uten grunnplate». Typisk måletid var minst 1 time for de korte vektorene og opp til *ca.* 4 timer for de lange vektorene på tvers av profilene. Måleopplegget tilsvarer metoden «klassisk statisk».

Figuren nedenfor viser punktenes beliggenhet i forhold til hverandre og vektorene som er beregnet i denne oppgaven er streket opp med grått. Punktene som er nummerert som 9401-9418 hører til dem som ble satt ned i 1994 med formål å skulle detektere jordskorpebevegelser.

Oversikt over punktplassering og vektorer:

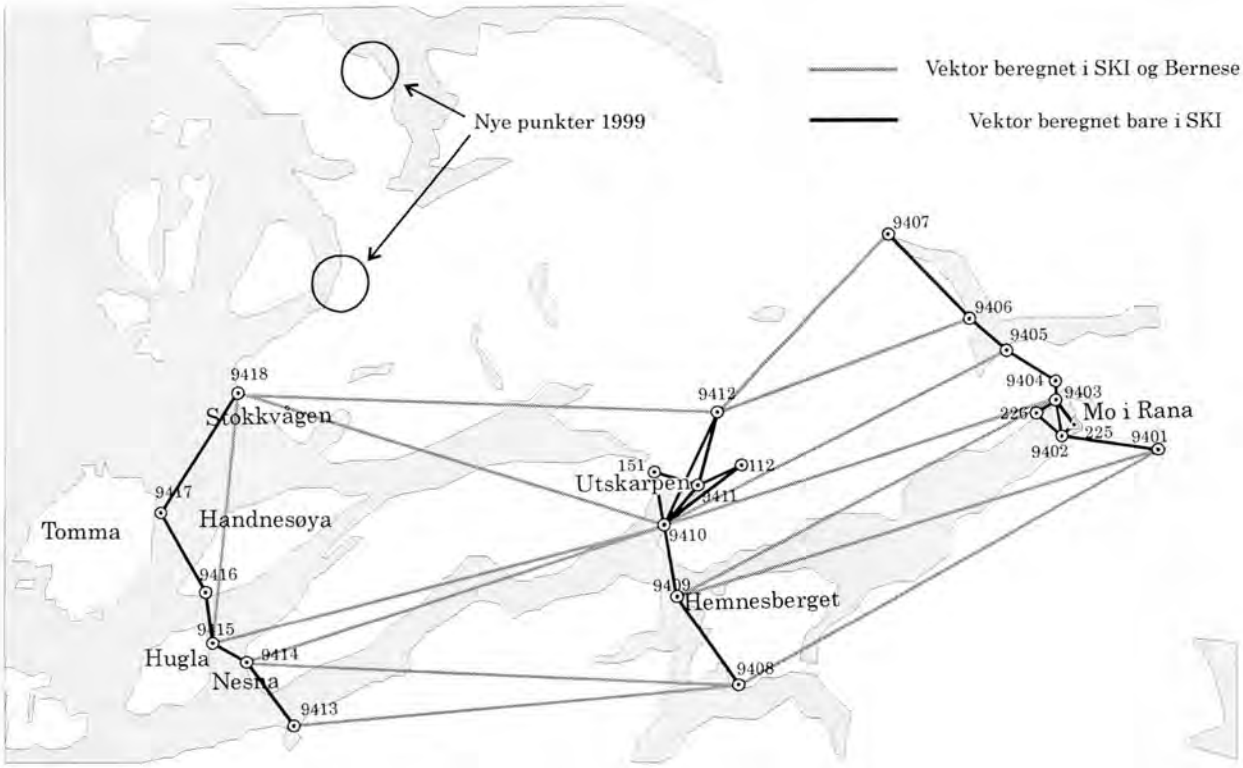

I tillegg ble det som figuren viser målt i punktene 151 og 112 ved Utskarpen samt 225 og 226 ved Mo i Rana. Disse punktene er etablert av Statens kartverk og er ikke angitt ved fullt navn i figuren. Fullt navn er J16T112, J16T115, J16T225 og J16T226. Videre i denne rapporten kan både den fulle betegnelsen og kortversjonene forekomme, men det skulle likevel være klart hva det er snakk om.

Blant disse punktene er J16T225 i Mo av spesiell interesse. Dette er et av 3D-punktene i det nye stamnettet som er basert på EUREF89-datumet og under utjevningene jeg har foretatt er dette brukt som fast punkt.

Punkt J16T225 eksisterte ikke da nettet ble etablert i 1994. Derfor finnes punkt 9402 selv om det ligger like ved. I 1999 ble 9402 derfor kuttet ut. Punkt 9407 ble heller ikke målt i 1999, i likhet med 112, 151 og 226, men det ble etablert to nye punkter på det ytterste profilet som ble målt.

Punktene som ikke hører til 94-serien (bortsett fra 3D-punktet 225) er hovedsakelig målt fordi det kreves startkoordinater som er bedre enn de som fås ved «Single Point positioning»/ navigasjonsløsning når en skal beregne vektorene. Det er oppnådd ved å bruke oppgitte koordinater for disse punktene som utgangsverdier.

8.5 BEREGNINGSSTRATEGIER

Dette kapittelet inneholder en beskrivelse av de forskjellige programmene som er benyttet til å beregne vektorer av dataene fra 1997-målingene. De to programmene jeg har vektorer fra er SKI Software fra Leica Geosystems AG og Bernese fra universitetet i Bern.

I SKI-programmet har jeg prøvd meg med litt forskjellige atmosfæremodeller og banedata, mens vektorene fra Bernese er slik som jeg fikk dem fra Morten Strand hos Fjellanger Widerøe, som var behjelpelig med selve beregningene. Uten denne assistansen ville mye tid gått med til å navigere i menyjungelen til Bernese-programmet og kanskje likevel ikke kommet ut med noe fornuftig resultat.

8.5.1 Leicas SKI-program

SKI står for Static Kinematic Software og navnet sier dermed noe om hva programmet gjør. Programmet inneholder moduler for planlegging av GPS-målinger, beregning av vektorer, utjevning og en modul hvor det går an å jobbe med datumtransformasjoner og kartprojeksjoner. I arbeidet med denne oppgaven er det vektorberegningsmodulen og utjevningsmodulen jeg har benyttet meg av.

SKI-programmet er primært laget for å jobbe mot Leicas eget format for backupdata. Det var dette jeg gjorde i arbeidet med denne oppgaven ettersom målingene var utført med utsyr fra Leica.

Det finnes imidlertid muligheter for import av RINEX-data fra andre mottakermerker.

For å bruke Leica-målingene i andre beregningsprogrammer, som Bernese, er en avhengig av å eksportere backupdataene på det interne formatet til RINEX.

Vektorberegninger i SKI

Alle vektorberegningene går automatisk, det er bare å markere stasjonene det skal beregnes vektorer mellom med «pek og klikk» og så går resten mer eller mindre av seg selv. Først kan det imidlertid være aktuelt å stille inn visse parametre for støy og atmosfære. Etterpå er det mulig å sjekke støymønsteret til de forskjellige satellittene ved å studere residualer fra vektorberegningene og så kjøre beregningene om igjen etter at en har utelatt satellitter.

Forskjellige beregningsparametre

I parameteroppsettet til SKI finnes blant annet følgende muligheter for å gjøre egne valg:

Cut-off angle

Satellitter som ligger under denne vinkelen blir ikke tatt med i beregningene. Standardverdi er 15 grader over lokal horisont og denne har jeg stort sett ikke endret på. Der hvor det var problemer med å få løst heltallene hadde ikke økning av elevasjonsmaske den ønskede innvirkningen.

Tropospheric model

Troposfæremodeller som er implementert i SKI er blant andre Hopfield og Saastamoinen. Hopfield er standard og jeg har holdt fast ved den når jeg har prøvd meg fram med å endre noen av de andre alternativene. Jeg har imidlertid brukt Saastamoinen til å beregne vektorene som skulle blandes med Bernese i fellesutjevning ettersom Bernese-vektorene var beregnet med Saastamoinen.

Ionospheric model

Hvis det foreligger med enn 45 minutter med observasjoner, noe det gjøre for alle vektorene i denne oppgaven, er det mulig å få SKI til å beregne en modell . (Computed model). Det er også mulig å importere ionosfæremodell i form av filer på IONEX-format. I hjelpefilene står

det listet opp ftp-adresser hvor slike filer kan hentes, men det var noe rart med filene og jeg fikk dem ikke til å virke. «Computed model» er sannsynligvis et bra alternativ.

Ephemeris

SKI kan enten bruke kringkastede banedata i beregningene eller presise banedata på NGS/SP3-formatet. Banedataene finnes med satellittposisjoner for hvert 40. og hver 15. minutt. SKI ville bare akseptere filene med data for hvert 40. minutt av en eller annen grunn. Det kan kanskje være årsaken til at beregning med disse dataene ikke ga noe særlig bedre resultater enn med «broadcast».

Ellers er vel 30 km vektorlengde (som i denne oppgaven) muligens grensen for når en har noe ekstrautbytte av presise banedata i det hele tatt med dagens software. Filene med data for hver 15. minutt fungerte ikke enda det var de samme som ble brukt under Bernese-beregningene. Jeg har ikke funnet noen forklaring på dette. Det kan knakke skyldes enn småfeil ved at det har sneket seg inn ikke-ascii-tegn i filene som SKI-importen ikke klarer å tolke, men det er fortsatt et åpent spørsmål.

De presise banedataene er gitt i ITRF-systemet mens GPS-beregningene skjer i WGS-systemet. SKI har ingen funksjon for å importere jordrotasjonsparametre som utgjør transformasjonen mellom disse systemene det jeg har funnet, dette har derimot Bernese. Kanskje er det en av årsakene til at det jeg ikke har oppnådd bedre resultater med presise banedata for så pass korte vektorer som 30 km.

A priori rms

Dette er en slags grense for tillatt støy på fasemålingene når SKI skal forsøke å løse heltallene med FARA-algoritmen. Standardverdi er 10 mm men det er mulig å øke denne hvis det oppstår problemer. Da må en imidlertid kontrollere resultatet med andre metoder i tillegg til å se på standardavviket på vektoren.

Test av forskjellige beregningsparametre

I tabellen som følger har jeg sammenfattet noen resultater fra beregning av trekanten som utgjøres av punktene 9401, 9402 og 9403 i Rana-nettet. En av vektorene er målt en annen dag en de andre, og de er derfor ukorrelerte så langt det lar seg gjøre. Lukking av trekant er brukt som nøyaktighetsangivelse.

Lukking av trekanter:

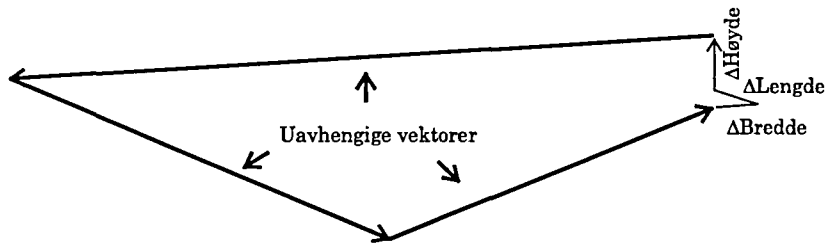

Forskjellige beregningsparametre, korte vektorer

	Alternativ 1	Alternativ 2	Alternativ 3	Alternativ 4	Alternativ 5
Tropospheric model	Hopfield	Hopfield	Hopfield	Hopfield	Hopfield
Ionospheric model	No model	Computed	Computed(?)	Computed(?)	Computed
Ephemeris	Broadcast	Broadcast	Broadcast	Broadcast	Precise
Data used	Code+Phase	Code+Phase	Phase only	Code+Phase	Code+Phase
Phase Frequency	Automatic	Automatic	L1	L1	Automatic
Code Frequency	Automatic	Automatic	---	L1	Automatic
Loop misclosure					
Lat:	0,0015 m	0,0015 m	0,0015 m	0,0015 m	0,0011 m
Lon:	-0,0035 m	-0,0046 m	-0,0039 m	-0,0039 m	-0,0058 m
Height:	0,0020 m	0,0009 m	-0,0034 m	-0,0034 m	0,0010 m
Total:	0,0043 m	0,0049 m	0,0053 m	0,0053 m	0,0060 m
ppm:	0,2795	0,3223	0,3507	0,3507	0,3955

Av dette ser en at «computed» ionosfæremodell ser ut til å være fordel for høydebestemmelsen, unntatt der hvor bare L1 er brukt. Ved å ta med presise banedata i tillegg fås ingen tilsvarende økning av høydenøyaktigheten. Det at alternativ 3 og 4 har identisk resultat viser at SKI ikke var avhengig av kodeinformasjon for å få løsning i dette tilfellet.

Forskjellige beregningsparametre, lange vektorer

Neste tabell inneholder tilsvarende informasjon for en lang trekant , nærmere bestemt den som utgjøres av punktene 9403, 9409 og 9410:

	Alternativ 1	Alternativ 2	Alternativ 3	Alternativ 5
Tropospheric model	Hopfield	Hopfield	Hopfield	Hopfield
Ionospheric model	No model	Computed	No model	Computed
Ephemeris	Broadcast	Broadcast	Precise	Precise
Data used	Code+Phase	Code+Phase	Code+Phase	Code+Phase
Phase Frequency	Automatic	Automatic	Automatic	Automatic
Code Frequency	Automatic	Automatic	Automatic	Automatic
Loop misclosure				
Lat:	-0,0075 m	-0,0059 m	-0,0044 m	-0,0028 m
Lon:	0,0030 m	0,0003 m	0,0021 m	-0,0006 m
Height:	0,0156 m	0,0095 m	0,0182 m	0,0109 m
Total:	0,0176 m	0,0112 m	0,0188 m	0,0112 m
ppm:	0,3168	0,2013	0,3386	0,2021

Her ser det ut som om det å benytte «computed» ionosfæremodell er viktigere for høydene enn hvorvidt det blir benyttet presise banedata eller ikke. (Med forbehold, ettersom det bare var de 40.-minutters banedataene som gikk an å importere som nevnt tidligere).

For å bli helt sikker i konklusjonene vil det være nødvendig å kjøre utjevning på hele nettet med vektorer som er beregnet med de forskjellige alternativene. Dette har jeg ikke gjort, bare benyttet disse resultatene for å få et hint om hva jeg skulle sette når jeg skulle beregne vektorer til den endelige utjevningen.

Loggfilene for disse beregningene finnes forøvrig på den vedlagte CDen under katalogen \Resultater_-_SKI\Lukkingstester\

Lukkingsfeilen kommer umiddelbart fram i det kartesiske systemet som ΔX, ΔY og ΔZ men er oppgitt som høydefeil og feil i horisontalplanet:

$$\Delta Bredde = \Delta Z \cos B - (\Delta X \cos L + \Delta Y \sin L) \sin B$$
$$\Delta Lengde = \Delta Y \cos L - \Delta X \sin L$$
$$\Delta Høyde = \Delta Z \sin B + (\Delta X \cos L + \Delta Y \sin L) \cos B$$

Geometri:

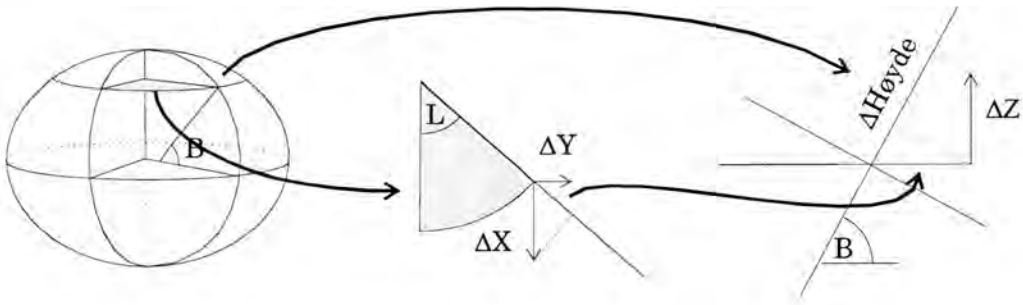

Hvorvidt B og L er bredde og lengde for trekantens tyngdepunkt eller lukkingspunkt spiller mindre rolle.

Loggfiler fra SKI

Det som ellers er mest interessant fra SKI-loggfilene bortsett fra rms og standardavvik på sluttresultatet av vektorberegningen er kanskje testene som blir utført for å godkjenne heltall-sløsningene. Det som listes ut er såkalte «FARA statistics», og viser at SKI benytter FARA-algoritmen omtalt i blant annet [Hofman-Wellenhof *et al.* 1993] for å finne heltallene.

8.5.2 Bernese-programmet

Bernese er en GPS programpakke som er utviklet ved universitetet i Bern i Sveits. Dette er et program hvor brukeren har mulighet til selv å gå inn å stille på parametre i større grad enn de kommersielle programpakkene, som Leica-SKI kan sies å være en representant for. Det stilles dermed høyere krav til kunnskapen hos brukeren, men hvis omstendighetene er de rette er det mulig å få mer nøyaktige resultater ut av en vektorberegning i Bernese enn om dataene er kjørt rett igjennom et program som Leica-SKI.

For beregninger med presise banedata bør en helst kjenne sammenhengen mellom ITRF(International Terrestrial Reference Frame) og ICRF (International Celestial Reference Frame) Forholdet er uttrykt ved rotasjonsmatriser og størrelsene som skal brukes er inn-fil ved beregningene i Bernese (Polfiler med/ jordrotasjonsparametre: ERP). SKI-programmet har ingen muligheter for å importere slike opplysninger det jeg er klar over.

Baneparametre

På grunn av de forstyrrende effektene nevnt tidligere avviker satellittbanene fra ellipsen. Fra SP3-filenes satellittposisjoner for hvert 15. minutt går det an å rekonstruere de virkelige banene ved hjelp av en matematisk modell.

Ellipsebane og interpolert bane:

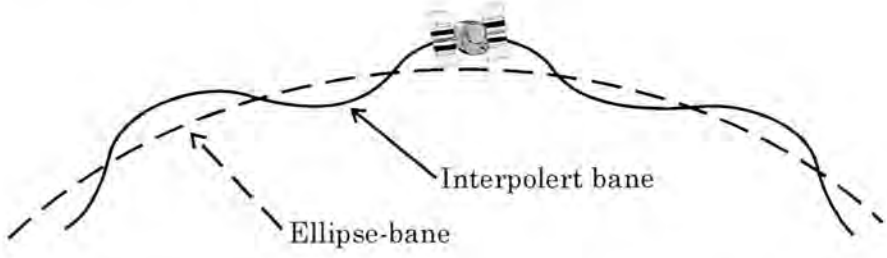

I Bernese-programmet benyttes en modell for dette som er utviklet ved universitetet i Bern «The new Bern orbit model». I loggen/resultatutskriften kommer det bekreftelse på at det virkelig er benyttet seg av de presise banedataene ved at beregnede bane-elementer for hver satellitt ved et tidspunkt t_0 er listet opp. Parametre for polbevegelser og tidsinformasjon er listet opp i sammenheng med dette.

Quasi-iono-free ambiguity sulution – QIF

Det som ellers er interessant med Bernese loggfilene er metoden som brukes i selve beregningene – Quasi-iono-free ambiguity sulution – QIF.

Dette er en litt annen algoritme enn den som SKI benytter for å finne heltallene. Benytter blant annet ionosfærefri lineær kombinasjon.

8.5.3 Metoder for å kontrollere målingene

Standardavviket på vektorberegningene er den første indikasjonen på om beregningene har gått greit eller ikke. Under SKI-beregningene var det spesielt 1 vektor som utmerket seg som spesielt «ugrei», nemlig 9416-9417 (anm: fra TS: Skyldes trolig et kraftig tordenvær/regnvær under deler av målingene). Av den grunn er verken punkt 9416 eller 9417 med i noen utjevning. Deretter går det an å sjekke lukking av trekanter for å avsløre grove feil. En sløyfe som inneholdt de to nevnte punktene passerte heller ikke denne «testen». En annen metode for å avsløre slike feil er fri utjevning.

Residualfiler

Det er mulighet å utelukke dårlige målinger/satellitter etter å ha inspisert residualfilene, sett på støymønsteret til satellitten og vurdert om det avviker fra det vanlige. Dette har jeg benyttet i liten grad. Det er heller ikke sikkert at resultatet blir noe bedre av den grunn. På CDen har residualfilene navnene L1c.txt, L1p.txt, L2c.txt og L2p.txt der hvor de er tatt med.

8.5.4 Andre programmer og metoder

GIPSY

Dette er en GPS programpakke som er utviklet ved JPL — Jet Propulsion Laboratory. Det er ikke gjort noen beregninger i dette programmet med målingene i denne oppgaven. Statens kartverk bruker imidlertid programmet til høypresisjonsformål og resultatene fra målingen i Rana-nettet i 1999 beregnes i dette programmet.

Absoluttbestemmelse

Ved absoluttbestemmelse beregnes ikke vektorer, man er derfor nødt til å måle i lengre tid for å få bra nok resultat. Står man lenge nok blir resultatet derimot bedre enn ved «klassisk statisk», som tilsvarer metoden som 1997-målingene i Rana-nettet ble foretatt etter.

For å utføre en slik beregning, er man avhengig av program som tar hensyn til alle feilkilder man ikke nødvendigvis bryr seg om ved vektorberegninger, f.eks. tidejord. GIPSY-programmet er et slikt program.

Det er mulig å inkludere data fra permanente GPS-stasjoner i f.eks. IGS-nettverket som også er bestemt med VLBI/SLR. («fiducial points»).

8.6 BEHANDLING AV RESULTATENE

Etter at de antatt dårlige vektorene er luket ut ved å se på standardavvik og trekantlukking, er det tid for å gå videre. Følgende momenter må vurderes:

- Utjevning direkte i det geosentriske kartesiske systemet eller utjevning i kartplankoordinater? Delprogrammet «SKI-adjustment» kan brukes til det første alternativet mens norske VG-land eller GEMINI vil være aktuelle programmer for den siste framgangsmåten.
- Fri utjevning kontra det å holde fast punkt(er)?
- Hvordan skal eventuelle forskyvninger bestemmes?

8.6.1 Utjevning og MKM

Den greieste måten å utjevne GPS-resultater på, er å gjøre det direkte i geosentriske kartesiske koordinater ettersom det er i dette systemet vektorene foreligger når de er etterprosessert. På denne måten slipper man transformasjoner til ellipsoide og kartprojeksjon før man har bruk for det. Minste kvadraters metode eller MKM gir det mest sannsynlige resultatet så fremt observasjonene er normalfordelte.

(Resten av dette kapitlet er ikke tatt med, det matematiske formelapparatet er beskrevet.)

8.6.2 GPS og vekting

(Også i dette kapitlet er det matematiske formelapparatet utelatt.)

Mange av feilkildene i forbindelse med GPS er vanskelige å måle direkte og en eksakt beregning av standardavviket vil derfor ikke la seg gjøre. Riktig vekting av observasjonene er derfor et problem man må ta hensyn til ved beregning av geodetiske nett.

Programmer for nettutjevning baserer som oftest beregning av vektsmatrisen $\underline{P}$ på standardavviket og korrelasjonsmatrisen, «the co-factor matrix», som følger hver vektor fra prosesseringsprogrammet.

$\underline{\Sigma}$ er bygd opp av varians-kovariansmatrisene for hver enkelt vektor. Vi kan skrive:

$$\underline{\Sigma} = \begin{bmatrix} \underline{\Sigma}_{vektor1} & & & 0 \\ & \underline{\Sigma}_{vektor2} & & \\ & & \vdots & \\ 0 & & & \underline{\Sigma}_{vektor\ n} \end{bmatrix}$$

hvor $\underline{\Sigma}_{vektor\ n}$ er varians-kovarians-matrisa for 1 vektor eller den inverse av normallikningsmatrisen, også dette opplysninger som stammer fra etterprosesseringen. Elementene utenom de 3 x 3 rundt diagonalen blir 0 hvis vi ikke regner med korrelasjon mellom forskjellige vektorer og beregningsomganger eller «sessions». Verdier for slike korrelasjoner har jeg ikke med på noen av beregningene i denne oppgaven.

Ved at det gjøres det på denne måten får vektorer med lavt standardavvik høy vekt mens vektorer med mindre bra standardavvik for lavere vekt.

Verdiene i $\underline{\Sigma}_{vektor\ n}$ er i regelen noe optimistiske og det kan være nødvendig å bruke skalafaktor fra 3 til 10 for å komme i nærheten av «sanne» verdier. Dette varierer imidlertid fra program til program og i praktisk bruk kan det være nødvendig å konsultere brukerveiledningen for å finne ut hva som er rimelig verdi å bruke.

Det å ha verdier for standardavvik og korrelasjoner som samsvarer noenlunde med virkeligheten har betydning når nettutjevningen skal testes for grovfeil, pålitelighet og andre ting. Hvis man i tillegg har med vektorer fra forskjellige programmer vil korrekt skalering ha avgjørende betydning for utjevningen på flere måter: Hvis den relative vektingen mellom to grupper settes som 1:10 mens virkeligheten ligger nærmere, la oss si 1:50, vil de resulterende utjevningstilleggene og feilellipsene bli mer villedende enn opplysende.

Vekting av forskjellige observasjonsgrupper

En måte å komme fram til fornuftig vekting på kan være å prøve seg fram med forskjellige skaleringen til resultatet samsvarer noenlunde med den nøyaktigheten man forventer etter å ha sett litt på lukkingsfeil i trekanter. Det er i alle fall ikke mulig å «jukse» seg til så små feilellipser man bare vil uten å manipulere med tallene inne i selve korrelasjonsmatrisen, og selv da vil det føre til at andre observasjoner igjen får større utjevningstillegg enn det som er rimelig.

En annen måte kan være å justere vektene for langvektorene til å få omtrent de samme verdiene som den har fra SKI-beregningen , eller litt mer ettersom Bernese er forventet å være mer nøyaktig.

I SKI-utjevningsprogrammet kan dette forholdet justeres omtrentlig ved å angi "user estimated accuracy" som svarer omtrent til "a priori varians". Har ingen absolutt kontroll i og med at det ikke kommer med noen vektingsopplysninger fra utskriften, bare residualer osv.

Problemet med vekting av forskjellige grupper står man også overfor innen tradisjonell landmåling ved blanding av vinkel og avstandsobservasjoner.

8.6.3 Resultater

Feilellipser med SKI og Bernesevektorer

Følgende tabell viser resutatet av en utjevning hvor det er blandet sammen vektorer fra SKI og Bernese. Utjevningen er foretatt i SKI-utjevningsprogrammet og gruppene er skalert utfra målsetting om å få et fornuftig resultat. Det er utført en friutjevning og en utjevning hvor minimum antall punkter er holdt fast. I dette tilfelle 3D-punktet 225.

Utjevningen er utført med uavhengige vektorer som jeg har plukket ut. Av den grunn er punkt 9407 utelatt. 9417, 9416 og 9415 er utelatt pga problemer med vektor 9416-9417.

SKI og Bernese

Punktnummer	Store halvakse:		Asimut:		Lille halvakse:		Høyde:	
	225 som fast	Fritt nett	225 som fast	Fritt nett	225 som fast	Fritt nett	225 som fast	Fritt nett
112	0,0098	0,0059	175,8	173,4000	0,008	0,0051	0,0375	0,0170
151	0,0095	0,0053	0,1	10,9000	0,0077	0,0045	0,0375	0,0170
225	---	0,0070	---	178,2000	---	0,0055	---	0,0285
226	0,0049	0,0073	135,8	171,8000	0,0042	0,0061	0,0067	0,0286
9401	0,0066	0,0076	145,9	179,4000	0,0061	0,0063	0,0086	0,0286
9402	0,0038	0,0068	148,8	179,0000	0,0034	0,0055	0,0051	0,0282
9403	0,003	0,0064	154,9	0,2000	0,0026	0,0049	0,0044	0,0282
9404	0,006	0,0079	129,9	174,0000	0,0055	0,0069	0,0074	0,0287
9405	0,0059	0,0071	131,4	9,9000	0,0058	0,0059	0,0066	0,0284
9406	0,0082	0,0082	147,2	10,5000	0,0079	0,0074	0,0096	0,0289
9408	0,0093	0,0049	178	167,3000	0,0075	0,0048	0,0373	0,0167
9409	0,009	0,0044	176,4	177,1000	0,0069	0,0039	0,0372	0,0165
9410	0,0087	0,0039	178,9	7,8000	0,0067	0,0030	0,0372	0,0164
9411	0,0089	0,0044	178,2	7,3000	0,0072	0,0038	0,0374	0,0167
9412	0,0088	0,0047	179,6	14,1000	0,0073	0,0042	0,0373	0,0167
9413	0,0143	0,0098	179,2	142,3000	0,0127	0,0096	0,0629	0,0409
9414	0,0141	0,0093	6,2	9,3000	0,0101	0,0064	0,0627	0,0405
9415	0,0143	0,0095	7,1	10,5000	0,0101	0,0065	0,0627	0,0405
9418	0,0119	0,0088	3,6	10,4000	0,0092	0,0066	0,0558	0,0424

Som ventet blir feilellipsene større jo lenger unna det faste punktet en kommer for den faste utjevningen. For høydene ser en at alle punktene på det innerste profilet har fått tilfredsstillende løsning mens alle andre har relativt store feilellipser. For friutjevningen har denne feilen feilen spredd seg utover.

Komplett resultat med residualer finnes på CD under katalogen \Resultater_-_Utjevning\SKI_og_Bernese\ i filene 95Fast225_med13-14.TXT og 95Fri_med13-14.TXT. Noen vektorer er markerte som grovfeil, men ettersom teststørrelsen er satt ganske strengt: «tuned Alpha: 0.16%» og utjevning sammen med bare SKI-vektorer viste noe annet har jeg tatt dem med likevel.

Feilellipsene er 95% med 2D-skaleringsfaktor 2.4477 og 1D skaleringsfaktor 1.9604. (Opplysning fra loggfil.)

Utjevningen av SKI og Bernese-blandingen

Koordinatene er transformert til UTM sone 33 og det er ellipsoidiske høyder

	Nord	Øst	Ell. høyde	
225	7355402.8839	461044.7870	40.2980	Fast
226	7356444.0902	459329.3242	36.6663	
112	7353940.1496	441140.1695	151.2225	
151	7353541.6199	435761.2690	80.5849	
9401	7354022.6959	466755.2900	160.9037	
9402	7354951.5090	460867.0618	34.4008	
9403	7357048.4919	460343.5632	35.8403	
9404	7357971.0773	460361.8266	62.5067	
9405	7360214.5449	457577.2806	152.8460	
9406	7362322.7371	455409.2286	93.1647	
9408	7340180.4964	440641.1093	41.9904	
9409	7345707.7465	437056.5965	49.9388	
9410	7350313.4680	436275.6041	35.4801	
9411	7352658.7069	438428.1642	35.4928	
9412	7357038.4198	439856.6538	303.1169	
9413	7338288.6904	413342.1316	42.7776	
9414	7342434.8467	410533.5320	37.7841	
9415	7343702.0587	408424.8520	36.2222	
9418	7359075.3578	410398.8767	43.8339	

Feilellipser med bare SKI-vektorer

Følgende tabell viser et utjevningsresutatet hvor det er med vektorer bare fra SKI-programmet. (Forøvrig akkurat de samme uavhengige vektorene). Utjevningen er fortsatt foretatt i SKI-utjevningsprogrammet, men vi slipper problemet med ulik skalering av observasjonsgrupper.

Bare SKI:

Punktnumme	Store halvakse:		Asimut:		Lille halvakse:		Høyde:	
	225 som fast	Fritt nett	225 som fast	Fritt nett	225 som fast	Fritt nett	225 som fast	Fritt nett
112	0,0127	0,01	145,1	143,5	0,0118	0,0092	0,0139	0,0104
151	0,0118	0,0089	161	28,6	0,0116	0,0088	0,0144	0,011
225	- - -	0,0085	- - -	137,3	- - -	0,0081	- - -	0,0101
226	0,009	0,0099	135,8	122,4	0,0077	0,0088	0,0123	0,0113
9401	0,0106	0,0086	127,3	103,6	0,01	0,0082	0,0122	0,0081
9402	0,007	0,0081	147,9	111,2	0,0063	0,0076	0,0093	0,0081
9403	0,0055	0,0069	154,8	103,1	0,0049	0,0066	0,0081	0,0064
9404	0,0111	0,0116	130	118,5	0,0101	0,0107	0,0137	0,0126
9405	0,0098	0,009	127,2	103,4	0,0094	0,0085	0,011	0,0083
9406	0,0127	0,0112	127,9	112,4	0,012	0,0105	0,0136	0,0106
9408	0,0109	0,0067	118	99,2	0,0104	0,0061	0,0118	0,006
9409	0,0096	0,0054	130,3	98,4	0,0092	0,005	0,0107	0,005
9410	0,0093	0,0052	133,9	98,5	0,0089	0,0048	0,0105	0,005
9411	0,0107	0,0074	123,4	106,5	0,0102	0,0067	0,0128	0,0088
9412	0,0111	0,0078	121,4	103,7	0,0105	0,0072	0,0121	0,0076
9413	0,0181	0,0133	103,9	99,3	0,0172	0,0124	0,0178	0,0119
9414	0,016	0,0112	98,4	91,4	0,0151	0,0104	0,0173	0,0116
9415	0,0168	0,0121	102,1	96,7	0,0159	0,0112	0,0175	0,0118
9418	0,0153	0,0129	119,9	111	0,0147	0,0123	0,0147	0,011

Her er ser det ut til å være mer samsvar mellom nøyaktigheten i høyde og grunnriss og vi ser ingenting til det merkelige fenomenet at kun punktene på innerste profil fikk OK høyder i fast-utjevningen.

I følge Morten Strand (FW) som utførte Bernese-beregningene var støynivået i målingene på grensen til hva som tåles for at Bernese-programmets fortrinn framfor kommersielle beregningsprogrammer skal komme til sin rett.

Det går likevel an å se at feilellipsene i grunnriss ble noe bedre for utjevningen som inkluderer Bernese-vektorer. Dette meg høydene er kanskje et vektingsproblem som ikke fikk helt tilfredsstillende løsning likevel.

Utjevningen av bare SKI-vektorer

Koordinatene er transformert til UTM sone 33 og det er ellipsoidiske høyder

	Nord	Øst		Ell. høyde
225	7355402.8839	461044.7870	40.2980	Fast
226	7356444.0900	459329.3245	36.6671	
112	7353940.1465	441140.1667	151.2017	
151	7353541.6173	435761.2665	80.5640	
9401	7354022.6979	466755.2881	160.9052	
9402	7354951.5091	460867.0619	34.4009	
9403	7357048.4919	460343.5634	35.8408	
9404	7357971.0773	460361.8259	62.5073	
9405	7360214.5450	457577.2802	152.8468	
9406	7362322.7355	455409.2279	93.1569	
9408	7340180.4934	440641.1056	41.9778	
9409	7345707.7439	437056.5937	49.9237	
9410	7350313.4649	436275.6023	35.4587	
9411	7352658.7043	438428.1616	35.4721	
9412	7357038.4185	439856.6507	303.0958	
9413	7338288.6901	413342.1265	42.7641	
9414	7342434.8488	410533.5269	37.7854	
9415	7343702.0611	408424.8467	36.2286	
9418	7359075.3620	410398.8672	43.8359	

Gitt koordinater for punktene 225, 226,112 og 151 var:

J16T225	7355402.884	461044.787	40.298
J16T226	7356444.095	459329.323	36.675
J16T112	7353940.152	441140.169	151.206
J16T151	7353541.623	435761.269	80.573

Hvis alle målinger var 100% feilfrie kunne det gått an å tatt koordinatdifferensen og kalt det «Forskyvning i forhold til J16T225», men det er jo ikke tilfelle.

Når det gjelder punktene 226,112 og 151 må det dessuten tas med at dette er stativ-oppstillinger og at sentreringsnøyaktigheten antakelig er deretter. Det er imidlertid bare stilt opp en gang i disse punktene, og en eventuell unøyaktighet i sentreringen vil derfor ikke bidra negativt til utjevningsresultatet heller.

Detektere forskyvninger

Ettersom de forventede forskyvningene (1,0-2,0 mm pr år??) knapt er større enn aksene i 95%-feilellipsene (0,5 - 1,0 mm) vil det bli vanskelig å estimere forskyvningen som antall mm pr år i løpet av de første årene.

Det går imidlertid an å sette det opp som en hypotesetest hvor svaret blir ja eller nei på om forskyvning har funnet sted. Det går an å si det slik at "sanne" forskyvninger (som vi ikke kjenner verdien på) vil da være nødt til å ligge i størrelsesorden 1,0 - 2,0 cm for at den skal kunne oppdages med høy konfidens. Det avhenger selvfølgelig også av nøyaktigheten på målingene vi skal sammenligne med (Har ingenting å sammenligne med hittil i år 1999).

For å bøte på det at feilellipsene blir større jo lenger unna det faste punktet (225) en kommer går det an å lage en forskyvningsmodelle hvor en definerer 0 forskyvning i nettets tyngdepunkt.

Hvis en har to nett fra to forskjellige år tilgjengelige vil en mulig framgangsmåte for å bestemme forskyvninger være å transformere det en nettet til det andre og holde fast et punkt hvor en definerer at det ikke har skjedd noen forskyvning.

For å sammenligne nett når det er brukt forskjellige beregningsmetoder kan en være nødt til å gjøre om til vektorer ut fra f.eks. absoluttbestemte koordinater.

VG-land

Ettersom bergeningsprogrammet VG-land fokuserer på omdanning til retning/avstand og ortometriske høyder, har jeg latt være å inkludere noen resultater derfra.

8.6.4 Sammenligning av vektorer fra SKI og Bernese

Ettersom det var noe forskjell på nøyaktigheten i grunnriss mellom utjevningen med bare SKI-vektorer og utjevningen hvor de lange SKI-vektorene var erstattet med Bernese-vektorer kan det være på sin plass å studere denne forskjellen fra en litt annen innfallsvinkel.

Andre har rapportert om antatt målestokkfeil i SKI og for å finne ut om dette gjelder for målingene i denne oppgaven, går det an å sammenligne vektorlengder og undersøke om det kan være noen systematisk forskjeller.

Diagrammet nedenfor er kommet fram ved å ta samme vektor beregnet i SKI og Bernese og sammenligne lengden av vektoren ved å ta (SKI / Bernese – 1) * 1 000 000.

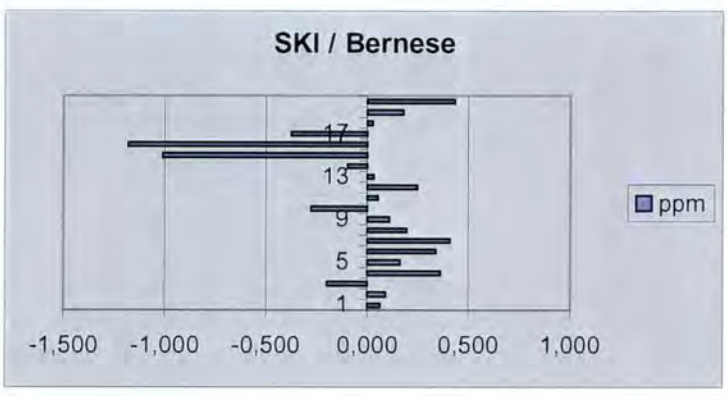

Gjennomsnitt:	-0,022 ppm
Median:	0,076 ppm
Standardavvik:	0,426 ppm

Ved første øyekast ser det dermed ikke ut til at det finnes noe system i forskjellen. 2 vektorer har spesielt store negative ppm-verdier (mindre enn -1). Ved å stryke ut disse 2 og samtidig stryke 2 i den andre enden av skalaen får vi:

Trimmet gjennomsnitt:	0,056 ppm
Median (Samme):	0,076 ppm
Standardavvik:	0,207 ppm

Det gjennomsnittet vi nå får samsvarer i større grad med medianen og ser vi bort fra standardavviket kan se ut som om en SKI-vektor gjennomsnittlig er lengre enn en Bernese-vektor.

Et slikt spørsmål går det an å sette opp som en hypotesetest:

H_0: k = 0 (H_1: k = 0 (Ingen målestokksforskjell)

hvor k er verdien fra diagrammet: (SKI / Bernese – 1) * 1 000 000.

For å utføre en hypotesetest må en først anta en fordeling. I et slik tilfelle med avledede størrelser er ikke det gitt av seg selv. Med det forholdet mellom verdier og standardavvik vi ser her (Målestokksforskjell) vil en i slik test imidlertid ende opp med å forkaste H_0 omtrent samme hva slags fordeling en antar, hvis ikke vil typeII-feil bli urimelig stor. (Sannsynligheten for å feilaktig akseptere H_0.)

Et forsøk på å sette opp samme diagram og bare ta med de 14 vektorene som er med i «hovedutjevningen» gjøre ikke en eventuell sammenheng mye klarere:

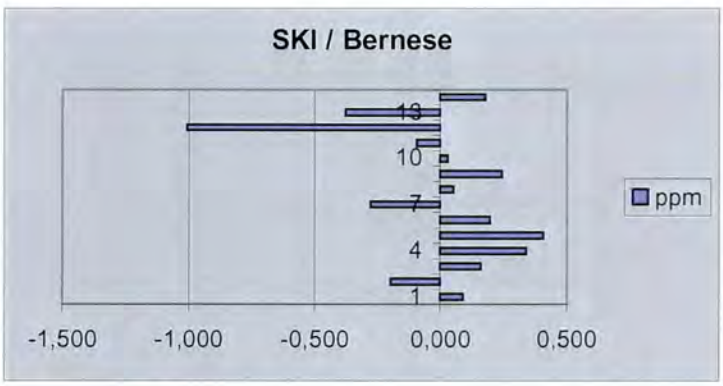

Gjennomsnitt:	-0,019
Median:	0,071
Standardavvik:	0,364

Det går også an å plotte datane på en spesiell måte for å undersøke hvor godt de passer med forskjellige fordelinger. En mer detaljert analyse av dette spørsmålet vil i tillegg måtte ta hensyn til at vektorene har forskjellig standardavvik.

Målestokkfeil i SKI?

Det er likevel mulig det eksisterer en slik systematisk feil ved lengre måleintervaller og mindre støy, men det er ikke mulig å trekke en slik konklusjon ut fra det vi har sett her.

8.7 7. MÅLEMETODER

Vurdering av ulike målemetoder

Etter det vi har sett er målingene fra 1997 for få til at det går an å detektere bevegelser ned til 0,5 cm -nivå med tilstrekkelig konfidens.

Med Statens kartverk sine målinger fra 1999 hvor det sto mottaker og målte i hvert punkt i fra 3 til 6 døgn og GIPSY-programmet benyttes skulle et slikt mål være oppnåelig. Det blir imidlertid ikke før nettet blir målt på nytt igjen med denne metoden om noen år(?) at målet om å kunne detektere bevegelser på 0,5 cm pr år vil bli realisert.

8.8 8. BAKGRUNN OG AKTUELLE PROSJEKTER

Teorien om kontinentenes drift ble først framsatt av geofysikeren Alfred Wegener i begynnelsen av dette århundret, men det var først når romteknologien nådde et visst utviklingsnivå at det ble mulig å måle platetektoniske bevegelser direkte: På slutten av 1980-tallet ble f.eks. bevegelsen av det amerikanske kontinentet i forhold til det europeiske målt til å være *ca.* 1-3 cm per år ved hjelp av de uavhengige metodene VLBI og SLR.

Platetektonikk etter [Tarbuch, Lutgens 1993]:

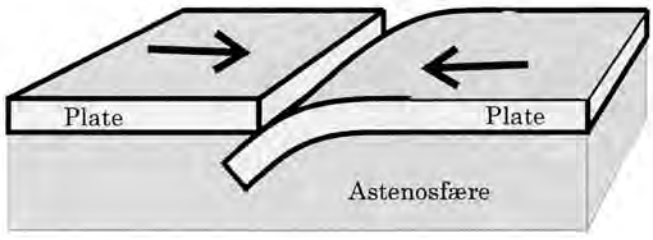

VLBI krever store antenner og det finnes bare et begrenset antall installasjoner, men i løpet av de siste 10 årene har GPS blitt nøyaktig nok til at dette alene kan brukes til overvåkning av forkastningsbevegelser innenfor mindre områder, også utenfor plategrenser. Dette åpner for mer omfattende kartlegging enn tidligere ettersom GPS er rimeligere enn SLR og de andre metodene og det nødvendige utstyret er allment tilgjengelig.

Vertikale bevegelser i jordskorpen har man vært i stand til å måle direkte helt siden teknikken for presisjonsnivellement ble så god at de årlige endringene oversteg tilfeldige målefeil. For eksempel har gjentatte målinger i presisjonsnivellementsnettene i Norge og Norden vist at landhevingen i de nordiske landene varierer fra et minimum på *ca.* 1-5 mm i året i Norge til *ca.* 10 mm i området rundt Bottenviken. Dette samsvarer med resultater fra andre metoder, eksempelvis tyngdemålinger og vannstands-observasjoner.

Presisjonsnivellement var og er fortsatt i noen grad metoden som brukes for å overvåke vertikale forkastningsbevegelser. De tradisjonelle metodene innen landmålingsfaget er av forskjellige årsaker ikke gode nok til at det går an å måle like nøyaktig horisontalt over lange avstander, men med GPS og romteknologien er dette nå mulig.

Forkastning hvor virkningen av erosjon er utelatt. Etter [Tarbuch, Lutgens 1993]:

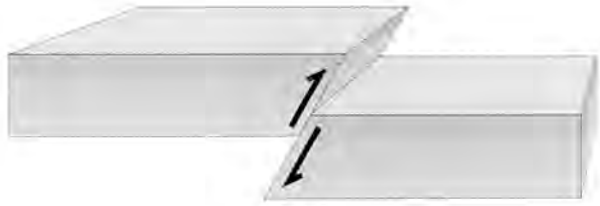

Figuren viser en forkastning tilsvarende den som er funnet i Rana hvor virkningen av erosjon er utelatt.

Califorina

I California finnes ifølge nettsidene til IGS over 50 permanente GPS-stasjoner med det til formål å overvåke San Andreas-forkastningen. Disse er en del av IGS-nettverket. Det er også aktuelt å kombinere det med seismiske data for å overvåke dette jordskjelvområdet. Et tilsvarende antall stasjoner (eller fler) er i drift i Japan

Skåne

Svenske geodeter har siden 1989 hatt et prosjekt på gang for å måle bevegelser i en forkastningssone i Skåne. Her er Bernese-programmet benyttet til beregninger og permanente IGS/EUREF-stasjoner som Onsala er benyttet som "fiducial points".

Ved gjentatte målinger fra 1989 til 1996 er det oppnådd å kunne bestemme verdier for "forskyvning/år" i størrelsesorden 2,0±0,7 til 5,0±0,5 mm/år.

8.9 LITTERATUR

Hofman-Wellenfof *et al.*: *GPS Theory and Practice.* Third edition. Springer Verlag – Wien New York 1994.

Kristiansen, Oddgeir: *Investigations Related To High Precision Analysis Of GPS Data.* Doktorgrad 1999

McCarthy, Dennis D. (ed.): *IERS Technical Note 21.* IERS Conventions 1996

Melchior, Paul: *The Earth Tides.* First edition. Pergamon Press 1966.

Revhaug, Inge: *Feillære og utjevningsregning.* Landbruksbokhandelen 1993. (Utdrag).

Rothacher, Markus and Mervart, Leoš (ed.): *Bernese GPS Software Version 4.0.* Astronomical Institute University of Berne, September 1996 (Brukerhåndbok)

Tarbuch, Edward J. and Lutgens, Frederick K.: *The Earth. An Introduction to Physical Geology.* Fourth edition. Macmillan 1993.

Vanícek, Petr and Krakiwsky, Edward J.: *Geodesy: The Concepts* North-Holland Publishing Company1982

Artikkel GFF volume 121 (1999): *GPS measurements of crustal deformations in Skåne, Sweden, between 1989 and1996*

Internettsteder (bl.a.):

http://geoyfsikk.ngu.no/neonor

http://www.oma.be//KSB-ORB/EUREF/eurhome.html

hhtp://igscb.jpl.nasa.gov/

http://hpiers.obspm.fr/

8.10 VEDLEGG

8.10.1 Oversikt over måleperioder